Indirect impact of landslide hazards on transportation infrastructure

.....

by

Benjamin Frank Postance

A Doctoral Thesis

Submitted in partial fulfilment of the requirements
for the award of

Doctor of Philosophy of Loughborough University

28/09/2017

CERTIFICATE OF ORIGINALITY

This is to certify that I am responsible for the work submitted in this thesis, that the original work is my own except as specified in acknowledgements or in footnotes, and that neither the thesis nor the original work contained therein has been submitted to this or any other institution for a degree.

Signed: Benjamin Frank Postance

Abstract

This thesis examines the indirect impact of natural hazards on infrastructure networks. It addresses several key themes and issues for hazard assessment, network modelling and risk assessment using the case study of landslides impacting the national road network in Scotland, United Kingdom. The research follows four distinct stages. First, a landslide susceptibility model is developed using a database of landslide occurrences, spatial data sets and logistic regression. The model outputs indicate the terrain characteristics that are associated with increased landslide potential, including critical slope angles and south westerly aspects associated with increased rates of solar irradiance and precipitation. The results identify the hillslopes and road segments that are most prone to disruption by landslides and these indicate that 40 % (1,700 / 4,300 km) of Scotland's motorways and arterial roads (i.e. strategic road network) are susceptible to landslides and this is above previous assessments. Second, a novel user-equilibrium traffic model is developed using UK Census origin-destination tables. The traffic model calculates the additional travel time and cost (i.e. indirect impacts) caused by network disruptions due to landslide events. The model is applied to calculate the impact of historic scenarios and for sets of plausible landslide events generated using the landslide susceptibility model. Impact assessments for historic scenarios are 29 to 83 % greater than previous, including £1.2 million of indirect impacts over 15 days of disruption at the A83 "Rest and Be Thankful" landslide October 2007. The model results indicate that the average impact of landslides is £64 k per day of disruption, and up to £130 k per day on the most critical road segments in Scotland. In addition to identifying critical road segments with both high impact and high susceptibility to landslides, the study indicates that the impact of landslides is concentrated away from urban centres to the central and north-west regions of Scotland that are heavily reliant on road and haulage-based industries such as seasonal tourism, agriculture and craft distilling. The third research element is the development of landslide initiation thresholds using weather radar data. The thresholds classify the rainfall conditions that are most commonly associated with landslide occurrence in Scotland, improving knowledge of the physical initiation processes and their likelihood. The thresholds are developed using a novel 'optimal-point' threshold selection technique, high resolution radar and new rain variables that provide spatio-temporally normalised thresholds. The thresholds highlight the role of the 12-day antecedent hydrological condition of soils as a precursory factor in controlling the rain conditions that trigger landslides. The new results also support the observation that landslides occur more frequently in the UK during the early autumn and winter seasons when sequences or 'clustering' of multiple cyclonic-storm systems is common in periods lasting 5 to 15 days. Fourth, the three previous elements are combined to evaluate the landslide hazard of the strategic road segments and a prototype risk assessment model is produced - a catastrophe model. The catastrophe model calculates the annual average loss and aggregated exceedance probability of losses due to the indirect impact of landslides in Scotland. Beyond application to cost-benefit analyses for landslide mitigation efforts, the catastrophe model framework is applicable to the study of other natural hazards (e.g. flooding), combinations of hazards, and other infrastructure networks.

Key words

Landslides, Landslide Susceptibility, Transport Infrastructure, Indirect Impacts, Initiation Thresholds, Landslide Hazard, Risk Assessment, Catastrophe Modelling

Glossary

NERC	Natural Environment Research Council
BGD	British Geological Survey
ONS	Office for National Statistics
mm	millimeter
m	meter
km	kilometer
k	Thousand
M	Million
pa	Per annum
hr	Hour
GBP	Great British Pound
USD	United States Dollar
NZD	New Zealand Dollar
CAT	Catastrophe Model
PBM	Physical-Process Based Model
LR	Logistic Regression
OLS	Ordinary Least Squares regression
ANN	Artificial Neural Network
SVM	Support Vector Machine
RF	Random Forest decision tree
WoE	Weights of Evidence
χ^2	Chi-square statistic
LLf	Log-likelihood function
AIC	Akaike Information Criterion
ROC	Receiver Operating Characteristic curve
AUC	Area Under Curve
TP	True Positive
FP	False Positive
TN	True Negative
FN	False Negative
TPR	True Positive Rate
FPR	False Positive Rate
TS	Threat Score threshold
OP	Optimal Point threshold
SRN	Strategic Road Network
LRN	Local Road Network
NR	Network Rail
DFT	Department For Transport
LRE	Landslide Rain Event
NRE	Non-Landslide Rain Event

SSR	Site Specific Rainfall record
ID	Rainfall Intensity-Duration
AD	Rainfall Accumulation-Duration
n	A count value (e.g. number of days)
D_n	Rain duration over past n days
I_n	Rain intensity over past n days (specify mean or max)
V_n	Rainfall accumulation over n days antecedence
$Imax_n$	Maximum rainfall intensity over n days antecedence
MAP	Mean Annual Precipitation
DR_n	Day with rain (>0.01 mm) over past n days
RDN	Rainy Day Normal (specify period e.g. month or annual)
$RDNI$	Rainy Day Normal Intensity (specify period e.g. month or annual)
NV_n	Normalised accumulation over n day's antecedence
RD_n	Duration of rainfall greater than $RDNI$ over n day's antecedence.
H	Hazard
C	Consequence
P	Probability
I	Intensity
E	Exposure
V	Vulnerability
$p(TH)$	Probability of threshold occurrence
$p(LS)$	Probability of landslide occurrence
$p(LS\|TH)$	Probability of landslide occurrence given threshold
p^T	Temporal probability of landslide occurrence
p^S	'Landslide susceptibility' the spatial probability of landslide occurrence
r	A road segment.
H_r	Landslide Hazard for a single unit area (i) of terrain.
$\|U_r\|$	A set of hillslopes intersecting a road segment.
J	Calibration coefficient for the average number of landslides per storm.
f	The approximate mean number of road segments effected by a storm.
OEP	Occurrence Exceedance Probability
AEP	Aggregate Exceedance Probability
AAL	Annual Average Loss
G	Network Graph formed of links and nodes
L	Set of Network Links
N	Set of Network Nodes
UE	User Equilibrium
SOE	System Optimal Equilibrium
DUE	Dynamic user Equilibrium
SUE	Stochastic User Equilibrium
DUA	Dynamic User Assignment
ΔT	Additional Travel Time
OSM	OpenStreetMap
ITN	Integrated Transport Network
OD	Origin Destination
ATC	Automatic Traffic Count

SUMO	Simulation of Urban Mobility
NLD	National Landslide Database
DTM	Digital Terrain Model
DEM	Digital Elevation Model
UCU	Unique Conditioning Unit
IHUS	Integrated Hydrological Unit Sections (Centre for Ecology and Hydrology)
PMM	Parent Material Model
S_i	Susceptibility on a road segment (i)
b	Spatial buffer distance (m)
At_b	Total area (m^2) within buffer
As_b	Area of susceptible ground (m^2) within buffer

Acknowledgments

The research was funded by the UK Natural Environment Research Council (grant number 1401793) and supported by the Department of Geography and the Department of Civil and Building Engineering at Loughborough University. I wish to thank the research council and the University for giving me this opportunity.

This thesis is the culmination of three and a half years of research that would not have been possible without the guidance and support from a number of individuals.

Firstly, I would like to thank the British Geological Survey (BGS) Landslides team for their assistance using the National Landslide Database. Permission was granted by the BGS to use the landslide database and others wishing to use this data should contact the BGS directly. I would also like to thank Katy Freeborough, Helen Reeves and Helen Glaves at the BGS for their more general guidance and support received whilst presenting this research at conferences in around the world.

Secondly, I would like to thank my supervisory team, Dr John Hillier, Dr Tom Dijkstra, and Prof Neil Dixon. To my first supervisor and good friend, John Hillier, whose ideas, advice and teaching in probability and statistics has helped me to develop a wide array of technical and programming skills. This training will no doubt open many opportunities to me in the future. John's continued encouragement and guidance throughout this entire process has also helped me to become an effective and confident researcher, and for that I am very grateful. Tom Dijkstra has been a continued source of enthusiasm. Tom's open-door policy, expertise and knowledge of landslides has given me the inspiration and insight to produce work of a high standard in the field. Lastly, my thanks go to Neil Dixon, who's reassuring feedback and big picture outlook has provided the solid foundation on which this project stands. It really has been an inspiration and a great pleasure to work with you all.

Thirdly, I wish to thank my friends (old and new) and family who have supported me in this endeavour in many ways.

Finally, to my fiancé Rosie, who has supported me through good times and bad, and who encouraged me not only to finish, but to start this work in the first place.

Table of Contents

List of Figures

List of Tables

Chapter 1 Introduction

1.1 Context and problem definition

Modern society is reliant upon a collection of infrastructure systems and networks to support and maintain economic growth and social standards. Highway networks are often considered one of the most important infrastructure networks as they provide cost-effective and flexible means of transportation, offer redundancy for other infrastructures (e.g. rail replacement bus services or water tankers during a pipe failure) and are generally available to most populations worldwide (Berdica 2002). There is growing awareness and concern for the vulnerability of these networks to damage and disruption by natural hazards, including landslides. The losses due to direct damage are often significant. For example, the remediation cost following landslides were upwards of $4.3M on highway 50, California in 1998 (Reid & Lahusen 1998) and £1.1M on the A83, Scotland in 2007 (Winter *et al.* 2014). But landslides, and other hazards, also have potential to inflict benign to catastrophic social and economic effects via 'indirect impacts', where losses are accrued via travel disruption or by increasing travel time and cost (Berdica 2002). Notable recent examples include: communities isolated from emergency responders by landslide blocked roads following the 2015 Gorkha earthquake, Nepal (Chiaro *et al.* 2015); and the widespread travel delay with daily economic losses of £2.3M due to flooding on a section of the M1 motorway, England following summer storms in 2007 (Chatterton *et al.* 2011; Dawson *et al.* 2016b).

The severity and extent of indirect impacts, thus vulnerability of affected populations, may extended far beyond the hazards physical footprint and can vary markedly according to which network locations are physically disrupted (Dalziell & Nicholson 2001; Murray *et al.* 2008). To limit these impacts and increase transport networks resilience requires more pre-emptive intervention by improving hazard identification in addition to developing a greater level of understanding for the behaviour of networks under disrupted conditions (Stern 2006; Dijkstra & Dixon 2010; DFT 2014b; Krebs 2017). These developments would enable the systematic evaluation of landslide indirect impacts using conventional hazard risk assessment methods, namely hazard risk and catastrophe models, for example those used to assess the potential losses due to flooding and earthquakes (Kappes *et al.* 2012; Mattsson & Jenelius 2015). Broadly, the aim and objectives of this thesis are to investigate and resolve issues related to: landslide hazard assessment; calculating the indirect impacts of landslides on national scale road networks; and to demonstrate a coupled hazard-network risk assessment framework. This framework may then be used to identify the road segments that are highly susceptible to landslides, are critical for the efficient operation of the road network, or a combination of the two.

In the UK, and other nations, weather driven hazards such as landslides and flooding pose a significant challenge to infrastructure operators, owners and policy makers (Eddington 2006; Stern 2006; DFT 2014b; Dawson *et al.* 2016b; Krebs 2017). Transportation networks are almost continuously exposed to these hazards and there is concern that their frequency and severity, and therefore potential for indirect impacts, may increase in the near future (Jaroszweski *et al.* 2010). However, predicting the occurrence of hazards is a complex task and is subject uncertainties for; the variability in network conditions due to changing travel demands and policy; changes in climate (Jenkins *et al.* 2009; Koetse & Rietveld 2009; Pachauri

et al. 2014) and its effect on the medium to long term feedbacks and responses of physical hazard processes including, slope stability (Kilsby *et al.* 2009; Dijkstra & Dixon 2010), flooding (McCarthy *et al.* 2016) and wind storms (Donat *et al.* 2011).

In recent decades, a specific issue has been shallow translational landslides and debris flows that have caused many disruptions on the strategic road network in Scotland (i.e. motorways and arterial roads). This presents a significant challenge given that, i) the hydro-geological factors associated with the occurrence of landslides are spatially distributed over a large area (Forster & Culshaw 2004; Milne *et al.* 2009; Dijkstra & Dixon 2010), and ii) as the road network is relatively sparse with few alternative routes. In addition, the main alternative modes of transport, primarily rail, are in many cases exposed to the same landslide hazards as on the road network (Dawson *et al.* 2016b). Identifying the road segments that are susceptible to landslides and that are important for maintaining the serviceability of the road network is therefore a high priority for the Scottish government (Winter *et al.* 2005; DFT 2014b; Dijkstra *et al.* 2016b). This case study is also relevant at broader scales as similar issues are faced in other nations and temperate mountainous regions including in Norway (Meyer *et al.* 2015), the Alps (Voumard *et al.* 2013), Japan (Tsukamoto *et al.* 1982), North America and Canada (Wilford *et al.* 2004; Chleborad *et al.* 2008).

The challenge to address the issues faced in Scotland is twofold. First, the landslides with the potential to disrupt the road network must be identified. For this the notion of landslide hazard is used, which is the probability of landslide occurrence within a given area and time period (Glade *et al.* 2005). The literature review finds that empirical assessments of landslide susceptibility and landslide initiation thresholds may be used to evaluate landslide hazard at the national scale. Landslide susceptibility is the likelihood of landslide occurrence within an area based on local terrain conditions (Brabb 1984). Landslide susceptibility is a measure of the spatial propensity to landslides and is generally based on analysis of terrain variables, such as slope angle and vegetation, derived from digital elevation and land cover models (Brabb 1984; Guzzetti *et al.* 2006; Van Westen *et al.* 2008; Walsby 2008; Budimir *et al.* 2015). Landslide initiation thresholds gauge the likelihood of landslide occurrence for different hydro-meteorological conditions, such as triggering and antecedent rainfall accumulation (Caine 1980; Chleborad 2000; Chleborad *et al.* 2006; Guzzetti *et al.* 2008). Landslide susceptibility and initiation threshold assessments provide information as to where and when landslides are most likely to occur, and these are combined to provide an evaluation of the landslide hazard. A literature review conducted for this thesis, identifies several interesting research questions and required developments so that these can be used effectively in Scotland. These include: identifying suitable data and explanatory variables for use in susceptibility modelling, as these can vary between different landslide regions (Budimir *et al.* 2015); to evaluate the use of hillslope sections in susceptibility modelling; and lastly to evaluate the influence of rain record length on landslide initiation thresholds (Chleborad *et al.* 2006; Staley *et al.* 2013).

The second challenge is finding suitable methods that can be used to approximate the indirect impact of landslide disruption events on the road network. For this, physical geographers and other hazard's researchers must draw upon and look to the methods used in other fields, such as transport engineering and modelling. In the past decade there has been a growing body of research on transport and infrastructure vulnerability that provides conceptual frameworks and methodologies that can be used to identify disruption events and to measure their impact on networks (Berdica 2002; Murray *et al.* 2008; Wang *et al.* 2014). For roads, this includes the

development and evaluation of different traffic simulation models used to calculate travel additional travel time and cost (Berdica *et al.* 2003; Knoop *et al.* 2007; Sullivan *et al.* 2010; DFT 2014a). Initially, these models were applied to examine the weaknesses of different network topologies (Murray-Tuite & Mahmassani 2004; Scott *et al.* 2006; Wang *et al.* 2013), but more recently they have been applied to assess the impacts of various hazards, including, urban flooding (Knoop *et al.* 2008, 2012; Burgholzer *et al.* 2013; Pregnolato *et al.* 2016), wind storms (Nyberg & Johansson 2013), and earthquakes (Khademi *et al.* 2015). These models are yet to be applied to landslide hazards on a national scale road network.

Individually, addressing these two challenges will provide new knowledge and improved understanding of the nature of landslide occurrence and of landslide impacts on roads in Scotland. Combined, they offer an assessment of the landslide hazard on any section of the road network. This provides one of the key requirements for the development of a working landslide-network catastrophe model. Catastrophe models (also termed hazard risk models) are computerised, probabilistic models designed to simulate the magnitude, intensity, and location of potential hazard events and to estimate hazard losses (Foote *et al.* 2017). A catastrophe model simulates hundreds to thousands of hazard events to extend the limited record of past events into the realm of what may plausibly occur. The catastrophe model then incorporates vulnerability, damage and financial functions to estimate the expected (or average) and the potential (or maximum) losses due to hazards occurring within a defined time period, for example the expected and potential losses per year or per decade. Catastrophe models are therefore used to aid in the understanding landslide hazard risk and improve risk management. Traditionally, the losses by catastrophe models are represented in terms of insured financial loss as most models are developed within the insurance industry. Yet the fundamental modelling principles are applicable to other loss metrics, such as, the number of fatalities or the traffic delay time due to hazards. In the context of landslides impacting traffic on road networks, the primary limitation to use of catastrophe models has been in the lack of appropriate models that may be used to approximate the travel disruption for a large number of potential hazard events. In this thesis, this is addressed by using a traffic simulation model and a prototype catastrophe model is produced.

1.2 Aim & objectives

1.2.1 Aim

To develop a method to systematically quantify and evaluate the indirect impact of landslide hazards on transportation infrastructure networks.

1.2.2 Objectives

1. To understand the present state of knowledge and its limitations with respect to quantifying the landslide susceptibility on slopes adjacent to transportation networks.
2. To develop a landslide susceptibility assessment for transportation networks.
3. To understand the present state of knowledge and its limitations with respect to quantifying the user-impact of disruptions on transportation networks.
4. To establish an appropriate traffic simulation model to quantify the indirect impact of landslide disruptions on a highway network.

5. To understand the present state of knowledge and its limitations with respect to the definition of landslide initiation thresholds.
6. To develop a set of landslide initiation thresholds utilising weather radar data.
7. To demonstrate a coupled hazard-network catastrophe model to quantify the annual average loss caused by road travel disruption due to landslides in Scotland.

1.3 Contribution to knowledge

Successful completion of the aim and objectives has contributed new knowledge on the indirect impact of landslides on transportation networks, a relatively new area of research. The indirect impact assessments are produced using a novel catastrophe modelling framework that provides a proof of the methodological concept for the study of network disruptions due to other hazards, combinations of hazards and on other transportation networks. Beyond cost benefit analysis, the framework may be used to identify the worst-case hazard scenarios, evaluate impacts to specific network users (e.g. specific industries or vulnerable groups), and to evaluate different hazard management strategies. It is therefore envisioned that the research outputs and framework yields value to policy makers, network users, infrastructure operators and owners, particularly within the case study area. The development of this framework was made possible and is based on three novel elements of original research conducted in this thesis:

The first is a new national landslide susceptibility model for the Scottish road network. The model uses logistic regression analysis to evaluate the geomorphological and geotechnical properties of hillslopes that are associated with decreased and increased landslide susceptibility. The model results indicate the spatial distribution of the most susceptible hillslopes in Scotland, and this is used to evaluate the landslide susceptibility of each road segment in the strategic road network.

Second, a network simulation model is developed that can be used to approximate the additional travel time and economic losses caused by network disruptions. The simulation is used to evaluate the indirect impact of disruption on the road segments identified as having a level of landslide susceptibility in Scotland. In addition to assessing the national economic loss, the model reveals the spatial distribution of impacts, or footprint, on road users according to the zones where they live, such as the additional travel time and cost per zone. These footprints show that the indirect impact of landslides is felt far beyond the hazards physical location.

Third, is a set of new landslide rain initiation thresholds. The research examines the effects of using different rain records on two techniques that are used to define landslide thresholds. The results indicate that threat score thresholds are more sensitive to changes in the rainfall record than optimal point thresholds: optimal point thresholds may therefore be of use to landslide warning systems. The thresholds are also derived using new spatio-temporally normalised rain variables and these help to account for seasonal and regional rainfall variation.

Initially, each of the research elements are used independently: to determine the terrain characteristics that are associated with increased landslide susceptibility, to identify the road segments that are highly susceptible to landslides, to calculate the indirect impact of network disruption, to identify the road segments that are critical to maintaining network serviceability, and to examine the rainfall conditions that are associated with landslide occurrence. Each

assessment is conducted at spatial resolutions relevant to the national government and organizations responsible for hazard risk management in Scotland and the wider UK.

The three elements are then combined to demonstrate a catastrophe risk model (hazard risk model). The catastrophe model includes a stochastic landslide event set of potential landslide hazards on the road network. The impact of each event is evaluated to give an exceedance probability distribution for the annual average loss due to landslides in Scotland. This framework, and its component elements, are applicable to the study of other hazard phenomena, such as severe gales or flooding, and it provides the groundwork for future investigations of landslide that consider: climate and land use change, changing travel demands, or other highway users and transport modes including public transport, emergency services and industrial freight.

1.4 Dissemination of research reported in this thesis

Two of the key elements of this research have been published in international peer reviewed journals. These are for: the development of the network model and evaluation of indirect impacts, and the development of the landslide initiation thresholds.

Postance, B., Hillier, J., Dijkstra, T. and Dixon, N. (2017b) Extending natural hazard impacts: an assessment of landslide disruptions on a national road transportation network. Environmental Research Letters. [Online] 12 (1), 14010. Available at: doi:10.1088/1748-9326/aa5555

Postance, B., Hillier, J., Dijkstra, T.A. and Dixon, N. (2017a) Comparing threshold definition techniques for rainfall induced landslides: a national assessment using radar rainfall. Earth Surface Exchanges In 'Earth Surface Processes and Landforms'. [Online] Available at: doi:10.1002/esp.4202

The research has also been the topic of several international conference papers and poster presentations including: two paper and three poster presentations at the European Geoscience Union annual meeting in 2015, 2016 and 2017; two paper poster presentations at the Royal Geographical Society annual conference; and one poster presentation at the Research Data Alliance 7th plenary meeting in Tokyo, Japan. In addition, the author has presented and discussed the practical applications of this research with stakeholders at two industry workshops hosted at the British Geological Survey and the Scottish local roads association.

Postance, B., Hillier, J., Dixon, N. and Dijkstra, T. (2015) Quantification of Road Network Vulnerability and Traffic Impacts to Regional Landslide Hazards. In: EGU General Assembly Conference Abstracts 2015

Postance, B., Hillier, J., Dijkstra, T. and Dixon, N. (2016a) Characterising regional landslide initiation thresholds in Scotland, UK using NIMROD c-band precipitation radar and the BGS National Landslide Database. In: EGU General Assembly 2016.

Postance, B., Hillier, J., Dijkstra, T. and Dixon, N. (2016b) Indirect economic impact of landslide hazards by disruption to national road transportation networks; Scotland, United Kingdom. In: EGU General Assembly 2016.

Postance, B., Hillier, J., Dijkstra, T. and Dixon, N. (2017c) Rainfall thresholds and susceptibility mapping for shallow landslides and debris flows in Scotland. In: EGU General Assembly Conference Abstracts 2017

1.5 Thesis structure

The following chapters explain the context, approach and findings of this research.

Chapter 2 provides a literature review, relating studies of landslide susceptibility, landslide initiation thresholds, indirect impact assessments, and landslide hazard and risk assessment.

Chapter 3 describes and explains the data sources and methodology used in this research.

Chapter 4 presents the results and discussion of the landslide susceptibility model developed for this research.

Chapter 5 presents the results and discussion of the traffic model and indirect impact assessments developed for this research.

Chapter 6 presents the results and discussion of the landslide initiation thresholds.

Chapter 7 presents the results and discussion of a prototype catastrophe model.

Chapter 8 provides a synthesis of the key discussions, conclusions and recommendations for further work.

Chapter 2 Literature Review

2.1 Landslides, Climate and Infrastructure: the UK perspective

2.1.1 Introduction

Section 2.1 presents a review and discussion of literature regarding landslide hazards in the United Kingdom. First, it provides a brief explanation of common landslide mechanisms. This is followed by detailed discussion for the spatio-temporal distribution and hydrogeological characteristics of past and present landslide activity in the UK. Third, a summary is provided of the key drivers and characteristics of UK climate and weather, the prospects of projected climate change in the 21st century, and the possible implications of climatic changes on landslides and slope stability. Fourth, it discusses the impact of landslides on critical infrastructure networks including evidence of direct and indirect impact of landslides and the challenges associated in quantifying them.

2.1.2 Landslides in the UK

'Landslides' is the collective term used to describe the movement of a material mass from a high to a low altitude on an inclined plane (shear surface) by gravitational force (Cruden 1991). As illustrated in Figure 2.1, landslides are classified by distinctions between movement and material types that include falls, topples, slides, spreads and flows of rock, earth or debris (Varnes 1978; Cruden & Varnes 1996). The stability of a slope, thus occurrence of a landslide (excluding falls), is determined by the ratio of resistive and driving forces, more formally, the equilibrium between the slope material shear strength and shear stress respectively (Terzaghi 1950; Cruden 1991). Shear strength is predominantly determined by the angle of slope (i.e. self weight), the internal friction coefficient and the cohesion of particles due to soil porewater pressure that influence the effective stress. The shear stress is the load from the above vertical mass per unit area. A landslide cannot occur whilst its shear strength and resistant forces due to material strength with the underlying strata is in equal proportion and opposing direction to the shearing stress driving force.

Landslides are "*the natural process of the landscape tending towards equilibrium*" Innes (1983 pg 470). Although landslides are fundamentally driven by gravity, there are many environmental, geological and anthropogenic factors that contribute to slope stability and initiate failure by increasing shear stress, decreasing shear strength or (most likely) a combination of the two. For instance, globally the majority of recorded landslides are associated to periods of prolonged and intense rainfall which causes changes to porewater pressure (Caine 1980; Iverson 2000) or by ground acceleration and liquefaction during earthquakes (Keefer 1984; Dadson *et al.* 2004; Meunier *et al.* 2008). These, and other common contributory factors are summarized in Table 2.1, which is based on comprehensive discussion (Varnes 1978; Van Asch *et al.* 1999; Leroueil 2001), and with reference to relevant supplementary material.

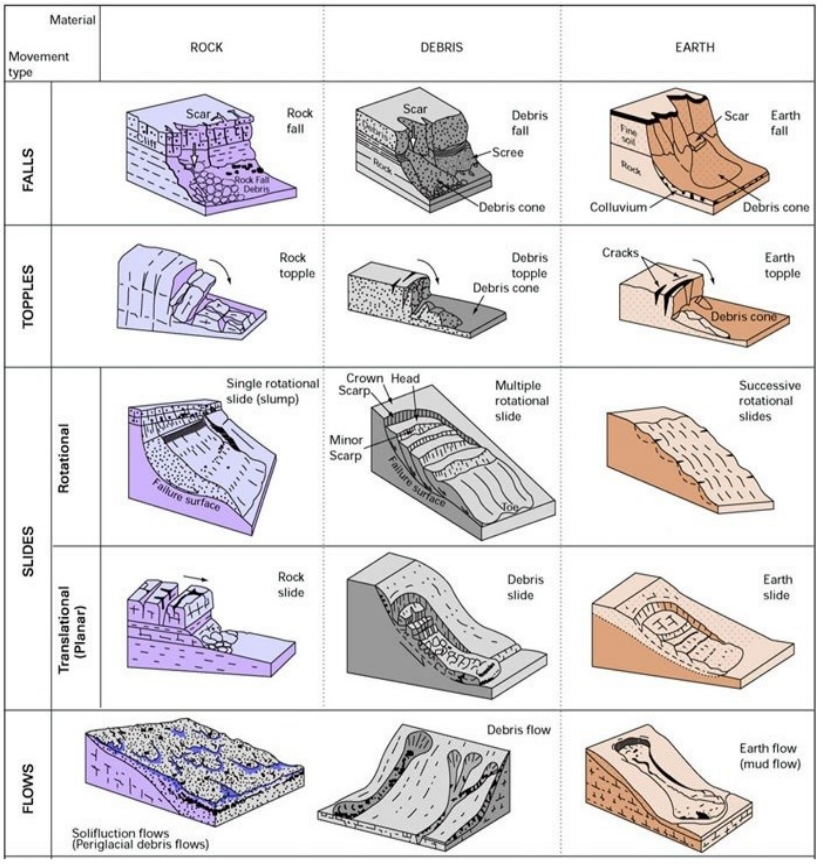

Figure 2.1. British Geological Survey landslide classifications after *Cruden and Varnes*, (1996) (BGS 2017).

	Factors contributing to increased shear stress
Erosion & Morphology	Removal of lateral and underlying support steepens the slope profile and alters hydrological pathways. This can be caused by road construction or fluvial, coastal and aeolian processes (Sidle & Ochiai 2013).
Surcharging	Increasing the slope material mass by deposition or sedimentation due to rock fall, erosion, other landslides, vegetation growth, glacial and fluvial deposition.
Seismicity	Ground acceleration reduces the cohesion and friction of soils and may cause liquefaction in saturated soils (Meunier *et al.* 2008). Increased permeability of soils due to perturbation and cracking.
Volcanic	Rock falls, tephra and other debris may interact with water or ice to form lahars. Volcanoes may also cause similar effects to those of seismic and surcharging factors.
	Factors contributing to decreased shear strength
Water Supply	Variation of soil pore-water pressure due to precipitation, surface runoff and ground water infiltration.
Weathering	Soil ratcheting and perturbation by freeze-thaw or shrink-swell cycles acts to reduce soil cohesion and friction whilst increasing surface permeability and water infiltration (Kilsby *et al.* 2009).
Vegetation & Land Use	Vegetation and land cover influences soil permeability and water infiltration. Root systems provide mechanical strength to slope materials and thus vegetation change or removal can reduce soil strength (Greenwood *et al.* 2004).

Table 2.1. Common factors associated to variations in slope shear-strength and shear-stress.

Globally, landslides are the main cause of fatalities and damage associated with storms and earthquakes in upland environments (Petley 2012; Swiss Re 2016). For example: 43 fatalities and damage on the SR530 highway by the Oso landslide Washington, US (Iverson *et al.* 2015); it has been estimated that from 2000 to 2016 landslides in Nepal have caused on average 80 fatalities per year to several thousand during catastrophic earthquake events (Petley *et al.* 2007; Grandin *et al.* 2015). Fortunately, the UK rarely suffers from large scale and catastrophic landslides, however, those that do occur often cause significant damage and disruption to infrastructure (Walsby 2007; Gibson *et al.* 2013). The most comprehensive record of UK landslide activity, with >17,000 records, is The National Landslide Database (NLDB) maintained by the British Geological Survey (e.g. Foster et al. 2008). National scale analyses of this database, supplemented with information for terrain morphology and geology, reveals the spatial distribution of the most common failure mechanisms in landslide domains (Figure 2.2A) and models of the terrain susceptibility (Figure 2.2B - C) (Foster *et al.* 2008; Dijkstra *et al.* 2014b). These indicate that approximately 10 % of the UK land area is classed of moderate or high landslide potential (Jackson 2004; Dixon *et al.* 2006).

The NLDB contains several records of large, complex and rotational landslides such as. at Trotternish, Isle of Skye (Ballantyne *et al.* 2014); Mam Tor, Derbyshire (Waltham & Dixon 2000); Crackenthorpe, Cumbria (Smedley *et al.* 2009); Leys Bend, Wales (Early & Jordant 1985) and in Southwest England and Wales (Pennington *et al.* 2014). These are often of ancient to early Holocene in origin and are reactivating failures driven by discontinuities within the underlying geology. Their spatial distribution is relatively limited as shown (blue shading) in Figure 2.2A (Forster & Culshaw 2004; Jenkins *et al.* 2011). The UK also features A large number of coastal landslides that generally occur due to the undercutting of slopes by coastal erosion processes and other phenomena, such as, storm surges and rising sea levels (Dawson *et al.* 2016b). There are varying rates of coastal erosion by location. These range in the order of 0.05 m yr^{-1} for hard crystalline rocks in the North and West, to 3 m yr^{-1} and significantly greater episodic erosion events in weak sedimentary materials in East Anglia and South England, such as chalks, glacigenic sands, gravels and tills (Lee *et al.* 2004a).

The majority (~ 53 %) of terrestrial UK landslides, and those that have the greatest impact on society, occur due to soil related processes (Dixon *et al.* 2006; Dijkstra & Dixon 2010; Mansour *et al.* 2011). The most active landslide mechanisms are: shallow translational landslides, including to debris flow in wetter upland regions (Figure 2.2B); and movements in natural or engineered slopes that contain clay soils liable to shrinkage and swelling (Figure 2.2C). The spatio-temporal distribution of these two hazards is non-uniform. They are primarily driven by the interactions between the UK's temperate maritime climate and seasonal weather conditions, the complex patchwork of bedrock and superficial lithologies, human factors, and topographic relief (Gibson *et al.* 2013; Dijkstra *et al.* 2016a). For instance, many of the ageing infrastructure embankments and cuttings were constructed using susceptible London Clay, Lias Clay and Gault Clay formations (Dijkstra & Dixon 2010; Harrison *et al.* 2012; Pritchard *et al.* 2014).

Though soil movements due to shrink-swell are not landslides, they are briefly discussed as shrink-swell can aid in the development and initiation of landslides. In addition, shrink-swell is responsible for a substantial amount of the ground related damage to buildings and infrastructure with an estimated cost £300 - 400M per year (Forster *et al.* 2006; Dijkstra & Dixon 2010). The shrink-swell volumetric changes of clay soils is driven by the seasonal soil moisture cycle and this gradually aids the development of shearing surfaces for other rotational

and translational failures (Leroueil 2001; Culshaw & Harrison 2010) and undermines engineered structures.

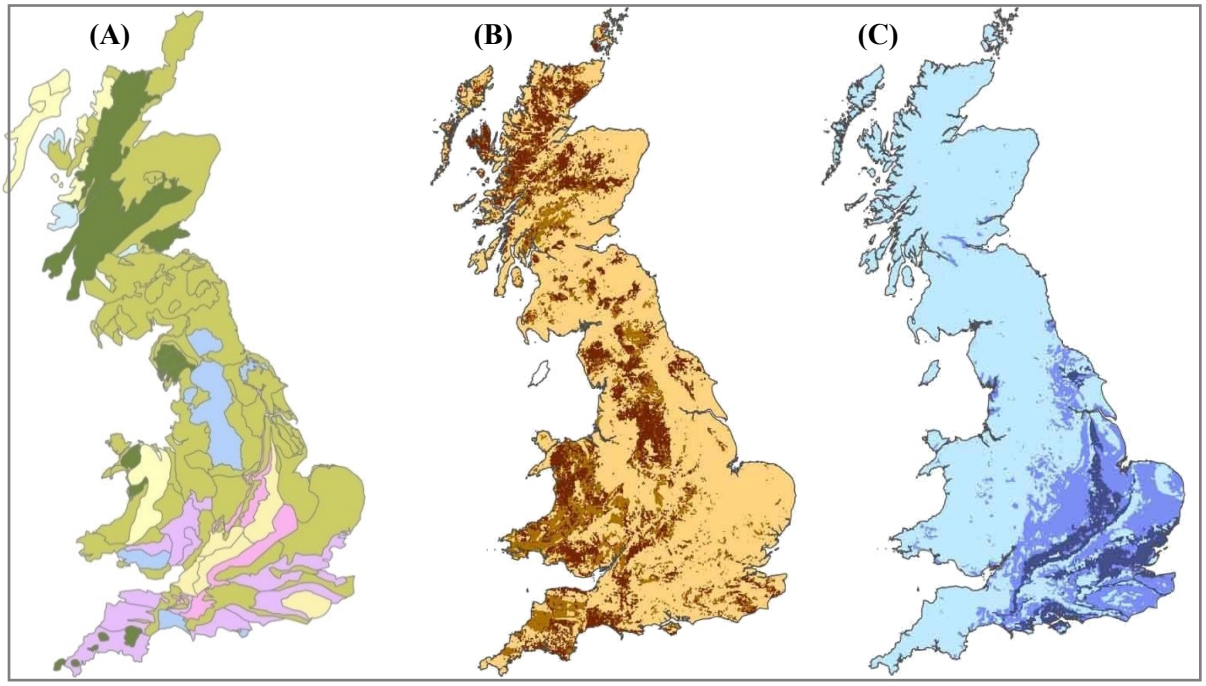

(A) Landslide domains

- Large, deep seated rotational landslides.
- Valley-side rotational and planar landslides.
- Shallow rotational and planar landslides.
- Landslides due to cambering.
- Planar slides, debris flow and rock slope failures in superficial deposits.
- Rotational landslides degrading to flows due to incompetent bedrock.
- Shallow rotational landslides with flow elements.
- Bedrock controlled landslides.

(B) Landslide susceptibility

- Low
- Moderate
- High

(C) Shrink-Swell susceptibility

- Low
- Moderate
- High

Figure 2.2. (A) Landslides domain map showing 8 groupings for broad spatial patterns in failure mechanisms and the influence of morphology and lithology after Dijkstra et al. (2014). (B-C) 3-tier landslide and shrink-swell susceptibility maps (Jackson 2004; Walsby 2008).

Platelets of susceptible clay minerals form in a layered-lattice structure with high surface area and bonded by water, such as smectite and vermiculite minerals that are common within the London, Lias and Gault clay formations of the Southeast UK (Entwisle *et al.* 2012). The interstitial space between the lattice layers expands with the influx of water (swelling), and contracts in drier conditions (shrinkage). To quantify this water content the soil moisture deficit (SMD) is the amount of water a unit of soil can uptake before reaching its 'field capacity'

(SMD = 0 mm) as the soil can no longer expand and any additional water becomes runoff (Ridley *et al.* 2004). Low SMD indicates a water surplus and this acts to reduce soil strength and increases the slope shearing stress by, for example, increasing the porewater pressure and mass of the slope material. Indeed, many recorded UK landslides are associated to low SMD conditions following antecedent and extreme precipitation sequences in winter months and storm events (Early & Jordant 1985; Waltham & Dixon 2000; G.O. Jenkins 2006; Pennington *et al.* 2014; Muchan *et al.* 2015; Petley 2015).

Slopes formed of clay materials may also be weakened by high SMD during warm and dry climatic conditions. High SMD leads to increased surface soil desiccation and drying of the soils downwards. In turn, this can lead to deeper drying of soils as roots are able to penetrate to greater depths (Glendinning *et al.* 2008). In the UK, the influence of SMD, and thus movements due to shrink-swell, is generally found within 0.5 - 1.5 m below the ground level (bgl). This corresponds well with the depths of 81 % of recorded failures on 570 km of surveyed motorway slopes (Perry 1989; Clarke & Smethurst 2010). The effects of positive SMD may also extend to greater depths of 2 - 4 m bgl during extremely warm periods and droughts (Glendinning *et al.* 2008; Clarke & Smethurst 2010; Davies *et al.* 2014; Gunn *et al.* 2015). In the summers of 2005, 2006 and 2007, extremely dry conditions led to the development of hardened, high-permeability surface soils that are believed to have contributed to several landslides in railway cuttings and embankments in low SMD conditions in the following winter months (RAIB 2008).

Illustrated by the dark green areas in Figure 2.2A, periods of prolonged and intense precipitation also trigger translational landslides and debris flows in areas with high topographic relief, such as Snowdonia, The Lake District and the Scottish Highlands (Addison 1987; Ballantyne 2002; Smedley *et al.* 2009; Petley 2015). These failures are typically initiated as planar movements in shallow permeable materials overlain on steep sided hillslopes and on gully walls, ranging between 28^{o} and 42^{o} (Innes 1983; Iverson *et al.* 1997; Wilford *et al.* 2004). The slope hydrology contributes to the rapid saturation of the slope materials, reduced effective stress and initial mobilisation that then develop into flows of dense, fine and coarse grained materials (60 – 80% by mass silt, sands, gravels, rocks and boulders) or 'slurries' (Varnes 1978; Iverson 2000; Milne *et al.* 2009). The potential velocity and volume of transported material spans several orders of magnitude from 10's mm yr^{-1} to 10's m sec^{-1} of individual boulders to hundreds of cubic meters of material (Jakob 2005; Hungr *et al.* 2014). High energy events cause significant erosion within the channels and substrates within which they flow that further increases the sediment charge, deposition and damage potential. Examples in the UK include: £53k worth of damage caused by two debris flows which deposited 820 tonnes of material on the A5 road in North Wales (Addison 1987); several large ~500 tonne debris flow depositions initiated during storm Desmond in Cumbria 2015 (Parry *et al.* 2015; Petley 2015); and at least 30 debris flow each depositing 100 - 1000 tonnes of material on the Scottish highway network and with £100 k's in engineered remediation costs in 2004, 2007, 2009, 2012 and 2015 (Milne *et al.* 2009; Pennington & Harrison 2013; Winter *et al.* 2014; Transport Scotland 2016a).

The initiation of translational slides and debris flows (hereafter 'landslides') is dependent on sufficient water infiltration into slope materials, that leads to a critical increase of porewater pressure and reduction of effective stress, so that shear strength is reduced and a landslide occurs (Crozier 1997; Iverson *et al.* 1997; Iverson 2000; Stoffel *et al.* 2014). The superficial deposits that form the slopes susceptible to landslides in the UK are listed in Table 2.2. The

materials include a wide range of rapidly-draining, loosely compacted, coarse-grained, unconsolidated materials formed and modified under various processes.

Material	Description	Typical size
Regolith	Weathering of the bedrock forms a covering layer of unconsolidated clay, silt, sand and rock fragments (gravels, cobbles, boulders).	0.01 mm - >5 m
Glacial	Unconsolidated soil mass including; clays, silt, sand, gravels, cobbles and boulders, formed during glacial (angular to rounded moraines, erratic's and till), proglacial (rounded and sorted lacustrine and fluvial), para- and post-glacial periods.	0.01 mm - > 5 m
Scree	Scree or Talus cones form on the slopes below cliffs and other exposed rock faces when angular rock fragments are dislodged by weathering (e.g. freeze-thaw).	1 mm - 1 m
Colluvium	Unconsolidated heterogeneous sediments of silt and rock fragments deposited by surface water run-off. Colluvium sedimentation acts to recharge gullies, accumulating on the channel floor and walls.	0.05 mm - 10 mm
Fluvial	Unconsolidated detrital sediments deposited by streams and rivers. Upland fluvial systems predominantly generate silt, fine sands and gravels.	0.01 mm - 3mm

Table 2.2. Description of superficial deposits, and their formation, that are susceptible to debris flows in the UK; based on descriptions in (Ballantyne 1986; McMillan & Powell 1999)

The deposits and slope materials listed in Table 2.2 are usually found in relatively shallow horizons of 0.5 to 3 m depth, but are also known to occur at up to 15 m depth within topographic depressions (Ballantyne 1986; Milne *et al.* 2009). The materials form a thin mantle of weakly structured and high permeability soils overlying hard and low-permeability substrata, such as, bedrock and layers of more cohesive and finer-grained material. These substrata provide potential shearing surfaces where slope failures can propagate. Subsequently, there are many recorded instances of landslides in uplifted and mountainous terrain where these types of conditions are prevalent and where periods of prolonged and intense rainfall are common. UK examples include: two landslides initiated following 118 mm of rain in 5 hours in North Wales (Addison 1987); three landslides initiated in Cumbria following 341 mm of rain in 24 hrs during Storm Desmond (Parry *et al.* 2015; Petley 2015); 30 landslides following 81 mm of rain in 24 hrs (peak intensities of 20 mm h^{-1}) at Glen Ogle in the Scottish highlands (Milne *et al.* 2009); and 8 landslides that occurred on days with 30 - 90 mm of rain in 2007, 2008, 2011 and 2013 on the A83 road in Argyle and Bute, also in Scotland (Winter *et al.* 2010; Winter 2014). There are similar records of landslide occurrence in other comparable mountainous regions including, in South Korea and Japan (Kim *et al.* 1991; Saito *et al.* 2010), New Zealand (Brooks *et al.* 2004; Welsh & Davies 2011), North America and Canada (Wilford *et al.* 2004; Chleborad *et al.* 2008; Staley *et al.* 2013) and Europe (De Vita *et al.* 1998; Meyer *et al.* 2012; Segoni *et al.* 2014b).

Even in such well-drained soils as discussed above, the antecedent soil moisture conditions can act to raise or reduce the short-term water supply required to reach critical effective stress so that a landslide occurs (Stoffel *et al.* 2014). The antecedent soil water conditions are determined by longer term (i.e. > 24 hours) to seasonal precipitation regimes. The characteristics of this relationship depend on the rate of interaction between the weather and climatic conditions of a region and the hydrology, geomorphology and geotechnical properties of the slope materials. For example, in Scotland, Winter *et al.* (2010) notes that the occurrence of 16 large debris flows were characterised by significant rates of rain accumulation in the 12-day antecedent period prior to failure. Conversely, landslides that occur in finer grained materials and in the Mediterranean climate of Emilia-Romagna, Italy are associated with a shorter, 3-day antecedent rain accumulation period (Berti *et al.* 2012). Globally, the rainfall antecedence periods associated with landslide occurrence are in the range of 2 to 35 days (Guzzetti *et al.* 2008). It is therefore important to regionally constrain assessments of the short and long-term rainfall patterns that lead to landslides to within areas where there is with a high degree of homogeneity in the factors that control the water content of slope materials, such as, weather and climate, terrain, and soil lithology.

It may also be important to consider other water sources on slopes. In high elevations and latitudes, snowmelt and drainage from water bearing peat soils has the potential to influence the slope material antecedent water conditions (Milne *et al.* 2009; Meyer *et al.* 2012). Catchment hydrology is another important factor. Translational landslides and debris flow form almost exclusively within existing hydrological units, including as slides and flows initiated on hillslopes and within existing fluvial channels or gullies (Iverson *et al.* 1997; Ballantyne 2002; Hungr *et al.* 2014): these forms are transitional as hillslope flows often propagate into gullies and those initiated in gullies often encroach on open ground and hillslopes (Ballantyne 1986; Iverson *et al.* 1997; Wilford *et al.* 2004). The geomorphology of these hydrological units, including their geometry, elevation and aspect, influence soil moisture content by channelling surface water flows and determining the slope exposure to incoming precipitation and solar radiation (Wilford *et al.* 2004; Van Westen *et al.* 2006; Dijkstra & Dixon 2010). Slope geomorphology also influences the rate of erosional processes, such as, aspect related weathering by inbound rain and freeze-thaw. Increased rates of erosion acts to supply or 'recharge' failure conduits with failure susceptible materials (Bovis & Jakob 1999; Jakob *et al.* 2005). In Scotland, radiocarbon and lichenometric dating of buried landslide deposits suggest that slope recharge intervals are in the order of 2 - 10 years to several decades over the past 7,000 years (Ballantyne 2002). Erosion can also disrupt or dam existing drainage pathways leading to an increase in the water content of slope materials (Bovis & Dagg 1992; Lane *et al.* 2007).

2.1.3 Weather and Climate

Despite its relatively high latitude (40–60^{o}N), the UK has a temperate maritime climate characterised by warm summers and mild winters, Cfc-Cfb in Köppen climate classifications (Met Office 2017). UK climate is moderated by the heat capacity of the Atlantic Ocean, specifically the Gulf Stream or North Atlantic Oscillation (NAO) of warm surface waters (7-22^{o} C) and moisture laden tropical air mass flowing North Westerly between the Azores High and Icelandic Low. As illustrated in Figure 2.3C, the effect to long term annual average rainfall patterns (1961-1990) is for a decreasing west to east precipitation gradient but this is also influenced by orographic affects in upland areas (Wilby *et al.* 1997). The annual average

temperature is also influenced by terrain elevation, but follows a decreasing south to north gradient due to reducing solar insolation at higher latitudes (Figure 2.3B). Short term weather patterns are highly variable. In addition to NAO, the UK is also situated at the polar front or path of the polar jet stream where low-pressure, cyclonic and frontal systems are common due to exchanges between several air masses, including the polar, returning polar, arctic and tropical maritime air masses and the polar and tropical continental. For example, Figure 2.3C shows the December 2015 precipitation anomaly for parts of England, Scotland and Wales were 125 – 300 % of the long term average (1981 - 2010) and this occurred following repeated cyclonic systems, such as the December storms Desmond 5th, Eva 24th and Frank 29th (McCarthy *et al.* 2016). There is also some evidence to suggest a trend of increased winter cyclone intensity 1871 – 2012, but this may be attributed improved data quality (Matthews *et al.* 2016). Oscillations in the polar jet stream can block cyclonic systems, leading to periods of calm, high-pressure, anticyclonic conditions typically lasting last 2-5 days. Prolonged blocking periods of up to several weeks are associated to summer droughts and severe winter cold spells, such as in the 2010 European heat wave (Francis & Vavrus 2012).

The 2009 UK climate projections (UKCP09) represent the current state-of-the art assessment of future climate change in the UK for the 21st century (Jones *et al.* 2009; Murphy *et al.* 2010). The projections are probabilistic assessments given by the cumulative distribution function and reported at 0.1, 0.5 and 0.9 probability levels (p) of climatic changes relative to the 1961-1990 baseline period. UKCP09 projections are reported for 30-yr overlapping periods ranging 2010-2039 to 2070-2099 and for low, medium and high emissions scenarios. The emissions scenarios are equivalent to the former Intergovernmental Panel on Climate Change (IPCC) B1, A1B and A1F1 emissions scenarios (Nakicenovic & Swart 2000).

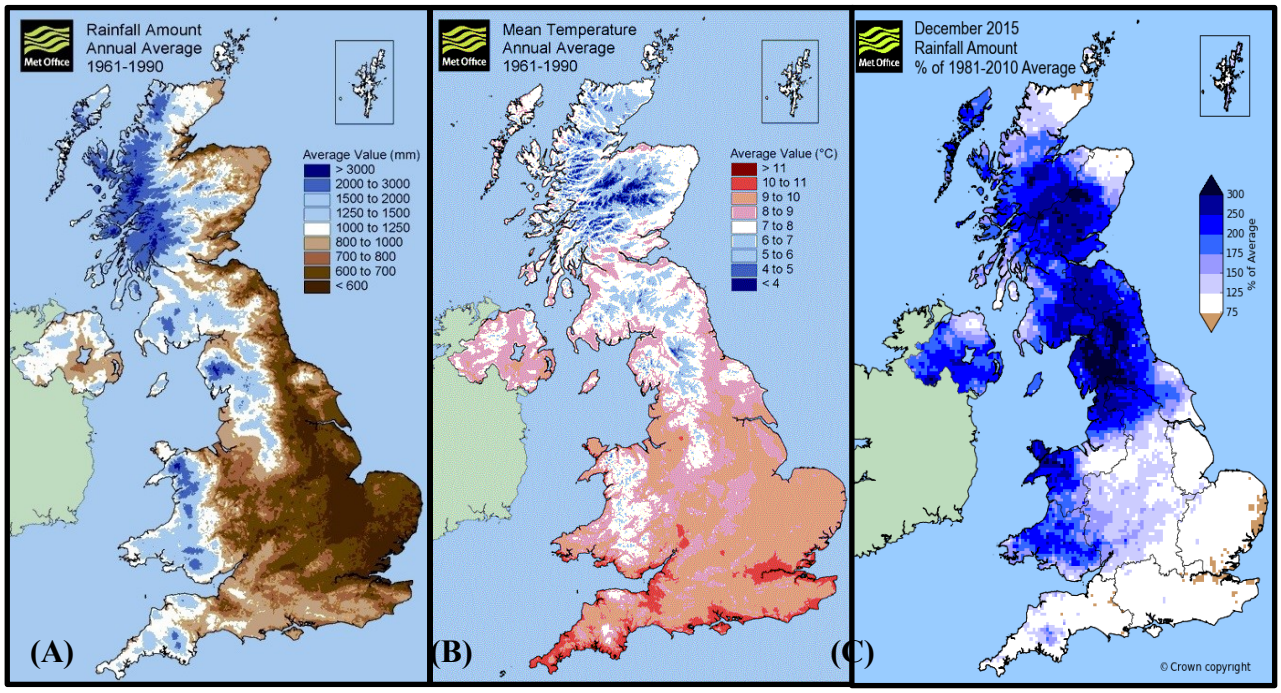

Figure 2.3. Climate and weather summaries for the UK: **(A)** annual average rainfall (mm) 1961-1990, **(B)** annual average daily temperature (°C) 1961-1990, and **(C)** December 2015 rainfall amount in % of the 1981-2010 averaging period. Figures are available (Met Office 2017).

The following discussion is of the UKCP09 projections for the 2050 period (2040-2069) under the medium emissions scenario. Mean annual precipitation shows relatively little change ±2 % ($p = 0.5$) or spatial variation across the UK (ranging -10 % to +10 % for the $p0.5$ and $p0.9$ levels, respectively). Seasonal changes are marked. In winter, mean precipitation change is +12 to +17 % across the western parts of the UK (+2 to +38 %) and +11 to +14 % in the east (+1 to +36 %). In summer, mean precipitation change is -17 to -20 % (-42 to +7 %) in the south of England, midlands and -11 to -15 % (-30 to +2 %) in Scotland. The seasonal mean temperature change is +1.6 to +2.2ºC in winter (0.7 to 3.4ºC) and +2.0 to +2.8ºC in summer (+0.9 to +4.6ºC). The spatial distribution of winter and summer temperature change is greatest in the south and reflects the decreasing south-north latitudinal temperature gradient (Figure 2.3B). UKCP09 also projects changes to the magnitude of extreme rainfall events, using the 99th centile of precipitation on the wettest day, and an indicator of prolonged heavy rainfall events by the number of days with rain > 25 mm. In winter, the magnitude of extreme rain is ±5 to +10 % across the UK (-10 to +30 %) and days with heavy rain are set to increase by a factor of 2 to 3.5. In summer, the number of days with heavy rain is set to increase by a factor of 1 to 2. The central estimate for extreme rain magnitude change is -5 to -10 % across the south of England. However, the 0.1 and 0.9 probability levels exhibit far greater spatial variability in extreme rain magnitude change with -30 % in the south of England and +30 % in upland parts of Wales and West Scotland.

The UK's projected climatic changes in seasonal and extreme weather conditions are likely to cause significant, but varying impacts on slope stability (Dijkstra & Dixon 2010). The combination of warmer, drier summers with wetter winters could intensify fluctuations in the seasonal soil moisture cycle, increasing shrink-swell movements in susceptible soils and the likelihood of progressive failures in natural and engineered slopes (Clarke & Smethurst 2010). Moreover, highly desiccated soils have higher permeabilities and may be more susceptible to rapid water infiltration and mobilisation during increased frequency and high magnitude precipitation events (Hughes *et al.* 2009; Kilsby *et al.* 2009; Kendon *et al.* 2014). Conversely, higher temperatures could increase evapotranspiration and high SMD conditions resulting in drier, more stable slopes due to decreased (Rouainia *et al.* 2009). The projected increase in prolonged and high magnitude precipitation events could likely generate more frequent low SMD conditions and increased rates of overland flow in unconsolidated upland soils, that are linked to landslide initiation (Ballantyne 2002; Milne *et al.* 2009). In addition, more extreme and frequent periods of heavy rainfall could exacerbate erosion rates increasing the sedimentation yield, inundation and recharge of upland fluvial systems and on hillslopes (Lane *et al.* 2007; Whitehead *et al.* 2009). This has the potential to increase the frequency of landslide failures by, for example, blocking drainage pathways and reducing the failure material recharge intervals of susceptible slopes (Bovis & Jakob 1999; Jakob *et al.* 2005).

In order to effectively manage and reduce slope instability and landslide risk requires a sound knowledge of landslide processes in their current environmental setting and under the potential effects of climate change (Dijkstra & Dixon 2010). However, there is limited understanding and modelling capability to evaluate long term hydrogeological processes and their influence on slope stability (Beven 2002). The current state-of-the-art includes: improving stakeholder communication and multi-disciplinary research networks, such as CLIFFS (Dixon *et al.* 2006) and BIONICS (Kilsby *et al.* 2009); developing full scale physical and numerical models of slope stability (Malet *et al.* 2005; Kilsby *et al.* 2009; Rouainia *et al.* 2009; Davies *et al.* 2014)

and, for shallow translational slides and debris flow, empirical investigations of past events to identify the most common failure conditions and to develop probabilistic hazard assessments (Guzzetti *et al.* 2005; Chleborad *et al.* 2006; Berti *et al.* 2012; Budimir *et al.* 2015; Rossi *et al.* 2017). However, assessments for the long term stability of slopes in the context of climate change are still of limited use as there remains a great level of aleatory uncertainty for future weather and climatic conditions (Jenkins *et al.* 2009; Murphy *et al.* 2010) and therefore for the actual physical response slope mechanisms (Dijkstra & Dixon 2010). In order to alleviate some of this uncertainty, it is suggested that landslide occurrence should be evaluated in a broader range of contexts, such as evaluating impacts to business, tourism and indirect impacts to transport, to more effectively communicate the spatio-temporal distribution and forecast severity of these hazards (Dijkstra *et al.* 2014a). Such assessments would also address a further limitation to effective landslide risk management which is associated to the need to further characterize vulnerability and exposure by improved understanding for the ways in which these hazards interact and cause impacts on transport infrastructure (Glade *et al.* 2005).

2.1.4 The Road Transport Network

Each year in the UK (England, Scotland and Wales) an estimated 440 billion road vehicle miles are driven and by volume road transportation accounts for 65% of all freight and 90% of commuter and passenger journeys (DFT 2013a). The strategic road network (SRN, motorways and significant arterial roads 'A-roads') forms just 2% (6,000km) of the nation's roads, yet includes the nation's busiest road sections and is used in two thirds of all freight and one third of all passenger journeys made by road (DFT 2013b, 2015a). The SRN is managed by the respective agencies of central government (i.e. Highways England, Transport Scotland and the Welsh Assembly). The remainder of road journeys are made on 394,000 km (98%) of local road network (LRN, connecting rural and urban roads) managed at the regional level by county council authorities (DFT 2013b).

At an estimated value of £99 billion, the road network is the UK's most valuable public asset (Cook 2011). Maintaining serviceability of this network is of critical importance to UK economic growth and for the provision of essential services to maintain social-welfare standards. 'The Transport Study' by Eddington (2006), estimated the annual economic cost of road maintenance, delay and congestion is approximately £8-12 billion, and projected to reach £22-25 billion by 2021. Only a small proportion of this figure is apportioned to annual road maintenance activities (planned upgrades and repair budgets), which averaged £1.1 billion per annum in the period 2012-2015 (DFT 2012), but that vary year-on-year and between regions due to the damaging weather phenomena (Butcher 2016). These weather phenomena also contribute to an increasing cost of travel delay and congestion by deteriorating road travel conditions, including, by surface ice and rain (Jaroszweski *et al.* 2010; Hooper *et al.* 2014), or by causing delays at weather related road traffic incidents and responsive repair works (Bourne *et al.* 2008; Notley *et al.* 2008). Though the cost of individual incidents vary, the combined influence during recent winter weather seasons is apparent by the low spikes in the 2010-2015 SRN journey reliability estimates in Figure 2.4; here, the reliability measure is the monthly percentage of 'on time' journeys based on a month-by-month comparison of road segment travel times and at similar times of day (DFT 2015a).

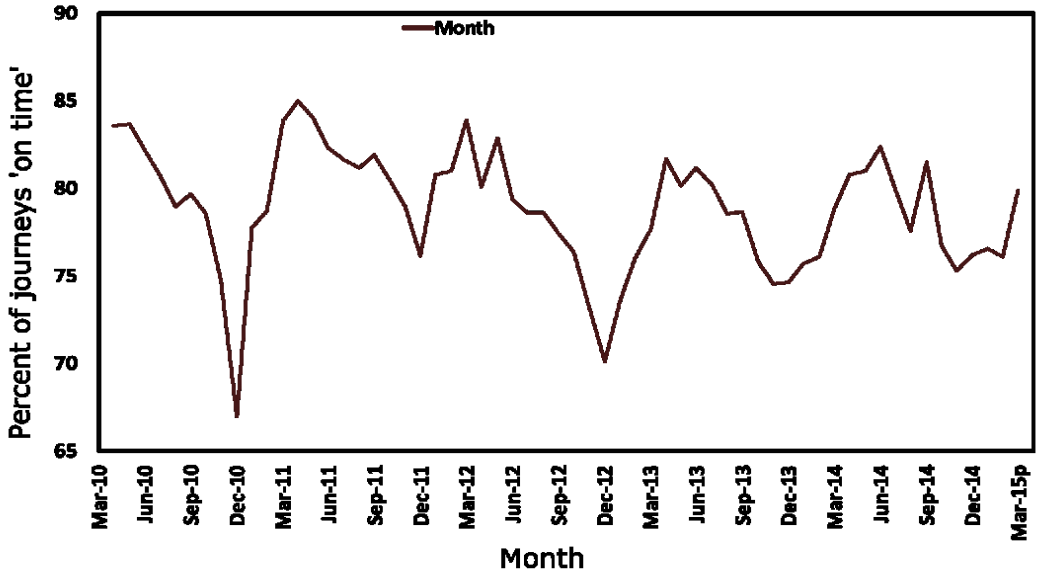

Figure 2.4. The percentage of journey's on time on the UK SRN March 2010 to March 2015, after (DFT 2015a).

At the level of the SRN (i.e. motorways and arterial roads), the consensus is that the issue of travel delay and congestion is not related to insufficient network connectivity (i.e. roads are available to and from most places). Rather, it is the case that given the current level of transport demand the SRN lacks the resilience and spare capacity to offset negative effects during periods of disturbance by regularly occurring or rare hazard phenomena (Eddington 2006; Glaister & Graham 2006; Banks *et al.* 2007; Levinson 2010; Cook 2011). It is foreseeable that these issues will be exacerbated in the future. The UK Department for Transport (DFT) National Transport Model (NTM) range of road transport demand forecasts indicate a 19 to 55 % increase in the nationwide road transport demand for the period 2010 to 2040. This forecast translates to increases of 19 to 60 % on the SRN and 10 to 50 % on local road network (DFT 2015b). Within this timescale, UK climate projections (median estimate for the 2050 period; see section 2.1.3) indicate that there is also likely to be an increase in the intensity and frequency of adverse weather, including, 10 – 20 % wetter winters, and a 2 - 3 factor increase in high magnitude precipitation events (Murphy *et al.* 2009, Kendon *et al.* 2014). Consequently, the impacts and economic losses due to road network disruptions are likely to be increased in the future and the economic argument for pro-active intervention is well defined (Stern 2006).

It is therefore essential that governments and network operators assign sufficient resources to address these future challenges. National guidelines for the management of highways state that the network segments and locations that support and maintain serviceability of the network, termed 'critical links', should be identified (DFT 2014b). The critical segments are defined as "*the road segments or assets that are essential for supporting the social and business needs of both the local and national economy. They will have a high consequence of failure, but not necessarily a high likelihood of failure*" (HMEP 2012). To improve the resilience of the road network to landslides (and other hazards), a pertinent question is therefore, at which locations in the network are landslide events least or most likely to occur? and what is the potential impact to traffic of these events? Similar themes were identified as a key priority in the recent

2017 UK Climate Change Risk Assessment and this included issues faced by other hazards and on infrastructures such as flooding and rail networks (Krebs 2017).

2.1.5 Landslide Impacts on Transport Infrastructure

Landslide hazards pose a significant threat to the UK's transport infrastructure (Forster & Culshaw 2004; Dijkstra & Dixon 2010; Krebs 2017). Approximately 7 % of the strategic networks (i.e. mainline rail, motorways and arterial roads) are located within areas considered to be of moderate to high landslide and shrink-swell susceptibility (Dijkstra & Dixon 2010). These networks traverse natural environments with factors associated to increased slope instability, such as on steep slopes and in valleys, and their foundations are typically found at depths of 1 - 2m bgl, depths associated to most recorded ground movements. In addition, these networks are often co-located with the conduits of other critical infrastructures, including water (0.5 - 1 m bgl), power (adjacent pylons or cables at 0.4 – 1 m bgl) and gas (0.3 - 0.9 m bgl) (HSE 2014). This physical coupling can generate compounded impacts and complex cascading failures which propagate between the interconnected systems (Little 2002; Dueñas-Osorio & Vemuru 2009).

The impact of landslides on transport networks can be categorised to two groups, 'direct' physical impacts and 'indirect' impacts that deteriorate travel conditions. But these impacts can also incur secondary impacts and broader socio-economic consequences such as disruptions to emergency responders and other public services, reducing levels of tourism, reducing business investment and employment.

First, landslides cause direct physical damage to engineered structures that require engineered remediation at a cost to transport network owners and operators. On average, some 50 landslide failures occur on UK railways each year (Loveridge *et al.* 2010). Network Rail (NR) is responsible for maintaining the entire 16,000 km rail network and spends in excess of £80M/pa on geohazards related activities (RAIB 2008). This figure includes ongoing damage and maintenance costs at problematic sites, such as, £800 k to £5M per year in engineered solutions to stabilise the South West line at Dawlish (Dawson *et al.* 2016a), and mitigating the effects of ageing railway slopes that are becoming increasingly susceptible to failure, inducing £5M at the Harbury landslide (Rail Engineer 2015). Ageing railway slopes are a significant issue as many embankments and cuttings were crudely constructed during the early 19th and 20th centuries using local earth or industrial by-product materials, including clay rich soils and high permeability ash (Skempton 1996; O'Brien 2007). For roads, the Department For Transport (DFT) budgets £700M per year maintaining the strategic road network (10,500 km) and a further £3.3 billion per year is distributed between 154 local authorities to maintain the rest of road the network (134,000 km of secondary to unclassified urban and rural roads) (PAC 2014; Butcher 2016). As the roads are managed by several different authorities the national cost attributed to landslide damage is unknown. The cost of individual incidents are demonstrated by the following examples: in 2013-14 severe winter weather led to 12 landslides damaging several SRN and local roads in Gloucestershire and the direct damages of £15M, equivalent to the county's entire annual road maintenance budget (GCC & Amey Ltd 2014); in 2004 £1.1M in direct damage was caused by a large debris flow on the A83 road in Scotland (Winter *et al.* 2014); and in the period 2010 to 2014 an additional £1 billion was distributed by the UK government to pay for the repair of damage to local roads caused by numerous cases of

subsidence and landslide damage to roads but also widespread flooding following several severe storms (PAC 2014).

Second are the 'indirect' impacts. These include charges collected from network operators failing to maintain network serviceability. For instance, the UK's rail network operator, NR, and rolling stock franchisees are subject to a statutory system of financial penalties, up to 10 % of their annual turnover, for the delay and cancellation of services (RailwaysAct 1993). This is levied to provide rail users with compensation (e.g. replacement bus services and ticket refunds), and each minute of delay costs rail operators an average of £70 (NAO 2008; ORR 2015). Analyses combining these values with rail delay data indicate that the cost of indirect disruption on the Dawlish-Teignmouth section of the Southwest main line are in the order of £270 k per annum for the period 1997-2009 (Dawson *et al.* 2016a). Applying this same technique, £70 k of indirect disruption is attributable to a single storm event in June 2012 that according to Jaroszweski *et al* (2015) caused 10,000 minutes of rail disruption. Such pricing schemes are not currently applied on UK road networks though this may change in coming decades as Transport-as-a-Service systems become more prevalent, such as shared vehicles autonomous transport services (Burns 2013).

Indirect impacts also include those related to functioning of the network from the aspect of different road user groups. For instance, emergency responders require access to all network locations and within mandatory response times, in particular to vulnerable populations such as the elderly (Chang & Nojima 2001; Nyberg & Johansson 2013). Travel disruption also generates impacts via macroeconomic factors, for example, varying the rates of business investment and tourism to affected areas, but these are not considered in this thesis. Two thirds of UK road traffic is for commuting, business and social purposes (Cook 2011). For each of these user groups, travel time is intrinsically linked to several microeconomic factors. To illustrate the economic importance of efficient travel time, Eddington (2006) notes that just a 5 % reduction to UK business trip travel times would alone generate annual savings in the order of £2.5 billion, equivalent to 0.25 % of UK GDP. The economic factors closely related to travel time are collectively termed the user generalised-cost and account for the travel expenses associated to: the cost of owing, running and maintaining a vehicle; and values of time spent working, non-working and socialising (MacLeod *et al.* 2005; DFT 2014a; Winter *et al.* 2014). As a result, indirect impacts can generate significant financial losses and population exposure is distributed far beyond the hazard's physical location. The severity and spatial extent of travel time delays, and economic losses as a function of generalised-cost, vary according to which network links are physically disrupted and by the level of user demand (Murray *et al.* 2008). Table 2.3 lists the indirect impact of several landslide hazard events that have been calculated by combining traffic counts and detour lengths with values of user generalised-cost.

Disruption Event	Direct Impact	Indirect Impact (total and currency)	Reference
Per lane closure on UK motorways	n/a	£10-15 k hr^{-1} (GBP)	(Lords Hansard 2007)
Per lane closure on M25 (London Ring Road)	n/a	£62 k hr^{-1} (GBP)	(Cook 2011)
M1 motorway closed for 40 hours due to a severe storm in June 2007 (Junction 31 to 34).	n/a	£58 k hr^{-1} (£2,300 k GBP)	(Chatterton *et al.* 2011; Dawson *et al.* 2016b)
A83 Rest and Be Thankful in Scotland was closed for 15 days due to landslides in October, 2007.	£1,100k	£49-80 k day^{-1} (£735-1,200 k GBP)	(Winter *et al.* 2014; Postance *et al.* 2017b)
A371 closed at Ansford rail bridge for 24 weeks of subsidence repairs in September 2012.	n/a	£1-4M loss for local haulage companies (GBP).	(Lords Hansard 2013)
US route 50 in California closed for 4 weeks due to 267k m^3 landslide deposition in January 1997.	$4,500 k	$1,000 k day^{-1} (USD)	(Reid & Lahusen 1998)
US Interstate Highway 10 closed after the Los Angeles North ridge earthquake, 1994	n/a	$1,000 k day^{-1} (USD)	(Yee *et al.* 1996)
State Highway 1 (Desert Road), New Zealand.	n/a	$8 k hr^{-1} (NZD)	(Dalziell & Nicholson 2001)

Table 2.3. Direct and indirect impacts of road network disruptions reported in the UK, US and New Zealand.

The examples in Table 2.3 clearly indicate that both the indirect impact of landslides on transportation networks contribute a significant proportion to total landslide risk (Glade *et al.* 2005). Despite this, relatively little research has been conducted on assessing the indirect impacts of landslides on national scale road networks. This is primarily since quantifying the additional travel at such scales time is a complex task. Whilst there is reasonably detailed empirical data for rail delays (e.g. Dawson, D. et al. 2016), this is not the case for road transport where traffic flows are the result of complex interactions between the topology of networks and the spatio-temporally varying levels of travel demand (Ortuzar & Willumsen 2011). State-of-the-art methods are adapted from industry techniques for road transport investment appraisal (DFT 2014a) and these couple models of network traffic flow with values of user generalised-cost of time: a critical review of these techniques is presented in Chapter 2.3. Limiting factors to the wider adoption of these models include their high computational requirements and the numerous ways in which landslide disruptions are manifest on large scale transport networks. In this thesis, research and analyses are conducted that seek to overcome these limitations.

2.2 Landslide hazard and risk analysis

2.2.1 Introduction

Section 2.2 presents a critical literature review regarding landslide hazard and risk assessment. The section is focussed on the different methods of landslide hazard assessment including the use of process based models and empirical methods for: landslide susceptibility, landslide initiation thresholds, empirical landslide hazard assessment and its application on infrastructure networks. Lastly, the components of a typical hazard risk assessment are introduced and discussed in relation to landslides.

2.2.2 Physically-based-models

Physically-Based-Models (PBM) are geotechnical and process-based models which analyse slope stability based on the Factor-Of-Safety (FoS) within morphologically meaningful units. The FoS is the ratio of a slope materials shear strength (e.g. internal cohesion, friction or other factors pertaining to shear resistance) to shear stress (e.g. modified by changing porewater pressures), with failure occurring at FoS $\leq$ 1.0 and increasing stability FoS > 1.0 (Duncan 1996). PBM are used to simulate FoS under various input conditions, such as different rainfall intensities or temperatures, by combining slope stability models with hydrological models of unsaturated and groundwater flow to iteratively calculate the porewater conditions throughout the slope.

PBM are constructed using detailed information for: the slopes geometry; shearing surface; material internal friction coefficient, material cohesion, the porewater pressure conditions; modifications to porewater by surface or ground water flow; vegetation; incoming precipitation and solar radiation amongst others. Models are calibrated using measurements of past movements in relation to variations in the input parameters. Probabilistic assessments of future slope stability are based upon the likelihood and return period of changes to these the input parameters. Approaches range from relatively simplistic 1-Dimensional infinite slope models of resistive and driving forces shown in Figure 2.5A (e.g. Brooks et al. 2004), to complex, temporally dynamic and spatially discretised 2D and 3D models in Figure 2.5B and Figure 2.5C (e.g. Hungr 1987, Anderson and Howes 1988).

One of the main advantages of PBM is that these models explicitly consider the hydro-geological parameters, physical processes and their interactions that control the stability of slopes. Although PBM are site-specific and deterministic by design, in general the processes can apply to larger areas which exhibit a degree of homogeneity for slope morphological, lithological and meteorological conditions (Dijkstra & Dixon 2010). For example, Brooks *et al* (2004) apply this rationale using a 2D PBM to determine precipitation initiation thresholds for shallow translational landslides in New Zealand: the PDM modelled the stability of high permeability colluvium and regolith assemblages 1 - 3 m in depth and on 34^{o} slopes. The PBM identified rain intensity thresholds in the order of 5 to 15 mm hr^{-1} over 24 hour periods with greater intensities required in deeper soils.

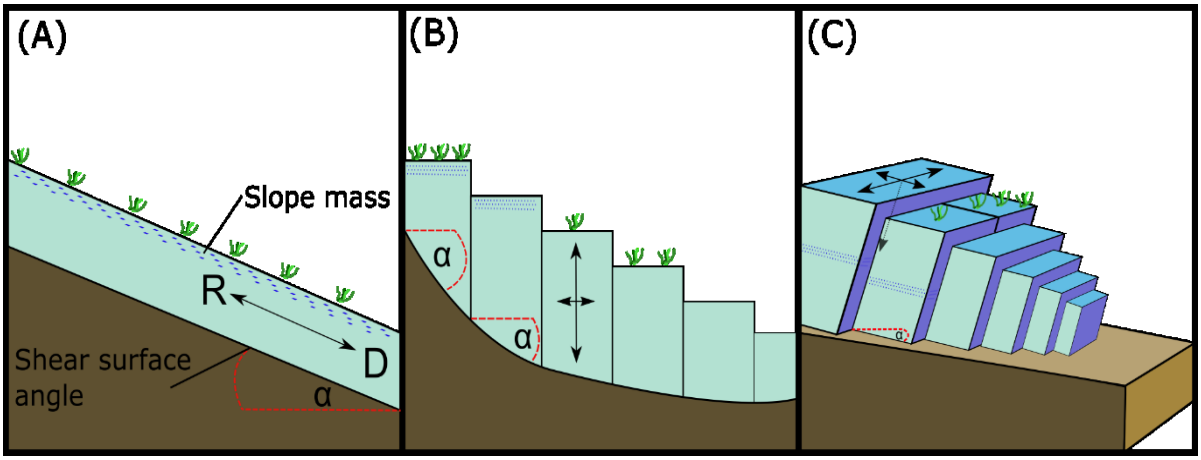

Figure 2.5. Different physically-based-models for slope stability assessment including arrows to indicate the direction in which resistive (R) and driving (D) forces are modelled in addition to α for slope angle, soil saturation (blue dots) and vegetation (green lines). (A) is a representation of a 1D infinite slope model with uniform parameters for the entire slope, whilst (B) and (C) temporally and spatially discretized 2 and 3D models with different parameter values in each model unit (blue boxes).

Another advantage is that PBM facilitate simulations to explore the specific slope conditions that led to historic failures or to explore the range of ultimate limit states (Davies *et al.* 2014). For example, a 2D PBM was used to examine the effect of climate change scenarios in southeast England by applying 20-year weather sequences (i.e. UKCP09 projections) to diagnostic London-Lias clay embankment model (Kovacevic *et al.* 2001; Davies *et al.* 2008; Rouainia *et al.* 2009). Each of these studies showed that the seasonal porewater pressure variation increased under climate change (60 to 100 kPa) and this led to the softening and displacement of the slope toe. These models also indicated that applied scenario of climate change did not lead increased rates of progressive slope failure, although there is now some evidence to the contrary in ongoing and unpublished research by the same authors.

The advantages of PBM are also directly linked to several of their limitations. Primarily, the use of PBM is limited due to their detailed data requirements. Sufficient data are generally only availably following resource intensive subsurface exploration and rigorous laboratory testing on a site-by-site basis, for example, to determine the location of shear surfaces and the physio-chemical properties of the slope materials (Van Asch *et al.* 1999; Glade *et al.* 2005). Many of the parameters are hard to determine, initial porewater pressure distributions are largely unknown and historical observation data is typically of insufficient quality to permit reliable model calibration due to unknown changes, such as, vegetation cover and weather conditions (Frattini *et al.* 2009). Even so, within the PBM these parameters are represented as area-averaged values whereas in reality there may be a high degree of spatial heterogeneity (Malet *et al.* 2005).

PBM are also limited by the level of understanding and modelling capability for physical slope processes and boundary conditions (Beven 2002) and developing representative sequences model inputs, such as sequences of future weather (e.g. Jones et al. 2009). These limitations

and the selection of input parameters can lead to contrasting evaluations for the stability of a slope. For example, Nyambayo *et al* (2004) also evaluated the stability clay embankments in southeast England, however using three conditions of soil permeability and water infiltration, including low ($1 \times 10^{-9} m/s$), medium ($1 \times 10^{-8} m/s$), and high ($1 \times 10^{-7}\, m/s$), to account for different surface desiccation scenarios under climate change. The high permeability condition ultimately led to the development of progressive failure mechanisms in contrast to the initial results of comparable studies (Kovacevic *et al.* 2001; Davies *et al.* 2008; Rouainia *et al.* 2009). In other similar studies using PBM, including vegetation cover was found to mediate the slope weakening effect of these climatic change scenarios (O'Brien 2007; Tsiampousi *et al.* 2016).

2.2.3 Empirical Models

To address and reduce landslide hazard risk, requires improved understanding of how landslides are distributed in space and in time. Establishing accurate distributions within areas covering tens to hundreds of square kilometres is non-trivial. As such, empirical assessments rarely involve the direct assessment of stress conditions as used in PBM. Instead they are based on analyses of the spatio-temporal distribution landslide occurrences and of explanatory variables that are of theoretical significance. These analyses are heuristic, statistical or probabilistic assessments conducted at different spatial scales (e.g. catchment, regional and global) to identify the conditions associated with past landslide events (Aleotti & Chowdhury 1999; Glade *et al.* 2005; Van Westen *et al.* 2006). Empirical landslide assessments are therefore based on the principle of uniformitarianism and the assumption that future landslides are likely to occur under similar conditions as those that occurred in the past (Varnes 1984). Provided that ongoing and accurate landslide records are kept, these empirical assessments provide meaningful insights on the landslide potential in the past, present and the near future (Chleborad *et al.* 2008).

Empirical landslide assessments may incorporate the spatial, temporal or combined spatio-temporal likelihood of landslides. To evaluate where a landslide might occur, the spatial component is addressed using terrain landslide susceptibility models. These models examine the geomorphological, geotechnical and environmental explanatory variables associated with landslides, such as, critical slope angles, slope aspect, vegetation and land use (Brabb 1984; Ayalew & Yamagishi 2005; Budimir *et al.* 2015). These models are generally constructed using geographic information systems and digital elevation models (Carrara *et al.* 1995; Dai & Lee 2001; Carrara & Pike 2008; Shahabi & Hashim 2015). To evaluate when a landslide might occur, the timing component of landslides is addressed using either: the recurrence interval between historic landslide events, such as using the Poisson or Binomial probability distributions (Crovelli 2000; Guzzetti *et al.* 2005); or through landslide initiation thresholds. These thresholds quantify the of hydro-meteorological conditions that, when exceeded, are likely to result in landslide initiation (Caine 1980; Chleborad *et al.* 2006; Guzzetti *et al.* 2008; Meyer *et al.* 2012; Segoni *et al.* 2014b).

2.2.4 Landslide Susceptibility

Landslides tend to occur in certain types of locations (Hungr *et al.* 2014). Landslide susceptibility models (e.g. in Figure 2.2B-C) calculate the spatial propensity or proneness of landslides to occur in a certain location (Brabb 1984; Aleotti & Chowdhury 1999; Ayalew &

Yamagishi 2005; Guzzetti *et al.* 2006). Alone, without the timing element, they do not show the number or annual probability of landslide occurrence as is done in landslide hazard models (Fell *et al.* 2008).

Landslide susceptibility assumes that the spatial distribution of landslides is not random but is determined by the distribution of one or more explanatory variables (Van Westen *et al.* 2003; Glade *et al.* 2005). The models are constructed by ranking each unit area based on a best fitting function that describes the relationship between the values of the explanatory variables and the presence or absence of landslides (Brabb 1984; Aleotti & Chowdhury 1999; Guzzetti *et al.* 1999; Dai & Lee 2001; Fell *et al.* 2008; Budimir *et al.* 2015). A large number of landslide susceptibility studies have been conducted in different landslide prone regions around the world and for different types of landslides. Subsequently, the literature includes a variety of methods, unit scales, and explanatory variables that are more or less applicable in different situations. The selection of appropriate analysis techniques depends on: the type of landslide phenomena to be studied; the scale of the investigation; the availability and suitability of analysis tools; and the type, quality, resolution and availability of data (Carrara *et al.* 1995; Guzzetti *et al.* 1999). These aspects are discussed in the following sections.

Explanatory variables of landslide susceptibility:

In general, the explanatory variables which are related to slope instability and landslide mechanisms are known. These are taken from the understanding of physical processes, geomorphological descriptions and site investigations (Varnes 1978; Phipps 2003; Milne *et al.* 2009; Hungr *et al.* 2014). Table 2.4 provides a comprehensive list of the most common variables that is based on those compiled in Guzzetti *et al.* (1999) and Süzen and Kaya (2011). These variables can broadly be categorised into four groups: environmental, geotechnical, geological and geomorphological. In several cases there are relationships between the variables of different groups, for instance, weathering characteristics may be implicit for different types of lithology. Some variables are used to provide by-product insights on the characteristics of landslides. For example, elevation is used to approximate the gravitational potential energy and run-out distance of landslides (e.g. Vandre 1985, Bathurst et al. 1997, Chen and Lee 2003), and the proximity of slopes to rivers and roads is often used to indicate the potential for lateral erosion and undercutting of a slope (e.g. Shahabi and Hashim 2015).

Group	Variable	Description and examples
Environmental	Land use & vegetation cover	Classification of forested or arable areas and dominant vegetation types or indices, such as NDVI (Marjanović *et al.* 2011).
	Precipitation	Long-term average or synoptic meteorological conditions (e.g. annual average rain or days with snow cover). Not to be confused with initiation thresholds.
	Temperature	Soil temperature influence on soil moisture content, ice formation and thawing.
	Catchment position	Upland vs. lowland environmental processes and distance to watershed, fluvial channels or other hydrological features.
	Human activity	Any human activity which alters one or many other factors for example, road construction which alters the profile and drainage of a slope (Larsen & Parks 1997), or trampling which increases soil surface permeability and erosion.
Geotechnical	Slope material properties	Physio-chemical characteristics including porosity, permeability, grain size and sorting. Strongly linked to lithology factors.
	Superficial deposit thickness	Material depth to bedrock or otherwise impermeable strata forming a potential shear surface.
	Weathering potential	Weathering characteristics of the slope materials (e.g. low, moderate and high).
Geological	Bedrock lithology	Rock lexicon and weathering characteristics.
	Bedrock-strata interaction	Proximity to faults and fracture zones or bedrock sequences overlaying weakened substrata (e.g. (Jenkins *et al.* 2011)).
	Seismicity	Hazard maps for annual average seismicity or ground acceleration during tremors and earthquakes (Meunier *et al.* 2008).
Geomorphological	Elevation	Terrain and slope elevation and range is related to the gravitational potential energy and runout distance (Vandre 1985; Bathurst *et al.* 1997; Lorente *et al.* 2003).
	Aspect	Slope orientation to incoming solar radiation, wind and precipitation.
	Angle	Critical angles of repose for common hillslope materials are in the range of 25 to 45° (Iverson *et al.* 1997).
	Curvature	Convexity or concavity of the slope profile. Curvature influences the direction and velocity of surface and ground water flow (Yilmaz 2010).
	Terrain roughness / ruggedness	Roughness is an indicator of steep and elevated terrain liable to increased erosion and gravitational potential energy. E.g. the Melton Ratio (Melton 1957): MR = $Elevation\ Range/\sqrt{Area}$
	Hydrology	Fluvial features (e.g. gullies or channels) in which sediment is entrained, and ground water flow from the above draining area.

Table 2.4. Explanatory variables used in landslide susceptibility models. Table adapted from Guzzetti *et al.* (1999) and Süzen and Kaya (2011).

Different combinations of explanatory variables will be important for studies conducted in different landslide regions. Landslides that are initiated during periods of prolonged and intense rainfall are generally distributed with respect to critical slope angles on hillslopes or in gullies featuring increased rates of ground water flow and erosion (Montgomery 1999; Iverson 2000; Milne *et al.* 2009). Conversely, landslides initiated during earthquakes are situated in areas attributed to the topographic amplification of seismic waves, such as on faults and ridge crests (Keefer 1984; Dadson *et al.* 2004; Meunier *et al.* 2008; Korup 2010). In spite of this, many susceptibility studies do not differentiate between landslide types (Van Westen *et al.* 2006). Budimir *et al* (2015) review the statistically significant factors ($p < 0.05$) reported at 91 study sites from 75 peer review studies over the period 2001 to 2013: 55 of the studies were for certain landslide types. The results show that:

- For all the sites examined the significant factors were: slope (95 % of study sites); aspect (64 %); elevation (50 %); vegetation, land cover or drainage (35-45 %); and only curvature, lithology, soil type, precipitation, and proximity to faults or roads (10-25 %).
- Landslides initiated by rain (23 sites) and earthquakes (9 sites) shared factors for: slope (95 %), aspect and elevation (50 %), and bedrock geology (30 %). Landslides initiated by rain also included vegetation (70 %), soil type (40 %), curvature (25 %) and distance to fault (13 %). For landslides initiated just by earthquakes (9 sites), these were 11, 0, 0 and 44 % respectively.
- For shallow slides and flows (33 sites) the significant factors were slope (83 %), aspect (40 %), elevation (40 %), land use and soil type (30 %), curvature (20%) and vegetation (10%).
- For complex landslides (20 sites) the factors were slope (85 %) and aspect (75 %). Complex landslides included a broader range of factors in the 30-50 % range, including, elevation, vegetation lithology, land cover, curvature, precipitation, distance to faults and roads. The wider range of factors reflects the presence of multiple different landslide mechanisms at complex landslide sites (Hungr et al. 2014).

A similar set of reviews that examined the variables used in 145 articles (1986 - 2007) also found that the majority of studies use slope angle, superficial lithology and elevation (100%), and 60 % of these used land use, drainage and aspect (Ercanoglu *et al.* 2004; Süzen & Kaya 2011). Whilst these reviews provide useful insights and may be used to guide the selection of explanatory variables used, the selection of variables should be based on independent and location specific analyses in order to account for the local landslide characteristics (Guzzetti *et al.* 1999; Carrara & Pike 2008).

Model units:

Susceptibility assessments are conducted using different modelling units, where each unit is a portion of the land surface that is internally homogeneous in terms of its explanatory variable values (Hansen 1984). The three most commonly used unit areas are: grid cells (e.g. the cells in raster images): unique-condition-units, polygons based on spatial joins of different input data, and geomorphic or hydrological units that are areas characterised by distinct suites of features and processes, such as river catchments, basins and gullies (Carrara *et al.* 1995; Soeters & van Westen 1996; Guzzetti *et al.* 1999; Montgomery 1999).

In grid based analyses, a grid is made up of uniformly sized cells (i.e. pixel resolution) and each grid and grid-cell represents a different explanatory variable and its value in a certain location. The grids of different variables are stacked on top of one another and the cell values where landslides are present are compared to the values of the cells that are without landslides. For example, Pareschi et al (2000) used a 10 m^2 DEM grid to evaluate the characteristics of 37 debris flow that occurred following 100 - 180 mm rainfall in 24 hours in Sarno, Southern Italy. Given the number and proximity of the landslides, the authors employed relatively detailed feature mapping based on aerial imagery and site investigations to identify the properties at the debris flow initiation zones (0.5 – 2.0 m depth volcanic rich colluvium on > 25^o slope angle).

Such detailed feature mapping is rarely available in other regions due to the longer recurrence interval between landslides and as much of the geomorphic evidence is removed by erosion, vegetation or other landslides (Ballantyne 1986; van Westen *et al.* 2006; Frattini *et al.* 2010). Most susceptibility assessments are based on landslide initiation zones recorded as point coordinates (Malamud *et al.* 2004; Glade *et al.* 2005; Guzzetti *et al.* 2008; Blahut *et al.* 2010). As the spatial accuracy of these coordinates is often in the order of 1 to 500 m several studies compare grids with different spatial resolutions, ranging from 5 to 200 m^2, to identify the most suitable resolution for landslide susceptibility modelling. These comparisons indicate that the most suitable resolutions are those equivalent to the average size of the landslide features being examined, ranging from 15 - 30 m^2 in South Korea and Hong Kong (Dai & Lee 2001; Lee *et al.* 2004b) to 50 - 100 m^2 in Guangdong, China and Tuscany, Italy (Tian *et al.* 2008; Catani *et al.* 2013). Therefore, higher resolution grid data does not necessarily improve the performance of models, however, high resolutions are required to capture accurate variable statistics, such as maximum slope angles, and these may then be resampled to broader resolutions. Guzzetti *et al.* (1999) advises that several grid resolutions should be evaluated to account for the regional characteristics of landslides and the quality of the landslide records.

Compared to grids, there are relatively fewer studies that use unique-condition-units (UCU) Guzzetti *et al.* (2005) examine 3,900 translational slides and debris flows in the Apennines Mountains, Italy by creating sub-basin slope units based on drainage divide lines (e.g. individual valley sides), and these were then split into 2,243 UCU based on a spatial overlay of 21 different susceptibility factors. Using a similar approach, Catani *et al*. (2005) examined 20,000 rotational and 7,000 shallow translational slides in Tuscany, Italy using UCU based on the overlay of lithology, land cover, slope, curvature and data for the above slope draining area. In each case, the adopted models were reported to accurately classify 75 to 85 % of the UCU when partitioned into training and test data sets. However, they do not report the accuracy for the minority class, the accuracy the model is able to predict just the UCU that contain landslides.

Hydrological units offer an appropriate unit for modelling landslide susceptibility since a clear physical relationship exists between certain landslide mechanisms and the morphological and hydrological properties of upland fluvial systems (Guzzetti *et al.* 1999; Montgomery 1999; Wilford *et al.* 2004; Welsh & Davies 2011). For instance, Korup (2004) notes that the occurrence of shallow-translational slides and debris flow in New Zealand are most often the result of a physical coupling to the fluvial systems and processes that operate on the same hillslopes and gullies. There observational evidence for these linkages in Scotland where many of the recorded landslides have been initiated on hillslopes or in gullies where multiple drainage

channels converge – increasing the saturation of the slope materials (Ballantyne 2002; Milne *et al.* 2009).

Studies in other fields (outside of landslide susceptibility) have examined the characteristics of different hillslopes and gullies to determine which units are more likely to produce flooding, debris flooding and landslides. Many of these studies use the Melton Ratio terrain roughness index (MR, in Table 2.4). In British Columbia, debris flow were found to occur on the hillslopes and gullies with MR > 0.64, with lower MR values found for the units that produce flooding (MR = 0.3 - 0.6) and alluvial fan (MR < 0.3) deposits (Jackson *et al.* 1987; Wilford *et al.* 2004). In New Zealand, a slightly lower criteria MR > 0.5 was found for the units associated with debris flow (Welsh & Davies 2011). Despite this, and as far as these authors are aware, MR and hillslope or gully hydrological units are yet to be applied in a landslide susceptibility model. Studies which use hydrological units are limited to the catchment scale (e.g. upland basins and valleys) in the Catalan Pyrenees (Chevalier *et al.* 2013; Berenguer *et al.* 2015). These studies achieved reasonable classification accuracy (69 %) for the detection of units both with and without landslides. Chevalier *et al*. (2013) note that the use of catchment scale units limits the use of certain explanatory variables, such as slope aspect, given that each catchment unit contains contain two or more slopes faces with different values. The use of higher resolution hydrological units, at the scale of hillslopes and gullies, may therefore prove beneficial to modelling the terrain landslide susceptibility to debris flow.

Analysis Technique:

Many analysis techniques have been applied to empirical landslide susceptibility assessments including: qualitative landslide distribution mapping and landslide inventories; heuristic knowledge based models; and quantitative statistical or probabilistic bi-variate and multi-variate models.

Landslide mapping and inventories (e.g. the NLDB) are of great importance as all studies rely on accurate and representative spatio-temporal landslide information for the development and validation of susceptibility models (Aleotti & Chowdhury 1999; Guzzetti *et al.* 1999; Glade *et al.* 2005). Landslide inventories are compiled from various sources including news articles, social media, infrastructure organizations or insurance claims (Pennington *et al.* 2015), and are complimented in particularly active regions by field surveys and remote sensing (Pareschi *et al.* 2000). Worldwide, these inventories have typical data and data quality for: landslide source locations as coordinate pairs at spatial accuracies ranging from 1m to entire catchments; the date and time of failure (5 % <12 h, 26 % 24 h and 70 % >24 h), and the type of movement and failure material based on common classification systems (Malamud *et al.* 2004; Guzzetti *et al.* 2008; Hungr *et al.* 2014). In addition, inventories are generally biased towards larger events or those with impact to society, and it is likely that many small magnitude landsides or those with little impact are unrecorded (Milne *et al.* 2009).

Heuristic landslide susceptibility models are developed using landslide inventories in combination with a priori knowledge, expert judgment and local experiences to assign weights for the relative importance of various explanatory variables within each terrain unit (Soeters & van Westen 1996; Cardinali *et al.* 2002). In the UK, the 1:50,000 scale landslide susceptibility model 'GeoSure' is based on a 5 tier (A = low-susceptibility to E = high-susceptibility) ranking of UCU according to 15,000 NLDB data points and expert weightings for slope angle (derived

from 25m2 NEXTmap DEM), geology and bedrock (1:10,000 to 1:50,000 geological maps) discontinuities, and with regional modifications based on factors related to superficial deposits such as past landslide deposits, unconsolidated glacial tills and clay soils (Foster *et al.* 2008); GeoSure is available nationwide and is the de facto product used by the UK insurance industry. Qualitative weightings are heavily dependent on the cognitive bias, experiences and knowledge held by the persons which develop such models. However, this does not render such assessments as invalid or inaccurate as the developers typically include experienced researchers and regional experts, rather that it is difficult to determine the objectivity and reproducibility of heuristic methods (Glade *et al.* 2005).

Bi-variate analyses overcome issues of subjectivity by apportioning each terrain unit into mutually exclusive conditions (units with landslides or units without or yet to have landslides 'non-landslide') and comparing these to the distribution of each explanatory variable mapped to categories, such as, categorical lithology types or slope angle categories of 0 - 10^{o}, 20 - 30^{o} etc. The tallies of each condition and unique factor-class are compiled in a contingency-table and cross tabulated to quantitatively derive weightings and conditional probabilities for each factor-class relationship to the presence or absence of landslides. Most methods are based on some variation of the Bayesian probability model including: Weights of Evidence (WoE), Weighted Overlay, Frequency Ratio or Information Value methods (Thiery *et al.* 2007; Pardeshi *et al.* 2013). WoE is by far the most common approach. In WoE, the conditional Bayesian probability of landslide or non-landslide occurrence is calculated for each factor-class and are transformed using the natural logarithm of their odds, which gives the odds-ratio between the landslide occurrence and non-occurrence probabilities (Bonham-Carter & Cox 1995). The odds-ratio is used to calculate weights which define the strength of the spatial association (positive weights) or separation (negative weights) of landslide occurrence to each factor-class. Thus, a probabilistic assessment of susceptibility is reached by summing the weights and retransforming the odds-ratios for each factor-class. WoE and the terrain factors slope, curvature and flow accumulation have been used to model landslide susceptibility in mountainous regions of Europe (Thiery *et al.* 2007; Blahut *et al.* 2010; Sterlacchini *et al.* 2011; Meyer *et al.* 2014), Malaysia (Pradhan *et al.* 2010) and with additional anthropogenic land-use and road proximity factors in Canada (Quinn *et al.* 2010), the Italian Alps (Piacentini *et al.* 2012) and the Indian Himalaya (Martha *et al.* 2013). The reported accuracy of these WoE models is in the order of 65 - 85% and the use of more complex models with more explanatory variables often fail to improve accuracy levels beyond this range (Blahut *et al.* 2010; Sterlacchini *et al.* 2011; Meyer *et al.* 2014). However, a pre-requisite of bi-variate models, including WoE, is conditional independence of explanatory variables and therefore including large numbers of factors is more likely to violate this condition (Thiery *et al.* 2007). The use of UCU can alleviate the requirement for conditional independence (Piacentini *et al.* 2012), however this would be at the expense of quantifying individual weights and the relative importance of individual factors and factor-classes on landslide occurrence.

Bi-variate techniques are not suited for susceptibility assessment in regions where landslides occur as the result of multiple explanatory variables and interactions between them (Thiery et al. 2007; Pardeshi et al. 2013). Multi-variate analyses are applied in order to consider the relative contribution of multiple factors and to quantify the strength and effect of interactions between different factors and factor-classes. Figure 2.6 illustrates the four most commonly used multi-variate methods in landslide susceptibility, including, Artificial Neural Networks (ANN),

Support Vector Machine (SVM), Random Forest decision trees (RF) and Logistic Regression (LR). These are statistical and assisted learning algorithms which are repeatedly trained and validated, using separate sets of labelled units (i.e. landslide and non-landslide), in order to improve their predictive accuracy.

ANN are a 3-tier system of decision neurons, or nodes, for input (factors and their values), hidden-layer (data transformations) and output (probabilistic classification of landslide and non-landslide units) connected by weighted links. Depending on the model and assigned problem, at each iteration the hidden layer recodes the input factor data (e.g. mean normalization, standardization, log transformation, resampling classes or Boolean), adjusts the link weights and the classification error is re-evaluated until no further reductions are reported (Bonham-Carter & Cox 1995; Lees 1996; Aleotti & Chowdhury 1999). ANN have achieved reasonable classification success rates using geomorphological and geological factors in a number of regions including: 85% for UCU in the Arno River Basin, Italy (Catani *et al.* 2005), 72-81% across 5 different sites in Penang, Malaysia (Pradhan & Lee 2009) and 84% in Koyulhisar, Turkey (Yilmaz 2010).

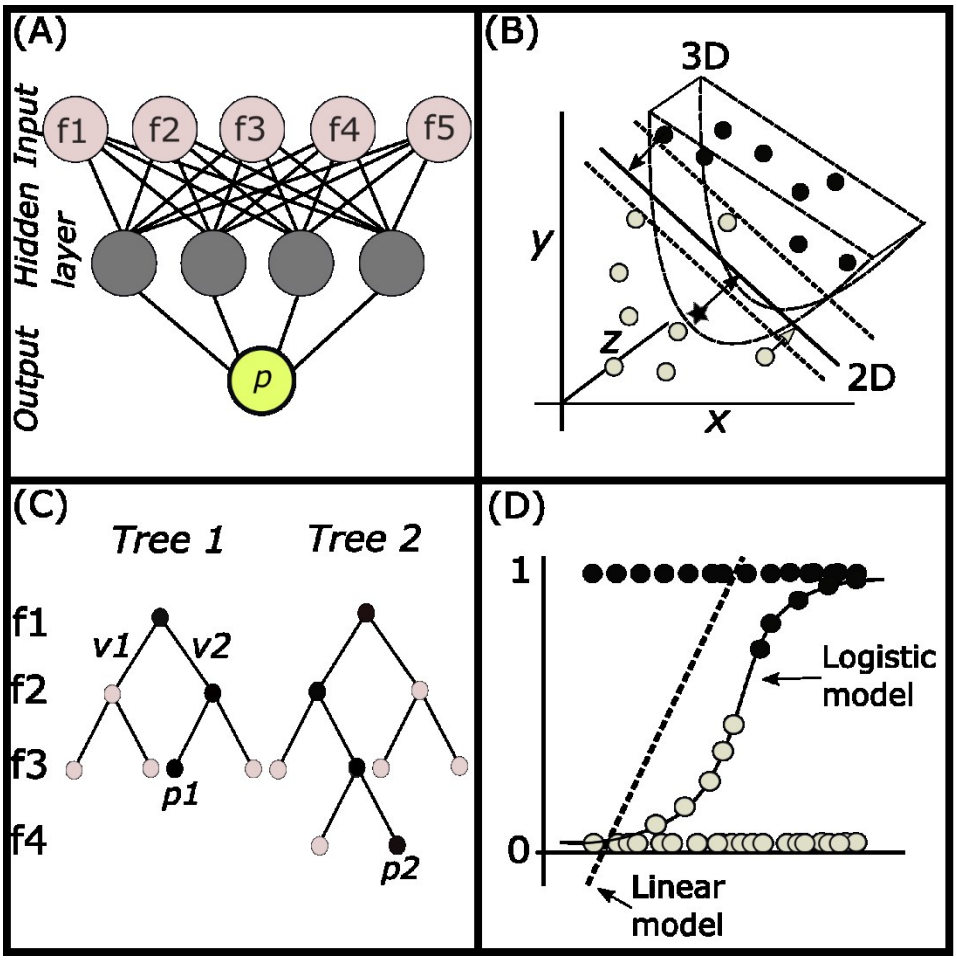

Figure 2.6. Conceptual diagrams of: (A) Artificial Neural Networks (ANN); (B) Support Vector Machines showing 2D separation (bold black lines) of landslides (black dots) and non-landslide (grey dots) and 3D separation (light grey lines); (C) two Random Forest (RF) decision trees with four tier logic decision gates; and (D) Logistic Regression showing the sigmoid log odds function (black solid line and bold points) as opposed to the multiple regression line (dashed grey line and light points).

LR is a useful tool to find the best fitting model to describe the relationship between a dichotomous or binary dependent variable (the presence or absence of landslides) and a set of independent explanatory variables which may be categorical (e.g. rock type and land use) or continuous (e.g. slope angle and curvature) (Menard 1997). Unlike multiple-linear regression, the model output is determined by the binomial distribution and logit that a terrain unit belong to the dichotomous landslide or non-landslide state. Logits are the natural logarithm of the odds ratio and, as in WoE, the odds ratio is the ratio between the probability that something does occur to the probability that is does not occur with values ranging from floor 0 to <1 (reduction in the probability or odds), 1 (the probability or odds are identical) and >1 to infinity (increase in the probability or odds). The logit is used so that the model outputs are symmetrical around zero and vary from negative to positive infinity within 0 and 1. It is stressed that probability, odds, and logits are three ways of expressing the same thing and one can easily be converted into the other. LR is given by Equation (2.1:

$$logit(Y) = \beta + \beta_1 x_1 + \beta_2 x_2 \ldots + \beta_i x_i \quad (2.1)$$

$$p = \frac{1}{1 + \exp^{logit(Y)}} \quad (2.2)$$

where Y is the dependent variable, β is the model constant, x_i and β_i are the i-th causative factor values and regression coefficients, respectively. The logit is transformed to a probability (p) using Equation 2.2. The LR model coefficients (β_i) are weights for the best-fit combination of explanatory variables which give the greatest log odds that a terrain unit is susceptible to landslides. A valuable output of LR is that taking the exponential of each model coefficient gives the odds ratio and probability that a factor-class (e.g. certain rock type) has on the probability of being in the landslide or non-landslide susceptible state. The significant predictor variables (Wald test $p \leq 0.05$) found for applications of LR to landslide susceptibility are: slope angle and elevation in Hong Kong (Dai & Lee 2001); slope angle and lithology in Kansas, US (Ohlmacher & Davis 2003); and slope angle, aspect, lithology and proximity to roads in Kakuda-Yahiko, Japan (Ayalew & Yamagishi 2005). In addition, slope angle and the adjacent draining area were the most important factors for the susceptibility of 1184 slopes and engineered cuttings on the Irish rail network and with 92 % LR classification accuracy (Martinovic *et al.* 2016).

SVM and RF are more recently developed and so called 'machine learning' methods (Hand 1997). As illustrated in Figure 2.6B, in 2-dimensions the SVM seeks to determine the maximum separating hyper-plane (solid black line) between landslide (black dots) and non-landslide (grey dots) support vectors (i.e. the scatter plot formed of slope angle (x-axis) and curvature (y-axis) for each terrain unit). The distance of separation (dotted lines and arrows) and systematic removal of the nearby 'support vectors' (star point) is evaluated in order to determine the strength and sensitivity of the separation. This same principle is then applied to distinguish three or multi-dimensional data separation (i.e. using more explanatory variables), but using kernel functions to determine complex hyper-plane (the z-axis and dashed black lines in Figure 2.6B) (Yao *et al.* 2008). In RF (Figure 2.6C), a decision tree 'ensemble' is formed of multiple individual decision branches, and each branch uses random sub-selection of factors or layers (i.e. each selected factor is a layer in each branch f1, f2, f3…etc.) and a random portion data for training and testing the classification probability of each branch. A branch is a multi-tiered series of logic decision gates, or rule-set, based on the factor values and classes (e.g.

slope ≥ 20° = landslide, slope < 20° = non-landslide). The successful tree series (chained black dots) and their classification probabilities are retained whilst the unsuccessful series (grey dots) are discarded. The process is repeated and the successful branches are accumulated until there are no further reductions in the net classification error of the tree ensemble (Brenning 2005).

SVM and RF are more recently developed methods and as such there is relatively limited application and evaluation of their suitability for landslide susceptibility mapping (Brenning 2005). Most comparisons are made to with respect to LR regression models which are by far by far the most common approach. For instance, Budimir et al. (2015) reviewed the explanatory variables used in 75 LR studies from a literature search containing some 1200 unique results for the terms "landslide" and "logistic" in Science Direct. Brenning (2005) notes that step-wise LR and SVM provide the lowest classification error whereas RF tend to over fit the training data when comparing different proportions of training and validation data from 2000 shallow-translational slides and debris flow in the Ecuadorian Andes. Similarly, Catani et al (2013) apply RF in the Arno basin, Italy and find that the training process and therefore model accuracy is strongly influenced by the factor distributions in the training data. Marjanović et al (2011) compare three susceptibility models for landslides in Fruska Gora, Serbia using 5, 10 and 15% validation data sets. The authors report that a similar range of classification success rates were found for each model, SVM (0.85-90%), LR (0.85-0.87%) and RF (0.82-0.85%). Similar results were found for ANN (0.85%), SVM (0.84%) and LR (0.83%) models of landslides in Sivas, Turkey (Yilmaz 2010) and for RF (0.77%) and LR (0.75%) models in Shaanxi Province, China (Chen *et al.* 2017). Though each of the multi-variate models seem to exhibit similar levels of performance, logistic regression is the most widely adopted method and performs consistently well between studies in different landslide prone regions.

2.2.5 Landslide Rain Initiation Thresholds

Globally, periods of prolonged and excess rainfall are the most frequent triggering mechanism of landslides (Ballantyne 1986; Crozier 1997; Aleotti 2004; Glade *et al.* 2005; van Westen *et al.* 2006). Landscapes containing slopes that are susceptible to generating landslides are often regarded as being in equilibrium with the long term environmental conditions, such as rainfall and land use, to which these have been exposed (Guidicini & Iwasa 1977; Cannon & Ellen 1985; Aleotti 2004; Giannecchini *et al.* 2016). It therefore follows that in landscapes where rainfall is the dominant factor (i.e. other contributing factors such as land use remain relatively constant), it is reasonable to analyse rainfall patterns in order to quantify thresholds which when exceeded trigger a hydro-geological response sufficient to disrupt the equilibrium and result in the triggering of a landslide (Caine 1980; Van Asch *et al.* 1999; Waltham & Dixon 2000; Pennington *et al.* 2014).

Empirical initiation thresholds are defined through statistical and probabilistic analysis of the past rainfall conditions that have resulted in landslides. The thresholds are categorized based on the method of analysis, the rainfall data used, the type of landslide mechanism, and the regions in which the thresholds apply (Caine 1980; Wilson & Jayko 1997; Guzzetti 1998; Guzzetti *et al.* 2008). Initiation thresholds, no matter how complex, are a simplification of the relationship between rainfall and landslide occurrence (Aleotti 2004). Establishing relevant initiation thresholds is a complex task given that there are many influential factors, for instance, the lag-time between rainfall infiltration and significant increases in porewater pressure on

deep failure surfaces that require prolonged or multiple rainfall periods to raise the antecedent slope material water content (Iverson 1997; Van Asch *et al.* 1999; Dijkstra & Dixon 2010). As a result, thresholds are rarely applied to large and complex rotational landslides unless complimented by detailed geomorphological and geotechnical knowledge of a specific site (Waltham & Dixon 2000; Dixon & Brook 2007).

The majority of landslide initiation thresholds are developed for shallow translational landslides and debris flow that occur in mountainous environments where there is a relatively high degree of homogeneity between the failure mechanisms and conditions at multiple failure locations (Innes 1983; Guzzetti *et al.* 2008). Moreover, there is often reliable evidence for the regular activation or re-activation of landslides in certain locations or of simultaneous failures occurring episodic weather events (Onodera *et al.* 1974; Guzzetti 1998; Pareschi *et al.* 2000; Ballantyne 2002; Jakob & Weatherly 2003; Guzzetti *et al.* 2007; Cannon *et al.* 2008; Chleborad *et al.* 2008; Winter *et al.* 2010; Staley *et al.* 2013; Søren *et al.* 2014). The following review and discussion of landslide threshold studies is therefore constrained to these types of landslide.

The first, and most common landslide threshold approach is the characterization of the intensity and duration of landslide rain events (LRE) by Caine (1980). As illustrated in Figure 2.7, Caine determined a lower-limit initiation threshold by examining and manually drawing a curve-line below the intensity-duration (ID) points of 73 24h LRE (days with landslides) which initiated shallow landslides (< 3m soil depth) in different climatic, geologic and topographic environments around the world.

Figure 2.7. A reconstruction of the Intensity-Duration threshold (thick solid line) for 73 24h landslide rain events (black crosses) reported in Caine (1980). The ID threshold (thin solid line) developed by Innes (1983) showing the effect of spatial variation between landslide regions. Three ID thresholds from the frequentist's method (Brunetti *et al.* 2010) are shown for 75% (best fit), 50% and 10% percentiles; legend in figure.

The ID-threshold is formalized by the power law Equation (2.3:

$$I = \alpha D^{-\beta} \qquad (2.3)$$

where I is the mean rainfall intensity (mm hr-1), D is the rain event duration (hours), α is the intercept and β is the shape parameter (scaling coefficients).

Initial developments to the methodology include: the determination of lower (as in Caine, 1980), intermediate (capturing ~50 % of landslide events) and upper limit (conditions that do not cause landslides) ID-thresholds (Onodera *et al.* 1974); the inclusion of longer antecedent rainfall information for landslide thresholds in the San Francisco Bay region, California (Cannon & Ellen 1985); ID-thresholds to best separate LRE which caused landslides from the non-landslide rain events (NRE) (Wieczorek & Sarmiento 1982); and threshold comparisons which led to the realization that they vary significantly between regions (plotting above or below one another, see Figure 2.7) and thus require calibration to the specific area of application (Innes 1983; Wieczorek 1987).

Guzzetti et al. (2007) compare the approaches of 27 ID-threshold studies in a variety of landslide prone regions around the world (e.g. the European Alps, Italy, South East Asia, Japan, China, Brazil, South and North America) and note that most define lower and upper limit ID-thresholds in order to form an envelope around the LRE within which landslides are most likely to occur. The range of reported average intensities for the 24 hour rainfall period (the day of landslide occurrence) is from 3.5 to 70 mm hr-1 (Guzzetti *et al.* 2007). The primary difference between these studies is in the rainfall variables used. As shown in Table 2.5, these include other standard variables (e.g. mean or maximum accumulation), antecedent and normalised rain variables.

Antecedent rain periods are those which condition the slope prior to failure. The principle pre-condition effect is for a rise in the slope materials moisture content, thus reducing the required infiltration, accumulation or intensity of rain to initiate failure (Iverson 2000). For example, Chleborad (2000) develop rain accumulation landslide threshold in Seattle, US combining the accumulated rain at 3 (A_3 mm) and from >3 to 18 (A_{15} mm) days antecedence ($A_3 = 88.9 - 0.67A_{15}$); in the Columbian dry season, ID-thresholds are three times greater than in the wet season (Terlien 1998), and significant antecedent rain accumulation periods were identified and ranged from two to 12 days for landslides initiated Scotland (Nettleton *et al.* 2005; Winter *et al.* 2010). Worldwide analysis of 2,200 landslides and ID-thresholds report that antecedent periods are in the range of two days to five weeks (Guzzetti *et al.* 2008), and suggest that rain events of duration <48 h should be considered 'triggering' rain events given the temporal accuracy of most landslide inventory data is ~24 h as landslides often reported on the day of failure.

Normalised rain variables are used in order to cope with the differences in rain intensity and accumulation between different climatic regions or within regions where there is likely to be differences due to orographic effects (Jakob & Weatherly 2003; Sidle & Ochiai 2013). Normalised thresholds represent the ratio between the landslide initiation value and the long term rainfall conditions in a location, for example the mean annual precipitation (MAP) (Cannon & Ellen 1985; Aleotti & Chowdhury 1999). The rainy day normal (RDN) is the average precipitation on days with rain (Wilson & Jayko 1997) and is a better indicator of

typical rain conditions, and thus for the extremes associated with landslides, as it reduces the effect of no-rain days (Guzzetti *et al.* 2007, 2008; Brunetti *et al.* 2010; Meyer *et al.* 2012).

Variable	Description	Units	Cited in:
n	Antecedence period. The preceding time period that each variable is calculated.	hours or days	
D_n	Rain duration. The duration of rain within the antecedence period; often defined by the period of time where rain intensity >0.01 mm/h.	hours or days	(Onodera *et al.* 1974; Caine 1980)
I_n	Rainfall intensity. The mean or maximum rate of precipitation falling within the antecedence period.	mm/h	(Onodera *et al.* 1974; Caine 1980)
V_n	Rain accumulation. The sum of precipitation falling within the antecedence period.	mm	(Chleborad 2000)
NV_n	Normalised rain accumulation. The normalised sum of precipitation falling within the antecedence period; also denoted by E_{norm_n}.	ratio	(Aleotti 2004)
DR_n	Days with rain. The number of days with rain accumulation above a certain threshold (>0.01 mm) within the antecedence period.	integer	(Wilson & Jayko 1997)
Normalisation variables			
RDN	Rain day normal. The average daily precipitation accumulation on days with rain (A >0.01 mm).	mm	(Wilson & Jayko 1997)
MAP	Mean annual precipitation. The annual average precipitation accumulation for a given location obtained from the historical range of observations.	mm	(Aleotti 2004)

Table 2.5. Rain variables used to determine landslide initiation thresholds.

The arbitrary selection of ID-threshold restricts ease of comparison and repeatability of methods between study areas or research and hazard management communities. In addition, deterministic ID-thresholds are of little value for early warning or landslide hazard and risk analysis as they do not indicate the recurrence intervals of significant LRE or the landslide likelihood when ID-thresholds are exceeded (Brooks *et al.* 2004). In the past decade developments have therefore been focused on objective threshold selection techniques and probabilistic assessments.

Guzzetti et al (2007) propose a 'Bayesian inference' model, which estimates a number of ID-thresholds that loosely support the LRE point data cloud. The model is based on a binomial distribution for the combined chances of, (i) a storm with peak intensity I and duration D, (ii) consequential landslide failure, and (iii) that the landslide is observed and reported. ID-thresholds are then selected which capture different percentiles of the LRE points, and the approach was used to determine a global ID-threshold using 2,200 landslides (Guzzetti *et al.* 2008). Another percentile based approach is the 'Frequentists' method (Brunetti *et al.* 2010). First, the intensity and duration values of LRE points are log transformed and a line of best fit is approximated using the least square method. Then, parallel lines with the same slope are calculated in order to define thresholds which capture different percentiles of the LRE points

or landslides (5%, 10%, 15% …100%). Figure 2.7 shows an approximation of the 10, 25 and 75% (75% is also the best fit line) frequentist ID-thresholds using the data from Caine (1980). Peruccacci et al (2012) assessed the sensitivity of 'frequentist' ID-threshold coefficients (intercept and slope) by bootstrap sampling different proportions of 753 LRE, finding ≥75 LRE resulted in stable coefficient means and standard deviations in Umbria, Italy. Assuming that the catalogue of rainfall events is sufficiently complete for the study area, each of these methods state that the probability of landslide initiation due to periods of exceeding rainfall is less than the corresponding threshold exceedance probability (i.e. the cumulative distribution function). However, this assumption and reporting is somewhat misleading given that NRE are not explicitly considered and as rainfall is not the only factor which causes landslides and so a degree of uncertainty is inevitable. For example, Meyer et al (2012) propose annual landslide trigger frequencies for Norway based on the recurrence intervals of the 90% (lower limit) 50% (middle) and 10% (upper) limit 'frequentist' ID-thresholds, but these are defined using only the LRE. Gariano et al (2015) developed ID-thresholds using the frequentist method for 223 LRE and 1250 NRE in the period 2002-2011 in Sicily, Italy. They then cross-validated each threshold and found that only the 7.5% percentile ID-threshold had the highest (76%) classification success rate, whilst the 50% percentile ID-threshold performed poorer (46%).

The problem of defining a suitable threshold value is analogous to the problem of estimating the probability of landslide occurrence and choosing an acceptable probability value. Furthermore, thresholds which are associated to a time discrete probability of landslide occurrence are applicable to hazard risk assessment (Chung *et al.* 1999; Glade *et al.* 2005). In one approach, ID-thresholds are again drawn by the line of best fit through the LRE of different probability levels (5%, 10%...90%), but using the probability of landslide occurrence calculated by a logistic regression model of LRE and NRE dependent variable and their ID, AD or normalised equivalent values as independent variables (Chang *et al.* 2008; Frattini *et al.* 2009; Giannecchini *et al.* 2016). In Seattle, Chleborad et al (2006) choose thresholds which maximize the conditional probability of landslide occurrence given different combinations of 3 and 15 day antecedent rain accumulation, equivalent to those for $A3$ and $A15$ reported in Chleborad (2000). The probabilities are calculated and reported on a day-by-day basis using a daily time series (not using rain events) and range 2-10% between regional domains based on the distribution of the available rain-gauge network. Conditional probabilities of a similar range 1-20%, were also found using LRE and NRE based analysis in Emilia-Romagna, Italy (Berti *et al.* 2012).

Landslides thresholds which are derived using conditional probability are in essence an attempt to solve a binary classification problem, where the rainfall conditions that coincide with the occurrence of landslides (LRE = 1) are separated from the rain conditions that do not coincide with landslides (NRE = 0); with increased probability at increased separation. Receiver Operating Characteristic (ROC) is a suite of diagnostic tests to assess the performance of classification models, for instance: the classification success rate or accuracy is the proportion of LRE and NRE that are correctly classified (true positives and true negatives) to those that are incorrect (false positives and false negatives); and the True and False Positive Rate (TPR and FPR) are the proportions of LRE and NRE correctly classified by each thresholds value, respectively. Staley et al (2013) apply the ROC measure 'threat-score' in an exhaustive approach (all possible ID values) to select the ID-threshold which minimizes any false results and is equivalent to the greatest conditional probability. However in medicine, meteorology

and many other fields, the use of the most accurate threshold often results in low detection rates (e.g. of cancers or rare weather phenomena) and instead a low number of missed alarms (false negatives) is desired when the threshold is to be used in an operational system where missed alarms could result in fatalities or severe loss, such as, a landslide early warning system. Therefore, other ROC measures are used to select thresholds for instance, the 'optimal point' which finds the greatest ratio of the TPR (landslide detection) over FPR (false alarms) (Schisterman *et al.* 2005; Fawcett 2006; Perkins & Schisterman 2006b). However, these are yet to be applied to determine landslide thresholds.

In summary, there are many different research studies and approaches which aim to determine objective and clear criteria to define landslides thresholds. Approaches which objectively select thresholds and report the probability of landslide occurrence are most applicable to landslide hazard and risk analysis. However, a major issue that is yet to be resolved is that threshold values, probabilities and their statistical significance are influenced by subjectivity in the criteria used to define each 'rain event' and effect on the proportion of LRE to NRE. There is little rationale or consistency between the adopted rain event criteria or for the number of events which are analysed. For studies which utilities rain gauge observations approaches include: 16 LRE (no NRE) ranging from 1hr to 150 days preceding failure in Scotland (Winter *et al.* 2010); Meyer et al (2012) analyse 700 LRE (no NRE) which are the four-week period preceding each landslide Norway; Jakob & Weatherly (2003) use equal numbers (25) of LRE and NRE defined as the four-week period prior to landslides and as a random selection of four-week periods with similar accumulation 1980-2001, respectively; Søren et al (2014) analyse rain values from 14 days before to 14 days after each landslide occurrence; Staley et al (2013) examine 43 LRE and 259 NRE which are defined between >8 h dry periods in a 16 month rain record (November 2008-June 2009 and October 2009- June 2010); Giannecchini et al (2016) examine 71 LRE and 120 NRE defined using two intensity criteria, >20 mm/h in 2-3 h or 0.1-2mm/h in 100-120 h, for the period 1950-2005; Berti et al (2012) define LRE and NRE by runs of days with positive rain accumulation (>0 mm) in the period 1939-2000; and others use criteria developed in Italy for minimum dry periods of > 48 h in the dry-season to > 96 h in the wet-season (Brunetti *et al.* 2010; Peruccacci *et al.* 2012; Gariano *et al.* 2015; Melillo *et al.* 2015; Piciullo *et al.* 2016). Similarly, for studies which use radar based rain observations event criteria range from > 1 h dry periods in the Central Pyrenees (Abancó *et al.* 2016) to > 24 h in Japan (Saito *et al.* 2010) and in the Italian Alps (Marra *et al.* 2014).

A criterion (e.g., 24 h) may not adequately separate two distinct convective rain storms events, whereas a shorter period (e.g., 2 h) may unnecessarily split longer duration storms into separate events. In addition, for slopes which consist of mixed to fine grained materials the longer-term antecedent conditions (e.g., > 100 h) may be significant, whereas high permeability and coarse grained materials (e.g. volcanic deposits) have shorter response times (Aleotti & Chowdhury 1999; Pareschi *et al.* 2000). As far as these authors are aware no study has compared and evaluated the influence of different event criteria on thresholds or conditional probabilities within and across different landslide prone environments. It is reasonable to assume that the least subjective, and therefore most accurate, approach involves using all of the available rain record data in a day-by-day time series analysis, retaining all rain record information, such as in Chleborad et al (2006) and Chleborad et al (2008). For application to hazard risk assessment or operational warning systems, when new landslides occur in a study area the data set changes and so the thresholds and probabilities should be recalculated (Glade *et al.* 2005).

One last caveat is related to source of the rain record information. In rain-gauge based assessments, a single rain record (and set of events) is associated to all of the landslides that occur within a single region or within spatial domains that are based on the distribution of available gauges (Chleborad 2000; Chleborad *et al.* 2006; Guzzetti *et al.* 2007; Brunetti *et al.* 2010). These regions and domains are subject to the assumption of uniform rain or rain is interpolated between gauges which are often of low density and low elevation (Guzzetti *et al.* 2007). Conversely, for assessments using remotely sensed rain data (i.e. satellite or radar) a unique site-specific-rain (SSR) series (or set of events) is created at each landslide location; with the exception of landslides occurring in close proximity to one another. As a result, threshold values selected using objective methods and using SSR data are likely to increase and the probabilities of landslide occurrence will reduce as the proportion LRE decreases with respect to NRE. Comparisons of thresholds derived using gauge and radar data note that significantly lower thresholds are obtained when using gauges (Marra *et al.* 2014; Abancó *et al.* 2016). However, probabilities are not reported and each study uses different criteria and quantities of LRE to NRE. These differences may also be attributed to the different data sampling point gauge observations and spatially averaged radar data (Austin 1987), although in many areas there is good agreement between gauge and radar observations (Cole & Moore 2008; Villarini *et al.* 2008; Harrison *et al.* 2009). Remotely sensed, spatially continuous observations are beneficial to the study of landslide initiation as rainfall patterns vary in both space and time and are strongly affected by topography, particularly in mountainous terrain (Sidle & Ochiai 2013). Remote sensing data also provide self-consistency between the measurements used to develop thresholds and those with desirable features for operational use, such as short and long range forecasts (Borga *et al.* 2014). In order to apply SSR data in a day-by-day analysis using all available rain data, such as in Chleborad et al (2006), thresholds and conditional probabilities of landslide occurrence must therefore be selected and expressed using normalised rain variables to allow the inter-comparison and analysis of the rain records from each landslide location. However, a thorough search of literature did not yield any such studies and this is therefore a gap in knowledge.

2.2.6 Empirical Landslide Assessments on Infrastructure Networks

Landslide susceptibility and initiation thresholds have been used to evaluate the landslide potential on infrastructure networks. In England, Freeborough *et al* (2016) assess the susceptibility of segments in the national rail network using a 500 m spatial buffer to evaluate the areas of adjacent susceptible ground as defined in the national landslide susceptibility model GeoSure (Foster *et al.* 2008). In South West England, network rail also operates a series of landslide warning thresholds to assess and monitor the condition of clay rich slope assets. These are for: wet conditions (in 24 h, >175 % average daily rainfall and SMD < 60 mm), dry to desiccated conditions (SMD 200 to > 250 mm). In Scotland, Winter et al (2010) examine the ID-thresholds of 16 landslides using Caines' (1980) method, reporting that the important rainfall durations and antecedence periods are likely in the range of 2 h to 12 days prior to landslide occurrence.

Many landslide susceptibility assessments report that proximity to roads within the range of 50 – 500 m is often one of the most significant explanatory variables to landslide susceptibility (Ayalew & Yamagishi 2005; Shahabi & Hashim 2015). However, this is likely attributed to the fact that most recorded landslides and inventories tend to have some bias toward events

with socio-economic impact – thus landslide are more likely to be recorded when they impact infrastructure (Malamud *et al.* 2004; Guzzetti *et al.* 2006; Stanley & Kirschbaum 2017). In order to alleviate this bias, it is recommended that independent landslide assessments are conducted for the slopes adjacent to infrastructure networks. For example, Martinovic *et al* (2016) use a logistic regression model to assess the susceptibility of engineered slope assets on the Irish Rail network: each slope unit was pre-defined by the rail network operator and natural slopes were not included.

2.2.7 Landslide hazard and risk

In recent decades landslide hazard and risk assessment has become a major field of interest and scientific of research due to an increasing awareness for the socio-economic impacts of landslides due to increasing pressures from human development, urbanisation and climatic change (Aleotti & Chowdhury 1999; Glade *et al.* 2005; Van Westen *et al.* 2006). Varnes (1984) defines landslide risk as "*the expected number of lives lost, persons injured, damage to property and disruption of economic activity due to a particular damaging phenomena for a given area and reference period*". In probabilistic hazard risk models (Grossi & Kunreuther 2005; Kappes *et al.* 2012; Lee & Jones 2014), risk is quantified using Equation (2.4:

$$Risk = \sum(PIEV) \qquad (2.4)$$

where P is a probability function expressing the spatio-temporal likelihood of a hazard within a specific period of time (e.g. per century, year or second) and I is the hazard intensity, which includes information for the duration and magnitude of a hazard (e.g. landslide volume and velocity). E is the exposure and spatio-temporal distribution of the elements at risk (i.e. hazard receptors, the net present value and location of a section of road, vehicles and people) in relation to the location of a hazard. Lastly, V is the vulnerability characteristics or resilience of each element at risk (e.g. reinforced and well drained vs. aged and weathered slopes).

The relative simplicity of the risk formula gives way to complexity when considering real world situations where lots of different aspects must be taken into account. Moreover, there are stark contrasts between the methods and techniques used at different scales of assessment. Hazard and risk assessments can broadly be categorised to those which are: site specific, deterministic and rely on physical-process based models; and those that are regional, empirically based and probabilistic models. For example, a site specific risk assessment generally requires comprehensive geophysical and geotechnical information for the susceptible slope hazard (e.g. of the slopes materials and their arrangement, shear surfaces, seasonal porewater pressures, vegetation, the rates precipitation and solar radiation), the section of road at risk (e.g. construction materials, design standard) in addition to detailed information for the hazard consequences (e.g. road asset value, repair cost, temporal user demands and cost of disruption). In contrast, for a regional scale assessments, covering areas of tens to hundreds of square kilometres, the analysis is generally based on the mapping and heuristic, statistical or probabilistic models of the factors associated to landslide occurrence (e.g. slope, elevation, vegetation cover and weather conditions), identifying the elements at risk and their basic properties (e.g. road geometry, classification and typical construction standard) and

probabilistic functions for hazard intensity (e.g. landslide volume, velocity and deposition shape) and damage (e.g. relationship of landslide volume-velocity to road damage cost).

As there are clear distinctions, and for ease of discussion, it is useful to further simplify the risk formula ($Risk = H \times C$) by combining the elements which are solely related to the physical properties of the hazard (H = *Probability* × *Intensity*) and those which determine the hazard consequences (C = *Exposure* × *Vulnerability*). For landslide risk assessment ($Landlisde\ Risk = H \times C$), the landslide hazard (H) is the probability of landslide occurrence within a discrete period of time (P_t) and space (P_s). The methods used to define the temporal (P_t) and spatial (P_s) probabilities are discussed below. The landslide hazard (H) may also include an approximation of landslide intensity (P_i), such as the landslide magnitude, speed and duration of disruption. Pragmatically, and particularly for large scale studies on infrastructure networks, it is often necessary to simplify hazard intensity, for example, by assuming that if a landslide occurs it causes a complete or partial closure of a road segment and for a discrete period (e.g. 24 hours).

As a first approximation, Crovelli (2000) considered the temporal probability of landslides as independent random events in Poisson (i.e. continuous-time) and Binomial (i.e. discrete-time) probability models. Each of the probabilities are derived by examining the recurrence interval between successive failures in historical landslide inventory. The approach assumes that landslides occur at a certain rate within a given area. For example, according to the landslide inventory obtained for the period 2004 to 2016 in Scotland, landslides occur at a rate of 6 landslides per year. Other than this information, the temporal distribution of landslide occurrence is assumed to be a completely random process (e.g. they occur independently of seasonal climate or rainfall conditions).

As an alternative approach to define P_t, one could use Bayes theorem and the conditional probability of landslide occurrence given the exceedance of a landslide initiation threshold. For landslides that are known to be initiated by periods of rain, the use of thresholds and their probabilities is desirable as rainfall provides a spatio-temporally distributed triggering mechanism (Glade *et al.* 2005; Pennington *et al.* 2014). In addition, this quantifies the uncertainty of landslide occurrence associated with each threshold (Berti *et al.* 2012). The probability of landslide occurrence (p^T) is obtained by Equation (2.5, combining the probability of threshold occurrence (pTH) with the conditional probability of landslide occurrence given threshold exceedance $p(LS|TH)$:

$$p^T = pTH \times p(LS|TH) \qquad (2.5)$$

To assess landslide hazard these temporal probabilities require input for the spatial components of landslides. These capture the critical homogeneities in the landscape that contribute to increased landslide susceptibility. In the case of landslide initiation thresholds, this indicates the locations where rainfall can act as a landslide trigger (Iverson 2000). Landslide susceptibility is the spatial probability (p^S) of landslide occurrence for a given unit of terrain (Brabb 1984). As discussed in section 2.2.4, landslide susceptibility attempts to answer 'where' landslides are expected to occur. Susceptibility may be approximated using a variety of different statistical and analytical techniques including, heuristic, bivariate (e.g. WoE) and multi-variate (e.g. ANN, LR and RF) models (Aleotti & Chowdhury 1999; Carrara *et al.* 2000; Pardeshi *et al.* 2013; Budimir *et al.* 2015; Segoni *et al.* 2015a).

Based on Guzzetti *et al*. (2005), the landslide hazard (H) of a terrain unit (i) may be expressed as:

$$H_i = {p^T}_i \times {p^S}_i \quad (2.6)$$

where ${p^T}_i$ is the temporal probability of landslide occurrence and ${p^S}_i$ is the landslide susceptibility on a terrain unit (i). The landslide hazard Equation (2.6) is the combined spatio-temporal probability of landslide occurrence. It is based on the simplifying assumptions that: (i) the probability of landslide occurrence and the spatial probability of landslide susceptibility are independent of one another; (ii) that future landslides will occur under the same rainfall conditions and in similar locations to those that produced landslides in the past; and (iii) that the average rate of landslide occurrence (per year or per decade) will remain constant with respect to rate observed in the historical landslide inventory. The main advantage of Equation (2.6) is that the resulting landslide hazard is based solely on and self-consistent with the empirical evidence gathered within a region. Although the availability and quality of landslide inventories is often poor, the simplicity of the model enables the landslide hazard to be regularly recalculated and updated as more data is obtained.

The main limitations of Equation (2.6) are related to the possibility that the landslide triggering and susceptibility conditions may change within the time period considered in the hazard assessment. For landslide susceptibility, it is reasonable to assume that many of the significant explanatory variables, including, slope lithology, proximity to faults, slope angle, aspect, curvature and elevation, will remain relatively constant over periods of several years to multiple decades. For example, In Italy, Guzzetti *et al* (2005) note that the expected validity of landslide hazard assessments based on these geological and geomorphological variables is in the order of 50 years. Other variables that are known to influence landslide occurrence are subject to more frequent and seasonal change, for example, the availability of failure materials (or erosion), land use and vegetation cover. Similarly, as weather and climate changes, so do the rainfall conditions that are most likely to lead the initiation of landslides (Dixon *et al.* 2008; Dijkstra & Dixon 2010). It is therefore vital that model creators pay careful consideration to the selection and the uncertainties of each explanatory variable used to develop landslide hazard assessments. For instance, whilst using just a few of the most constant susceptibility variables is desirable (e.g. slope angle and lithology), this may overlook the more subtle and seasonal changes that occur in other factors, such as vegetation cover, and that condition the slope ready for failure (Pardeshi *et al.* 2013; Meyer *et al.* 2014). In any case, obtaining high resolution data and at regular intervals is not possible using current technology. An exception to this is remotely sensed precipitation data, such as from satellite or weather radar sensors (e.g. Hong *et al.* 2006). Hazard assessments that utilise thresholds based on such data are therefore a relatively new and important area of research.

A literature search returned no examples the landslide hazard model outlined in Equation (2.6) and using the conditional probability of landslide occurrence given threshold exceedance. However, this is likely due to the fact that it is only in recent years that the conditional probability of landslide thresholds have been reported (Chleborad *et al.* 2008; Berti *et al.* 2012). Analogous approaches, using other methods to determine the temporal probability, include: combining categorical (i.e. low, medium and high) initiation thresholds and susceptibility in a qualitative 3×3 matrix (Berenguer *et al.* 2015); and multiplying the recurrence interval of

'frequentist' ID-thresholds (i.e. low-90 %, medium-50 %, high-10 %) to landslide susceptibility (Meyer *et al.* 2015).

The approach taken by Meyer *et al* (2015) is most relevant to this thesis as the hazard is calculated for individual road segments in Norway. This is achieved by using the intersection of the road network segments to river catchment units. The susceptibility and temporal probabilities are calculated using a grid. For each road segment, the landslide hazard is calculated as the landslide susceptibility multiplied by the threshold mean annual recurrence interval within each catchment. Where a network segment intersects multiple catchments, the landslide hazard is the sum of the susceptibilities multiplied by the maximum annual recurrence interval for the intersecting catchments. The critical limitation of this study is that the temporal probability value is the recurrence interval for the lower limit rain ID-threshold (i.e. the annual frequency of rainfall conditions above which 90% of past landslides have occurred). This value does not consider the days where landslides did not occur under the threshold conditions and as a result the recurrence interval is likely to be greater than that of the historical landslide inventory, thus the landslide hazard may be overestimated.

2.2.8 Catastrophe models

A catastrophe model is a computerised model designed to simulate the magnitude, intensity, and location of possible hazard events and to calculate their losses (Foote *et al.* 2017). First developed in the 1980s, catastrophe models have been applied to model a wide range of hazards including tropical cyclones, earthquakes, storm surges and flooding (Grossi & Kunreuther 2005; Sampson *et al.* 2014; Foote *et al.* 2017). The models combine knowledge and techniques form multiple disciplines including, natural hazards (e.g. assessments of where, when and how a hazard occurs), engineering (e.g. the structural resilience of buildings) and socio-economics (e.g. the response of humans, financial markets or technological systems that are directly or indirectly effected by a hazard). As such, operational catastrophe models are extremely complex systems operated by large multidisciplinary teams of hazard, actuarial and computer scientists. The fundamental concepts and key components of a catastrophe model are discussed below for the level of understanding required in the context of the models implemented in this thesis. For a comprehensive review see Foote *et al* (2017).

A catastrophe model, such as those implemented by insurance companies, can be considered as a computerised, practical implementation of the risk formula in Equation (2.4). As in Equation (2.4), catastrophe models have a typical modular structure.

- The hazard module incorporates information of the probability and intensity of a hazard event within a given period of time. Each 'event' includes information for the relative likelihood and the characteristics of a single hazard occurrence, such as a landslides timing, location and magnitude. The 'event set' is a catalogue of multiple hazard events. At its simplest, the event set can be a catalogue of the events from the observed historical record. More commonly, the event set contains many thousands of events that are generated through random sampling (e.g. Monte Carlo simulation) of the hazard probabilities. These stochastic and simulated event sets are produced in order to extend the limited record of past events into the realm of what may plausibly occur. The stochastic element is usually based on the probability density function and the expected return periods of relevant phenomena, such as extreme rainfall or earthquakes.

- The exposure module. This module contains information for the objects being modelled. This typically takes the form of an exposure database that includes, the location of buildings and assets, their physical value, the value of a buildings contents, the value of business disruption, amongst others. In traditional risk assessment, the exposure module is comparable to the register of the elements at risk. For operational catastrophe models, the exposure model also includes information on the financial structures and obligations of the insurance policies for the modelled objects.
- The vulnerability module represents the interface between hazard and exposure modules. It estimates the damage to buildings or assets given the characteristics of each hazard event. The components of the vulnerability module can range from relatively simple and deterministic operations for example, if there is a landslide then the road can be considered to be blocked, to complex damage functions such as those that relate building and contents damage to flood inundation depth (Grossi & Kunreuther 2005).
- The financial module translates the expected physical damage and the monetary losses (hazard + exposure + vulnerability) to quantify the probability distribution of loss. These distributions include several useful metrics. Annual Average Loss (AAL): the average loss of all simulated events weighted by their annual probability of occurrence. ALL indicates the losses that are expected within a typical year. Occurrence Exceedance Probability (OEP) curve: the probability distribution that a loss will exceed a certain value within a year. OEP can be used to determine the likelihood of high losses due to rare and extreme events. Aggregate Exceedance Probability (AEP): the probability that the sum of event losses exceeds a certain amount within a year. These metrics are the primary output of the catastrophe model and combined are used to inform hazard and risk managers of the expected losses so that they can better apportion mitigative measures.

The models can operate in two ways: deterministically, to approximate the loss of a particular or hypothetical hazard event; and probabilistically, to approximate the full range of potential hazard events and their losses. In the probabilistic case, the model is calculated for numerous iterations that often represent the passing of time (e.g. > 10,000 years) and potential events are created by repeated random sampling of the hazard probabilities. For each of the sampled events the expected losses (e.g. AAL and AEP) and the potential maximum loss (i.e. OEP) is evaluated and aggregated for a defined time period, for example the losses expected per year, per decade or for specific recurrence intervals (e.g. the 1 in one-thousand-year loss).

As with all models, catastrophe models provide an abstraction of real world processes and the suitability and interpretation of the model outputs is determined by the quality and availability of empirical data (i.e. the primary model input), the specialist assumptions and the scientific knowledge on which they are based. The models are calibrated so that the frequency or rate of hazard event occurrence (i.e. how many events occur within a given period) is consistent with the historical record or of a hazard modelling methodology. This enables modellers to evaluate how changes to individual or combinations model parameters, such as the number of buildings within an area or the duration of hazard disruptions, can influence the expected level of loss. This information can be used to implement mitigative measures and to enact management strategies to minimise hazard impacts.

2.3 Quantifying Impact on Transport Infrastructure Networks

2.3.1 Introduction

Section 2.3.1 presents a critical literature review regarding road transportation networks in the UK, key concepts within the fields of transport and network vulnerability research, and the methodologies used to calculate indirect impacts on road networks.

2.3.3 Road Network Vulnerability

Within the past two decades the concept and study of 'network vulnerability' has been of growing interest within the fields of complex networks and transportation research. These efforts are often cited as being in response to an increased awareness of the vulnerability of transport networks and the potential for catastrophic, far reaching socio-economic consequences following events such as the 1994 Northridge, California and 1995 Kobe, Japan earthquakes or the 2001 World Trade Centre, New York terrorist attacks (Boarnet 1996; Berdica 2002; Srinivasan 2002; Murray-Tuite & Mahmassani 2004). In this body of literature there are two prevailing definitions. First, and for studies which often focus on a specific threat, network vulnerability is equivalent to vulnerability in hazard risk assessment - a function of the probability and consequences of a threat (Berdica 2002). In the second definition, network vulnerability is related solely to the consequences of disruption irrespective of any specific threat or its likelihood (Taylor & D'Este 2007). The latter is based on the principle that multiple known and unknown threats exist and which may have a low, unknown or random occurrence probability, yet society may consider the consequences to be unacceptable and worthy of safeguarding against (Evans 1994; Haimes 2006). This definition is also analogous to the concept of 'criticality' and critical-link identification that is now commonplace in operational infrastructure management guidelines (HMEP 2012; Mott MacDonald & Patterson 2014).

Table 2.6 lists several other concepts in transportation network research that are more or less related with network vulnerability. Reliability measures assess the probability of a network to provide a defined level of service or performance (Berdica 2002). Measures of network robustness and resilience compare the relative (un)reliability of two or more sections of transport network with greater robustness and resilience at sections which act to alleviate the impact of disruption (Chen & Miller-Hooks 2012; Dijkstra *et al.* 2014a). Reliability measures include: *Travel Time Reliability* is the likelihood of trip completion within a given time threshold (Bell & Iida 2003), *Capacity Reliability* is the likelihood that the network has sufficient capacity to accommodate the level of demand whilst limiting delay or congestion (Yang *et al.* 2001), and *Connectivity Reliability* considers the number of connections or accessibility between different locations by the probability that a link remains in the event of a disruption (Iida 1999; Chen *et al.* 2007).

	Definition	Cited in:
Risk	Risk is the network disruption probability of occurrence multiplied by its consequences.	(Nicholson & Dalziell 2003)
Reliability	Reliability is the probability that a network will deliver a required level of serviceability or performance	(D'Este & Taylor 2001)
Resilience	Resilience is the networks ability to resist and recover from a disruption.	(Dijkstra *et al.* 2014a)
Robustness	Robustness is the extent to which a network can maintain the function for which it was originally designed	(Sullivan *et al.* 2010)

Table 2.6. Concept definitions used in transportation and network research.

Network reliability and network risk are similar in that they both focus on the probability of occurrence for a disruptive phenomenon. Reliability measures provide information relevant to managing the day-to-day performance of transportation networks and for relatively common disruption phenomena, for instance due to diurnal temporal demand fluctuations (e.g. rush hour) or non-severe, inclement weather conditions (Clark & Watling 2005; Bourne *et al.* 2008; Hooper *et al.* 2014). The short duration and regular occurrence of these disruptions enable relatively thorough assessments of their impacts for instance, by measuring and comparing the travel time or capacity on each road link under various situations.

The limitation of network reliability is that it may obscure potential network problems in large scale national road networks where there is limited understanding and past experience for the impact of certain threats or for events with low and unknown probabilities of occurrence. It is often very impractical and financially infeasible to conduct detailed hazard risk assessment for each threat on large networks and therefore there is the requirement for methods to target resources in order to get the best value from them (Nicholson & Dalziell 2003). D'Este and Taylor (2001) highlighted the limitations of network reliability by considering low probability events on the Australian rail and road networks. Figure 2.8 shows their example for a 1 in 500-year flood event on a section of coastal highway and rail where the measures for travel time and connectivity reliability remain high despite a significant 5,000 km detour which would likely cause significant but unknown socio-economic consequences. Thus, each of these concepts is closely related to one another but studies network vulnerability are most closely aligned with determining the consequences of failure.

Studies of transport network vulnerability (and risk or reliability) follow a similar conceptual framework. The focus of this thesis and the majority of transport network vulnerability studies is on road networks (70%), yet the same basic principles hold for other transport networks such as rail, aviation, shipping or power and gas infrastructure (Wang *et al.* 2014). First, a geometric and topological model of the transport network is constructed in a graph of road links and junction nodes, often with details for link speed, capacity and turn restrictions. Second, a set of hypothetical network disruption events, scenarios or a disruption strategy is selected. Lastly, an impact measure of disruption is defined in order to evaluate the impact of each disruption event before and after its occurrence.

The impact measure is critically dependent on the aim of the investigation, and this in turn influences the representation of the network, its users and demand. For instance, one may

examine the shortest routes and uncongested travel times of emergency responders to certain network locations or consider the routes and congested travel times for groups of road users each with different transport modes, costs, trip origins and destinations. For each stage in this framework a variety of approaches and methods exists, each with varying levels of theoretical and practical trade-offs. In the following sections, each of these stages is discussed.

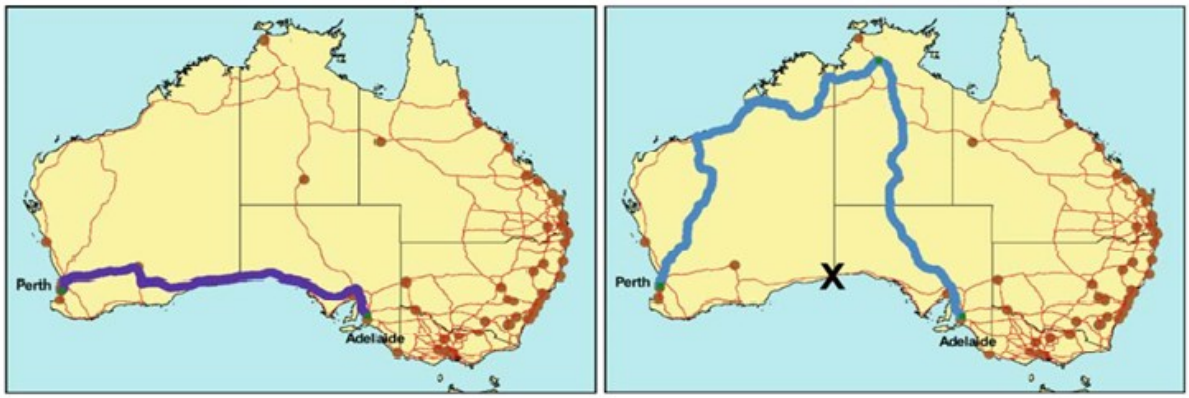

Figure 2.8. The diversionary route following a low probability flood event on the Eyre Highway, Australia after D'Este and Taylor (2001).

2.3.4 Network Definition

Transportation networks are geo-spatial structures located in Euclidean space. A network is comprised of road links and junction node elements that have relative spatial position and to other objects and facilities, such as, engineered assets, natural terrain and populations. As illustrated in Figure 2.9A, at the most basic level a transport network is represented by its topology in a 2-dimensional graph $G(L, N)$ formed by a set road links (L) and a set of nodes (N) in an adjacency matrix. Each row and column in the adjacency matrix describes each how road-link (L_i) is (un)connected to each node (N_i), for instance, the link (L_1) connects N_1 to N_2 and is represented by a 1-digit in the $(x = 1, y = 2)$ and $(x = 2, y = 1)$ matrix positions, whereas a 0-digit indicates that no connection exists from N_4 to N_5. Figure 2.9A is a diagonally symmetric and un-weighted adjacency matrix therefore it assumes that each road-link can be traversed in either direction and at the same cost, which in this case, the cost value per link is 1. The un-weighted adjacency matrix provides the basic topological information about the network such as: node degree, which is the number of link connections incident at each node (e.g. N_1 = 3 and N_5 = 1) and is given by the sum of each row or column in the matrix; or path costs which are the sum of the link weights between a series of nodes (e.g. N_4 to N_3 has a cost of 3 via N_2 and N_1, red arrow).

The realism and detail of network topology models is increased using directional and weighted adjacency matrices. In Figure 2.9B, the black arrows indicate the permitted direction of travel on each link and the cost of traversing each link is now given by weighted links (w^n). The link weights reflect the cost of traversing each link and range from simple 'link-level' measures of distance to (un)capacitated and dynamic weights calculated traffic flow algorithms.

Both the un-weighted and weighted matrices are aspatial, but are readily represented in Euclidean space and maps by assigning coordinates to each node and link. The definition of transport network matrices and coordinates is rarely conducted by hand. Instead, the network topology and weights are derived from national road-highway mapping and GIS data products including OpenStreetMap (OSM) or the UK Ordnance Survey.

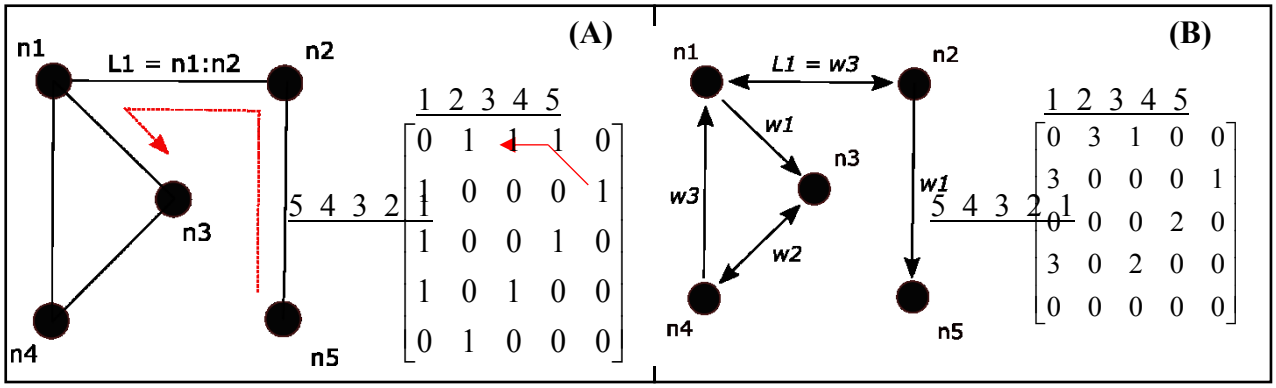

Figure 2.9. (**A**) Adjacency matrix and graph for an un-weighted and un-directed road graph. (**B**) A weighted and directional adjacency matrix and road graph.

2.3.5 Disruption Events

Network vulnerability is the study of disruption events and their consequences. A disruption event is a unique set of conditions which have some disruptive effect on the network including: the time of occurrence and duration; its location and the link effected in the network; the physical effect it has on the weight of the disrupted road link, including complete or partial road-link failure; and the number of road-links that are disrupted simultaneously (and how) in the case of area covering and dispersed disruption events. The inclusion or exclusion of certain disruption events could lead to an incomplete picture of network vulnerability. Therefore, the approach used to determine disruption events is of critical importance and concern for researchers, transport mangers or network analysts whose goal is to identify all relevant network vulnerabilities (Murray-Tuite & Mahmassani 2004; Wang *et al.* 2014; Mattsson & Jenelius 2015). In the review by Murray et al (2008) three different disruption event selection methods were identified which are simulation-, strategy- and scenario-assessments.

In *simulation-assessment*, the full extent of network vulnerability is assessed by exhaustive calculation of all possible disruption events. Simulation adheres to Taylor & D'Este (2007) definition of network vulnerability, which makes no a priori assumption for occurrence probability. The approach provides information for the full range of possible impacts which is used to rank and identify critical-links or events with unacceptable consequences that may not have been identified otherwise (Haimes 2006). However, simulation assessments are often unfeasible for all but small scale road networks and for studies which employ mathematically efficient impact measures such as the disrupted link length or increased path length between nodes in weighted graphs (e.g. in Figure 2.9B). This limitation is a combinatorial problem as

the number of single link disruption scenarios $\binom{n}{1}$ is equal to the total number of links (n) factorial:

$$\binom{n}{1} = \frac{n!}{(n-1)!} \qquad (2.7)$$

Therefore, the total number of disruption events is given by the sum of equation (2.7) for all 1, 2, 3…n combinations. The total number of disruption events soon becomes intractable for even modest size networks. For instance, Matisziw & Murray (2009) note that there are 17 billion possible events in the 24 node 34 link undirected graph of the Ohio interstate highway network, and it would take approximately two years to calculate each of the 39,018 single road-link disruption events using a capacitated traffic model of Chicago's urban road network (Wang *et al.* 2014). For capacitated impact models and measures, the number of disruption events is further increased by considering the potential for partial link closures or reduced serviceability (Sullivan *et al.* 2010). Most simulation-assessments are thus limited to all single link failures on, (i) national scale road networks using graph theoretical and link-level impact measures (D'Este & Taylor 2001; Murray-Tuite & Mahmassani 2004; Jenelius *et al.* 2006a; Jenelius 2009), or (ii) using more computationally intensive, traffic models and system-operation impact measures in small scale and urban networks (Knoop *et al.* 2007; Sullivan *et al.* 2010). Therefore, the potential for compounding impacts due to simultaneous link disruption events is often overlooked. One possible solution suggested in Murray et al (2008), is to examine a representative number of simultaneous 1, 2, 3,… n link failure disruption events in order to get a view for the range of potential impacts and network vulnerabilities.

Strategy-assessment examines the vulnerability of networks in response to a coordinated strategies or sequences of attack (Murray *et al.* 2008), and are often described in terms of 'game theory'. The general approach is to rank each network element using an initial measure of their importance such as the node or link degree (i.e. number connections), average traffic flow or their 'betweeness centrality', which is a measure for the number of paths that depend on a network element (Newman 2003). Then, the most important network elements are disrupted 'attacked' individually or in sequence and the network impact is re-evaluated after each successive attack (Bell 2000; Murray-Tuite & Mahmassani 2004; Bell *et al.* 2008; Yi-Ming *et al.* 2009; Duan & Lu 2014). Conversely, one may disrupt network elements believed to be of low importance until only the critical network elements remain and a certain level of network serviceability is maintained. Strategic-assessment has proved beneficial to identify worst case scenarios and for the study of how varying network topologies (e.g. grids and hub-and-spoke) respond to identical attack strategies (Albert & Barabási 2002; Srinivasan 2002; Murray *et al.* 2008; Wang *et al.* 2013; Mattsson & Jenelius 2015). Indeed, Jordan (2008) reported that the three London Underground stations targeted in the 7/7 2005 bombings were all within the top six most important targets identified using the betweeness measure. A potential disadvantage of this approach is that the not all disruption events are considered and these are themselves determined by the choice for different attack strategies which may be more or less relevant for networks exposed to different threats and in different environmental and socio-political settings.

Scenario-assessment evaluates the network vulnerability by analyzing a finite number of disruption events. Limiting the number of disruption events is achieved by constraining the

analysis to a particular threat or to a particular sub-section of the road network, enabling more computationally intensive impact measures and therefore more detailed vulnerability assessments (Murray *et al.* 2008).

There are relatively few examples of scenario-assessment as the majority of literature concerns the development of suitable network models and impact measures (Wang *et al.* 2014). Nonetheless, hazard and risk analysis provide suitable conceptual frameworks and tools (Chapter 2.7) that can be applied in order to select disruption events and constrain network vulnerability assessment to specific threats. Examples include: link-level impact measures for single link disruption events on national road networks subject to earthquakes (Khademi *et al.* 2015), severe wind storms (Nyberg & Johansson 2013) landslides (Meyer *et al.* 2015), sea-level rise (Demirel *et al.* 2015) and urban flooding (Green *et al.* 2017); and system operation measures for urban road networks subject to flooding (Dawson *et al.* 2011; Pregnolato *et al.* 2016). Alternatively, the scenario-assessments are constrained to disruption events which occur on a particular road link and the impact is constrained to the local diversionary links which form a sub-section of the larger network. For example, Dalziell & Nicholson (2001) assess disruption events due to snow, flooding, severe wind, earthquake and volcanic eruptions on the State Highway 1 'Desert Road', New Zealand, whereas the impact of local traffic diversions due to landslide hazards are evaluated in the Swiss Alps by Voumard et al (2013) and in Scotland by Winter et al (2014). Scenario-assessments provide detailed understanding for the ramifications and of the ways in which particular threats interact with transport networks. However, as in strategic-assessment, a potential disadvantage is that network vulnerability is assessed only in relation to the disruption events identified allowing potential vulnerabilities to go unnoticed (Murray *et al.* 2008). Moreover, the relative impact and criticality of disrupted links is constrained to the type of events identified and, in the case of local diversion or sub-networks, only for the links included in the network model.

2.3.6 Network Impact Measures

As indicated, in recent decades there has been increasing interest in network vulnerability from researchers within the fields of complex networks, transportation, and systems optimisation. As a result there are two distinct types of impact measure (Murray *et al.* 2008; Wang *et al.* 2014; Mattsson & Jenelius 2015). First, there are 'link-level' measures which use static values of the level of transport demand, topological and spatial properties networks, such as, connectivity, shortest path distances and daily average traffic counts, calculated using abstract road graphs formed by weighted and un-weighted adjacency matrices. The second are 'system-operation' impact measures. System-operation seek to measure impacts from the perspective of entire groups of transport users and are therefore based on the interactions that occur between factors related to network capacity and supply and the factors related to traffic demand and user cost.

As described in detail below, both link-level and system-operation approaches include impact measures and different techniques to calculate additional travel time. Measures of additional travel time provide the most suitable network impact measure as, (1) additional travel time reflects the concerns of both transport users and operators, (ii) travel time is readily converted to economic losses by values for user generalized-cost, and (iii) travel time takes account of different speeds and demands allowing comparisons for the relative performance and efficiency of individual links and different networks with contrasting topologies and levels of demand

(Berdica *et al.* 2003; Scott *et al.* 2006; Qiang & Nagurney 2008; Tampère *et al.* 2008; DFT 2014a).

Link-level measures:

Link-level measures include those which describe the relative criticality (importance) of individual network nodes and links based on their connectivity. The *degree* of a node (or link) is a measure for the number of connections it supports to other nodes within the network. For example, in well-connected urban grid networks, each node has relatively equal degree and number of connections to its neighbours. Conversely, for networks that have random or hub-and-spoke topology (e.g. railways and supply chains) the hub node(s) have relatively high degree, and are therefore critical, as they offer the only connection point between otherwise unconnected nodes (Watts & Strogatz 1999; Albert & Barabási 2002; Newman 2003). *Gamma index* is a network-wide measure of connectivity, it is the ratio between the actual number of links between network nodes of the network and the total number of links when all nodes are completely connected to one another (Scott *et al.* 2006). *Gamma index* provides a measure to compare the relative connectivity of different networks ranging from 0 (no connections) to 1 (fully connected).

Many link-level measures are related to the number and the distance of paths (routes) between pairs of nodes. In un-weighted networks, the shortest-path is the least number sequence of links connecting two nodes. In weighted networks, the shortest-path is the link sequence with the minimum sum of link weights between nodes, such as the link lengths. Comparing the minimum, mean or maximum shortest-paths of different networks provides another indicator of overall network connectivity (Newman 2003). *Betweeness centrality* is a measure for the number of shortest-paths that utilize each link, thus indicating the relative importance of each link by the number of shortest-paths it supports (Albert & Barabási 2002; Mattsson & Jenelius 2015). *Cut-links*, are road links which provide the only, therefore also the shortest, path to certain nodes. When a disruption event severs a cut-link, the node is no longer connected to or reachable from any other node within the network. Several authors note that cut-links and those featuring high Betweeness centrality are the most important links for maintaining connectivity in strategic-assessments of disruptions on urban road transport networks (Porta *et al.* 2006; Demšar *et al.* 2008; Duan & Lu 2014) and for scenario-assessments of urban flooding (Pregnolato *et al.* 2016).

A great deal of research has been conducted for the identification and optimization of shortest-paths (Pallottino & Scutell 1998). Some of the earliest and most notable contributions were those of efficient shortest-path algorithms by Dijkstra (1959), and their application by Garrison (1960) who examined link disruptions on the US interstate highway network which led to the largest increase in the shortest-path distances between pairs of major cities. For a vehicle travelling within an un-capacitated network (no other vehicles), one can infer a simple estimate of increased travel time by knowing the detour distance and the approximate speed of travel based on the free-flow speed (e.g. road speed limit). Therefore, in some cases, examining shortest-path distances with free-flow speeds provides a sufficient measure of network vulnerability. For instance, consider emergency responders, their primary concern is for network connectivity or 'accessibility' as they travel relatively unimpeded and regardless of other road users, congestion and costs of travel (Taylor & D'Este 2007). Therefore, the most vulnerable, conversely most critical, links are those where a disruption event causes a cut-link

or a detour that dramatically increases the travel distance and time between origins (e.g. police, fire or ambulance stations) and destinations (e.g. vulnerable populations, schools or hospitals).

This approach has been applied to examine travel distance-time between urban centres in simulation-assessments of all single link disruption events in national road networks (D'Este & Taylor 2001; Taylor & D'Este 2007) and in scenario-assessments of road networks susceptible to earthquakes (Sohn *et al.* 2003; Peeta *et al.* 2010) and flooding (Sohn 2006). In Sweden, Nyberg & Johansson (2013) consider the accessibility of O-D pairs for emergency responders and elderly populations residences under road disruption events caused by felled trees during severe wind storms, and Green et al (2017) consider similar situations and develop contingency plans for emergency responders during flood events in the city of Leicester, UK.

The additional travel time provides a holistic, system-operation based vulnerability measure (Murray *et al.* 2008; Wang *et al.* 2014; Mattsson & Jenelius 2015). For link-level assessments, these are based on the same shortest-path, free-flow speed and travel time calculations as above, but with additional information for traffic volume. Traffic volume is often represented by the sum or average traffic count measure on a link.

In Norway, Meyer et al (2015) assessed network vulnerability to landslides using a measure of displaced traffic flow distance (vehicle km day^{-1}), given by the shortest-path detour (km) connecting the start-end nodes of a disrupted link multiplied by its daily average traffic volume (vehicles day^{-1}). As illustrated in Figure 2.10A, this approach may underestimate the additional travel time by assuming that detours only occur around the disrupted link (links a,d,e and c), whilst shorter routes may be available (link f). A similar approach and traffic displacement measure is adopted in single link simulation-assessment by Jenelius et al (2006), however, using the shortest-path distances of trips between population O-D zones derived from a national transport model in Sweden (Beser & Algers 2002); illustrated by the blue nodes in Figure 2.10A. On busy links, traffic volumes are in the order of 10,000 to 35,000 vehicles per day but are much lower 500 – 2500 on the majority of links (Jenelius *et al.* 2006b; Meyer *et al.* 2015). For this reason, un-capacitated travel time is assumed using the function of distance and free-flow speed, enabling the use of simpler and faster shortest-path algorithms (Dijkstra 1959), but irrespective of traffic volume, link capacity and the potential for congestion.

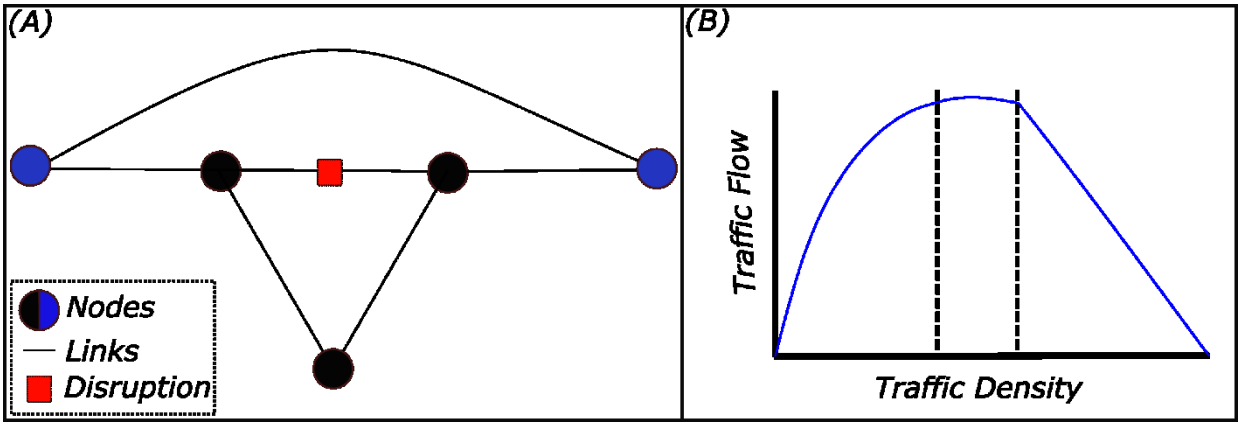

Figure 2.10. (**A**) Abstract road graph showing the link weights (a4, b2) and two methods for defining the shortest-path around a disrupted road link (red box). (**B**) A plot showing the road link traffic-flow relationship for capacitated network conditions.

Though lacking a generally accepted formal definition, link capacity is a measure for the physical space available on a road link to accommodate vehicles, such as the width and number of lanes (DFT 1999). However, link capacity is also time dependent, as vehicle speed increases the capacity of a road link is reduced as a greater proportion of the link area is occupied per unit of time. Figure 2.10B shows the density-flow relationship for a single road link where: at low traffic density there is spare road capacity and traffic flow can adhere to the link free-flow speed; synchronized-flow occurs when the maximum number of vehicles are travelling at the free-flow speed and spare capacity is limited; and as traffic density increases, vehicle speed is reduced leading to travel delay and congestion on links (Ortuzar & Willumsen 2011). As a result, delay and congestion can develop in even low to moderate traffic flow conditions if there is limited or reduced road capacity (Berdica *et al.* 2003; Bourne *et al.* 2008; Notley *et al.* 2008). Several authors have attempted to resolve this issue using link-level capacity measures in order to define the spare capacity on individual links and to sum these values across detour shortest-paths with other measures for: the link flow-density relationship, and the time needed to fully congest a link (Murray-Tuite & Mahmassani 2004; Taylor & D'Este 2007; Tampère *et al.* 2008; Knoop *et al.* 2012; Watling & Balijepalli 2012). However, empirical estimation of link capacity using point source traffic count data is non-trivial as link-level traffic flow and density is significantly affected by the traffic flow and capacity conditions on upstream and downstream links within a network (Minderhoud *et al.* 1997). In addition, for disruption events that displace a large proportion of traffic flow the detour shortest-path may lack sufficient spare capacity leading to widespread changes in route choice, traffic displacement and cascading congestion effects (Cascetta 2001; Knoop *et al.* 2008, 2012; DFT 2014b; Mattsson & Jenelius 2015; Peeta *et al.* 2015). Un-capacitated link-level travel time impact measures may therefore underestimate additional travel time, cost and thus network vulnerability.

System-operation measures:

System-operation impact measures are based on time discretized model simulations of traffic flow in capacitated networks (Berdica 2002). Transport models are generally created in a four-

step process: (i) trip generation determines the level of travel demand between O-D zones based on population demographics and social or economic factors; (ii) trip distribution portions the travel demand into distinctive O-D node trips within the network; (iii) mode choice allocates a proportion of O-D trips to specific modes of transport; and (iv) route assignment determines which path, therefore time and cost, is taken by each trip (Ortuzar & Willumsen 2011; Peeta *et al.* 2015). Ortuzar & Willumsen (2011) define these models as 'a simplified representation of a part of the real-world system of interest, which focusses on certain elements considered important from a particular point of view'. Models are therefore both problem and perspective specific. For instance, the construction of rail link between two previously unconnected locations requires detailed assessment of the present and expected future trip demand, the proportion of trips that will utilize the new link, and how these new trips and routes will interact with the route choices and travel costs for all other modes of transport available between the locations (Burton 2010; DFT 2014a). In the case of transport network vulnerability studies, the primary aim is to provide network wide measures of additional travel time as disruption events represent time discrete and short duration road closures typically lasting ≤ 1 day, or daily values are summed for the duration of an event lasting one or more days (Voumard *et al.* 2013; Winter *et al.* 2014; Meyer *et al.* 2015). Therefore, it is assumed that disruption events necessitate a recalculation of mode choice and route assignment, but are short enough to have little effect on longer term trip generation and trip distribution (Berdica 2002; Murray *et al.* 2008; Wang *et al.* 2014; Mattsson & Jenelius 2015). Instead, transport demand, trip generation and trip distribution is based on predefined O-D matrices for each transport mode derived from a variety of sources including census, travel survey, traffic count or national traffic model data provided by national statistics bureaus and road authorities (Beser & Algers 2002; Murray-Tuite & Mahmassani 2004; Taylor & D'Este 2007; Kraan *et al.* 2008; ONS 2011a; DFT 2015b). A major benefit to the transport model approach is that simultaneous link disruption events are readily evaluated (Murray *et al.* 2008). Multi-modal modelling is in its relative infancy (Krajzewicz *et al.* 2012; Burgholzer *et al.* 2013; Wang *et al.* 2014), therefore most investigations focus on individual transport modes and the selection of suitable route assignment procedures.

Real world traffic flow and its representation in modelled route assignment are each an attempt to optimize the equilibrium between transport utility over transport cost (Glaister & Graham 2006; Bourne *et al.* 2008; Burton 2010). Wardrop & Whitehead (1952) propose two principle conditions that formalize the notion of equilibrium within road transportation networks. First, 'user equilibrium' (UE) states that drivers act in a 'selfish' manner selecting a path through the network that minimizes their own personal cost of travel. UE is generally accepted as the most appropriate principle to model the day-to-day behaviour of road users in capacitated and congested networks (Ortuzar & Willumsen 2011; Peeta *et al.* 2015). At UE conditions, traffic flow is arranged in such a way that no individual vehicle can reduce its own travel cost by altering its path or route, thus capturing any cascading congestion effect due displaced traffic. Moreover, although a complete UE state is unlikely to arise in reality due to aleatory uncertainties, including human behaviour, weather or other factors effecting road capacity, UE models provide a 'best case' user response to disruption events and therefore provide an approximate minimum estimate of additional travel time for vulnerability studies (Berdica *et al.* 2003; Scott *et al.* 2006; Knoop *et al.* 2012; Wang *et al.* 2014; Mattsson & Jenelius 2015). Wardrop & Whitehead's (1952) second principle is 'system optimal' equilibrium (SOE), stating that drivers act cooperatively in order to minimize the system wide travel time at the expense

of individual efficiency, arising in organized traffic flows such as autonomous vehicle, rail and urban metro transport systems. SOE assignments can be applied in order to realise the potential benefits of managed traffic flow, including, SOE conditions for lowering transport greenhouse gas emissions (Nagurney *et al.* 2010).

To achieve UE conditions, models follow an iterative procedure whereby the O-D trip paths and link weights are calculated using a shortest path algorithm, such as Dijkstra's (1959), and these are then updated and recalculated in successive iterations until no further decreases in trip travel times are achieved. Additional travel time is defined as the increase in UE travel time between the un-disrupted and disrupted network (Berdica *et al.* 2003; Scott *et al.* 2006; Murray *et al.* 2008; Wang *et al.* 2014; Mattsson & Jenelius 2015). There are several variations of UE assignment relating to the technical aspects of different traffic models, including, the representation of time, spatial resolution and path uncertainty. These can be broadly categorized according to increasing model complexity and required computation time as follows.

Macro-simulation UE models are computationally efficient as they formulate the traffic flow-density relationship using aggregated components of vehicle quantities on links, and are comparable to the modelling of fluid flows. Moreover, these models are temporally discretized by a single time-step for the model period, typically 24 hours, and the vehicle paths, link weights and costs are only updated after each successive iteration. As a result, additional travel time delay due to congestion which spills onto multiple links may be underestimated (Berdica *et al.* 2003; Knoop *et al.* 2007, 2008). Macro-simulation UE models have been used to assess network vulnerability on: conceptual road networks (Scott *et al.* 2006), national road networks (Dalziell & Nicholson 2001; Jenelius *et al.* 2006a; Kraan *et al.* 2008; Erath *et al.* 2010), urban scale networks (Berdica *et al.* 2003; Berdica & Mattsson 2007; Issacharoff *et al.* 2008; Sullivan *et al.* 2010; Pregnolato *et al.* 2016) and for individual links with specified diversions (Tampère *et al.* 2008; Winter *et al.* 2014).

In meso and micro-simulation models, the link flow-density relationship is calculated for individual vehicles and the vehicle paths, link weights and costs are updated periodically at multiple time-steps within each iteration. Meso-simulations allow for aggregated and efficient computation of vehicles passing link junctions and intersections whereas in micro-simulation models, these are modelled explicitly, including, traffic control signals and turning priorities. Link congestion is taken into account by the regular updating of travel paths and costs (Berdica *et al.* 2003; Peeta *et al.* 2015). Given the increased number of computations, these models are typically created for periods of peak demand, lasting 1-12 hours, and with time-step intervals in the order of 1 second to 10 minutes (Ortuzar & Willumsen 2011; Krajzewicz *et al.* 2012). Such models are sub-categorized according to the information used to update vehicle paths at each time-step. In Dynamic User Equilibrium (DUE), vehicle paths are updated according to the link weights calculated at each time-step. Therefore, in DUE, road users have perfect knowledge of the network conditions at each time-step, degrading between time-steps, and is analogous to modern in-car navigation systems and intelligent-transport-systems which inform drivers of the shortest route according to network congestion (Burghout *et al.* 2006; Knoop *et al.* 2007; Burgholzer *et al.* 2013). In Stochastic User Equilibrium, vehicle paths are updated at each time-step according to link weights based on probability distribution in order to account for driver uncertainty of network conditions, for instance, high uncertainty during sudden

disruption events caused by terrorism (Murray-Tuite & Fei 2010; Mattsson & Jenelius 2015) or urban flooding (Dawson *et al.* 2011; Lu & Peng 2011).

Berdica et al (2003) compare macro, meso and micro DUE models for simulation-assessment of single link disruption events in a small urban network and varying levels of traffic demand. Berdica et al (2003) note that the impact disruption events varies significantly according to model used. Whilst computational efficiencies are achieved through macro-scale DUE models, the resulting levels of disruption are found to be higher in the meso and micro models due to increased traffic queuing, flow displacement and spillback (congestion) onto other links. Knoop et al (2008) conduct similar assessments evaluating the effect on travel times calculated by DUE micro-simulations with fixed or flexible-route-choices and spillback or non-spillback conditions in the city of Rotterdam, Netherlands. With fixed-route-choice, spillback leads to a 6.6 factor increase in travel times compared to the non-spillback model, whereas with flexible-route-choice, the increase due to spillback is only 2.3 times greater than in the non-spillback model. Consequently, most network vulnerability studies employ meso and micro-simulation DUE models which include consideration for flexible route choice and congestion, including for disruption events on individual links with specified diversions (Voumard *et al.* 2013) and for link disruptions in urban networks (Burghout *et al.* 2006; Knoop *et al.* 2007; Qiang & Nagurney 2008; Nagurney *et al.* 2010; Sullivan *et al.* 2010; Burgholzer *et al.* 2013). However, these are yet to be applied to assess impacts and network vulnerability in larger scale, national road transport networks.

2.4 Summary of the Literature Review and Research Gaps

The literature review has provided an in-depth discussion of the issues and present level of understanding of landslide activity in the UK, landslide hazard and risk analysis, and evaluating the indirect impact of landslides on road transport networks. The key findings and research gaps are summarised below.

The literature review began by considering the processes and distribution of landslide activity in the UK and the issues they cause on transportation infrastructure, finding that:

- The direct and indirect impact of landslides represent significant economic losses that are in the range of tens of thousands to tens of millions of pounds per single event. For several high-profile events in recent years, the estimated economic loss due to road and rail transport disruption has far exceeded those caused by direct physical damage. These impacts therefore represent a significant proportion of total hazard risk which is largely unaccounted for in state-of-the-art hazard risk assessment. In addition, identifying the critical network segments where the potential for indirect impact is most severe is therefore a strategic priority for the national governments in Scotland and the UK.
- A high proportion of the UK's strategic transportation networks are situated in locations considered to be of heightened landslide susceptibility. In Scotland, and other upland regions, the threat of landslides effecting road networks is particularly severe as the availability of alternative transport routes and modes is relatively limited. Shallow translational landslides and debris flows (hereafter 'landslides') are the dominant failure mechanisms these regions.

- Most of the reported landslides have occurred following periods of prolonged or intense rainfall and in locations that feature landscape characteristics that are known to be associated with heightened landslide susceptibility.
- The literature review has identified several empirical analysis techniques that can be applied to quantify and model the landslide potential at scales relevant for national infrastructure management. These include landslide susceptibility modelling and threshold analysis. Using these techniques, it is possible to develop a modelling framework that can be used to systematically evaluate the present-day landslide hazard, and the risk of indirect impacts due to transport network disruption.

The methods used to evaluate landslide hazard were investigated in detail. It was found that:

- Risk assessment provides a suitable framework to evaluate the combined effect of landslide hazard and impacts on transport networks.
- Physically-based-models (PBMs) provide detailed hazard analysis based on the modelling of physical processes and with specific parameter values, including, slope angle, the geotechnical properties of soils and the location of potential shearing surfaces. However, PBMs require large quantities of high resolution and detailed data that are generally unavailable at scales applicable to national scale infrastructure networks.
- Logistic regression has been identified as a suitable method to model landslide susceptibility. The most significant input variables are for the slope: elevation, angle, aspect, curvature, lithology, drainage and land-use. The use of hydrological terrain units, including hillslopes and gullies, and slope roughness indices has proven beneficial for the identification of debris flow deposits in other fields, but are yet to be applied for landslide susceptibility assessment.
- Landslide initiation thresholds can be used to provide the conditional probability of landslide occurrence for various sequences of triggering and antecedent rainfall conditions. Nonetheless, current thresholds are influenced by the subjective selection of rain event criteria, the number of rain events and the use of selection techniques that do not consider non-landslide conditions. As a result, threshold values may be biased and the reported probabilities do not adhere to the assumption of uniformity in hazard risk assessment models.
- To be of use, initiation thresholds must be derived using rainfall records characteristic of the conditions at each landslide site and the effect of record length must be evaluated.
- For a landslide risk assessment, the landslide hazard can be determined by combining the landslide susceptibility and the initiation thresholds to produce a spatio-temporal probability of landslide occurrence. This technique is applicable at scales spanning tens to hundreds of square kilometers, and thus is suited to assessments of large infrastructure networks.

The methods used to quantify network impacts were investigated, focussing on conceptual models and techniques used to evaluate the effect of disruptions on road transport networks. It was found that:

- Studies of network and transport vulnerability offer suitable conceptual frameworks to evaluate transport impacts. Whilst most studies consider the topological weaknesses of networks, scenario-assessments are focused on specific hazard and disruption events are therefore applicable to studies of landslides on transport networks.

- In transport planning and appraisal, the economic outcomes of changes to transportation supply or demand are evaluated by combining measures of additional travel time with monetary values of transport user generalized-cost.
- Link-level impact measures indicate the relative importance of individual links and nodes based on their level of connectivity and position within the network. Link-level calculations of additional travel time are applicable for un-capacitated travel conditions.
- More realistic, system-operation impact measures of additional travel are calculated using dynamic user equilibrium (DUE) traffic flow models. These models consider the interactions between link capacity, user demand and route choice which have been shown to have a large influence on system wide travel times in urban road networks.

Based on the above assessment of the literature review and the research gaps identified the proposed approach is to:

- Develop and apply a logistic regression analysis to identify the terrain characteristics associate with increased landslide activity and to model the landslide susceptibility of hillslopes adjacent to the highway network.
- Develop and apply a dynamic user equilibrium traffic simulation model to calculate the indirect impact of network disruptions.
- Develop landslide initiation thresholds using normalised radar rainfall data that characterize the rainfall conditions associated with landslide occurrence and to estimate their likelihood.
- Develop a catastrophe model to evaluate the risk due to indirect impact of landslide on traffic. The hazard module will be driven by landslide hazard derived from the combination of the results of the landslide susceptibility and initiation threshold assessments.

Chapter 3 Methodology

3.1 Introduction

3.1.1 Overview and justification of the method

The aim of this thesis is to develop a method to systematically quantify and evaluate the indirect impact of landslide hazards on a national highway network. To achieve this aim A literature review was conducted to evaluate the present state of knowledge (Chapter 2) and to inform the development of a methodology to: evaluate the spatial distribution and susceptibility (or proneness) of the terrain to potential landslide hazards; to quantify the rainfall conditions, and their likelihood, that are most commonly associated with landslide occurrence; to develop a model that can calculate the impact of landslides on road transportation at the national scale (i.e. the objectives in section 1.2). These constitute three components of novel research conducted for this thesis (Chapters 3.2, 3.3 and 3.4). They are combined to produce a fourth component, that is, to demonstrate a catastrophe model that estimates the potential losses due to landslide travel disruption (Chapter 3.5). Conceptually, it is convenient to consider how these four components of research and their methods fit together within the context of the simplified hazard risk formula (e.g. $Hazard \times Consequence = Risk$). First, the landslide hazard is determined by combining landslide susceptibility with the initiation thresholds (i.e. section 3.2 and section 3.3). Second, the consequence is determined using the traffic simulation model (i.e. section 3.4). Third, the hazard and consequence are combined to evaluate the landslide risk (i.e. section 3.5). Figure 3.1 is a schematic illustrating how each of these components are linked together. Figure 3.1 schematic shows the raw and primary data sources used in the study and how these are processed and analysed, the arrows and boxes indicate the transition and flow of data through each component of the thesis.

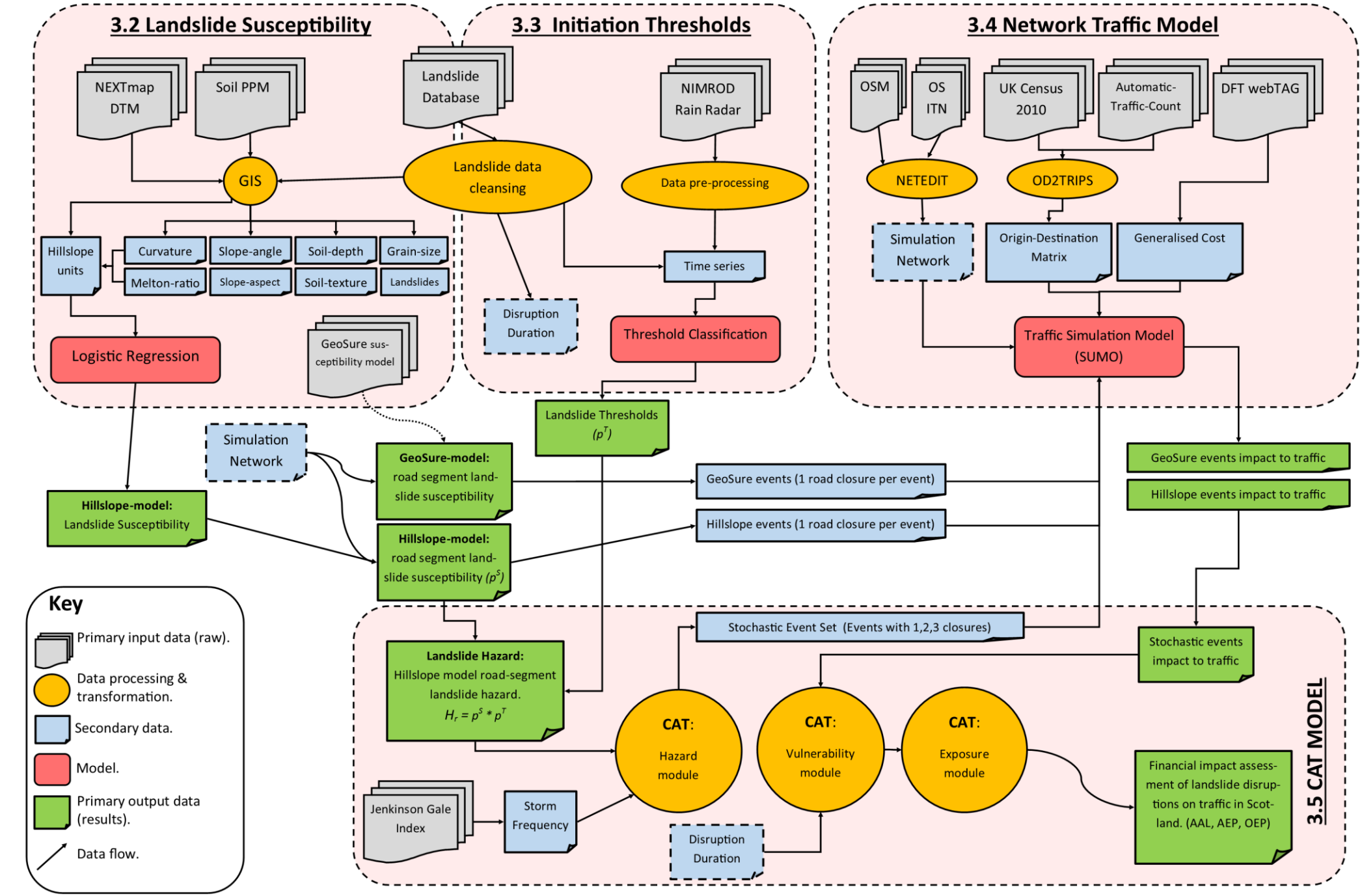

Figure 3.1. Conceptual framework of the method used.

To assess landslide susceptibility (Chapter 3.2), the general approach is to use logistic regression to model the landslide susceptibility of areas adjacent to a highway network. Logistic regression was identified as suitable method in the literature review (Chapter 2.2.4). The modelling approach enables the evaluation of each explanatory variables contribution to increased or decreased landslide susceptibility, such as the slope angle, elevation, aspect, superficial lithology and proximity to roads. This information makes it possible to identify the most active landslide processes and to map the relative landslide potential (i.e. spatial probability) in different locations and at scales relevant to national infrastructure networks. Though logistic regression is widely used for landslide susceptibility modelling, several research gaps were identified that need to be addressed to achieve the aim and objectives of this thesis.

- First, a selection of suitable explanatory variables need to be identified for the study area. Although a list of relevant candidate variables is provided in the review of previous studies (Chapter 2.2.4), this study requires an independent evaluation to account for the availability and quality of input data, the landslide mechanisms, and the landscape and terrain characteristics that are unique within each study area.
- Second, the review of literature identified that the Melton Ratio terrain roughness metric has been successfully applied in hydrological investigations to differentiate hillslopes and gullies that are likely (or unlikely) to produce landslides with flow components, such as debris flows (Wilford *et al.* 2004; Welsh & Davies 2011). Despite this, the metric and hillslope and gully terrain units are yet to be applied in landslide susceptibility modelling. As there are multiple size criteria that may be used to define these terrain units, the performance of susceptibility models that use these different units needs to be systematically investigated.
- Third, most landslide inventories are known to exhibit recording biases since most landslides are reported when they have had some interaction with the built environment, such as on roads (Malamud *et al.* 2004; Kirschbaum *et al.* 2015). To limit the influence of this bias, the models are developed using only the terrain units and landslide records that are found adjacent to the road network. This approach improves the reliability and relevance of the model in the areas of interest (i.e. on the road network). However, this is at the expense of increased uncertainty if the model were to be applied in other areas, such as on new roads or hillslopes away from the road network.

In section 3.3, a set of empirical landslide initiation thresholds are developed. The literature review established that for landscapes where rainfall is a dominant factor, and other contributing factors such as land use remain relatively constant, it is reasonable to use empirical thresholds, and the conditional probability of threshold-landslide occurrence, to quantify the rainfall conditions in which the hydro-geological responses are sufficient to result in the triggering of a landslide (Caine 1980; Van Asch *et al.* 1999; Waltham & Dixon 2000; Pennington *et al.* 2014). Empirical and probabilistic rainfall thresholds have been shown to be of particular practical use for: examining the hydrological processes and conditions conducive to landslide initiation (Brunetti *et al.* 2010; Segoni *et al.* 2014b; Abancó *et al.* 2016); determining the likelihood and return period of landslide triggering conditions (Chleborad *et al.* 2008; Berti *et al.* 2012); and early warning systems that consider forecast weather conditions several days in to the future (Martelloni *et al.* 2013; Segoni *et al.* 2015a).

In recent decades several different threshold selection techniques have been developed including methods to objectively choose the thresholds that provide the highest predictive accuracy (Jakob & Weatherly 2003; Staley *et al.* 2013; Segoni *et al.* 2014b, 2015a; Giannecchini *et al.* 2016; Piciullo *et al.* 2016). Based on a review of past studies (Chapter 2.2.5) it is evident that the threshold values and their probabilities are likely to be influenced by several factors of uncertainty that restrict their wider use, such as in landslide hazard assessments and in early warning systems (Guzzetti *et al.* 2008; Kirschbaum *et al.* 2012). These factors are addressed in this thesis:

- First, many thresholds are derived by analyzing the rain events that co-occur or do not occur with landslides. However, there is no common or agreed criteria to define these events and there is little consistency between the approaches adopted in the literature (Chapter 2.2.5). Alternatively, thresholds may be based on an analysis of time series data to avert this issue by including all available rain information at the expense of greater numbers of time periods without landslides (Chleborad *et al.* 2006, 2008).
- Consequently, the second factor is related to the type and length of the rain record used. Increasingly, thresholds are derived using remotely sensed data, including by high resolution satellite (Hong *et al.* 2006; Kirschbaum *et al.* 2012) and weather radar systems (Winter *et al.* 2010; Marra *et al.* 2014; Abancó *et al.* 2016). These spatially continuous observations provide a site-specific-rain record (SSR) at each landslide location. This is beneficial in the study of landslide initiation thresholds due to high spatial variability of rainfall, particularly in mountainous terrain (Sidle & Ochiai 2013). The use and length of these SSR can lead to a significant increase in the number of days without landslides and so places an additional influence on threshold selection, particularly, the sensitivity of threshold values and their occurrence probabilities. These effects are yet to be systematically evaluated for different threshold selection techniques.

In section 3.3, thresholds are derived using radar SSR time series, as applied to gauge records and by Chleborad *et al* (2008). A receiver operating characteristic (ROC) analysis is used to select two types of threshold. First, 'threat score' (TS) is used to select the threshold that offers the greatest level of predictive accuracy and minimizes false results (Staley *et al.* 2013). Second, the 'optimal point' (OP) threshold is selected to provide the highest rate of landslide detection for the lowest number of false results. OP is yet to be applied to landslides, but is common in other disciplines for the detection of rare phenomena, including disease and signal processing (Schisterman *et al.* 2005; Perkins & Schisterman 2006a; Rota & Antolini 2014). For each threshold, the effect of varying the SSR record length is systematically evaluated using 10 different record lengths representative of those implemented in past studies. The coefficient of variance quantifies the relative sensitivity of the thresholds. The adopted approach is the first to demonstrate the threshold sensitivity in relation to changes in the rain records used.

Section 3.4 of the methods chapter details the development of a traffic model that can calculate the indirect impact of network disruptions. The rationale and benefits of such models are discussed in the literature review (Chapter 2.3) and summarised here. Road transport networks are continuously exposed to weather driven hazards including landslides (Jaroszweski *et al.* 2010). The economic impact of these hazards is accrued by direct physical damage or by indirect impacts and disruptions to network operation, such as travel delays, costlier routes and reduced accessibility to vital services. Due to the indirect impacts, the effect of landslide

hazards and population exposure is distributed far beyond the hazard's physical location. A poignant example is the estimated £2.6M regional economic losses incurred in the West Midlands, UK due to the 40 hr closure on the M1 motorway following a storm flood event in June 2007 (Chatterton *et al.* 2011; Dawson *et al.* 2016b). Critical network segments are those characterised by a high consequence of failure generally irrespective of the likelihood of failure (Kaplan *et al.* 1981; Murray *et al.* 2008). The identification of critical segments is integrated within network management guidelines (HMEP 2012; Mott MacDonald & Patterson 2014). However, current assessments are limited to static indicators of, for example, road segment classification and the long-term average traffic flow (Jenelius *et al.* 2006b; Sullivan *et al.* 2010; Nyberg & Johansson 2013). These assessments do not capture the traffic flow element of transport systems. Consequently, they fail to capture the potential for cascading and propagating disruption effects where network serviceability is reduced across a wide area, for instance by increasing congestion and travel time on alternative routes (Knoop *et al.* 2008; Mattsson & Jenelius 2015). At present, there is a lack of analysis techniques and models that can be used to pre-emptively identify the network segments (or the hazard events) that have the potential to generate high indirect impacts on national scale infrastructure. This was identified as a key priority in the 2017 UK Climate Change Risk Assessment (Krebs 2017).

To evaluate the indirect impact of landslide hazards, a road network traffic model at peak flow conditions is developed. The model is developed using Simulation of Urban Mobility (SUMO), an open source, meso-microscopic and time continuous traffic simulation software package developed by the German Aerospace Center - Institute of Transportation Systems (Krajzewicz *et al.* 2012). The SUMO software is executed from the command line and includes all applications for running the simulation and handling input and output files. The online documentation provides comprehensive guidance on developing traffic simulations using SUMO. In addition, the approach follows guidance set out in the UK Department of Transport website Transport Analysis Guidelines 'WebTAG' (DFT 2014a). The development of the SUMO model follows: i) to define the road transport network, ii) to generate the network demand using Origin-Destination matrices, iii) to develop a road transport model to simulate the network traffic flows, iv) create a set of network disruption events, and v) to measure the impact of each event on the road transport system.

Section 3.5 details the steps taken to produce a prototype catastrophe. As set out in the literature review (Chapter 2.2.8), catastrophe models (also termed 'hazard risk models') are primarily used within the insurance industry to produce probabilistic assessments of natural hazard risk and to estimate potential losses. Though they have been applied to assess risk for a number of different hazards, such as property damage from flooding and hurricanes, this is a first application of the approach to evaluate the indirect impact of landslides (a hazard-network catastrophe model). The absence of such models is primarily due to: one, the challenges associated to assessing the level of the landslide hazard across large and expansive infrastructure networks; and two, the lack of available techniques that can be used to calculate indirect impacts for a large number of potential hazard events.

The catastrophe model developed here illustrates how these issues may be addressed and provides a basic modelling framework for future studies. The landslide hazard is determined by combining the landslide susceptibility and the initiation threshold assessments (Chapters 3.2 and 3.3). The landslide hazard represents the spatio-temporal probability of landslide occurrence as defined by equation 2.6 (Guzzetti *et al.* 2005) and is used to generate many

stochastic events (the event set). The landslide hazard used to generate the event set is based on the analysis of landslides for the period 2004 to 2016, and so the modelled events can be interpreted as producing multiple different realisations of the conditions that occurred in this period. Based on the premise that the conditions that caused landslides are unlikely to vary significantly in the short term, the event set can be construed as a list of potential landslide scenarios that may occur in the future. The model then uses the traffic model (Chapter 3.4) to evaluate the economic impact of each of event by its disruption to traffic.

3.1.2 Case study area

The aim and objectives of this thesis are to quantify the indirect impact of landslide hazards on a national scale highway network. As established in the literature review and the text above, landslide susceptibility modelling and initiation thresholds are to be used to evaluate and assess the landslide hazard on a large scale and expansive highway infrastructure network. These empirical methods utilise historical records and observations to improve understanding of the landslide processes involved in the past and these are then used to inform expectations for the future. Though empirical models provide insight and knowledge of the fundamental landslide mechanisms and processes, and that are applicable in other landslide prone regions around the world, the models are specific to the local conditions on which they are based (Carrara *et al.* 1995; Chau & Chan 2005; Glade *et al.* 2005; van Westen *et al.* 2006). Consequently, a case study area with data of past landslide occurrences is required to develop and validate these model's.

Suitable case study areas will feature the following basic characteristics:

- Detailed observations and data of historic landslide activity including, time of occurrence, location, and the landslide mechanisms involved.
- High resolution and timely data for landslide susceptibility and initiation variables, such as, digital elevation models, superficial and bedrock geology, and precipitation.
- A highway road network and sufficient origin-destination and traffic counting data to construct and validate a traffic simulation model.

In addition to fulfilling these criteria, pragmatically, Scotland was selected as a case study as it offers a unique research setting and several methodological advantages.

First, the impact of landslides in Scotland is primarily due to a limited number of landslide mechanism and this constrains the complexity of the study and limits the number and variety of analyses required. The study area is characterized by post-glacial upland and mountainous terrain which features many incised valleys and steep slopes. In high elevations (≤ 1346 m asl), escarpments expose the bedrock and the slopes are overlain by unconsolidated regolith, glacial and post-glacial deposits which are generally 1 - 5 m bgl in depth but can reach depths of up to 15 m bgl in hollows and other depressions (Ballantyne 1986; 2002; Trewin 2002). In such shallow, coarse grained materials there is often a rapid response to rainfall, while finer materials have lower permeabilities or have deeper slip surfaces, which may see delays between 'triggering' rain conditions and landslide occurrence of several days or more (Iverson *et al.* 1997; Stoffel *et al.* 2014). As a consequence, although there is evidence of complex rotational landslides and rock falls or topples such as at Trotternish on Skye (Ballantyne *et al.* 2014), most of the reported landslides are planar slides with a flow component or planar slides that develop into debris flows in response to a short term influx in the slope water content, such as during storms (Ballantyne 2002). As this relatively straightforward conceptual model of the

landslide failure mechanism is reasonably well understood, including knowledge of the relevant geomorphological conditions and the hydrological triggers, they are most suited to the empirical approach; in contrast to larger and more complex landslides such as rotational failures. In addition, the data required for these studies (e.g. landslide database, elevation models, land cover and precipitation) are widely available; the landslide data used in this study is described in section 3.2.1. Subsequently, empirical analyses have been conducted in a wide variety of regions prone to shallow failures and debris flow including in, North America and Canada (Jakob & Weatherly 2003; Cannon *et al.* 2008; Staley *et al.* 2013), Italy and the European Alps (Guzzetti *et al.* 2008; Catani *et al.* 2013; Segoni *et al.* 2015b) and Norway (Søren *et al.* 2014; Meyer *et al.* 2015).

Second, debris flow and planar slides are responsible for most of the damage and disruption caused by landslides on Scotland's strategic infrastructure, including the highway, rail and

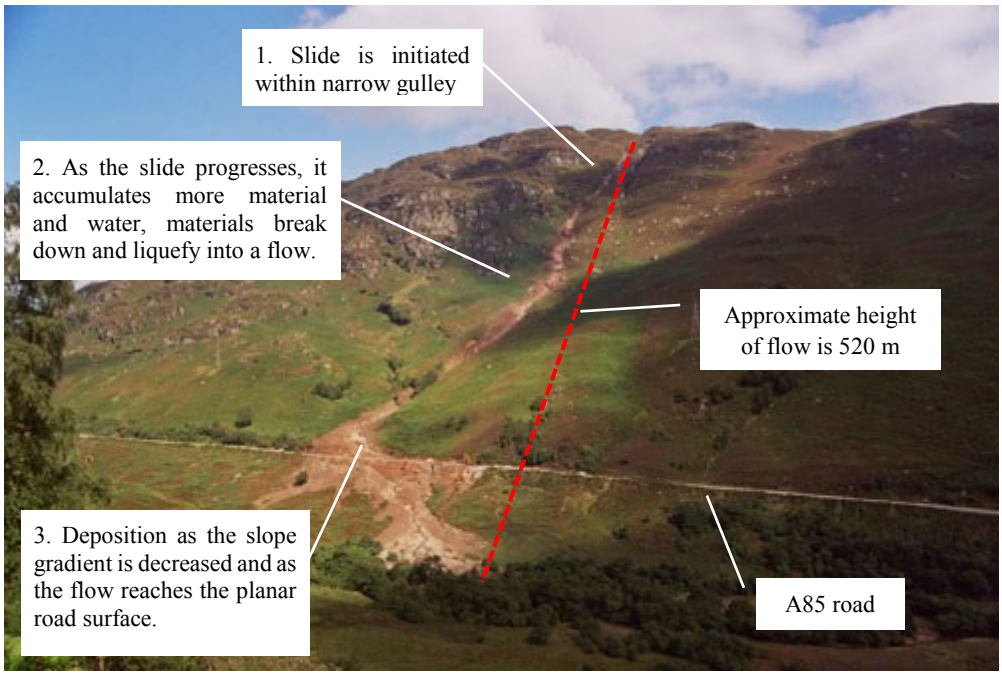

Figure 3.2. Debris flow on the A85 road at Lochernhead 18/08/2004. Adapted from BGS report http://www.bgs.ac.uk/landslides/GlenOgle.html

power networks (Winter *et al.* 2005; Dijkstra *et al.* 2016a). For example, Figure 3.2 shows a landslide which resulted in the closure of the A85 road at Lochernhead. This landslide was one of seven similar scale events to occur following a series of low pressure weather systems and heavy rain in August 2004. These landslides caused disruption on three separate sections of the road network and for a combined duration of 18 days. Figure 3.3 shows a more recent landslide that occurred on 28th October 2014 and that resulted in the closure of the A83 road for a total of 11 days (see also section 2.1). The research is therefore of strategic importance to the national government in Scotland (and wider UK) and is also of high public interest.

Figure 3.3. Debris flow on the A83 road near the Rest and Be Thankful pass 2014. Image taken from http://forargyll.com/?p=90101

Third, there are benefits related to the geography of Scotland. Figure 3.4 shows the case study area which comprises the Scottish mainland including the Isles of Sky, Mull and Bute, an area of approximately 70,100 km^2. The islands are included as they are connected to the mainland, and the wider strategic road network (SRN), via bridges or year-round and short duration (< 45 min) ferry services. The lack of national borders (except to England) simplifies the development of the traffic model by limiting the potential for model boundary effects. The area population is approximately 5.20 M and represents 98.3 % of the total population of Scotland (5.29 m) based the most recent 2011 UK census; this data is also used as input to the network model (ONS 2011a, 2011b). Some 73.4 % of the study area population reside within moderate population density sub-urban to urban areas (purple shading and circles in Figure 3.4), whilst the remaining 26.6 % (1.4 m) are reside in lower population density and rural locations (blue shading). The study area has global significance as the geographical setting is analogous (i.e. in terms of size, population and population density) to other landslide prone regions, including Norway, Malaysia and New Zealand. In addition, the traffic model may be used to evaluate the impact of other hazards and multi-hazards in Scotland, such as flooding and severe wind. The process to develop the traffic model and evaluate the impact of hazards is portable to these and other regions around worldwide.

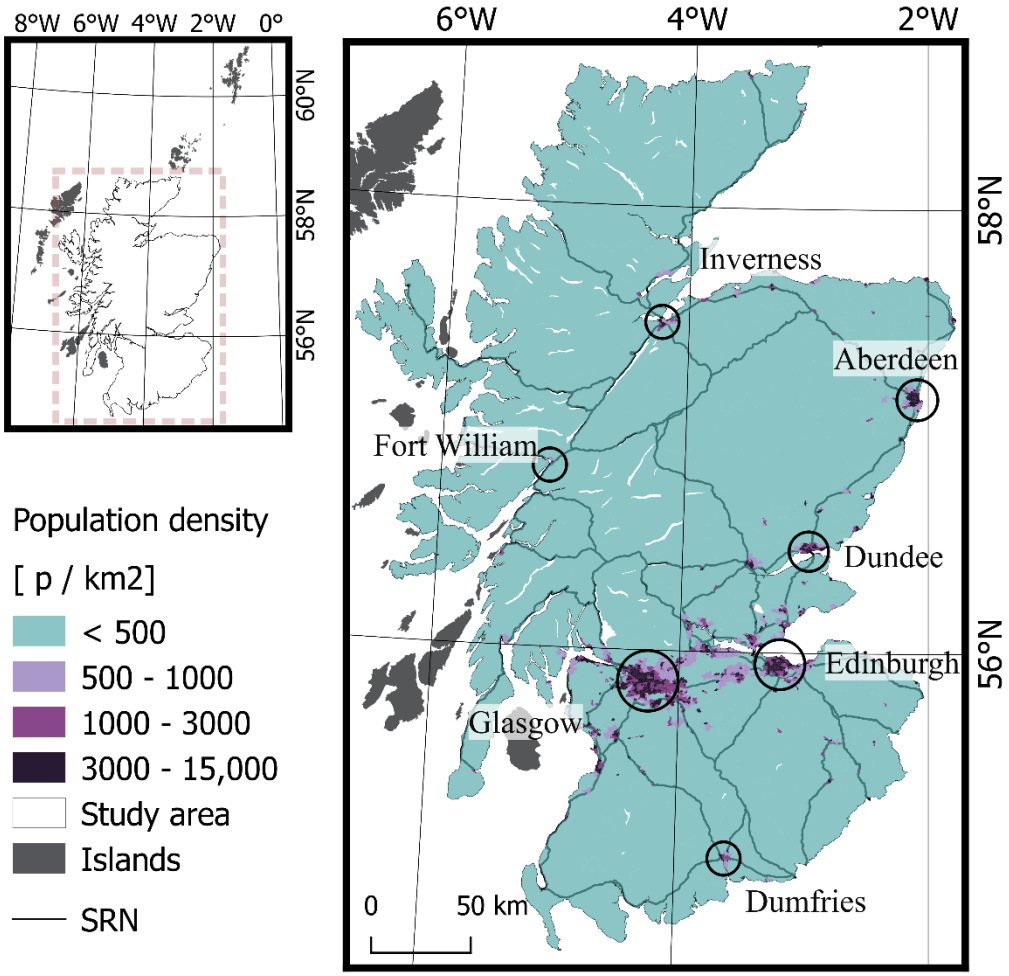

Figure 3.4. Map showing the study area (white and colours) and the other islands which are not included (grey shading). Blue and purple shading illustrates population density (p / km^2) and the major urban areas are shown using circles.

3.1.2 Landslide database

The landslide information used in this research is provided by the British Geological Survey (BGS). The BGS develops and maintains the National Landslide Database (NLD) which, with over 17,000 records, is the most extensive source of landslide information in Great Britain (Foster *et al.* 2008). The data are gathered through a range of sources and procedures including: incorporation of other databases; scientific literature; field and desk-based surveying; reports from infrastructure, insurance and other private organisations; social and broadcast media; and citizen science (Pennington *et al.* 2015). Whilst each of these sources provide valid landslide reports, when using the NLD it is important to consider the following assumptions and limitations: (i) the NLD provides a comprehensive record of all landslide activity; (ii) the NLD is biased toward landslides which occur in close proximity or cause impact on human activity, such as by damage to roads or buildings, as these are more likely to be reported; (iii) the NLD underestimates the number of landslides which occur in remote locations and where there is little to no impact on human activity; and (iv) the NLD is biased toward large landslide events as these are more likely to cause societal impact and are more easily detected, for example, visually or using aerial imagery.

The above limitations are true for almost all national scale landslide database around the world (Malamud *et al.* 2004; Guzzetti *et al.* 2008). For this research, the data issues related to the underrepresentation of landslides is likely to have limited negative effect as the analyses is focussed on the threat of landslides impacting the road transport network – and such events are relatively well represented in the NLD. Indeed, some 68 of the 75 verified (see below) landslide records in Scotland are situated on slopes adjacent to the road network. The clear recording bias toward the landslides occurring in proximity to the road network calls into question the validity of the analyses for small scale landslides and those occurring at distance to the road network. Since 2016, several strategies have been proposed that could be employed to limit this bias (Steger *et al.* 2017). The simplest approach, and that generates the most plausible results, is to constrain the analyses to the slopes adjacent to the road network (Freeborough *et al.* 2016; Martinovic *et al.* 2016). This approach is applied here.

The variety of NLD data sources means that the data are of varying levels of detail, for example, the spatial and temporal accuracy of landslide records, information on the landslide mechanism or slope material and as to whether the landslide datum has been quality checked by the BGS. As illustrated in Figure 3.5, a set of procedures were followed to verify and select NLD records with the following attributes:

- Database Query to select:
    - Landslide records with date of occurrence.
    - Landslide records within the period of radar data (01/03/2004 to 31/08/2016).
- Landslide Classification to determine:
    - Record Flow type and select planar slides with a flow component or debris flows (PS-FL).
- Source Check to remove PS-FL records:
    - With temporal accuracy of ≤ 48 h and spatial accuracy of ≤ 2500 m.
    - Records enriched solely using Google aerial imagery. To remove NLD records with no text source for flow type.

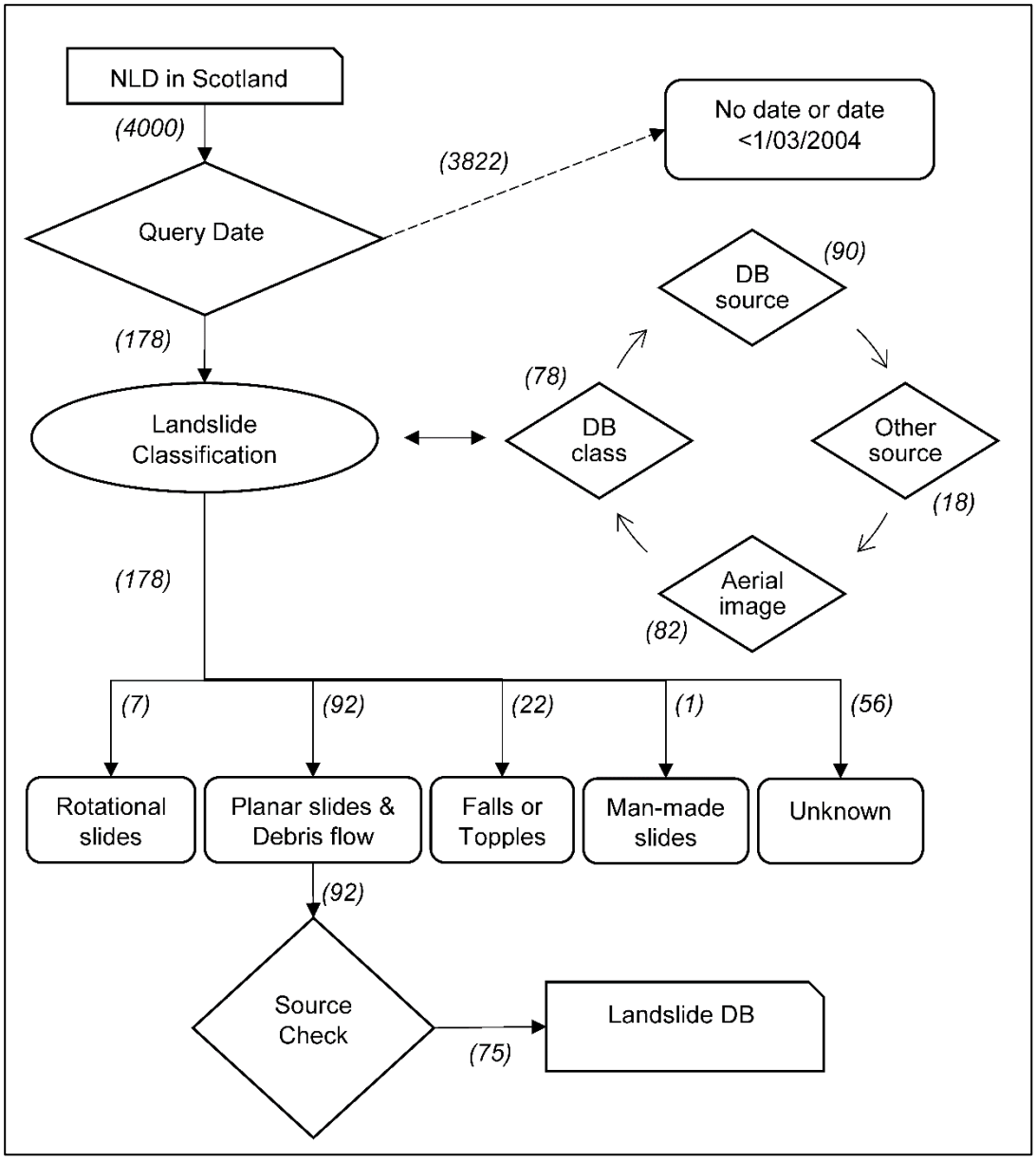

Figure 3.5. Process to update and select NLD records.

In practice, the classification and selection process involved the cross-validation of the NLD records with information internal to the NLD including: the NLD landslide comment fields; examination of the NLD data sources or BGS site-survey reports; and liaison with the BGS NLD personnel. NLD records were also cross-validated with external information not included in the NLD including: peer reviewed literature; print and online media; and visual inspection of annual time-step aerial imagery via Google Earths timeline feature (1984 – 2016). During this process many NLD records were updated with new information and some previously unreported landslides were detected that have now been incorporated into the NLD. The output is a verified landslide database or inventory of 75 landslides with the required attributes. In the remainder of this section, the attributes of the 178 NLD records that were successfully classified are summarised.

A total 178 landslides were classified according to failure type. PS-FL comprise 52 % (92) of the records, 31 % (51) are unknown, 12 % (22) are falls or topples, 0.4 % (7) are rotational landslides and one landslide was classed as 'man-made' which occurred due to a burst water main. Figure 3.6 shows the proportions of each landslide type per year and per month. The average rate of occurrence is 13.7 and 7.7 landslides per year for all and PS-FL classes, respectively. The landslide date of occurrence accuracy indicates the period within which the landslide is known to have occurred, for example, 24 h indicates that the day of landslide occurrence is known and confirmed. For all the NLD records the temporal accuracy is 12 h (5.6 %), 24 h (72.5 %), 48 h (0.6 %), 1 week (5.6 %) and 1 year (0.6 %). Some 15.2 % of the records have an unknown temporal accuracy, that is, the day of occurrence is recorded but is not confirmed within publicly available print media or site-survey report. It is likely that many of these were reported via informal communication to the NLD team.

Figure 3.7 shows the location of each landslide. The location information specifies the grid

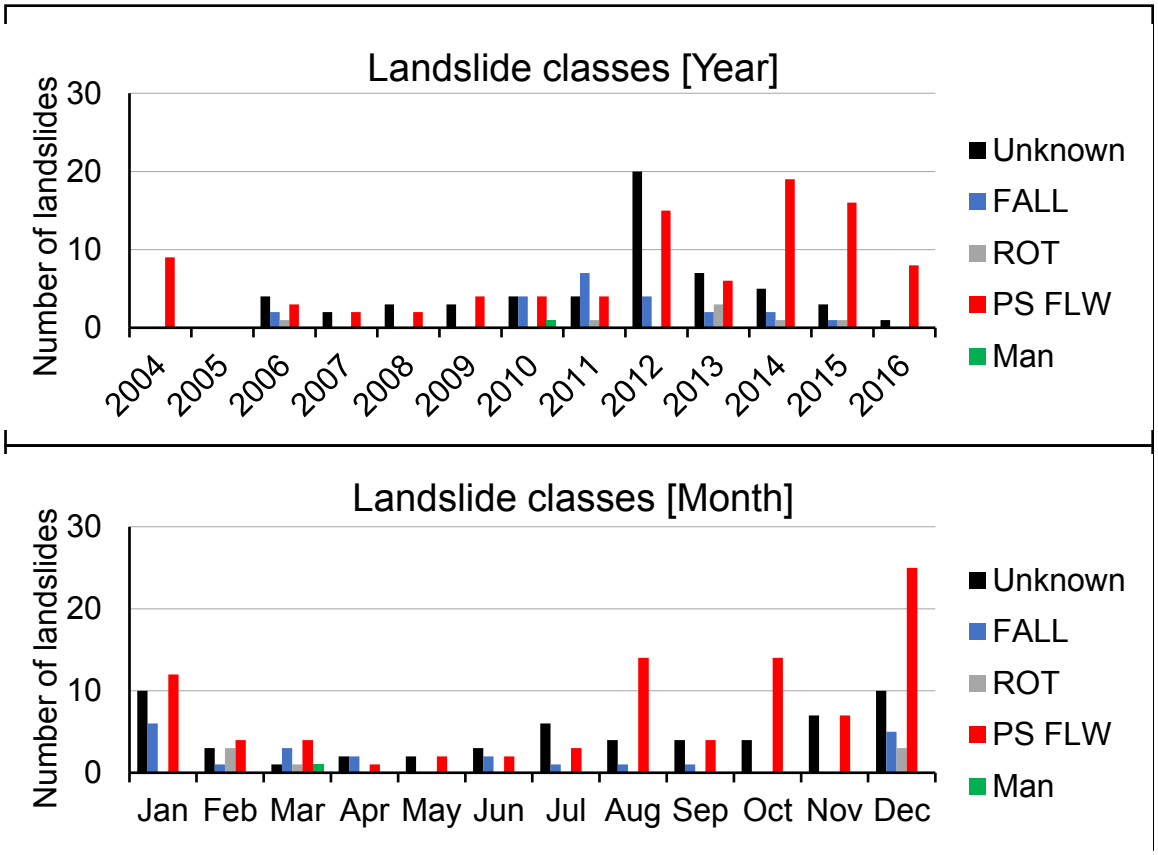

Figure 3.6. Landslide classes by year and by month for the period March 2004 to September 2016.

reference of the landslide source area and ranges in quality from several meters obtained by site-surveys and aerial imagery (19 % of records), 100 m - 2 km from 1:10,000 scale maps and aerial imagery (73 %) or they are recorded for entire valleys or by sections of road which can exceed 5 km in length (8 %). These coordinates allow further landslide properties and attributes such as geology, slope angle and elevation to be derived from other datasets using geographical information systems (GIS).

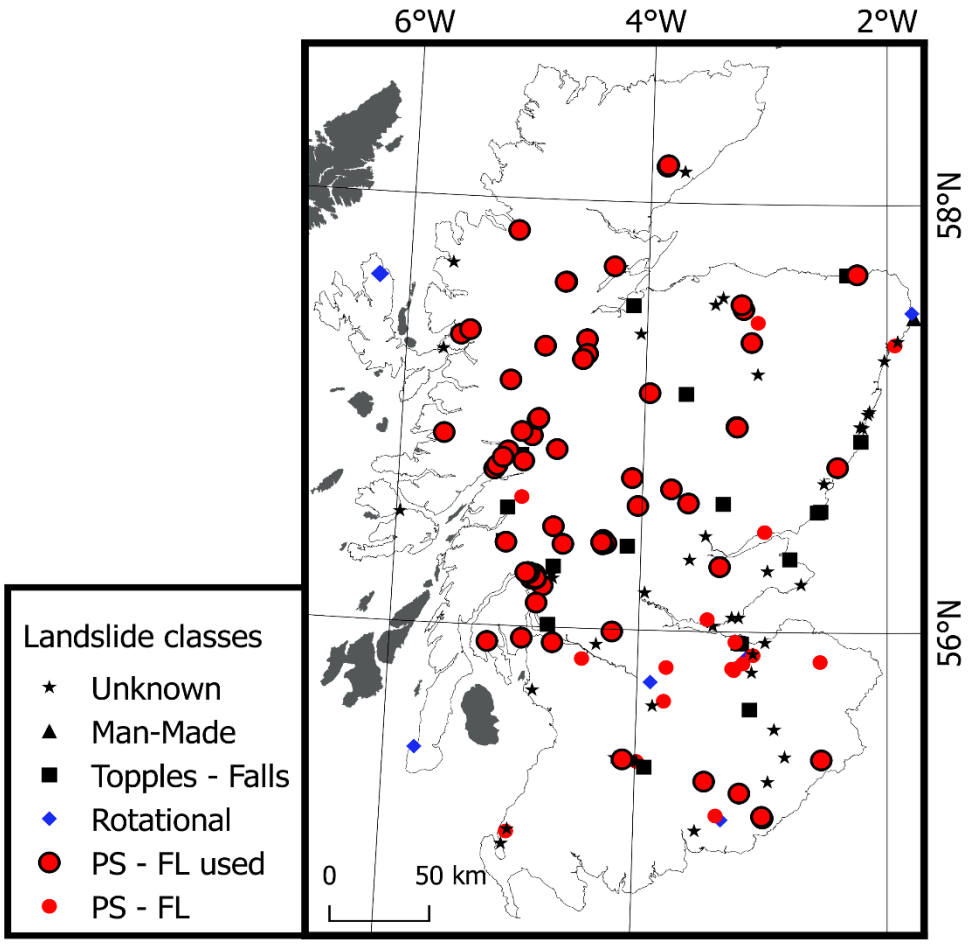

Figure 3.7. Landslide classes and location for the period March 2004 to September 2016.

The rainfall conditions prior to and at the onset of failure are also of particular interest. Figure 3.8 shows the amount of rain accumulation on the day of landslide occurrence (1-day) and for the 12-day antecedent rain accumulation. These are selected to illustrate the significant triggering (i.e. day of failure) and antecedent rainfall periods as noted in previous studies (Milne *et al.* 2009; Winter *et al.* 2010). Rain accumulation is shown as multiples of the rainy-day-normal (RDN), the average rain accumulation that falls of days with rain per location. For reference the RDN values in Scotland are in the range of 3 to 20 mm of accumulation varying by location and season (see Figure 6.1). Figure 3.7 shows that a large proportion of PS-FL, in addition to many unknown classified landslides, occur on days with more than two days' worth of rain and following 12-day periods with 10 to 30 days' worth of rain. Conversely, many of the recorded topples-falls and rotational landslides are shown to occur in relatively dry conditions and irrespective of increases in the 1-day rain accumulation. The rainfall data was obtained from the UK Met Office Nimrod weather radar system (Met Office 2003).

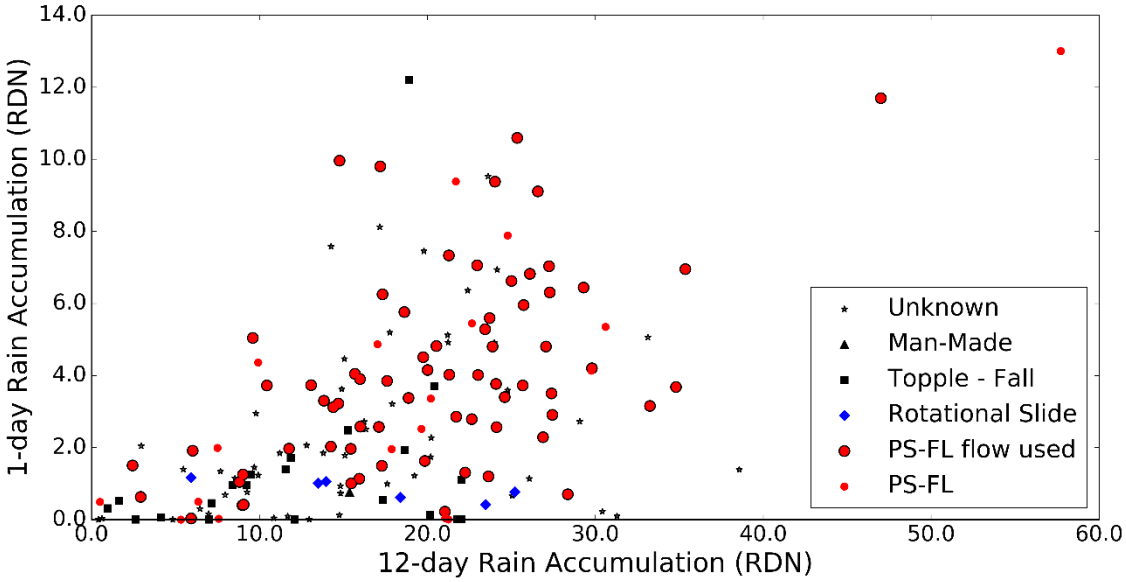

Figure 3.8. Scatter plot showing rain the 1 and 12-day rain accumulation for landslide classes in the period March 2004 to September 2016. Rain accumulation is given as multiples of the landslide location rainy-day-normal (not mm), which is the average amount of rain falling on days with rain in the location of the landslide.

3.2 Landslide Susceptibility

3.2.1 Input data

In this study, two primary data sources are used in addition to the NLD. First, is the 5 m^2 digital terrain model NEXTmap (DTM) which is available under academic or commercial license. The DTM is available across the British Isles and was produced from airborne Interferometric Synthetic Aperture Radar. The DTM is a so called 'bare earth' product that has had artefacts due to vegetation, roads, buildings and other cultural features removed via orthorectification with aerial photography, high resolution mapping and digital surface and elevation models (IntermapTechnologies 2009). The DTM is used to determine the hillslope units and to derive 5 m^2 resolution arrays (raster's) of the geomorphological factors slope angle, aspect, roughness, curvature and elevation. The arrays for slope angle, curvature and aspect are generated using the 'r.slope.aspect' procedure in GRASS GIS 7 which employs a 3×3 pixel kernel window and is equivalent to the procedures implemented in most other mainstream GIS software including the geospatial data abstraction library (GDAL), SAGA and ArcMap 10 (Horn 1981; Hofierka *et al.* 2009).

The second data used is the 1 km^2 soil parent material model (PMM) developed by the BGS (Lawley & Smith 2008). The PMM was generated using lithological maps, borehole records and other physical soil survey data in a combined spatial-generalisation and heuristic GIS modelling procedure. The data is distributed under an open commons license by the BGS. The PMM represents the very near surface geology and provides geotechnical factors and

information on the weathered material from which the superficial and subsoil horizons form including arrays for: soil material grain size, soil depth and soil texture.

Measures of central tendency and summary statistics are calculated for each of the factors, including the mean, median, mode, minimum, maximum and range, as each hillslope unit may contain one or more unique values. The selection of suitable statistics is informed by the literature review and by knowledge of landslide processes. For example, minimum elevation is likely to provide little insight on landslide processes whereas the maximum elevation or elevation range is indicative of the slope gravitational and weathering potential. A description of each factor is included below:

- Slope angle: the mean, median and maximum slope angle in decimal degrees.
- Elevation: the range and maximum slope elevation in meters.
- Slope aspect: mean slope aspect is included as a proxy for several environmental factors such as wind, rain and solar insolation which are related to weathering processes (Hughes *et al.* 2009; Budimir *et al.* 2015).
- Curvature: Three measures of curvature are used: profile curvature is the slope curvature parallel to the direction of the steepest slope (vertical plane of flow), plan curvature is perpendicular to the direction of the steepest slope (horizontal or contour), and general (total) curvature is the overall curvature of the slope surface. Each is measured by the radius of curvature in 1 / meter units (e.g. a slope with a radius of curvature of 0.04, is equivalent to a circle with radius 1 / 25 m).
- Terrain roughness: Melton Ration (MR), higher values indicate steep and elevated terrain which are more liable to increased erosion and gravitational potential.
- Soil depth: PMM has 5 classifications of soil depth listed in Table 3.1.

Class	Description	Depth (m)
Deep	A thick soil profile is likely. Soil should be easily dug to a depth of 2 to > 5 m.	2 - > 5
Deep-intermediate	The soil profile may vary from thick to intermediate. Soil can be dug to a depth of 1 m and possibly more in some places.	1 - 2
Intermediate	A ‘typical’ soil profile is likely. Soil can be dug to a depth of 1m	1
Intermediate-shallow	The soil profile may vary from thin to intermediate and is potentially difficult to dig at depths greater than 0.5 m	0.5 - 1
Shallow	A thin soil profile is likely. The soil will be extremely difficult to dig at depths of 0.5 m or less.	< 0.5

Table 3.1. Soil depth categories from PMM.

- Grain size: PMM has seven categories for soil material grain size listed in Table 3.2.

	Class	Description	Size (mm)
Non-igneous	Argillaceous (Argillic)	Materials that are dominantly fine grained (clay and silt grade)	< 0.06
	Arenaceous	Materials that are dominantly medium grained (fine to medium sand grade)	0.06 - 2.0
	Rudaceous	Materials that are dominantly coarse grained (coarse sand to gravel grade)	> 2.0
	Peat*	Material is Peat	NA
Igneous	Fine	Materials that are dominantly composed of fine crystals.	< 0.25
	Medium	Materials that are dominantly composed of medium crystals.	0.25 > 2
	Coarse	Materials that are dominantly composed of coarse crystals.	> 2.0

Table 3.2. Soil material grain size categories from PMM.

- Soil texture: soil texture classifications that are based on a UK classification scheme (Hodgson 1997). PMM has five generalized textures that are moderated (e.g. Silty – clay) to produce 25 unique classifications listed in Table 3.3.

Class	Description	Size (mm)
Clay	Soil is generally dominated by clay grade particles.	< 0.002
Silt	Soil is generally dominated by silt grade particles.	0.002 < 0.06
Sand	Soil is generally dominated by sand grade particles.	0.06 < 2.0
Loam	Loam soils are soils with a distributed/even mix of particle sizes	-
Peat	Not a texture term, but defines areas dominated by Peat materials	-

Table 3.3. Soil texture classifications from PMM.

3.2.2 Generating hillslope sections

Hillslopes are characterised by distinguishing areas with similar geomorphic features and hydro-geological processes. In the literature review it is shown that the characteristics of different hillslopes may be used to identify the slopes which are more or less prone to generating landslides. However, there is limited application of hillslopes in landslide susceptibility modelling which is instead limited to pixel, UCU or watershed basin scale units. In addition, there is no universally accepted criterion for the size of a hillslope and this very much depends upon the resolution of the input data (e.g. the terrain model) and the scope and

purpose of the investigation. Below, the procedures used to generate hillslopes and the criteria to select a suitable hillslope size are outlined.

Hillslope sections are generated using the 'r.watershed' procedure in GRASS GIS 7 (Ehlschlaeger 1989). R.watershed uses an A* least-cost path algorithm and a terrain elevation model to calculate hydrological parameters including flow accumulation, drainage direction, stream locations, watershed basins and half-basins. Half-basins divide the watershed basins into their left and right constituent slopes and are here used as the hillslope sections or 'hillslopes'. The default (recommended) r.watershed settings are used for all of the model parameters and the maximum computing RAM is set to 3000 mb. A comprehensive description of r.watershed with reference to the relevant peer reviewed literature is available online. Comparisons of r.watershed outputs to those of other software and of ground observations, including r.terraflow and ESRI ArcGIS watershed, suggest that r.watershed produces more realistic stream locations and watershed basins and is less sensitive to low slope areas or to elevation data containing vegetated areas or missing data values (Holmgren 1994; Kinner *et al.* 2005; Metz *et al.* 2011). The NEXTmap DTM used by this study is void of vegetation and missing data and so this should have little effect on the model outputs. Nonetheless, for the purpose of hillslope creation the DTM is resampled to 25 m^2 as the majority of literature on r.watershed uses SRTM DEM data at resolutions of 10 to 90 m^2 and the performance of r.watershed at resolutions < 10 m^2 is uncertain (Metz *et al.* 2011).

The DTM registers water bodies as missing data, including oceans, seas, inland lakes and lochs. This can lead to the production of erroneous hydrological flow profiles and hillslopes at shorelines where the water flows into these natural depressions and water bodies. To overcome this issue, the water body areas were assigned a value of -50 m which is below the minimum elevation of the DTM (-23 m). An alternative solution which involved the coupling of the DTM to bathymetry data was attempted, however, it is uncertain how the software may respond to any boundary artefacts and to using different data resolutions. The result of the adopted solution is to produce hillslopes which flow into the natural depressions and water bodies, as is expected. Lastly, the hillslope sections are clipped to the original DTM shoreline to re-introduce and preserve the original water body areas.

To determine the size of the generated hillslopes, the 'basin threshold' parameter is altered to control the minimum number cells of upland flow required for a basin to be formed. For example, if the threshold parameter is set to 100 then the minimum allowed size of a basin is equal to 62,500 m^2 (100 × 25 m^2 cells) – with the two hillslopes which form this basin having an equivalent sum area.

Six basin threshold values were evaluated for 100 to 1600 cells in 300 cell increments (e.g. 100, 400…, 1600). The range of threshold values is determined by visual inspection of the generated hillslope sections and by comparing these to integrated hydrological unit sections (IHUS) – the smallest official hydrometric area used in the UK and developed by the Centre for Ecology and Hydrology (Kral *et al.* 2015). These are shown in Figure 3.9.

A lower limit threshold value of 100 cells is used as lesser values were found to result in poorly defined hillslope sections. For example, many hillslopes were formed of single-cell width columns parallel to the angle of slope. Lower threshold values (< 100 cells) may be suitable for higher resolution DTM yet this is beyond the scope of this study. Threshold values greater than 1600 cells result in hillslope sections that capture large slope faces and that are generally

in line with the topography and borders of the IHUS, this is therefore used as the upper limit threshold. Figure 3.9A and Figure 3.9B illustrate the IHUS (blue lines) and the 100 (black lines) and 1600 (orange lines) threshold hillslope sections created by r.watershed at the Ben Nevis mountain complex. The IHUS blue lines extending beyond the mountain illustrate how the official IHUS are relatively large scale areas which capture both sides of a drainage basin. These are unsuitable for measuring several of the factors related to landsliding, for example slope aspect or curvature. The 1600 hillslopes follow the primary drainage divide lines of the IHUS (e.g. ridge crests and watersheds) and separate the left and right hillslope faces by the valley-floor divides. The 100 hillslopes are also terminated at the drainage divide lines and delineate many smaller areas of flow accumulation on hillslope faces. The selection of the most suitable threshold value is determined by comparing the performance scores of logistic regression models using the hillslopes with different basin threshold values.

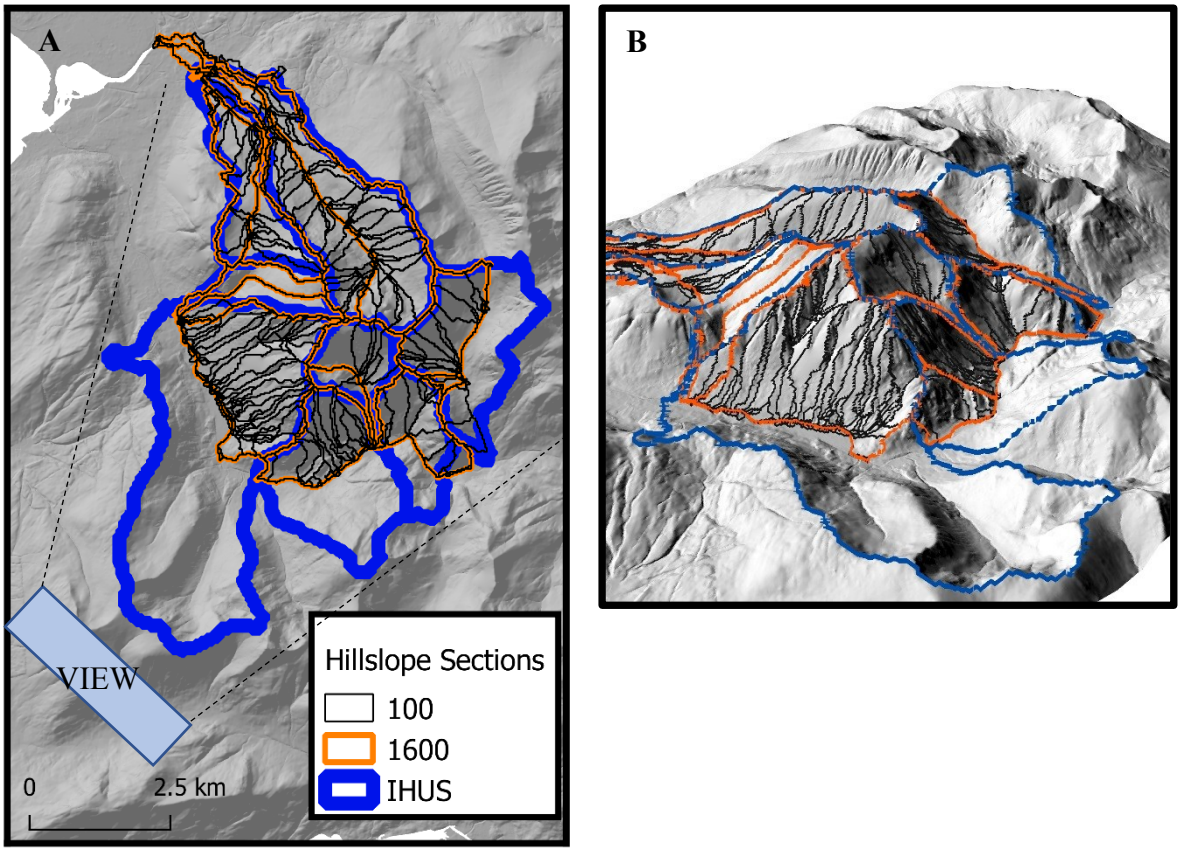

Figure 3.9. Plan (A) and 3D (B) views of Ben Nevis with overlaying IHUS (blue) and r.watershed generated hillslopes with 1500 (orange) and 100 (black) minimum cell thresholds. The 'view' box and dashed lines in A display the field of view in figure B.

3.2.3 Logistic regression modelling

Logistic regression (LR) models quantify the relationship between a series of independent explanatory variables and a binary dependant variable. In the case of landslide susceptibility mapping, the objective of LR is to produce the best-fit model which describes the relationship between the input variables of each hillslope (e.g. its environmental or geotechnical characteristics) and the presence or absence of a landslide. LR is used as it has been extensively applied and validated in studies of landslide susceptibility and has been shown to outperform other multi-variate classification techniques (Ayalew & Yamagishi 2005; Brenning 2005; Budimir *et al.* 2015). A LR model is developed using the python StatsModels package (Oliphant 2007; Seabold & Perktold 2010). A detailed description of the modelling process is provided.

The result of the LR model is a landslide susceptibility probability (p) for each hillslope ranging from 0 to 1 (Chapter 2.2.4 pg 31). The probabilities are determined by logit and the linear combination of the input variable coefficients. The natural exponent of the model coefficients gives the odds-ratio for a given independent variable. The higher the value of the explanatory variable coefficients and odds-ratios, the greater the influence the variable has on increasing the susceptibility of a hillslope. One of the main advantages of LR is that odds-ratios can be used to compare the relative contribution of each input variable on susceptibility. In addition, both continuous and categorical data are accommodated. For continuous data, the odds-ratio indicates the change in the odds for a 1 unit increase in a variable.

The Wald test is used to test the statistical significance of each explanatory variable in the logistic regression model (Dai *et al.* 2001; Agresti 2002). For a given explanatory variable, if the Wald test is significant ($p < \alpha$), then the variable coefficient is not zero (i.e. a coefficient of zero has no effect). If the Wald test is not significant ($p > \alpha$) then the explanatory variable can be omitted from the model. A critical p-value of $\alpha = 0.1$ is used as a threshold as suggested by Dai *et al* (2001).

Feature-engineering is the nomenclature term for the process of re-coding input variables, such as converting continuous data to categorical data. The purpose of feature engineering is to improve model fit by reducing the effect of the input data variance by applying heuristic or theoretical knowledge of the modelled processes. For example, in the UK one might assume that west facing slopes may be more susceptible to landslides as most weather systems move westward across the UK – driving wind and rain. The variable for slope aspect may therefore be engineered in to two or more distinct classes to compare the relative contribution of each class on susceptibility, for instance: east and west (0 - 180^o and 180 - 360^o); four cardinal classes (e.g. N, E, S and W) or inter cardinal classes (e.g. NW – NE, NE – SE) or eight 45^o classes and so on.

Feature-engineering and the selection of suitable classes is primarily determined by the investigators domain knowledge and modelling experience. Quantitative selection of classes may be achieved by examining the class frequency tables and histograms of the landslide and non-landslide data. For continuous data, the overlapping area between the two probability density functions (pdf) is a useful measure for the skill of the input variables to discriminate between landslide and non-landslide slopes (Cho *et al.* 2006; Berenguer *et al.* 2015). For categorical data, for instance the PMM soil depth classes, each class is mapped to a binary dummy variable which take on the value of 1 if a class is present and 0 if otherwise. A model

coefficient and odds-ratio is generated for each dummy variable. One of the dummy variables is used as the reference class to which all other classes are compared (Dai & Lee 2001; Wilks 2006). For example, for the different PMM soil textures, one may use peat soil as the reference class. The model coefficients and odds-ratios for each other soil texture class indicate the change in the odds relative to peat soil class. Reference classes are typically selected to ease interpretability of the results, for example, by selecting the class with the smallest number of landslides or selecting the class which capture the minimum value within a range.

Model over-fitting can occur due to: (1) high collinearity between the input variables, and (2) perfect separation errors that are caused by input variable classes that match those of the dependant variable (Suits 1957; Konis 2007). First, Pearson's product-momentum correlation, Spearman's rank-order correlation and chi-square tests are used to identify input variables that are highly correlated with one another (Thiery *et al.* 2007). Second, in most modelling applications it is very unlikely to be unaware of, or to find a single input variable that perfectly predicts the dependent variable. Instead, these separation errors are often caused by the over-engineering of input variables or are by-products of the data sample, such as using low resolution spatial data so that all of the hillslopes with landslides are within a single class. Class frequency tables are again used to identify the variables with class imbalances that may cause separation errors and these are removed from the model (Konis 2007). As a check, the performance of the model is evaluated both with and without the offending classes.

Four statistical measures are produced and used to evaluate the goodness of fit and statistical significance of the LR model (Oliphant 2007; Seabold & Perktold 2010).

- Chi-square test: used to determine if there is a significant difference between the log-likelihood function of the null model ($-2LLo$, no input variables) and that of the new model ($-2LLf$). The log-likelihood is multiplied by -2 to convert the values to the chi-square distribution. The difference between the log-likelihood of the null and new model is referred to as the model chi-square test (x^2). The significance level of the chi-square test is used to determine the statistical significance of the new model and to reject or accept the null. A 95 % ($\alpha = 0.05$) significance criteria is used to reject the null model.
- The Akaike Information Criterion (AIC) is a goodness of fit measure that favors smaller residual model error, but penalizes for including additional predictors and helps avoiding overfitting. AIC is given by: $-2 \times (LLf - n)$, where n is the number of input variables including the intercept. For a collection of different models of the data, AIC estimates the relative quality of each model with lower vales indicating greater model fit and model simplicity. Hence, AIC provides a means for model selection.
- McFadden pseudo R^2: used to assess the model goodness of fit (McFadden 1974). The interpretation of the pseudo R^2 is equivalent to that of ordinary least squares linear regression (OLS). However, pseudo R^2 values are considerably lower than those of OLS and values of 0.2 – 0.4 indicate very good fit (McFadden 1974; Clark & Hosking 1986). As a guide, Domencich and McFadden (1975) state that this range is equivalent to R^2 0.7 – 0.9 in OLS regression.
- Area Under Curve (AUC): the AUC of the receiver operating characteristic (ROC) is a measure of model accuracy (Fawcett 2006). AUC measures the ability of the model to correctly classify landslide and non-landslide slopes.

Cross-validation is the iterative process of fitting and evaluating a model using many unique training and validation dataset samples. As a rule of thumb, the data set is split 70 – 80 % for training and 20 – 30 % for validation. First, a model is created using a selection of the independent variables. For each iteration, the training data are used to fit a new instance of the model and the performance of the model instance is evaluated using the validation data. Once all of the iterations are complete, the performance scores of each model instance, such as the AUC and pseudo R^2 values, are averaged to assess the overall ability of the model to learn and predict the data (Wilks 2006; Kuhn & Johnson 2013a). The purpose of cross-validation is not to select the single best performing model instance to generate the result. The purpose of cross-validation is to evaluate the overall skill and validity of the model (and selection of variables) to accurately predict susceptible hillslopes given all possible combinations of the dataset or given a sufficiently large number of random samples.

To produce the LR model investigators must: i) select a suitable sample size for use in cross-validation, and ii) select the most suitable model instance to generate the final results. Firstly, in the literature several approaches are offered to select suitable sample sizes. Many studies use all of the available data within a study region and this typically leads to highly unbalanced samples of landslide and non-landslide units (Ohlmacher & Davis 2003; Ayalew & Yamagishi 2005; Catani *et al.* 2013; Meyer *et al.* 2014; Martinovic *et al.* 2016). Others recommend the use of more balanced or equal sample sizes to avoid the underprediction of landslide occurrence (Can *et al.* 2005; Jaiswal *et al.* 2010; Yilmaz 2010) and in applications of logistic regression to other rare phenomena (King & Zeng 2001; Kuhn & Johnson 2013b). Second, to produce the final model instance, there are two generally accepted approaches. One approach involves using all the available data to train the model and to generate the result (i.e. unbalanced sampling). This is done following a cross-validation process to provide an overall estimate of model performance (i.e. with balanced sampling). Alternatively, one can use the 'ensemble' or 'majority-vote' method. Here, each of the model instances created in cross-validation are used to make a prediction for every hillslope. The average value of the predictions across each of the cross-validation iterations is used as the result, termed an 'ensemble result'. The primary advantage of the ensemble approach is that it reduces the effect of model variance between cross-validation data samples.

Here, the latter, balanced sampling approach is adopted due to the relatively limited number of hillslopes with landslides in comparison to those without. For cross-validation, a repeat random sub-sampling without replacement is used. In each iteration, the landslide slopes are randomly split to training and validation samples of 75 and 25 %, respectively. An equivalent number of randomly selected non-landslide slopes are added to each of the samples and a model instance is fitted and a prediction is made. The process is repeated 30 times and the model predictions are averaged to provide an ensemble result.

The results of LR model is a value for each hillslope that indicates the landslide susceptibility between 0 and 1. To produce a landslide susceptibility map, the susceptibility values are split into four bands using ROC threshold selection: the bands are zero, low, moderate and high susceptibility. The zero and low susceptibility bands are selected using the optimal point threshold: the optimal point is the threshold that maximises landslide detection and minimises false positives. Values below the optimal point threshold are considered as 'zero' or uncertain susceptibility. The threat score threshold maximises accuracy, and selects the threshold with the greatest number of true positives to the lowest number of false negatives of false positives.

The susceptibility values above the threat score thresholds are in the 'high' susceptibility class. The threshold value that divides the range between the optimal point and threat score threshold is used to defined the low and moderate classes.

3.2.4 Limiting the influence of landslide database bias

Complete landslide databases are rarely available. Of particular concern is the systematic reporting bias due an abundance of landslides recorded adjacent to infrastructure networks (e.g. road, rail and power networks). Nonetheless bias databases are widely used to calibrate and validate empirical landslide susceptibility models (Malamud *et al.* 2004; Guzzetti *et al.* 2007; Kirschbaum *et al.* 2015). Recently, several studies attempt to quantify these biases by comparing real world databases to synthetically generated data sets (Stanley & Kirschbaum 2017; Steger *et al.* 2017). However, these assessments are subject to many uncertainties as the synthetic data sets are themselves generated using the statistical properties of ostensibly 'complete' landslide databases gathered at smaller spatial scales, such as in individual valleys or mountain sides. The degree that the properties of these smaller scale databases can be appropriately extrapolated to broader spatial scales is a prominent challenge.

To overcome this issue, several authors note that landslide susceptibility maps generated using biased databases are still relevant and accurate for the areas adjacent to infrastructure networks (Chau & Chan 2005; Van Westen *et al.* 2008; Jaedicke *et al.* 2009). In addition, slope proximity to infrastructure networks is often reported as one of the most significant indicators of increased landslide susceptibility (Dai *et al.* 2002; Budimir *et al.* 2015). In this authors opinion, a more appropriate approach is to constrain the analyses to only those slopes that are situated adjacent to or are intersected by the infrastructure network. The benefit of this is that all modelled slopes share the property of being next to the infrastructure network thus limiting the influence of both bias in the landslide database and the effects of close network proximity. Though suitable in the context of this study, a clear downside is that susceptibility is only modelled for the slopes next to these networks.

Two types of model are created. The first is a network-specific-model, that uses only the landslides and hillslopes adjacent to the road transport network. The second model is a nationwide-model that uses all landslides and hillslopes.

3.2.5 Susceptible road segments and model validation

As a means of validation, the logistic regression susceptibility model is compared to the existing British Geological Survey GeoSure landslide susceptibility model (Walsby 2008). GeoSure was produced using a combined heuristic and deterministic modelling of environmental and hydrological factors (e.g. soil permeability). The model was developed using ~15,000 landslide records and includes all types of failure, such as falls, topples, slides or flows. The data is supplied as unique-condition-unit polygons 0.5 – 5 km^2 in size and in 5 classes of increasing landslide susceptibility (i.e. compounding causative factors A – E; Table 3.4) at 1:50,000 scale. GeoSure is available nationwide and is widely used by insurers and infrastructure operators. This study uses categories D and E as these represent areas that are most susceptible to landslides (See Table 3.4).

GeoSure category	Description
A	Slope instability problems are not thought to occur but consideration to potential problems of adjacent areas impacting on the site should always be considered
B	Slope instability problems are not likely to occur but consideration to potential problems of adjacent areas impacting on the site should always be considered
C	Slope instability problems may be present or anticipated. Site investigation should consider specifically the slope stability of the site
D	Slope instability problems are probably present or have occurred in the past. Land use should consider specifically the stability of the site.
E	Slope instability problems almost certainly present and may be active. Significant constraint on land use.

Table 3.4. GeoSure landslide susceptibility categories.

A direct comparison of the two models is not possible given the different output scales (e.g. polygons and hillslopes). Therefore, the two models are compared by examining the number and spatial distribution of road segments that are found to be susceptible to landslides in Scotland's 4,300 km strategic road network. This has the additional benefit of comparing the two models in the locations where most landslides are recorded (i.e. along transport corridors). The susceptible road segments are identified as follows:

- For the hillslope susceptibility model developed in this study, the road segments that are susceptible to landslide are identified using a spatial join to the hillslope sections.
- For the GeoSure model of landslide susceptibility a spatial buffer analysis is used to identify road segments with areas of neighbouring susceptible ground using the GeoSure data. The search area is selected using two different buffer values to account for the fact that the GeoSure data does not distinguish between different landslide mechanisms. Each road segment (r) is classified as susceptible when segment susceptibility ($S_r > 0$), as given by Equation 3.1 and 3.2:

$$\alpha_r = As_b / At_b \qquad (3.1)$$

$$S_r = \alpha L \qquad (3.2)$$

where α_r is the fraction of susceptible ground area (As m^2, i.e. GeoSure categories D and E) to total ground area (At m^2) within a 50 m or 500 m buffer (b) of a road segment, and L is the segment length in meters. The buffer distance (b) is set to 500 m if a segment intersects a basin with a maximum slope angle ≥ 26^o. This is based on analysis of shallow translational slides and debris flow in Scotland noting that they most often occur on steep slopes (≥ 26^o) producing deposition run-out distances of up to 500 m (Winter *et al.* 2005; Foster *et al.* 2008; Milne *et al.* 2009). In other regions road segments are more likely to be susceptible to underlying and closer proximity slope movements and for all other cases a 50 m buffer is used. A 50 m road buffer is also used in other landslide studies (Shahabi & Hashim 2015) and by UK insurance and infrastructure organisations using GeoSure (Booth *et al.* 2010; Mott MacDonald & Patterson 2014).

3.3 Landslide Rain Initiation Thresholds

3.3.1 Input data

The rainfall data are radar quantitate precipitation estimates produced by the UK Met Office network of 15 C-band Doppler radar sites (Met Office 2003). The radar system provides precipitation observations at 5 km^2 resolution for 15 min intervals over the entire UK and Western Europe for the period March 2004 to present. The radar is calibrated to account for, amongst others, echoing, beam blockage and attenuation as described in Harrison et al (2000; 2009). At ≥ 1 h aggregations the radar data adequately reproduce gauged precipitation observations, however, the accuracy for short duration and low intensity precipitation is uncertain as most gauges require ≥ 0.2 mm per record (Harrison *et al.* 2000; Villarini & Krajewski 2008; Villarini *et al.* 2008). The data represent the state-of-the-art in UK weather radar and it is widely applied for national meteorological forecasting and research on flooding (Schellart *et al.* 2012; Parkes *et al.* 2013), climatology (Fairman *et al.* 2015), and water management (Harrison *et al.* 2009).

3.3.2 Rain variables

The rain variables used are summarised in Table 3.5 and include: non-normalized, total rain accumulation (V mm); rain-day-normal (RDN) normalized rain accumulation (NV); hourly maximum rain intensity ($Imax$ mm h^{-1}) and rain duration (RD h). The data are prepared as daily time series. Rolling window statistics are used to calculate the variables over antecedent periods of 1, 2, 3, 6, 12, 18, 24, 30, 50 and 60 days (e.g. 12 days = NV_{12}). The range of antecedence periods were chosen and skewed more to shorter durations (i.e. 1 to 18 days) based on the identification of significant thresholds for these periods in other temperate climates including Scotland (Guzzetti *et al.* 2007; Chleborad *et al.* 2008; Winter *et al.* 2010; Meyer *et al.* 2012; Søren *et al.* 2014).

Thresholds are developed using RDN normalized rain accumulation variables as thresholds which apply in one region do not apply to regions with different climatic regimes and weather variability (Jakob & Weatherly 2003). An empirical measure of local climate is used to normalise the rainfall values, for instance mean annual precipitation (Cannon & Ellen 1985). In this study the RDN is used for normalisation (Wilson & Jayko 1997). RDN is a more appropriate measure than mean annual precipitation for assessing rain events associated with landslides as it is not influenced by periods of no rain (Wilson & Jayko 1997; Guzzetti *et al.* 2007, 2008; Brunetti *et al.* 2010; Meyer *et al.* 2012; Gariano *et al.* 2015). As shown in Table 3.5, for each radar pixel and landslide location the RDN indicates the mean daily rainfall accumulation on days with rain. In addition, and in contrast to past studies, monthly RDN values are used to account for the seasonal variability in rain accumulation. Therefore, the RDN provides spatially and temporally normalised thresholds.

The rain duration (RD) variable is a new measure for the hours of rainfall above the monthly rainy-day-normal-intensity (RDNI = I / t). Like RDN, RDNI is the average of the rainfall intensities (I) recorded for all time periods (t) with > 0.01 mm h^{-1} rain.

Variable	Description	Units	Reference
RDN	Rainy Day Normal: the average of total accumulation (A) and the number of days with > 0.01 mm rain (D) in a month. ($RDN\ mm\ =\ A\ /\ D$)	mm	(Wilson & Jayko 1997)
$RDNI$	Rainy Day Normal Intensity: the average of the rainfall intensities (I) recorded for all time periods (t) with > 0.01 mm hr^{-1} rain in a month. ($RDNI\ =\ I\ /\ t$)	mm/hr	
V_n	Rainfall accumulation over n day's antecedence calculated by sum rolling window.	mm	(Innes 1983)
NV_n	Normalised accumulation over n day's antecedence. ($NV_n\ =\ V_n\ /RDN$)		(Wilson & Jayko 1997)
$Imax_n$	Maximum rainfall intensity over n days antecedence calculated by rolling window.	mm/hr	(Onodera *et al.* 1974)
RD_n	Duration of rainfall greater than $RDNI$ over n day's antecedence. Calculated by applying a binary filter to the 15-minute rainfall intensity data ($1\ IF\ \geq RDNI, ELSE\ 0$). The sum of the binary columns over n day's gives the count of 15-minute periods above RDNI.	hours	

Table 3.5. Precipitation variables used to define landslide thresholds and their common description, units, antecedence period and known earliest reference.

3.3.3 Selecting thresholds

The determination of thresholds is approached as a binary classification problem (Staley *et al.* 2013; Segoni *et al.* 2014b; Gariano *et al.* 2015). The classification seeks to find the threshold that best separates the rainfall conditions that coincide with landslide occurrence from the rain conditions that do not coincide landslides. A systematic classification procedure is applied to the daily time series data as follows.

- For each rain variable, a set of 250 candidate thresholds are created at equal increments between the observed minimum and maximum values for all days with landslide occurrence. The number of candidate thresholds (250) is selected to give small increments (e.g. 5 mm rain accumulation) between potential threshold values.
- For each candidate threshold, a binary classification procedure is applied to the time series data. The time series values are assigned a value of one if they are equal to or exceed the candidate threshold value and a value of zero if otherwise. The binary classification yields four mutually exclusive contingencies that are used to evaluate each threshold (see below).
- The process is repeated until contingencies are calculated for all rain variables and candidate thresholds.

As illustrated in Figure 3.10b, the binary classification generates four contingencies: true positive (TP) is when a threshold is exceeded and a landslide occurs; false positive (FP) is when the threshold is exceeded but no landslide occurs (a false alarm); false negative (FN) is when rainfall is below the threshold yet a landslide occurs (a failed alarm); and true negative (TN) is when neither the threshold is exceeded or a landslide occurs.

ROC analysis is applied to evaluate each rain variable (Wilks 2006; Gariano *et al.* 2015; Abancó *et al.* 2016; Giannecchini *et al.* 2016; Piciullo *et al.* 2016). The contingencies are used to calculate the skill scores, true-positive-rate (TPR) and false-positive-rate (FPR). For each rain variable, an ROC curve is formed by plotting FPR and TPR. The area under curve (AUC) provides a formal measure for each rain variables classification performance between 0 and 1 (Bradley 1997; Wilks 2006; Staley *et al.* 2013; Carvalho *et al.* 2014; Giannecchini *et al.* 2016). An ROC curve which tends toward the upper left portion of the chart indicates a variable that distinguishes useful information from the data. The diagonal, no-gain-line (AUC = 0.5) indicates a variable with random performance, with equal FPR and TPR. AUC is used to compare the performance of each rain variable.

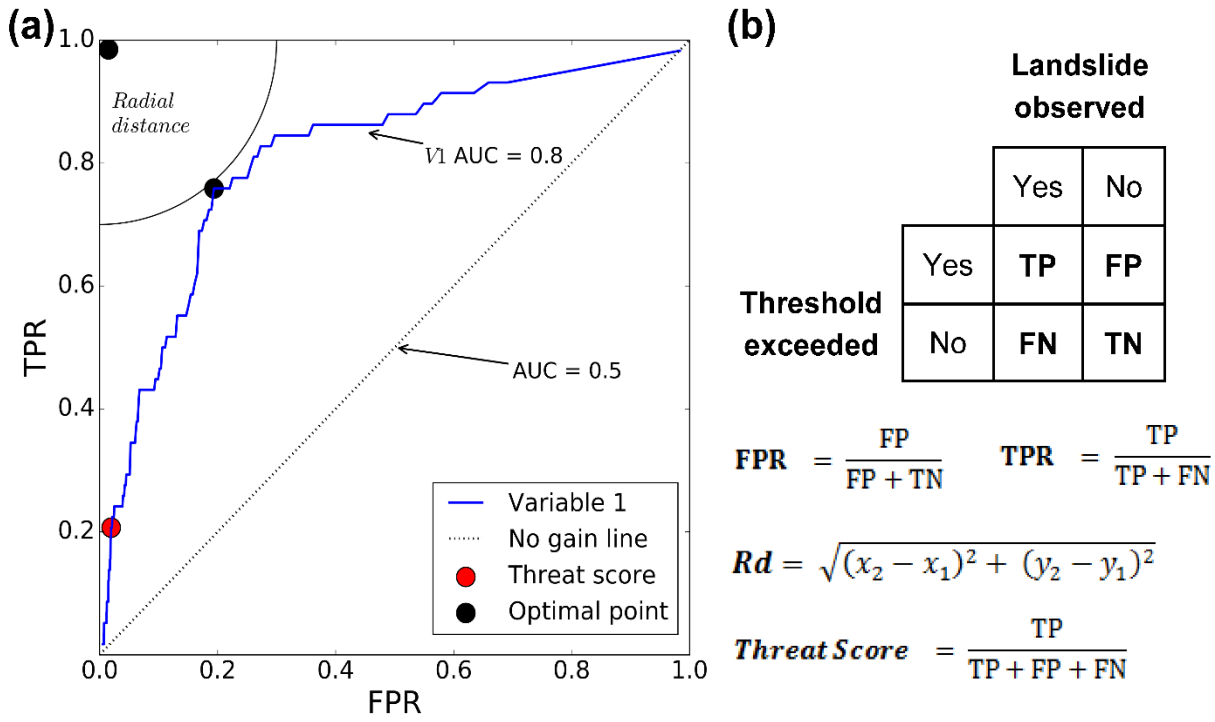

Figure 3.10. (**a**) Example ROC curve for a rain variable (V1, blue line). AUC indicates the predictive performance of a variable, and the no gain line (AUC = 0.5) indicates a variable with random performance. The two ROC threshold selection metrics are shown, (i) optimal point (black points), and (ii) threat score. (**b**) Is a contingency table and formulae for true positive rate (TPR), false positive rate (FPR), Pythagoras theorem to find the radial distance (Rd) and threat score.

Each point on the ROC curve corresponds to the candidate threshold values. As illustrated in Figure 3.10a, two types of threshold are selected at different cut points on the ROC curve. First, Staley *et al* (2013) demonstrate that landslide thresholds can be selected by maximising 'Threat Score' (TS). TS measures threshold accuracy after correct negatives are removed and ranges from 0 to 1, with each incorrect classification reducing TS (Schaefer 1990). In the ROC space the 'optimal point' (OP) represents a hypothetical threshold which classifies all outcomes correctly. Therefore, second, thresholds are selected with minimum radial distance (Rd) to OP to maximise landslide detection whilst minimising errors. Rd is found using Pythagorean

theorem. In other fields, OP thresholds are applied for the detection of rare phenomena and in situations where missed alarms (false negatives) may result in fatalities or unacceptable losses (Schisterman *et al.* 2005; Rota & Antolini 2014). OP thresholds may therefore be appropriate for use in landslide early warning but are yet to be applied. Conceptually, the OP and TS thresholds are similar to the lower and upper limit thresholds used in early investigations (Caine 1980). Like lower limits, OP thresholds capture the rainfall conditions below which it is unlikely for landslides to occur. Conversely, TS thresholds capture the upper limit rainfall conditions above which landslides are most likely to occur.

3.3.4 Threshold probabilities

In addition to the threshold values, a probability analysis is conducted to quantify the likelihood of landslide occurrence, the uncertainty, and the statistical significance of each threshold (Glade *et al.* 2005; Chleborad *et al.* 2008; Berti *et al.* 2012). The probabilistic assessment is also used in the quantitative landslide hazard assessment (Chapter). Bayes theorem (3.3) is applied to determine conditional probabilities:

$$P(LS|TH) = \frac{P(TH|LS) \times P(LS)}{P(TH)} \quad 3.3$$

Where: $P(LS|TH)$ is the posteriori conditional probability that a landslide (LS) occurs given the exceedance of a threshold (TH), $P(TH|LS)$ is the conditional probability of observing the TH when a LS occurs, $P(LS)$ is the priori probability that a landslide occurs regardless of rainfall conditions, and $P(TH)$ is the marginal probability of TH regardless of landslide occurrence.

The terms in Bayes theorem are calculated using the contingencies computed in the binary classification (Figure 3.10b). Where: N_D is the total number of days recorded in the rainfall time series (= TP + FP + FN + TN); N_{LS} is the total number of landslides recorded (= TP + FN), N_{TH} is the number of days with threshold exceedance (= TP + FP); and $N_{(TH|LS)}$ is the number of days with threshold exceedance and landslide occurrence (= TP). The Bayes terms are approximated by:

$$P(LS) = N_{LS} \,/\, N_D \quad 3.4$$

$$P(TH) = N_{TH} \,/\, N_D \quad 3.5$$

$$P(TH|LS) = N_{(TH|LS)} \,/\, N_{LS} \quad 3.6$$

Equation 3.3 is therefore equal to Equation 3.7:

$$P(LS|TH) = N_{(TH|LS)} \,/\, N_{TH} \quad 3.7$$

The statistical significance of the thresholds is assessed using Bernoulli trials to approximate the binomial probability density function (i.e. a coin toss experiment):

$$P(k\ out\ of\ N) = \frac{N!}{k!\,(N-k)!} P(TH)^k \left(1 - P(TH)\right)^{(N-k)} \qquad 3.8$$

Where: $P(k\ out\ of\ N)$ is probability of getting k landslides out of N independent trials, and N is equivalent to the total number of landslides recorded (N_{LS}). The cumulative binomial probability density function (CDF_k) states the probability of getting between 0 and k landslides.

The test answers 'given the probability of observing the threshold within a given time period, $P(TH)$, how many landslides are expected to co-occur with the threshold by random chance?'. Thus, a threshold is statistically significant if ($1 - CDF_k \leq \alpha$), when k is the number of landslides that co-occur with a threshold (i.e. TP) and α is the confidence level. For example, consider a threshold that is exceeded on 80 days out of 1000, so $P(TH)$ = 80/1000 = 0.08. During 1000 days, 60 landslides were recorded and 45 of these occurred on days when the threshold was also exceeded (i.e. TP). For the 95 % confidence interval ($\alpha = 0.05$), the null and alternative hypotheses state:

$H_0 : c \geq \alpha$; the occurrence of landslides is not related to threshold exceedance.

$H_1 : c \leq \alpha$; the occurrence of landslides is related to threshold exceedance.

In the example, the critical value to reject H_0 at the 95 % confidence level is 13 landslides, so H_1 is accepted as 45 landslides were recorded.

3.3.5 Effects of rainfall record length

To evaluate the influence of rain record length, the contingency scores, AUC, threshold values and Bayesian probabilities are calculated using ten different rainfall record lengths which reflect the approaches taken in previous landslide threshold investigations. The process involves using different proportions of the landslide site-specific-rainfall records (SSR), or time series, obtained from the precipitation radar. The different SSR lengths used are: 10, 20, 30, 45, 90, 180, 365, and 730 days before each landslide event, all days before ('Prior'), and all ('All') which includes all available data either side of landslide occurrence (March 2004 to August 2016). The 'Prior' record is influenced by the date of landslide occurrence.

In addition to graphical plots, the mean (μ) and standard deviation (σ) of the rain variable AUC scores and thresholds probabilities are used to assess the effects of varying rainfall record length. For the 'Threat Score' and 'Optimal Point' threshold values, the coefficient of variation ($CV = \frac{\sigma}{\mu}$) is used to measure the amount of threshold variability. CV is used because it is a unit-less measure and can be used to compare the relative variance of the threshold values for different rain variables, units and means.

3.3.6 Threshold combinations

In addition to finding thresholds for each individual rain variable, the above processes are used to determine combined thresholds for pairs of rain variables. Combinations can produce more robust threshold as they are able to capture both the short-term, landslide triggering rainfall conditions (e.g. 1 - 2 days) and the long-term antecedent rainfall (e.g. 3 – 20 days). The inclusion of antecedent rainfall is of particular importance as this is known to increase the slope

material pore water pressure and to reduce effective stress, so that shear strength is reduced and a landslide occurs (Iverson *et al.* 1997; Wieczorek & Glade 2005; Napolitano *et al.* 2016).

It is meaningless to examine all possible threshold combinations because many of the rainfall variables may be poor predictors of landslide occurrence and many variables may be highly correlated with one another. For example, the 1 and 2-day rain accumulation variables are likely to be highly correlated. Including highly correlated variables may over or under-estimate the threshold probabilities. In addition, this is an exhaustive and inefficient process given that there are some 500,000 possible threshold combinations ($\frac{10{,}000!}{2!(10{,}000-2)!}$, 10,000 is the total number of candidate thresholds = 4 variables × 10 antecedence periods × 250 candidate thresholds).

A criterion is applied to select suitable pairs of rain variables. First, the AUC scores are used to identify the best performing rain variables. Second, statistically independent and weakly correlated pairs of variables are identified using Spearman's rank order correlation (R). To avoid issues with the large sample sizes, the average R is used from a 500 random sub-sampling tests of the data ($n = 300$). The cut off values of AUC and R are selected based on the range of obtained values and is also guided by values used in previous studies. Søren et al (2014) use $R < 0.8$ and several studies report good AUC ≥ 0.85 (Staley *et al.* 2013; Giannecchini *et al.* 2016).

3.4 Network Traffic Model

3.4.1 Definition of the road transport network

The road network is obtained from OpenStreetMap (OSM), the native input for the SUMO simulation software used. The OSM network data is supplied in a OSM extensible markup language format (OSM-XML) that describes the network as a directed graph. The OSM-XML network contains the following information: each road segment is a collection of road lanes with information on their classification (e.g. secondary roads or motorways), location, geometry, direction of travel and speed limit; junction nodes provide the connections between the road segments and lanes, including rights of way and turn restrictions.

As the OSM network data is open source, the network is validated using a proprietary integrated transport network (ITN) produced by the Ordnance Survey (Ordnance Survey 2016). The ITN is the official dataset developed and maintained by regional and national road authorities in the UK. The two networks share the same geometry and topology (i.e. the road segment lengths and connections are correct). The validation ensures that the attributes of each road segment in the OSM network reflect those recorded in the ITN, including the turn restrictions, road speed limits, and road segment classifications. The validation is an attribute table comparison conducted within a geo-spatial SQL database PostGIS. Only a small number (24) of road speed corrections were made to reflect the speed limits recorded in the ITN.

The simulation network includes roads classified as strategic (e.g. motorway and arterial), primary and secondary (e.g. inter-regional and regional) in mainland Scotland. The roads on the Isles of Sky, Mull and Bute are also included as these are connected by bridges or regular ferry services. Roads classified as tertiary, residential and unclassified are omitted, such as residential streets, cul-de-sacs and single lane tracks. Omitting these minor roads significantly increases the computational efficiency of the traffic simulation. In addition, this strategy is consistent with previous studies that note that minor roads contribute little to regional and inter-regional traffic patterns (Dalziell & Nicholson 2001; Jenelius & Mattsson 2012; El-Rashidy & Grant-Muller 2014; Demirel *et al.* 2015; Meyer *et al.* 2015).

3.4.2 Network disruption events

A network disruption event is a hypothetical and/or historical event designed to represent conceivable manifestations of a landslide hazard on the road network. Each event represents a road segment closure which lasts for the duration of the traffic simulation. To clarify the adopted terminology, ‘event’ (i.e. single hazard occurrence) and ‘event set’, is widely used in this way in probabilistic risk assessment, hazard analysis, and catastrophe models (i.e. in insurance) (Kappes *et al.* 2012). This terminology is also applied in past network studies (Murray *et al.* 2008; El-Rashidy & Grant-Muller 2014), however, others also use ‘scenario’ specifically for potential hazard occurrences restricting ‘event’ to actual past occurrences (Meyer *et al.* 2015). At its most basic, an event set could simply be compilation of the historical occurrences of a hazard, but are commonly supplemented by physical or statistical modelling to extrapolate beyond experience to potential and extremely rare events.

For this study three sets of landslide events are created. First, an event set is formed using the known historical landslides that caused disruptions on the road transport network. Then, two event more sets are created using the landslide susceptibility models. One of these event sets

is created using the logistic regression model described above, whilst the other is created using the BGS GeoSure susceptibility model. The process to select each landslide event is identical to the steps to identify susceptible road segments in section 3.2.5 Susceptible road segments and model validation

The landslide event sets are generated on Scotland's 4300 km strategic road network. This network is the main transport connection between regions, population centres and key infrastructure; locally termed the "trunk" road network. Landslide events are defined for individual road segments (i.e. between junctions) and assume complete closure (i.e. all lanes in each direction). Events are not created on junctions (i.e. intersection or slip roads) or on primary and secondary roads (e.g. interregional and local roads). This is to constrain the scope and complexity of the study (Jenelius 2009; Nyberg & Johansson 2013; Demirel *et al.* 2015; Meyer *et al.* 2015) and to align with national level management of the strategic road network; all other roads are managed at the local authority level.

3.4.3 Creating an Origin-Destination matrix of road traffic demand

An OD matrix describes the start and end location of every trip made within the network. As illustrated in Figure 3.11a, trips are usually distributed between transport analysis zones and the OD matrix classifies the number of trips coming from and going to each zone. Note that trips with the same origin and destination zone represent internal trips (e.g. local trips).

(A)

OD Matrix		Destination Zones	
		A	B
Origin Zones	A	$Trips_{AA}$	$Trips_{AB}$
	B	$Trips_{BA}$	$Trips_{BB}$

(B)

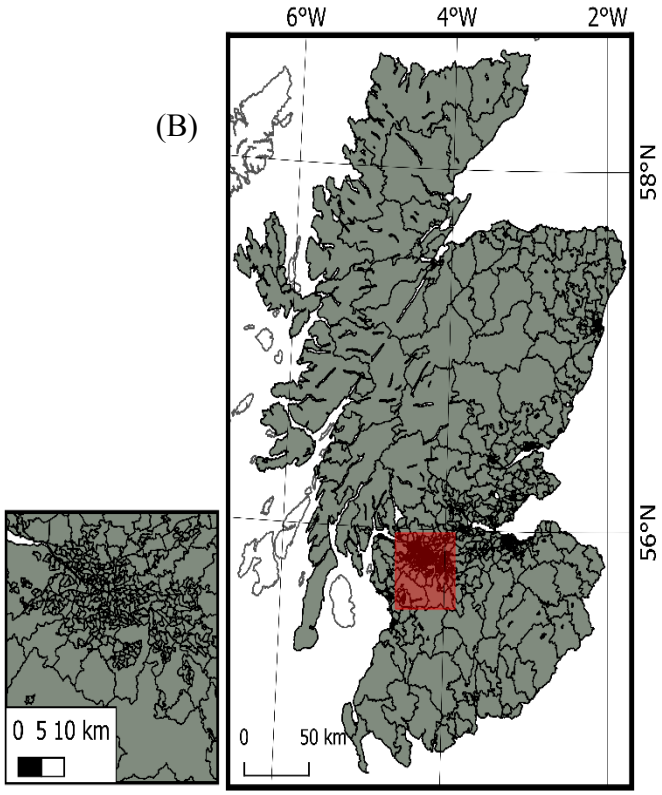

Figure 3.11. (A) example of an origin destination matrix. (B) A map showing the 1212 transport analysis zones for Scotland in the 2011 census; the insert (red box) shows the zones for Glasgow city.

A UK wide OD matrix data was obtained from the recent 2011 census that is available on safeguarded release for academic research (ONS 2011a). The dataset represents the "location of usual residence and place of work by method of travel to work" on a typical weekday and for all residents aged over 16. The OD trips are made between different geographical zones including: middle super output areas in England and Wales, super output areas in Northern Ireland, and intermediate zones in Scotland. In the study area (Figure 3.11b), the 1212 intermediate zone boundaries were designed to represent areas of 2500 to 7000 residents based on similarities in small area statistics including, population demographics, housing, health, crime and education (Flowerdew & Feng 2005). These zones have mean and median area of 57.8 and 1.7 km^2, with smaller zones in urban areas with higher population density.

	Method of travel to work	**Count**	**%**
Road	Car or small van	1,374,018	73.20
	Bus	271,337	14.46
	Passenger in a car or van	145,996	7.78
	Bicycle	35,521	1.89
	Other	28,696	1.53
	Taxi	14,377	0.77
	Motorcycle or scooter	7135	0.38
	Sub-total	***1,877,080***	***100.00***
Non-Road	Work from home	276,628	
	Pedestrian	265,413	
	Train	101,109	
	Underground, light rail, tram	7590	
	Sub-total	***650,740***	
	Total: all categories	**2,527,820**	

Table 3.6. The number and percentage of trips made by different methods of transportation in the study as reported in the 2011 Census.

Table 3.6 lists the number of trips made for different methods of transport collected in the census OD matrix. The census captured 2.52M respondents, approximately 50 % of the study area population. Table 3.6 is split into road and non-road based methods of transport as the focus of this study is the road transport network. For road based methods, the percentages show that trips made using cars or small vans and their passengers comprise 81 % of all trips made on the road network. The information for the number of passengers enables the calculation of the vehicle occupancy rate in each zone. Vehicle occupancy is the average number of persons per vehicle per trip and is used when estimating the travel time and economic impact of disruption. For example, WebTAG gives a UK average vehicle occupancy rate of 1.16 (DFT 2014a). Pragmatically, the traffic model is constructed using only the car or small van OD matrix and the vehicle occupancy rates calculated from the passenger OD matrix. This is because: i) these data represent a large majority (81 %) of the total daily trips made in Scotland; ii) trips made by other methods, such as by bus, taxi or motorcycle, are likely to be most prevalent within urban areas where landslide activity and thus the potential to be disrupted is limited; iii) other modes will have little or no effect on road traffic flows, such as cycles and

pedestrians; and iv) as multi-modal trip modelling although possible in SUMO is still in its relative infancy.

Traditionally, OD matrices were generated using surveys of road users travel characteristics, such as trip start-end locations and frequency (Ortuzar & Willumsen 2011). These surveys were conducted either at the road side or at home addresses and this was very expensive, disruptive to travel, cumbersome and hence many people were reluctant to participate. Consequently, data quality is usually very poor. Recently, other techniques have been used to generate OD matrices including, 'activity generation' using population statistics, and maximum entropy estimation from traffic count data (Ortuzar & Willumsen 2011; Peeta *et al.* 2015). Approaches using traffic count data are attractive as this data provide a continuous record of traffic patterns, is relatively abundant and cheap to obtain. The OD matrix used in this study partially overcome issues related to data quality as all eligible persons are required to reply to the census by UK law (Census Act 1920). To protect personal identities the OD matrix only specifies the method of transport, the number and the start and end zone of each trip. It also lacks information on the time of day that trips are made. In reality, the traffic demand represented within the OD matrix is time dependant and during rush hour increasing levels of demand often exceed road capacity leading to congestion. Therefore, to create the traffic model the OD matrix must be spatially and temporally discretised.

SUMO includes applications to overcome these issues. First, spatial discretisation of the OD matrix. The trips in the OD matrix are assigned specific start and end locations in the network by the following steps:

- The 'EdgesInDistricts' application is used to create a list of all the road segments and nodes within each transport analysis zone. The application also flags any zones that are not connected to the network by any road. Five unconnected zones were found and these were reconnected by re-building the network and including the minor roads that intersect these zones (e.g. tertiary or residential roads).
- The 'OD2TRIPS' application uses the list of road segments and nodes in each zone created in step 1 to split the OD matrix into a list of individual trips with distinct start and end locations. OD2TRIPS randomly assigns start-end locations at any position along a link or start-end positions can be fixed to nodes. The start-ends were limited to node positions as this is typically where the minor roads were connected to the major road network (e.g. to residential areas or places of business). Internal trips starting and ending within the same zone were also assigned random start-end nodes.
- Second, the trips are temporally distributed by analysing traffic count records from across Scotland. The Department for Transport, Scotland provide 15-minute resolution automatic traffic count data from 40 sites on the major road network over the period January 2004 to March 2015. Figure 3.12 illustrates the average hourly traffic count at each site on weekdays for the 11-year period. The traffic model is constructed to represent the weekday morning rush hour from 03:00 to 10:00 am (vertical dashed lines). This period is selected since it represents one third of the weekday traffic count and as the census OD data characterises commuter trips that are predominantly made during these hours (DFT 2014a). Additionally, the level of traffic demand goes from near zero to the daily peak over these 7-hours. In terms of traffic simulation, it is a far more logical approach to gradually increase the number of vehicles in the model as opposed to starting from a congested situation. The traffic count data is used to temporally distribute the OD matrix trips:

- The hourly proportion of traffic 03:00 to 10:00 am is calculated using the annual average weekday traffic count data illustrated in Figure 3.12. These are: 03:00-04:00 am 1.03 %, 04:00-05:00 am 1.15 %, 1.84, 4.20, 11.70, 24.56, 29.49, and 09:00-10:00 am 26.01 %. OD2TRIPS uses these proportions to assign a start time to each trip. A known limitation to this approach is due to the fact that the hourly traffic proportion is known to vary by day of the week and seasonally. For example, the mean hourly proportion of traffic in the network on a Monday during a summer month is different from a Friday during a winter month. This study uses the mean annual weekday proportions for simplicity. Other studies focussing on, for instance, the impact of landslides initiated solely by winter storms may therefore wish to use seasonally adjusted values.

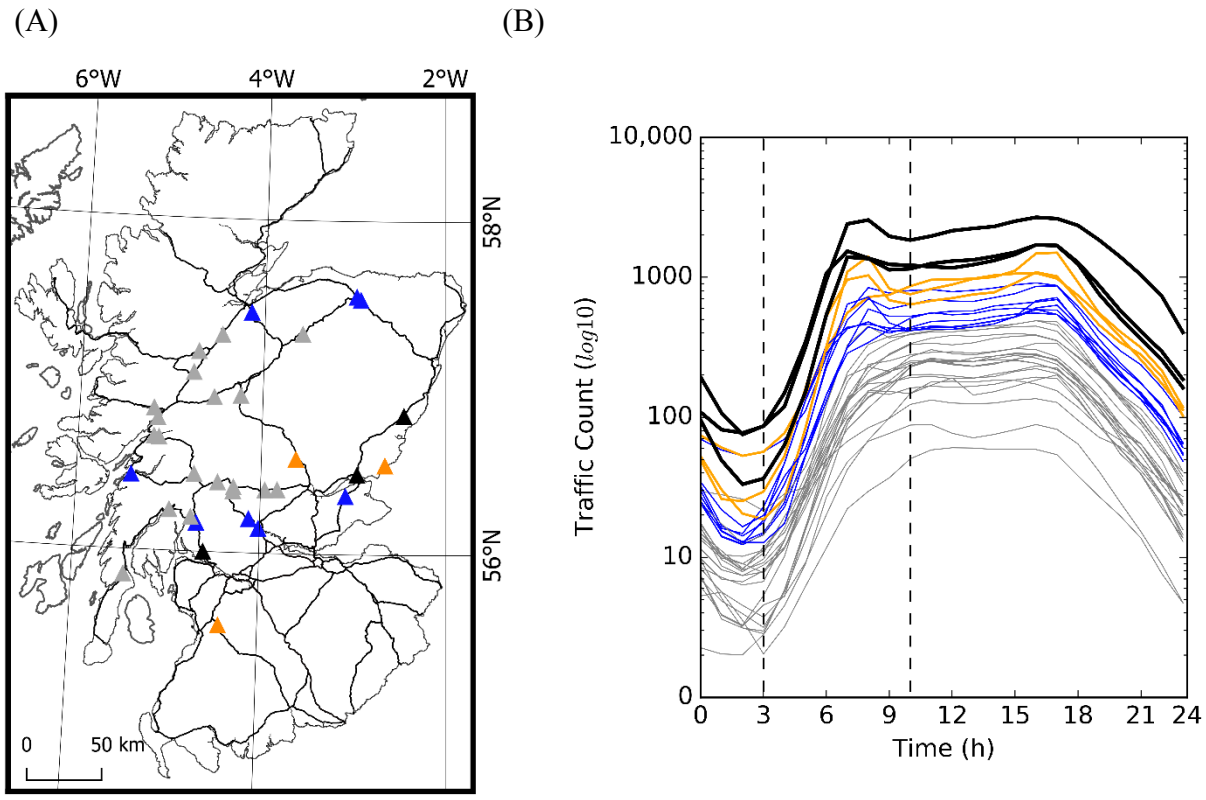

Figure 3.12. A) Map showing the location of 40 automatic traffic counting sites on the major road network. B) The hourly average traffic count (log scale) on weekdays January 2004 to March 2015.

3.4.4 Traffic simulation

The traffic simulation was conducted using a Windows 7 operated Intel Xeon CPU E5-2450 v2 @2.50 GHz with 128 GB ram. The traffic simulation, including the time and cost of travel, can be seen as the result of combining the OD matrix trips (i.e. traffic demand) and the route choice behaviour. In the literature review it is established that Wardrop's (1952) user equilibrium principle (UE) is an accepted model of route choice for congested networks: every vehicle chooses the route that minimises its travel cost, and a UE state is reached when no more routes can be adjusted to reduce the cost of travel. UE assumes that as the level of trip demand increases on certain routes and road segments, so too will the cost of travel and at some point it will become cheaper to use alternative routes. For this reason UE is widely applied to model the spill-over effects and self-optimising nature of road network traffic (Ortuzar & Willumsen 2011; DFT 2014a).

The SUMO application 'DuaIterate' performs an iterative procedure of dynamic user assignment to calculate a user equilibrium state. The mathematical implementation of this procedure was first developed by Gawron (1998) and is described below:

1. The SUMO application 'DUAROUTER' is called by 'DuaIterate' to calculate the initial route of each trip using the Dijkstra shortest path algorithm. For each trip (i) in the OD matrix, the shortest path route is calculated as a function of the uncongested travel-time (i.e. road distance × road speed) between the origin (O_i), destination D_i and departure time (T_i).
2. The simulation application 'SUMO' is used to calculate the 'real' travel times of the calculated routes, such as trip travel time, average speed and queuing time; the technical aspects of the simulation are described below. SUMO also generates a series of dump files that hold aggregated information on the travel-time cost of traversing each road segment at regular intervals throughout the simulation. The simulation ends once all trips are complete.
3. The next iteration begins by re-initializing DUAROUTER to recalculate the shortest routes in step 1. The new routes are calculated taking network congestion into consideration by using the road segment costs held within the simulation dump files from step 2.
4. Steps 2 and 3 are repeated until a user equilibrium state is achieved and the DuaIterate process is terminated. The convergence of the simulation to UE is measured by the standard deviation of the trip travel times across each iteration. The UE convergence criteria used is for standard deviation < 0.01, as indicated in the SUMO documentation.

The key publications regarding the technical aspects of the core 'SUMO' traffic simulation application used in step 2 include: the car following model (Kraus *et al.* 1997), the dynamic user assignment procedure as described above (Gawron 1998), and their implementation within an open source software package (Krajzewicz *et al.* 2012).

The car-following model is used to define vehicle speeds in relation to other upstream vehicles. The model and its default parameters allow vehicles to travel at the maximum possible speed so that a vehicle could stop without causing a collision. It also enables vehicle acceleration and speed to deviate by 10 % so that overtaking is possible, such as on dual carriageways, but without violating the condition for no collisions.

The SUMO model is a time-discrete and space-continuous traffic flow simulation. The default time step length is 1 second, this is recommended for the car-following model which treats vehicle speed as a constant in each time step (i.e. the Euler method). A first order 'Ballistic' method is planned for future SUMO releases (Treiber & Kanagaraj 2015). Spatially, SUMO is an integrated micro-meso scale traffic simulation (Burghout *et al.* 2006; Krajzewicz *et al.* 2012). The model supports micro-scale considerations of for example, calculating the least cost routes of each trip, and facilitates extensions for possible areas of future interest, such as intelligent transport control systems, partial road closures and multi modal transportation. In addition, it enables efficient meso-scale computation of traffic patterns at junctions and intersections, such as aggregating traffic movements over complex nodes, that cannot be realistically modelled at the micro scale in large and complex networks. These features mean that SUMO is designed to handle very large networks, with no hard limits on the number of roads or vehicles.

3.4.5 Model validation

Several statistical and semi-qualitative procedures are applied to in order validate the traffic simulation model:

- The undisrupted network simulation (e.g. no landslide events) is calibrated SUMO's Calibration of Dynamic Traffic Simulations (CADYTS) application (Flotterod *et al.* 2012). The tool bridges the gap between empirical traffic flows, in the form of automatic traffic count data, and the traffic flows produced by the simulation. First, the calibration computes the normalised Root Mean Square Error ($nRMSE$) between the observed and modelled traffic counts. The error value is calculated using the same automatic traffic count data used to define the OD matrix trips. The $nRMSE$ measure is widely used in transportation modelling and values of 2.5 – 25 % are reported for the best models in (Smilowitz *et al.* 1999; Brockfeld *et al.* 2003; Ortuzar & Willumsen 2011). Second, if poor error values are obtained, CADYTs follows a stochastic route re-assignment procedure whereby vehicle routes are randomly re-calculated until the $nRMSE$ value is reduced.
- In addition, a sensitivity test and mean error value for each OD zone (e.g. $\pm$5 minutes) is determined by simulating 30 disruptions on segments expected to have little effect (i.e. road segments with no undisrupted traffic flow).
- The results of the model are compared to the results obtained using other models by Winter *et al.* (2014).

3.4.6 Impact measures

For each event the travel delay and economic impact is considered nationally and within each OD zone. Economic impact is derived using UK national average value for travel time generalised cost (i.e. the market price value of occupant time and vehicle operation). This value is used in transportation planning and appraisal (DFT 2014a), and in previous impact assessments (Winter *et al.* 2014). The nationwide impacts (NI) are given by Equation 3.9:

$$NI = \Delta T_{o,d} Cost \qquad 3.9$$

where the additional travel time (ΔT) between all OD zones (o, d) in the undisrupted and disruption event simulation is multiplied by the user generalised cost ($Cost$).

The spatial distribution of impacts is illustrated in terms of extended hazard impact footprints. These footprints are constructed by aggregating the NI values of individual trips by their zone of origin (i.e. their zone of residence).

Some disruption events may completely disconnect OD pairs and produce isolated sub-networks. Travel to and travel from these sub-networks to the primary network is impossible (i.e. taking infinite time within a simulation). Therefore, the travel time measures outlined above are not suitable. In the literature several approaches and measures have been demonstrated to handle sub-network scenarios, including: not fully closing disrupted segments (e.g. reducing speed to 99.9 %) (Sullivan *et al.* 2010); using a measure for the proportion of unsatisfied demand (Jenelius *et al.* 2006a; Rupi *et al.* 2014); or by setting travel time delay equivalent to the disruption duration (Jenelius 2009).

This study uses a new approach based on the rational that initially, in undisrupted network conditions, a trip is made to gain some economic or social benefit. It is reasonable to assume that the value of the benefits received by making the trip are equivalent or greater than the cost of travel (e.g. an employee must receive the same or more money in their daily pay than the cost of commuting to work). Therefore, in this study, trips are omitted from the simulation if an event disconnects their OD pair (i.e. there is no possible route). The impact of these trips is taken as equivalent to the undisrupted value of the trip. For instance, consider a trip that has an initial, undisrupted duration of 1-hour. During an event the trip's OD pair is disconnected and so the trip is omitted from the simulation. However, as the trip was not possible a +1-hour travel time impact is still accounted for at the origin zone and national aggregation level.

3.5 Catastrophe model

3.5.1 Catastrophe model framework

The catastrophe (CAT) model framework developed in this study adopts the logic and modules used by best practice academic and state-of-the-art proprietary models, such as those used in insurance and re-insurance (Grossi & Kunreuther 2005; Foote *et al.* 2017). The framework is comprised of four modules: hazard, exposure, vulnerability and finance or loss. This enables controlled and repeatable experiments to be conducted. A description and details of each module, including the input data and the modelling assumptions, is provided in the following sections.

3.5.2 The hazard module

The hazard module utilises the results of the empirical landslide hazard analyses and a Monte Carlo sampling procedure to create thousands of potential landslide events (the event set) on the road network in Scotland. Each event is associated with a probability of occurrence and the event set is used to drive the exposure, vulnerability and financial modules of the CAT model.

The criteria for each event is as follows:

- Each event represents the occurrence of a landslide on a strategic road network (SRN) segment and each event must contain one landslide (single segment closure) or multiple simultaneous landslides (multiple segment closures).
- For each event, it is assumed that landslide occurrence causes the complete closure of road segments along their entire length (i.e. all lanes are closed between the segment start and end nodes). This assumes that the landslide magnitude and intensity is sufficient to completely disrupt the road segment. Therefore partial road closures are not considered and this is a necessary simplification to constrain the scope and complexity of large network studies (Jenelius 2009; Nyberg & Johansson 2013; Mattsson & Jenelius 2015; Meyer *et al.* 2015). A closure duration variable is introduced in the vulnerability module to account for landslides that do not cause network disruptions (Chapter 3.5.4 The vulnerability module).

To generate the stochastic event via Monte Carlo simulation, the landslide hazard of each road segment must be quantified. The landslide hazard (H) is the probability of landslide occurrence within a discrete period of time and space. As defined in Equation 2.6, H may be derived from the multiplication of: the landslide susceptibility (p^S) calculated by the hillslope scale landslide susceptibility model; and annual the probability of landslide occurrence (p^T) calculated by the landslide initiation thresholds on 5 km^2 radar arrays, according to Bayes theorem (Equation 3.3 to Equation 3.7). The following steps describe the technical procedures used combine p^S and p^T to calculate the landslide hazard at the road segment scale.

1. Spatial database software (PostgreSQL) is used to perform intersections and joins between: a raster layer containing the landslide probability of occurrence per pixel, the hillslope section units used to model terrain susceptibility, and the road network segments. A set of candidate initiation thresholds is selected according to the threshold results (Chapter 6).
2. The landslide hazard (H_r) for each road segment (r) is defined by Equation 3.10:

$$H_r = \sum_{i=1}^{|U_r|} p^S{}_r \times max\left(p^T{}_{U_r}\right) \quad 3.10$$

where $\sum p^S{}_r$ is the sum landslide susceptibility for the set of hillslopes ($|U_r|$) that intersect each road segment (r), addressing the spatial component of the landslide hazard. And $max\left(p^T{}_{U_r}\right)$ is the annual maximum probability of landslide occurrence within the set of intersecting hillslopes on the road segment, addressing the potential loading by rainfall or temporal component of the landslide hazard. This definition of landslide hazard is consistent with those used in previous studies (Chapter 2.2.7).

The stochastic event set is then generated by Monte Carlo sampling of the landslide hazard on road segments for a representative number of years. In the study of natural hazards it is common to use 10,000 years to capture the rare, low probability events (Foote *et al.* 2017).

For each simulated year, the occurrence of landslide events is conditioned by an empirical distribution for the frequency of storms per year. Therefore, within the simulation the occurrence of landslide events is conditional on the occurrence of a storm. It is important to stress that the storm conditioning variable does not influence the annual probability of landslide occurrence due to calibration of the model, but it provides several modelling advantages. First, conceptually the use of storms is a rational approach given the present level of understanding for the active landslide process, mechanisms and the observational records obtained in Scotland, that indicate a strong association between landslide occurrence and periods of prolonged and intense rainfall during storms (Ballantyne 1986, 2002; Milne et al. 2009; Winter et al. 2010; Dijkstra et al. 2016b). Second, pragmatically the use of storms enables an estimation for the likelihood of storms and events with two or more simultaneous landslide occurrences in addition to evaluating how different spatial distributions of storm footprints (e.g. size and location) might influence the expected level of loss. Third, it enables the model to be used by future investigations of other storm driven hazards (e.g. flooding) and to evaluate other factors, including: varying the frequency of storms to reflect scenarios of future climate change (Murphy et al. 2010) Lastly, the configuration of the model enables future investigations to experiment with alternative conditioning variables with relative ease.

The storm conditioning variable represents a simplification, necessary in the scope of this study. In the most sophisticated catastrophe models the stochastic event sets are created by sampling the outputs of complex physical-process-based projections or stochastic weather generator models of, for example hourly and daily rainfall and wind speed. For the British Isle, a relevant current data set is the weather sequences produced by the stochastic weather generator of the UK Climate Impact Programme 2009 (Jones *et al.* 2009). However, several challenges remain as these data are not currently resolved for cell resolutions of < 25 Km^2 and for spatially coherent projections across groups of cells. These and other limitations are expected to be resolved in the next iteration of the weather generator expected in 2018.

The procedure used to simulate the event set is as follows:

- The procedure is initialized to run for 10,000 years (iterations).

For each year, the expected number of storms is sampled from an empirical probability mass function for the annual frequency storms of in the UK. This distribution is constructed using very-severe-gales in the Jenkinson Gale Index (Jenkinson & Collison 1977; Jones et al. 2013); the index is compiled of three gale classifications for increasing wind vorticity including, gales, severe-gales and very-severe-gales. The gale index is available for the period 1871 to present day and the 2004 to 2016 period of the index is used to provide consistency with the period of the landslide observations and the rainfall data used in by study (Chapter 3.1.2). The gale index and other comparable indices, for instance the 1871–2012 record of cyclone frequency, intensity and 'storminess' derived from the 20th Century Reanalysis V2 (20CR), have shown cyclonic activity to serve as a meaningful proxy of seasonal precipitation patterns in the British Isles (Matthews *et al.* 2016). The 20CR data was not used as the period of landslide data extends beyond 2012.

- The landslide hazard of each road segment (H_r) is calibrated to account for the observed number of landslides per storm in the period 2004 to 2016 in Scotland. The calibrated landslide hazard (Hc_r) is:

$$Hc_r \frac{(H_r \times f)}{J} \qquad 3.11$$

where H_r is the uncalibrated landslide hazard on each road segment and J is a calibration coefficient for the average number of landslides per storm; J is calculated using the number of landslides and the number of very-sever-gales in the gale index for the period 2004 to 2016. The f variable is the approximate mean number of road segments effected by a storm and is used to account for storm size. For instance, for a very large storm covering all of Scotland $f = 1$. This variable allows for smaller storm footprints that cover a portion of the spatial domain to be included. For each storm in each year, the landslide events are sampled using Monte Carlo simulation of the calibrated landslide hazard on each road segment. The sampling is conducted in an independent fashion so that the occurrence of one landslide does not influence the occurrence of another. By this technique, the simulation provides a robust estimation for the number of events with 0, 1, 2…∞ simultaneous landslide occurrences. It is important to highlight that this reflects the estimated likelihood of landslides occurring on one or more individual road segments. It does not reflect the likelihood of multiple landslide occurrences along the length of a single road segment.

The result is of all the above procedures is an event set that represents 10,000 years' worth of randomly sampling the storm frequencies and the road segment landslide hazard for the period 2004 to 2016 in Scotland.

3.5.3 The exposure module

The exposure module contains information on the objects being modelled and their monetary values. In this study, the objects being modelled are the SRN segments and their exposure values are the indirect economic impacts calculated using the traffic model (Chapter 3.4). The event impacts calculated by the traffic model indicate the additional cost of travel during a single period of peak traffic flow.

For events with one landslide occurrence (single segment disrupted), the full range of impacts is calculated by applying the traffic model to all 580 SRN segments in Scotland. For the events with two or three simultaneous landslides there are approximately 170,000 and 32,000,000 possible combinations. As each traffic simulation takes 6 – 10 hours, simulating the traffic for each combination would likely take tens of years without a significant increase in the available computing resource. Subsequently, the traffic impacts of 300 events with two landslide occurrences and 100 events with three landslide occurrences were calculated to provide a 10 % margin of error at the 95 % confidence level. The events with two and three simultaneous landslides were sampled from the stochastic event set without replacement – each one is represents a unique combination of roads. For simplicity and computational efficiency, the events with four or more landslides were not included in the CAT model. In addition, the simulated probability of these events was found to be very low (Chapter 7.2).

The CAT model is run for a set number of years. For each year there is a sampled number of storms, and within each storm the landslide hazard is sampled to generate one or more landslide occurrences on the roads in Scotland. For the storms with one landslide, the exposure module retrieves the event losses from an empirical distribution lookup table for each of the 580 SRN segments in Scotland. When a storm produces two or three landslides, the exposure module samples the event losses from a skewed normal distribution. The skewed normal distributions are generated by maximum likelihood estimation for the samples of 300 two landslide events and 100 three landslide events described above. Future investigations may reduce the margin of error by simulating more events.

3.5.4 The vulnerability module

The vulnerability module provides the interface between the hazard, exposure and loss modules. Usually this involves a series of damage functions that are used to provide a look-up between the hazard intensity and the estimated damage caused to a modelled object as a proportion of its total exposure or total value (Foote *et al.* 2017). For the hazards where loss data are generally available (e.g. insurance claims due to flooding), a variety of damage functions have been constructed that account for different characteristics including, geographic region, flood inundation depth, replacement costs, building construction, and building usage (Merz *et al.* 2004; Sampson *et al.* 2014).

In this study, the simplifying assumption is made that when a landslide event occurs its magnitude and intensity is sufficient to completely disrupt the road segment and partial road closures are not considered (Chapter 3.5.2). However, the duration of a landslide disruption is determined by a complex combination of factors including, the hazard magnitude and intensity, the complexity and cost of remediation, and the availability of resources. To account for event duration, an empirical distribution of road closure duration is constructed using records contained in the landslide database obtained for Scotland (3.1.2). The records indicate that the range of disruption durations are in the order of 0 (< 12 hours), 1 (12 to 24 hours) to 15 days. The CAT model is applied with and without these durations to illustrate the effect of disruption duration on landslide losses. For the latter, the duration of disruption is assumed to be 1 day.

3.5.6 The Financial Module

The financial model provides the primary outputs of the CAT model. This includes metrics and probability distributions of loss. The Annual Average Loss (AAL) is the average loss of all simulated events weighted by their annual probability of occurrence. AAL indicates the losses

expected within any given year. The Occurrence Exceedance Probability (OEP) is the probability distribution that a loss from a single event will exceed a certain value within a year. OEP is be used to determine and identify the likelihood of losses due to rare and extreme events. The Aggregate Exceedance Probability (AEP) is the inverse of cumulative probability distribution function that the sum of event losses is equal to or greater than a certain amount within a year. AEP indicates the likelihood of a certain level of loss. The AEP may also be calculated in terms of the losses expected for a certain return period (e.g. the annual losses for a 1 in 100-year return period).

Chapter 4 Landslide Susceptibility

4.1 Introduction

Chapter 4 presents the results and discussion of the landslide susceptibility modelling. Landslide susceptibility is the spatial propensity or landslide occurrence and it attempts to answer 'where' and on which roads are landslides most likely to occur in Scotland. In the literature review (Chapter 2.2), logistic regression was identified as a suitable method to construct a landslide susceptibility model and a set of candidate explanatory variables were found. The susceptibility model is trained and tested using A database of 75 shallow translational and debris flow landslides for which the landslide source location and date of occurrence is known (Chapter 3.1.2). The study area is apportioned in to hillslope units and the landslide susceptibility of each hillslope is evaluated. The effect of hillslope size on model accuracy is systematically evaluated by comparing the model results for different sized hillslope units. The model results examine how each explanatory variable contributes to increased or decreased hillslope susceptibility and this is used to inform of the landslide processes. A map of the hillslope landslide susceptibility is produced and this is used to assess the landslide potential on each road segment in the strategic road network of Scotland. The selection of susceptible roads is compared is those selected using a different susceptibility model (i.e. GeoSure).

4.2 Generated hillslopes

One of the objectives of this study was to develop a technique to create different sized catchments and their component hillslopes, and to evaluate what size hillslopes are most suitable for modelling landslide susceptibility. To this end, six different sized sets of catchments-hillslopes were created. Only the hillslopes that intersect the road network are used in the logistic regression models and the properties of these hillslopes are shown in Table 4.1. The 'catchment threshold' is the minimum drainage area required for a catchment to be formed by the number 25 m^2 DEM cells. For example, the 100 and 1600-cell thresholds create catchments of > 0.0625 and > 1.0 km^2 and the hillslopes have smaller areas (Table 4.1). A total 75 landslides are recorded in the landslide inventory. However, the number of landslides situated on the hillslopes that intersect the road network varies with the size and shape of the different hillslopes.

Catchment threshold	Total area (km^2)	Number of hillslopes	Number of landslides	Mean area (km^2)	Min area (km^2)	Max area (km^2)	Mean elevation range (m)
100	9,915.65	81,352	52	0.12	0.0025	1.94	116.47
400	15,584.30	41,792	56	0.37	0.0119	4.01	127.85
700	18,640.25	31,852	59	0.59	0.0119	6.91	132.87
1000	20,882.17	26,580	61	0.79	0.0119	6.96	136.09
1300	22,594.18	23,086	60	0.98	0.0119	8.53	138.74
1600	24,130.92	20,653	62	1.17	0.0119	10.08	141.40

Table 4.1. Summary statistics for six sets of hillslopes created in Scotland.

4.3 Input variables

Exploratory data analysis was used to examine the ability of the different explanatory variables to classify landslide occurrence and to create a selection of variables most suitable for use in the logistic regression model. With this aim, each variable is analysed using class frequency tables, histograms and the empirical probability distribution (pdf). The proportion of hillslopes in each class and the overlapping area between the pdf curves (A) are used to evaluate the skill of each variable at distinguishing between landslide (LS) and non-landslide (NLS) hillslopes (Cho *et al.* 2006; Berenguer *et al.* 2015). The smaller the overlapping area between the LS and NLS pdf curves, the more skill the variable has.

Figure 4.1 shows the results of the exploratory data analysis for the 14 explanatory variables. For brevity, only the plots of the hillslopes generated using the 1000-cell catchment threshold are shown: nonetheless the variables with the highest and lowest skill scores are consistent across the five other catchment threshold values. As indicated by the overlapping area of the pdf's, some of the best performing variables include maximum elevation ($A = 0.40$), median slope angle ($A = 0.46$) and general curvature ($A = 0.65$). Melton ratio performs relatively poorly ($A = 0.82$).

The classes in the soil depth and soil grain size variables exhibit little variation between landslide and non-landslide hillslopes (Figure 4.1K-L). In addition, a large proportion of hillslopes are characterised by a single soil depth (70 % 2 - > 5 m deep) and grain size class (85 % Argillaceous). Subsequently, soil depth and soil grain size are not used in any models. The classes in the PMM soil texture variable exhibit a more even frequency distribution (Figure 4.1J). There are very few hillslopes in the silt and peat soil texture classes, however, most silt and peat soils are confined to lowland river channels and on upland moors situated away from the major road network and its intersecting hillslopes.

For the average aspect of hillslopes, two sets of bins are displayed to demonstrate the consequence of feature engineering. Figure 4.1N shows the four cardinal aspect classes (bottom bars showing NE 0 – 90º, SE, SW, NW) and four intercardinal aspect classes (top bars showing NW - NE 315 – 45º NE – SW, etc.). Both sets have an equivalent pdf overlap ($A = 0.80$). The greatest proportion of landslides are found in the SE-SW and SW-NW intercardinal classes, capturing 62 % of all landslides. In contrast, the landslides are distributed more evenly by the cardinal aspect classes – albeit still showing a tendency for the SE and SW facing hillslopes.

The intercardinal classes may therefore be more suitable for use in susceptibility modelling. Figure 4.1 O shows the distribution of aspect average in a radial plot.

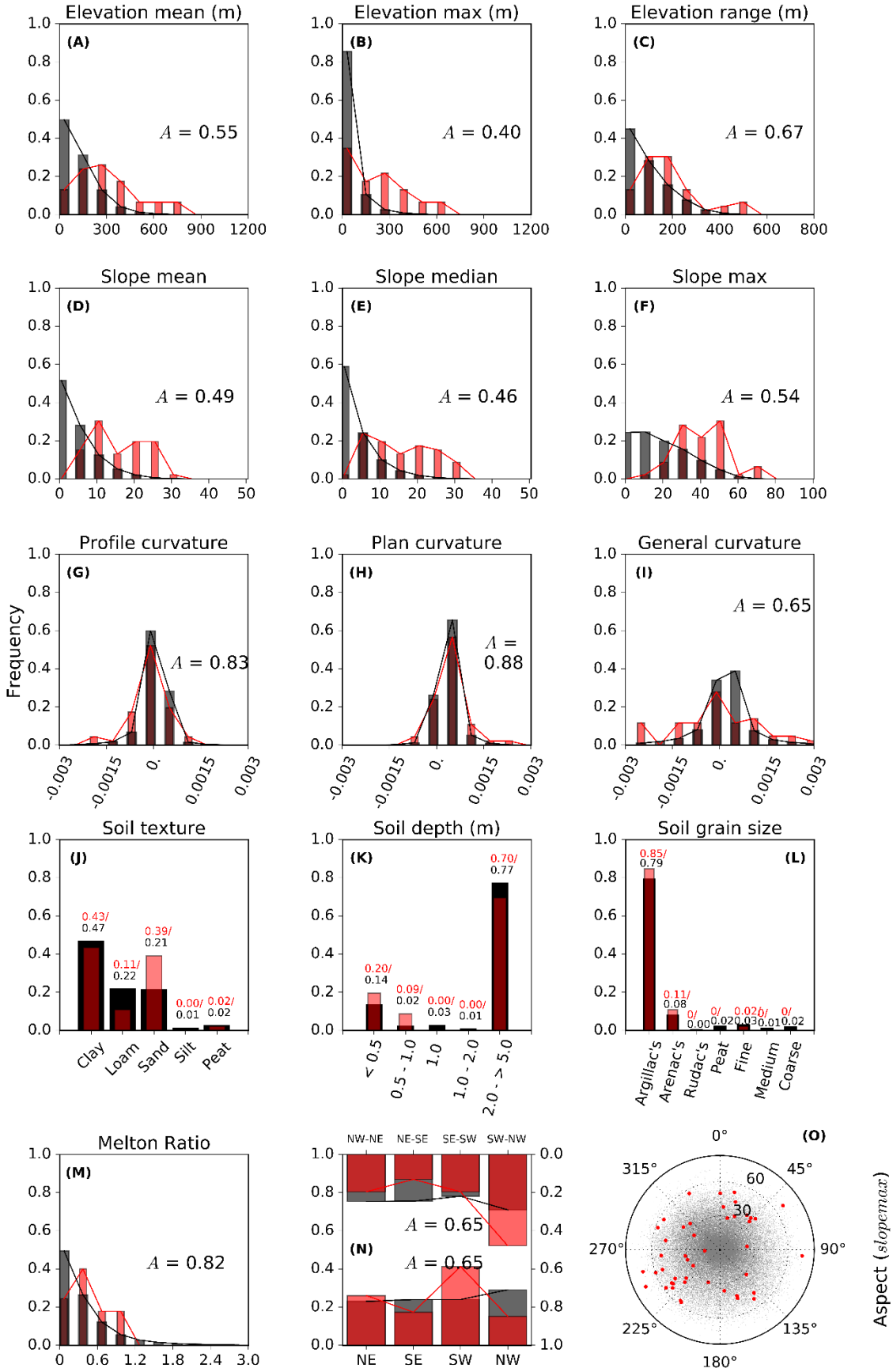

Figure 4.1. A – O histograms and probability distributions of the explanatory variables used to model susceptibility. The red bars and lines correspond to landslide hillslopes, the black ones to non-landslide hillslopes. The pdf overlap (*A*) is the shared proportion of the two distributions. Plot O is a radial plot of hillslope aspect, scaled on the *y-axis* using slope max (0 – 90º).

Correlation analysis and chi-square tests are applied to ensure that the explanatory variables used in the model are independent. The following figures are again for the hillslopes generated using the 1000-cell catchment threshold. Figure 4.2 is a matrix plot that illustrates Pearson's correlation coefficient (r) for the explanatory continuous variables. The matrix is colour shaded for negative (Blue) to positive correlation (Red) and asterisks indicate significance at the 95 % confidence interval ($p < 0.05$). A threshold of r ±0.35 is used and only one variable from each of the different values are taken (e.g. using mean slope angle eliminates median or maximum slope angle). The r threshold is based on the absolute mean of the r values obtained and is within the range of thresholds ($r = 0.25 - 0.45$) used in similar studies (Ayalew & Yamagishi 2005; Brenning 2005; Berenguer *et al.* 2015).

The chi-square statistic tests that the categorical explanatory variables independent of one another. For this test, a high p-value ($p > 0.05$) rejects the hypothesis that the variables are dependent on one another and can therefore be used together in the model: indicated by the red boxes in Figure 4.2. The blue boxes and asterisks indicate that a significant association between the variables exists. Figure 4.3 displays the chi-square statistical significance for the categorical variables aspect (i.e. cardinal and intercardinal), soil depth, soil texture and soil grain size. In addition, the curvature variables are classified in to three classes for concave (< -0.001), flat (-0.001 to 0.001) and convex (> 0.001) hillslopes: the 0.001 interval is equivalent to a radius of curvature of 10 km. This classification to makes it easier to interpret the influence of hillslope curvature on susceptibility using the logistic regression model coefficients and odds-ratio.

Two different selections of high skill and independent variables are made to use as inputs to the model. These selections are as follows:

- The first, selection A, includes elevation mean ($A = 0.55$) and maximum slope ($A = 0.54$) that exhibit a weak positive correlation ($r = 0.34$). Melton ratio is excluded due to high positive correlation to mean elevation ($r = 0.81$). Selection A also contains the categorical variables, soil texture, intercardinal aspect ($A = 0.80$) and the engineered general curvature classes ($A = 0.65$, i.e. concave, flat and convex).
- Second, selection B, includes median slope ($A = 0.46$) and Melton ratio ($A = 0.82$), also with weak positive correlation ($r = 0.32$). This eliminates all the elevation variables ($r > 0.81$). Selection B includes the same categorical variables as selection A.

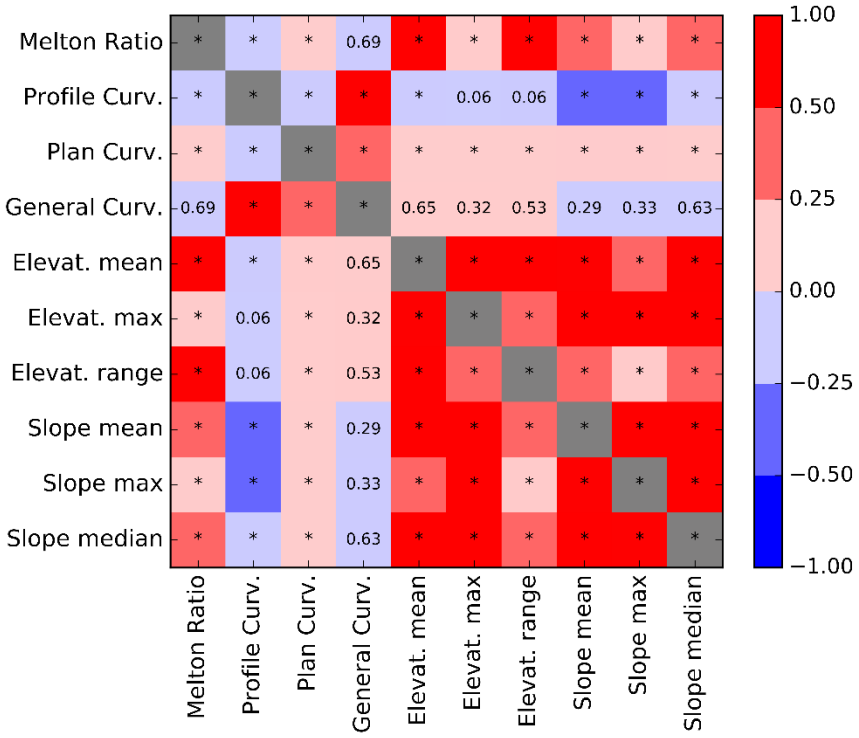

Figure 4.2. Matrix showing the explanatory variable Pearson product momentum correlation coefficients from negative (blue) to positive (red). The asterisk (*) symbol indicates that the correlation between a pair of variables is highly significant ($p < 0.05$). Correlated variables must not be included in the logistic regression model.

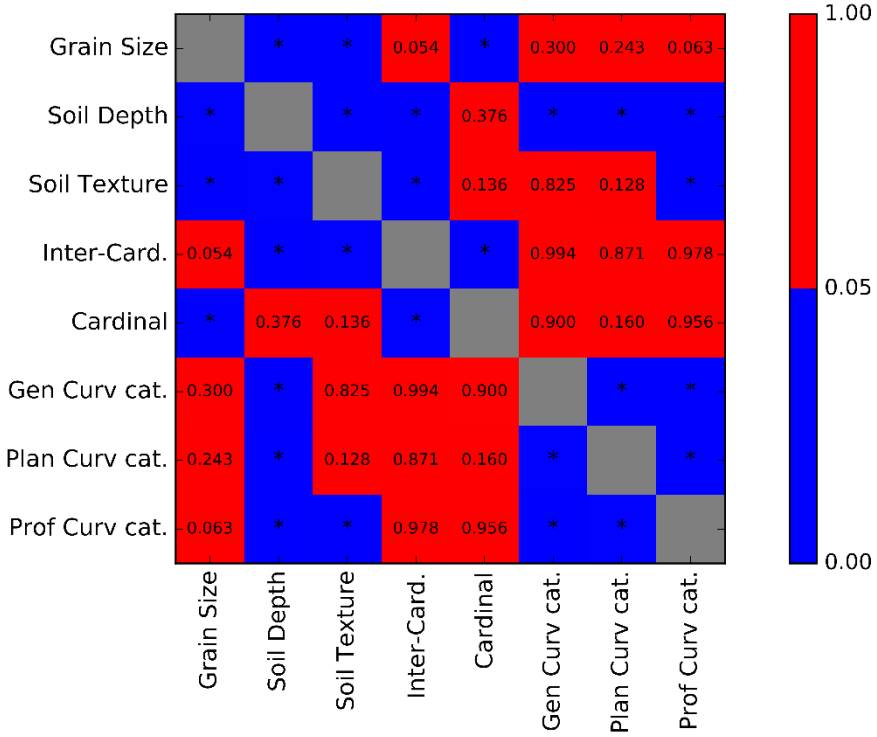

Figure 4.3. Matrix showing the explanatory variable chi-square test. The blue squares with an asterisk (*) symbol indicate that the association between a pair of variables is highly significant ($p < 0.05$). Associated variables must not be included in the logistic regression model.

4.4 Logistic regression modelling

The logistic regression model (LR) of hillslope landslide susceptibility is developed using a cross-validated and ensemble prediction approach. Briefly, the hillslope data, including the explanatory variable values and landslide records, were compiled into a single hillslope-database. To avoid known biases in the landslide database, the hillslope-database contains only those hillslopes that were found to intersect the major road network.

To fit the LR models, k-fold cross-validation ($k = 30$) is used to randomly split the hillslopes with landslides in to model training (75 %) and model validation (25 %) datasets. To each of these datasets an equivalent number of randomly selected non-landslide hillslopes is added. Producing datasets with equal number of landslide and non-landslide hillslopes. A LR model instance is fitted to each of the training datasets and predictions are made for the hillslopes in the validation dataset and for all other hillslopes in the hillslope-database. For the validation datasets, several statistics are calculated to evaluate the LR model's accuracy and goodness of fit (i.e. AIC, AUC, R^2 and chi-square p-value). In addition, the explanatory variable odds-ratios show the change in the odds for a one unit increase of a continuous variable or between each class and the reference class: higher odds-ratios (> 1) indicate that a variable contributes to increased susceptibility. The LR model prediction results for the entire hillslope-database are averaged to give an ensemble prediction of landslide susceptibility across the entire road network. The entire process is repeated for hillslopes created using six different thresholds, 100, 400, 700, 1000, 1300 and 1600 cells (i.e. hillslopes increasing in size).

A unique LR model and set of results is created for each set of input explanatory variables outlined in Chapter 4.1 (i.e. the variables selected using the correlation scores in Figures 4.2 and 4.3: selection A = Model A, selection B = Model B etc.). The following sections present the results for each of these models. The tables summarise the model performance statistics across hillslope sizes and the plots show the ROC curves and odds-ratios obtained for the 1000-cell hillslopes.

Model A:

Model A is comprised of five explanatory variables including the continuous variables for: elevation mean (1) and maximum slope (2), and the categorical variables, intercardinal aspect (3), general curvature (4) and soil texture (5). The reference classes for the categorical variables are as follows: north east to south east "NE-SE2 (3); flat general curvature (4); and for soil texture (5), the loam, peat and silt soil classes are combined due to them having low frequency amongst landslide hillslopes – leaving only the sand and clay classes.

Table 4.2 summarises the statistical measures used to evaluate model A. Smaller AIC values indicate models with fewer number of input variables (e.g. simpler) and a larger log-likelihood function (e.g. better model fit). As the number of input variables used is constant, increasing the hillslope size is shown to increase Model A's goodness of fit. The models AUC (0.79 – 0.83) and R^2 (0.27 – 0.28) also indicate a relatively good fit, yet these do not appear to be associated with changing hillslope size: pseudo R^2 values of 0.2 – 0.4 indicate very good fit (McFadden 1974; Clark & Hosking 1986). Crucially, only the 400-cell hillslope chi-square test (x^2) between Model A and the null model is significant at the 95 % confidence interval ($p = 0.035, < 0.05$). Though the p-values are close to significance for the 700 and 1000-cell hillslopes (0.057).

In Table 4.2, Table 4.3, Table 4.4 and in section 4.5 it is shown that each of the LR models performed greatest when using the 1000-cell hillslopes. As such only the plots for the 1000-cell hillslope models are shown.

Figure 4.4 displays three plots of results for Model A using 1000-cell hillslopes. Plot (A) shows 30 ROC curves for each validation dataset used in cross-validation. This illustrates the variance in model fit across the model training and validation samples. Plot (B) shows the ROC curve (grey line) for all the hillslopes on the road network in Scotland, the AUC and error (pink shading) are the mean and one standard deviation of the AUC values obtained in cross-validation (i.e. the ROC curves shown in plot A). Plot (B) also shows three susceptibility levels, 'Low' (yellow), 'Moderate' (amber) and 'High' (red). The low and high levels are the optimal point and threat score thresholds, the moderate level threshold is exactly halfway between the low and high levels. The accuracy of each level is reported (Ac) and the threshold values are given in brackets (i.e. the cut points in the modelled susceptibility probabilities between 0 and 1). Lastly, plot (C) shows the variable odds-ratios and their statistical significance (p) given by the Wald test: a critical p-value of < 0.1 is suggested by Dai *et al* (2001). Categorical variables are deemed significant if at least one of their classes is significant.

For model A using 1000-cell hillslopes (Figure 4.4C), all variables are shown to induce increased hillslope susceptibility and are significant at the 95 % confidence level. The odds-ratios (OR) may be converted to probabilities using: $P = (OR - 1.0) \times 100$. For example, a one unit increase in the mean elevation (OR = 1.003) or maximum slope (OR = 1.042) of a hillslope translates to a P = 0.3 % and 4.2 % increase in the likelihood of a hillslope being susceptible, respectively. To calculate the odds-ratio for a specific value of a continuous variable, take the OR to the power of the number of units. For example, if the maximum slope on a hillslope is 30°, $1.042^{30} = OR$ 3.435 = P 243.6 %.

For soil texture, clay (P = 17.4 %) and sand (P = 71.7 %) soils increase hillslope susceptibility relative to the reference class of loam, peat and silty soils. Figure 4.4C also displays several interesting associations between the general curvature and intercardinal aspect of hillslopes to increased susceptibility relative to their reference classes. The odds-ratio of the model intercept can be interpreted as the likelihood that a hillslope is susceptible for the reference classes and when all continuous variables are zero.

Model A				
Catchment threshold	**AIC**	**AUC**	**R^2**	**x^2 p-value**
100	121.57	0.83	0.27	0.119
400	92.12	0.83	0.28	0.035
700	80.24	0.79	0.28	0.057
1000	80.34	0.83	0.28	0.057
1300	71.47	0.82	0.27	0.156
1600	65.07	0.82	0.27	0.183
Mean	85.14	0.82	0.27	0.101

Table 4.2. Model A – statistical measures to evaluate the goodness of fit and significance of logistic regression models. AIC: the Akaike information criterion. AUC: the area under the receiver operating characteristic. R^2: McFadden's pseudo r square. x^2 p-value: the p-value of the chi-square statistic between model A and the null model.

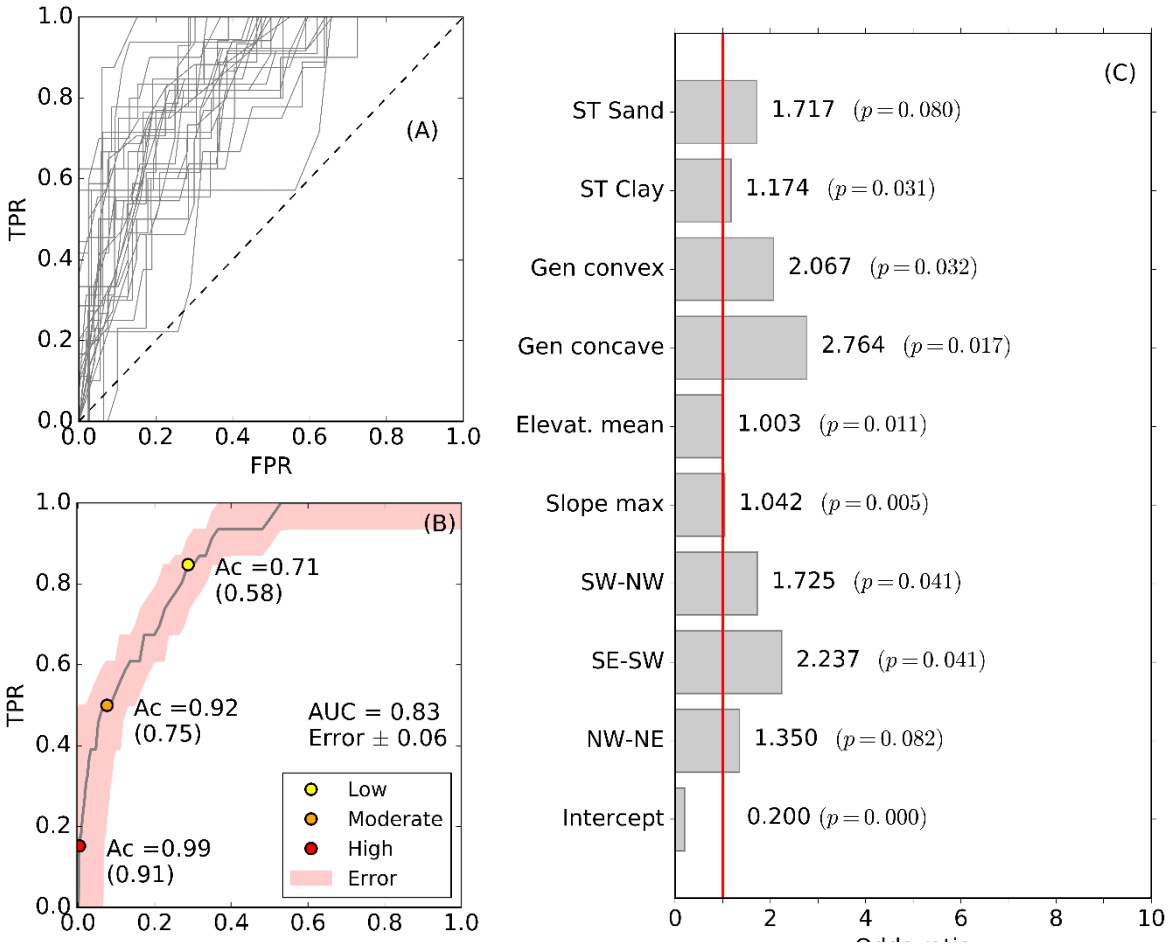

Figure 4.4. Results of Model A using 1000 cell hillslopes. (A) 30 ROC curves for each dataset created in cross-validation. (B) ROC curve (grey line) for all hillslopes on the road network; the average AUC and error values (red shading); and the low, moderate and high susceptibility cut points '(values)' and their accuracy (Ac). (C) Odds-ratios for the model explanatory variables and their statistical significance (α). The red line indicates no change.

Model B:

In Model B, median slope and Melton's ratio are used instead of elevation mean and maximum slope. Model B also includes the same categorical variables and reference categories as model A (i.e. NE-SE, flat general curvature, and the combined loam, peat and silt soil texture classes). As for model A, Table 4.3 shows that model B's AIC values decrease for increasing hillslope size, indicating improved goodness of fit. The AUC (0.85 – 0.87) and R^2 (0.34 – 0.43) values are higher for model B than model A and all hillslope sizes feature significant p-values. Figure 4.5A-C shows the ROC plots (A-B), susceptibility levels (B), and odds-ratios (C) for model B using 1000-cell hillslopes. Compared to model A, Plot A illustrates that model B produces more uniform ROC curves in the cross-validation datasets. This translates to a higher mean AUC (0.87) and lower error (± 0.06). There is also a 10 % increase in the accuracy of the low-yellow susceptibility level. The accuracy of the other susceptibility levels is unchanged (Figure 4.5B). All the model's explanatory variables are shown to increase hillslope susceptibility and are statistically significant. Each unit increase in the median slope angle of hillslopes exerts a greater influence (OR = 1.329 or P = 32.9 %) on slope susceptibility than the maximum slope angle variable used in model A: as expected given the smaller overlapping area of the median slope pdf's (Figure 4.1). A hillslope with Melton's ratio of 0.5 and > 0.65 increases the likelihood of hillslope susceptibility by 37.7 and > 51.6 %.

Each of the statistical measures used to evaluate the logistic regression models show that model B performs better than model A. In multi-variate modelling, the overarching aim is to develop the simplest possible model (i.e. fewest input variables) whilst maximising the model fit to the data. The benefits of reducing the number of input variables are twofold: first, it improves prediction accuracy by limiting the variance of multiple coefficients; second, it eases interpretation by focussing on the predictors with the strongest effects (Menard 1997; Brenning 2005). With this aim, many past studies attempt to remove input variables in a stepwise fashion and using a threshold of variable significance (Dai & Lee 2001; Brenning 2005). Here, a different approach is adopted given that each of the variables in model B are significant. Model B is re-run following a leave-one-out strategy in which one of the input variables is omitted and the model is re-evaluated. The process is repeated for each input variable. Removing the general curvature variable marginally improves the model. The removal of all other variables leads to a decrease in model performance and these iterations are subsequently discarded. The new model is named 'Model C'.

Model B				
Catchment threshold	**AIC**	**AUC**	**R^2**	**x^2 p-value**
100	107.58	0.87	0.38	< 0.000
400	89.26	0.85	0.35	0.008
700	81.27	0.87	0.34	0.003
1000	71.86	0.87	0.39	0.008
1300	69.37	0.88	0.38	0.003
1600	60.32	0.87	0.43	0.012
Mean	79.94	0.87	0.38	0.006

Table 4.3. Model B – statistical measures to evaluate the goodness of fit and significance of logistic regression models. AIC: the Akaike information criterion. AUC: the area under the receiver operating characteristic. R^2: McFadden's pseudo r square. x^2 p-value: the p-value of the chi-square statistic between model B and the null model.

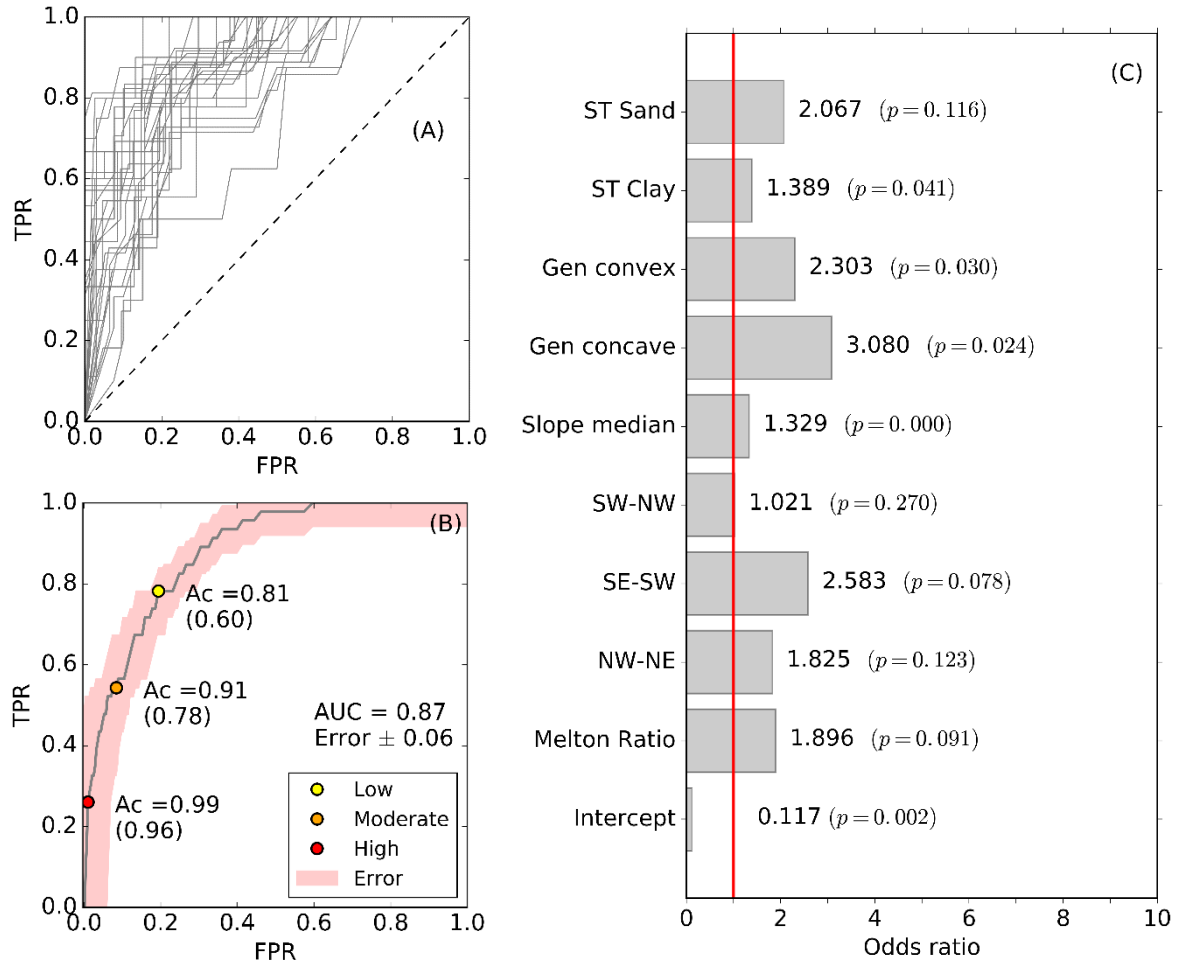

Figure 4.5. Results of Model B using 1000 cell hillslopes. (A) 30 ROC curves for each dataset created in cross-validation. (B) ROC curve (grey line) for all hillslopes on the road network; the average AUC and error values (red shading); and the low, moderate and high susceptibility cut points (values) and their accuracy (Ac). (C) Odds-ratios for the model explanatory variables and their statistical significance (α). The red line indicates no change.

Model C:

Model C includes the continuous variables: median slope (1), Melton's ratio (2), and the categorical variables, intercardinal aspect (3) and soil texture (4). The reference categories are NE-SE (3) and the combined loam, peat and silt soil texture classes (4). Table 4.4 summarises the performance statistics of model C across the different hillslope sizes. In comparison to model B (Table 4.3), the most significant changes are the reduced AIC values and chi-square test p-values. Improved AIC scores are most likely due to the removal of the general curvature input variable (i.e. a simpler model). This is supported by the fact that the AUC and R^2 scores exhibit little change. Figure 4.6A-B also shows that there is little change in the average AUC scores or in the susceptibility levels and their accuracy for the 1000-cell hillslopes. In comparison to model B, the variables feature increased odds-ratios indicating that they have a stronger effect at increasing hillslope susceptibility (Figure 4.6C). Nonetheless, the relative strength of each explanatory variable is unchanged. For instance, the sand soil class still has a stronger influence than the clay class.

Model C national:

Models A, B and C are trained and tested using the hillslopes that intersect the major road network in Scotland to avoid the bias in the landslide database. To evaluate the effects of this bias, a new implementation of Model C is trained and tested using all of the hillslopes in the study area – it is not limited to the hillslopes adjacent to the road network. In summary, this national model provides similar AUC (0.84 – 0.87) and R^2 (0.24 – 0.28) values as the models constrained to the hillslopes on the road network. The AIC values are notably higher (86.95 – 243.90) indicating reduced goodness of fit. The chi-square test p-values (0.1 - < 0.001) indicate that there is still a significant relationship between the independent and dependent variables used in Model C in comparison to the null model. Crucially however, the Wald Test significance of the coefficients and odds-ratios of each individual variable are now found to be insignificant ($p > 0.1$). In other words, an insignificant relationship was found between each input variable and the dependent variable when controlling for all the other input variables.

Model C				
Catchment threshold	**AIC**	**AUC**	**R^2**	**x^2 p-value**
100	102.94	0.86	0.38	< 0.000
400	83.64	0.86	0.36	< 0.000
700	75.37	0.88	0.36	< 0.000
1000	67.97	0.88	0.38	0.001
1300	64.43	0.88	0.39	0.002
1600	59.63	0.87	0.38	0.014
Mean	75.66	0.87	0.38	0.003

Table 4.4. Model C – statistical measures to evaluate the goodness of fit and significance of logistic regression models. AIC: the Akaike information criterion. AUC: the area under the receiver operating characteristic. R^2: McFadden's pseudo r square. x^2 p-value: the p-value of the chi-square statistic between model C and the null model.

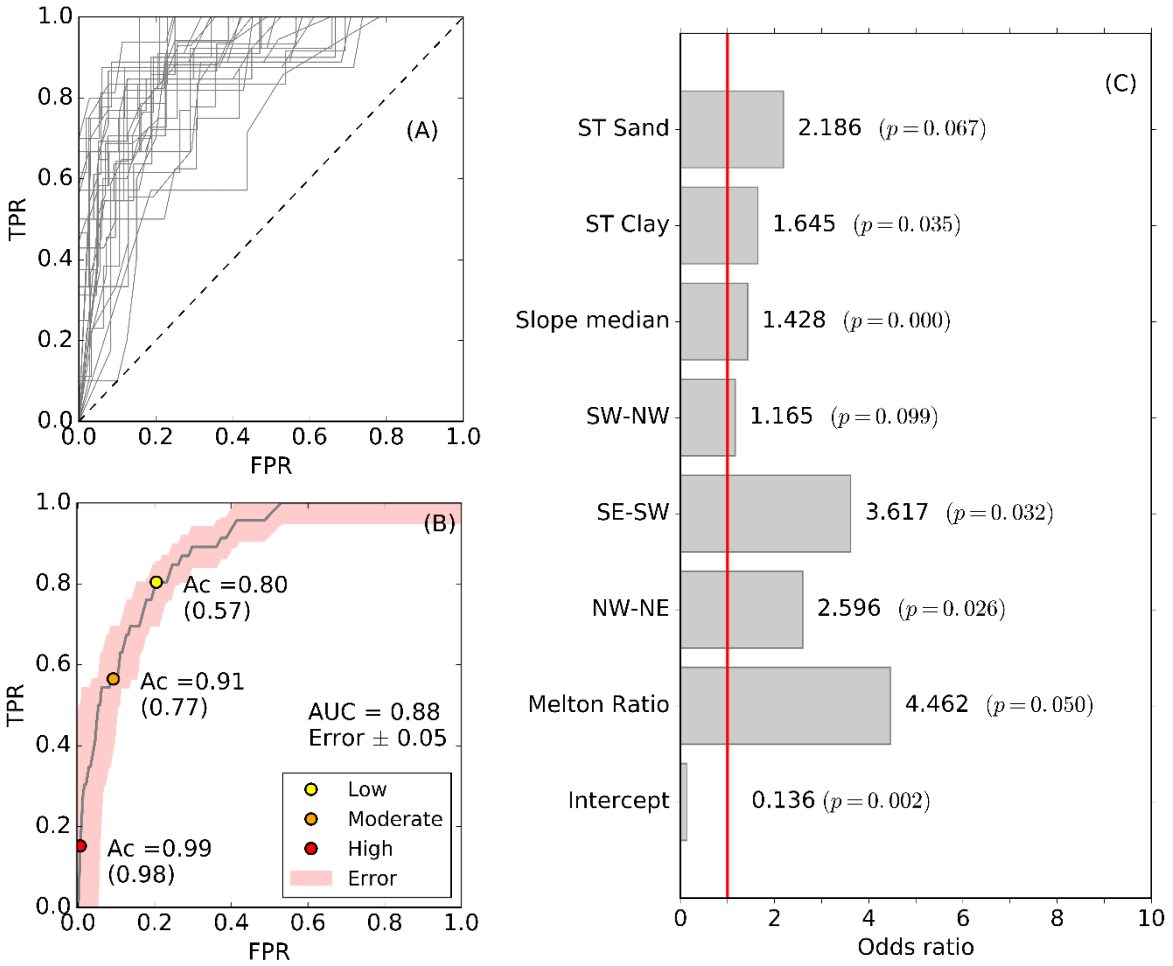

Figure 4.6. Results of Model C using 1000 cell hillslopes. (A) 30 ROC curves for each model validation dataset created in cross-validation. (B) ROC curve (grey line) for all hillslopes on the road network; the average AUC and error values (red shading); and the low, moderate and high susceptibility cut points (values) and their accuracy (Ac). (C) Odds-ratios for the model explanatory variables and their statistical significance (α). The red line indicates no change.

4.5 Selecting the optimal hillslope size

One of the objectives of this study was to evaluate what size hillslopes are most suitable for modelling landslide susceptibility. Six different sets of hillslopes were created and these were used to develop logistic regression models of hillslope landslide susceptibility: the properties of the different hillslope sets are summarised in Table 4.1. Four statistical measures are used to evaluate each model and to select the optimal set of hillslopes. In order of decreasing importance based on their prevalence within the literature the measures include: the chi-square test statistic p-value (x^2 p-value), the statistical significance of the model compared to the null model with no input variables; AIC, a measure of model simplicity and goodness of fit (lower AIC values indicate simpler and better fitting models); AUC, a measure of the model's accuracy to independent validation datasets created in cross-validation; and Mc Fadden's pseudo R^2, another indicator of goodness of fit.

Figure 4.7 illustrates each different set of hillslopes and their susceptibility as calculated using model C. The plots in Figure 4.7 are centred on the A83 trunk road (dashed line) between Arrochar and Cairndow (i.e. the Rest & Be Thankful pass), one of the most active landslide regions in Scotland. The plots illustrate the merging of hillslopes as the catchment cell-threshold is increased. The 1000-cell hillslopes are selected as the most optimal for modelling the susceptibility of the hillslopes that intersect the road network in Scotland. Pragmatically, these were selected based on an evaluation of the statistical measures obtained for models A, B and C. Table 4.5 shows the average value of these measures across the three models: individual model values are in Tables 4.2, 4.3 and 4.4. For each model, only the AIC measure is shown to improve for increasing hillslope size. However, for model A, the > 1300-cell hillslopes produced insignificant models. The other measures show no clear association to varying hillslope size yet many of the highest scores are obtained for the 1000-cell hillslopes. In addition, the 1000-cell hillslopes capture 61 (81 %) of the 75 landslides recorded in Scotland: only the 1600-cell hillslopes capture more with 62 landslides (Table 4.1).

Average of models A, B and C				
Catchment threshold	**AIC**	**AUC**	**R^2**	**x^2 p-value**
100	110.70	0.85	0.34	0.040
400	88.34	0.85	0.33	0.015
700	78.96	0.85	0.33	0.020
1000	73.39	0.86	0.35	0.022
1300	68.42	0.86	0.34	0.054
1600	61.67	0.86	0.36	0.070

Table 4.5. Average values of the statistical measures to evaluate the goodness of fit and significance of the logistic regression models A, B and C.

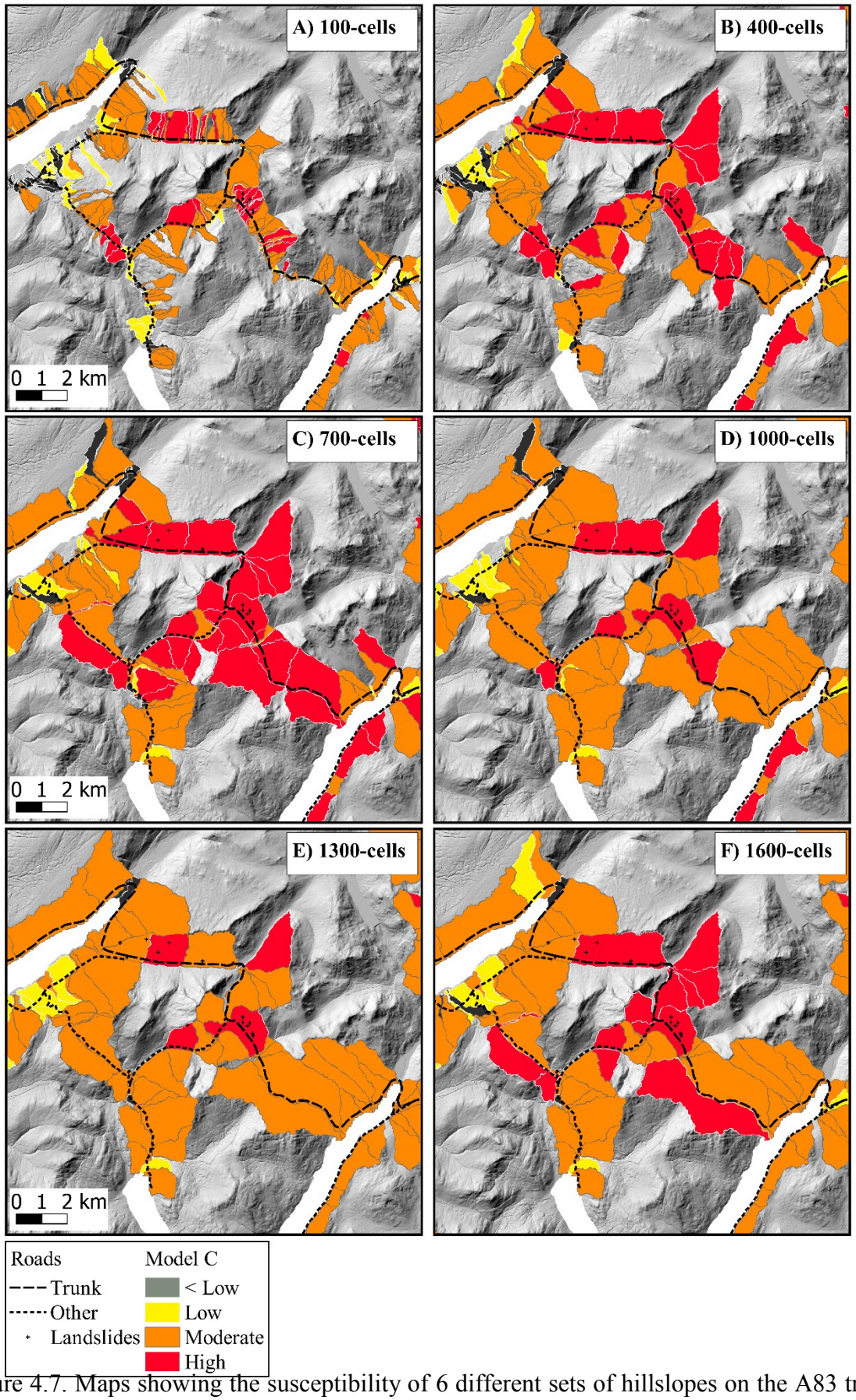

Figure 4.7. Maps showing the susceptibility of 6 different sets of hillslopes on the A83 trunk road between Arrochar and Cairndow (Rest and Be Thankful Pass): hillslope susceptibility is calculated using model C.

4.6 Hillslope Landslide Susceptibility on the Scottish road network

Hillslope susceptibility is evaluated according to the results of Model C using the 1000-cell hillslopes. Pragmatically, Model C is selected as it features the least number of input variables, high goodness of fit, significance ($p < 0.05$) and high prediction accuracy. The results are displayed in Figure 4.8. Most hillslopes that are found to be of low (yellow), moderate (amber) and high (red) susceptibility are situated in the central, west and north-west highland regions of Scotland. As may be expected, there are notably fewer susceptible hillslopes on roads in urban areas and in the lower lying eastern and coastal regions. Hillslopes that were less than 'low susceptibility' are not shown. The dark shading indicates areas and hillslopes that do not intersect the road network. The major road network is displayed in thin grey lines.

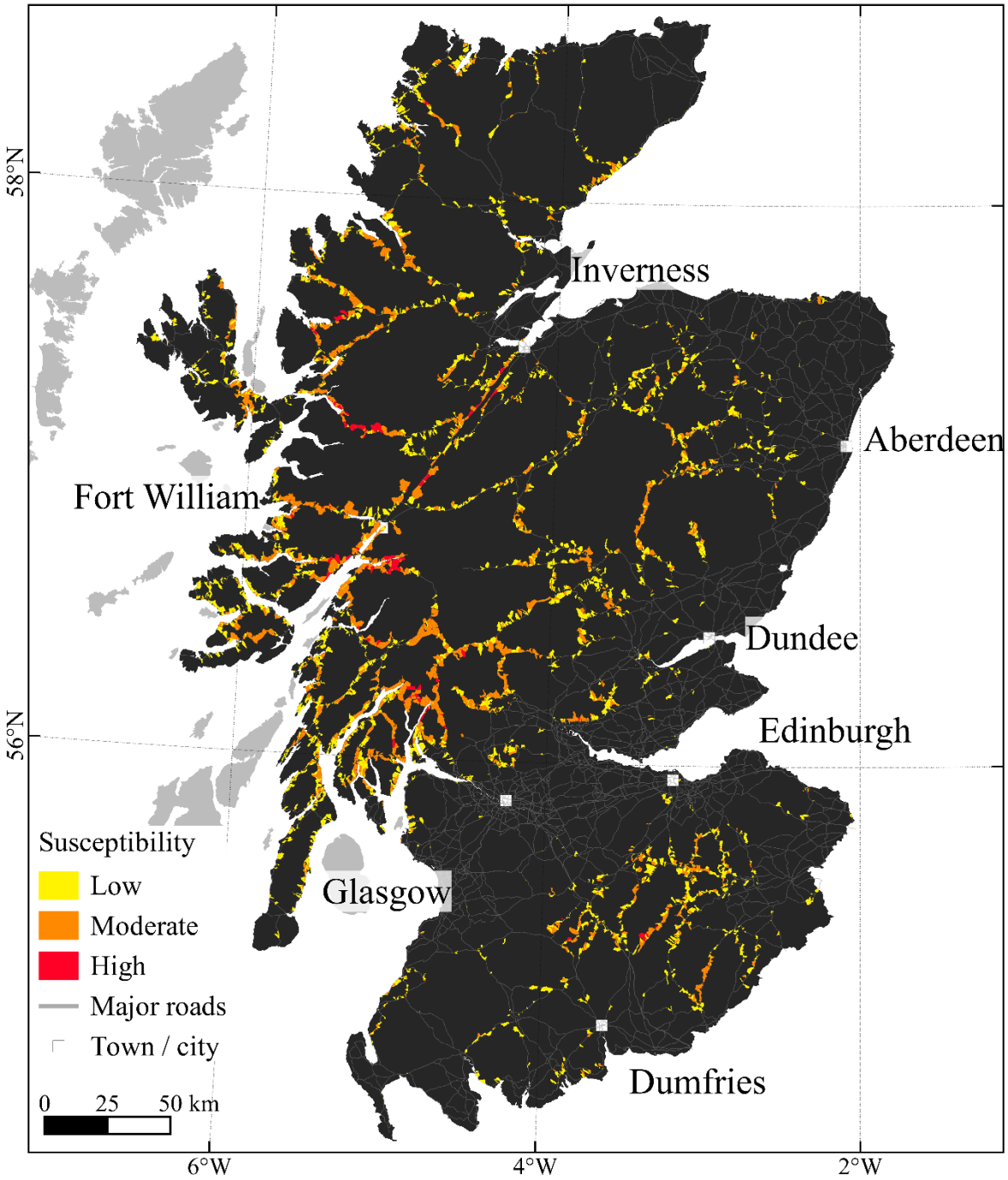

Figure 4.8. Map of Scotland showing susceptible 1000-cell hillslopes on the major road network: susceptibility is calculated by model C. The major road network (white-grey lines) includes all the motorway's, arterial, primary and secondary roads in the study area (dark shading).

4.7 Road segment susceptibility on the Scottish road network

The major road network is comprised of road segments between network nodes (i.e. road links between junctions). The susceptibility of each road segment is given by spatial analysis of the intersection of road segments and hillslopes, taking the highest hillslope susceptibility band: as shown in Figure 4.9. Approximately 37 % of the major road network is of low to high susceptibility (6,500 km / 17,600 km). Individually this is: 40 % of the strategic road network is susceptible, comprised of motorways and arterial roads (1,700 / 4,300 km); 39 % of primary roads (2,600 / 6,600 km); and 33 % of secondary roads (2,200 / 6,700 km). By warning level, 10 % is of low susceptibility (1,800 km), moderate 21 % (3,600) and high 4 % (700 km).

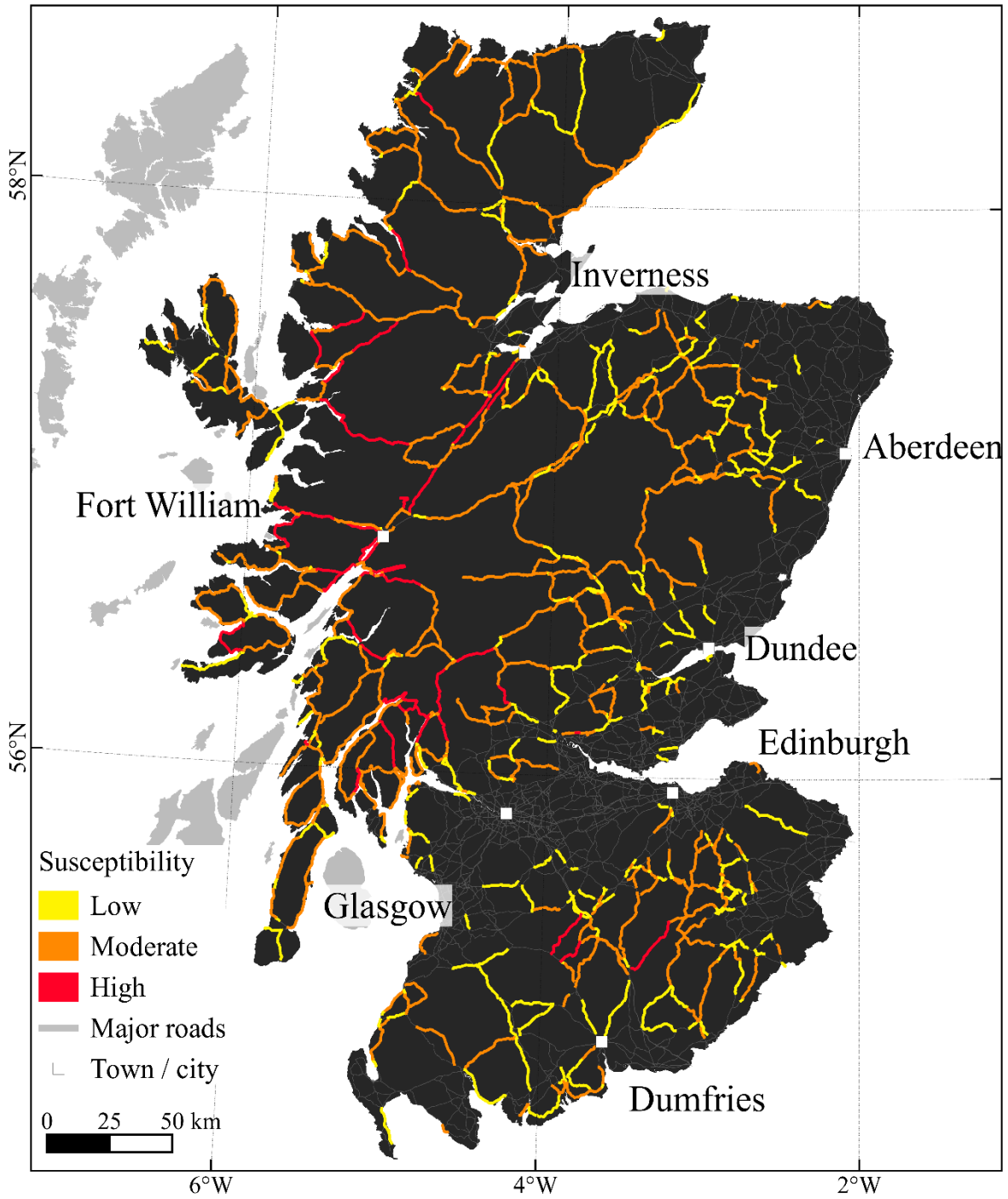

Figure 4.9. Map of Scotland showing susceptible road segments on the major road network: susceptibility is calculated by model C and using 1000-cell hillslopes. The major road network (grey lines) includes all motorway's, arterial, primary and secondary roads in the study area (dark shading).

The SRN is the primary means of transport between regions, population centres and other key infrastructure in Scotland, such as ports, airports and rail terminals. As such, the SRN is the focus of this investigation. Additionally, focussing on the SRN constrains the scope and complexity of the analysis (Jenelius 2009; Nyberg & Johansson 2013; Demirel *et al.* 2015; Meyer *et al.* 2015) and aligns with national government level management of the SRN; all other roads are managed at the local authority level. Figure 4.10 displays the 161 susceptible SRN road segments (yellow, amber and red lines), the non-susceptible SRN segments (thick grey lines), and the other major road segments, including primary and secondary roads (thin grey lines). Approximately 9 % (400 km) of the SRN is high susceptibility, 20 % moderate (850 km) and 10 % low (450 km). The blues labels in Figure 4.10 highlight several road corridors which were subject to repeated disruption by landslides 2002 to 2009 and that were indicated as highly susceptible in the 2005 Scottish road network landslide study (Winter *et al.* 2005). The new model also categorises these roads in the high susceptibility level.

Please turn over.

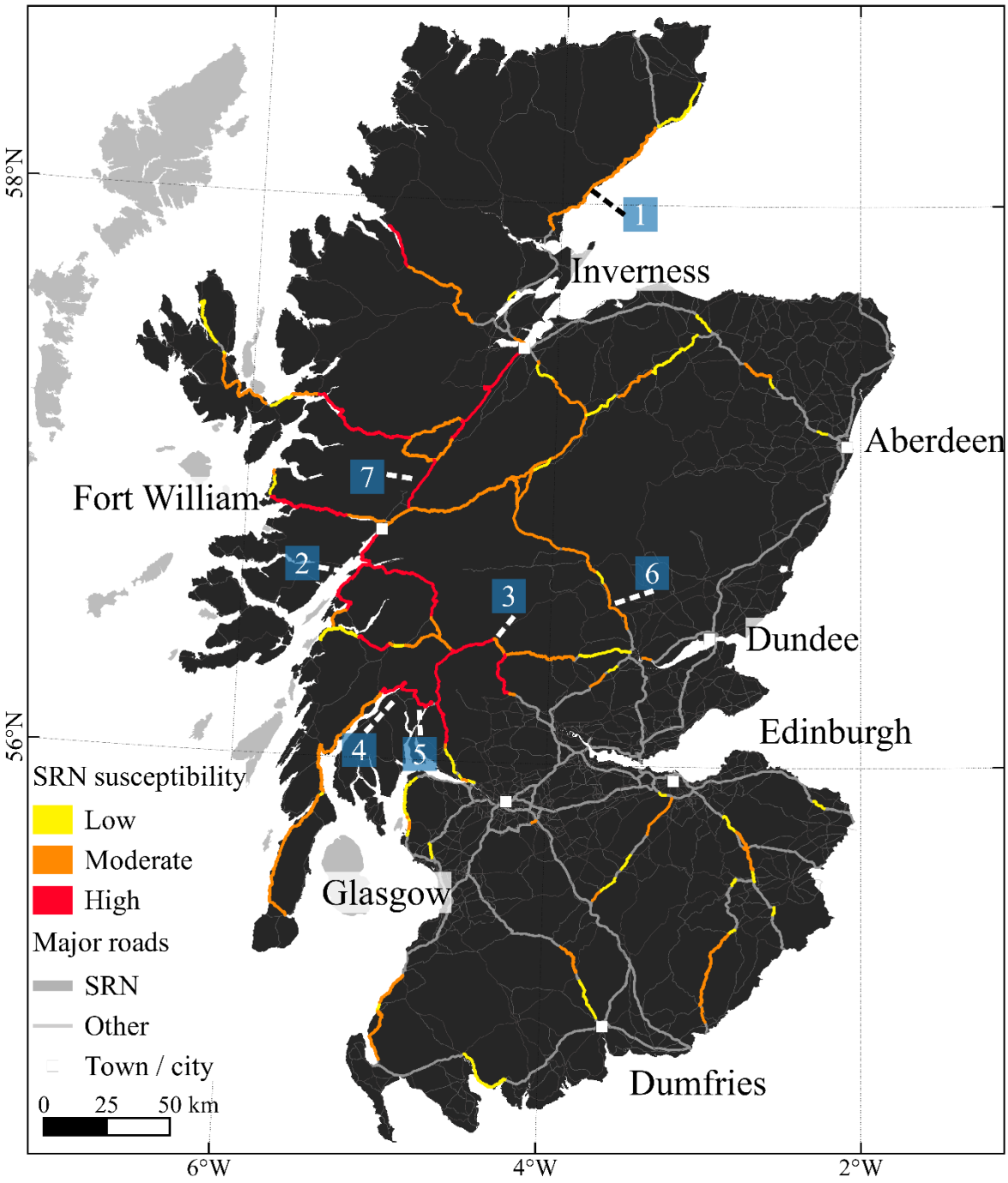

Figure 4.10. Map of Scotland showing susceptible SRN road segments: susceptibility is calculated by model C and using 1000-cell hillslopes. The major road network (grey lines) includes all motorway's, arterial, primary and secondary roads in the study area (dark shading).

The Blue labels highlight roads disrupted by landslides: 1 the A9 at Helmsworth (01/02/2016), 2 the A82 south from Fort William (multiple recorded instances, latest in 17/10/2014), 3 the A85 north from Lochearnhead (multiple, 18/08/2004), 4 and 5 are the A83 south and north sections at Rest and Be Thankful (multiple instances in 09/08/2004 and 28/10/2007, latest on 04/01/2016), 6 the A9 north from Dunkeld (11/08/2004), and 7 is the A82 at Letter Finlay (29/01/2016).

4.8 Comparison to the GeoSure susceptibility model

A comparison is made between the road segments identified as susceptible to landslides by the logistic regression model C to those segments identified using the GeoSure susceptibility model. GeoSure is a national model of landslide susceptibility produced by the British Geological Survey. The GeoSure model differs from the models developed in this study in several ways, including: i) GeoSure was produced using a combined heuristic and deterministic methodology; ii) GeoSure indicates terrain susceptibility to a wider variety of landslide mechanisms, including topples, falls, flows and rotational slides; and iii) GeoSure is supplied as 1:50,000 scale unique-condition-unit polygons in 5 classes (A-D) of increasing susceptibility (Chapter 3.27).

Figure 4.11A shows the susceptible SRN road segments according to the GeoSure susceptibility model. Figure 4.11B illustrates how spatial analysis is used to select susceptible SRN road segments by evaluating their proximity to GeoSure polygons. A 50 m buffer is used to measure the total area of GeoSure classes D or E in proximity to each road segment. A 50 m buffer is selected as this is the distance used in similar studies (Shahabi & Hashim 2015) and by other GeoSure users, such as UK insurers and infrastructure operators. For road segments in upland regions featuring higher elevation and steeper slopes (max slope > 26 °), a 500 m

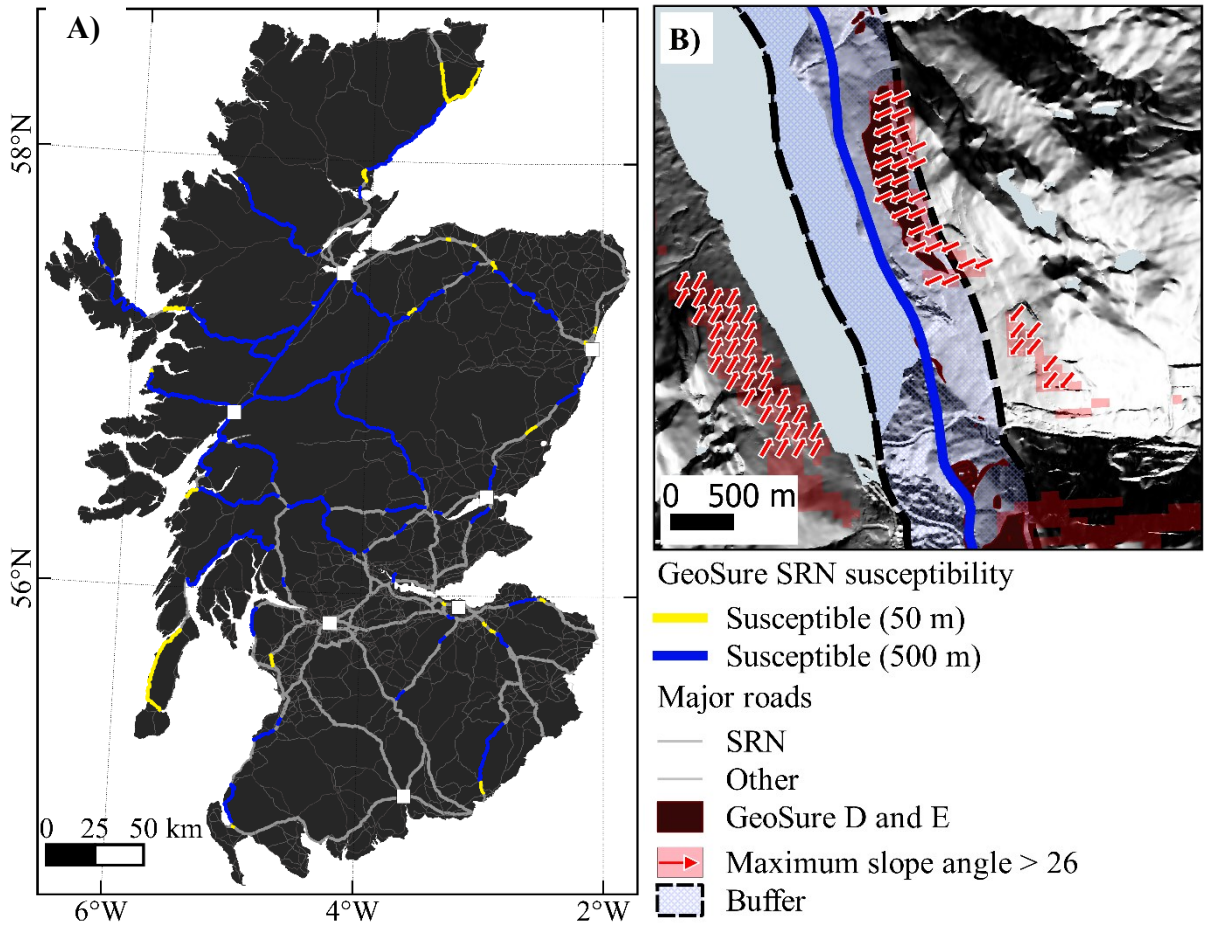

Figure 4.11. (A) Map of Scotland showing susceptible trunk road segments according to GeoSure classes D and E. (B) Illustrates a road segment with a 500m buffer (dashed black line), GeoSure polygons (grey area) and areas where the terrain slope angle is ≥26° (red shading and arrows).

buffer is applied to each road segment to account for the potential for longer landslide run-out distances (Chapter 3.27).

The GeoSure model categorises 152 SRN road segments, or 35 % of the SRN, as susceptible to landslides (1,500 / 4,300 km); approximately 200 km less than for model C. Figure 4.12 shows the SRN road segments identified by both model C and GeoSure (green lines), and those solely from model C (orange lines) and GeoSure (pink lines). A chi-square test indicates that there is a highly significant association ($p < 0.001$) between the road segments marked as susceptible and non-susceptible by each of the models.

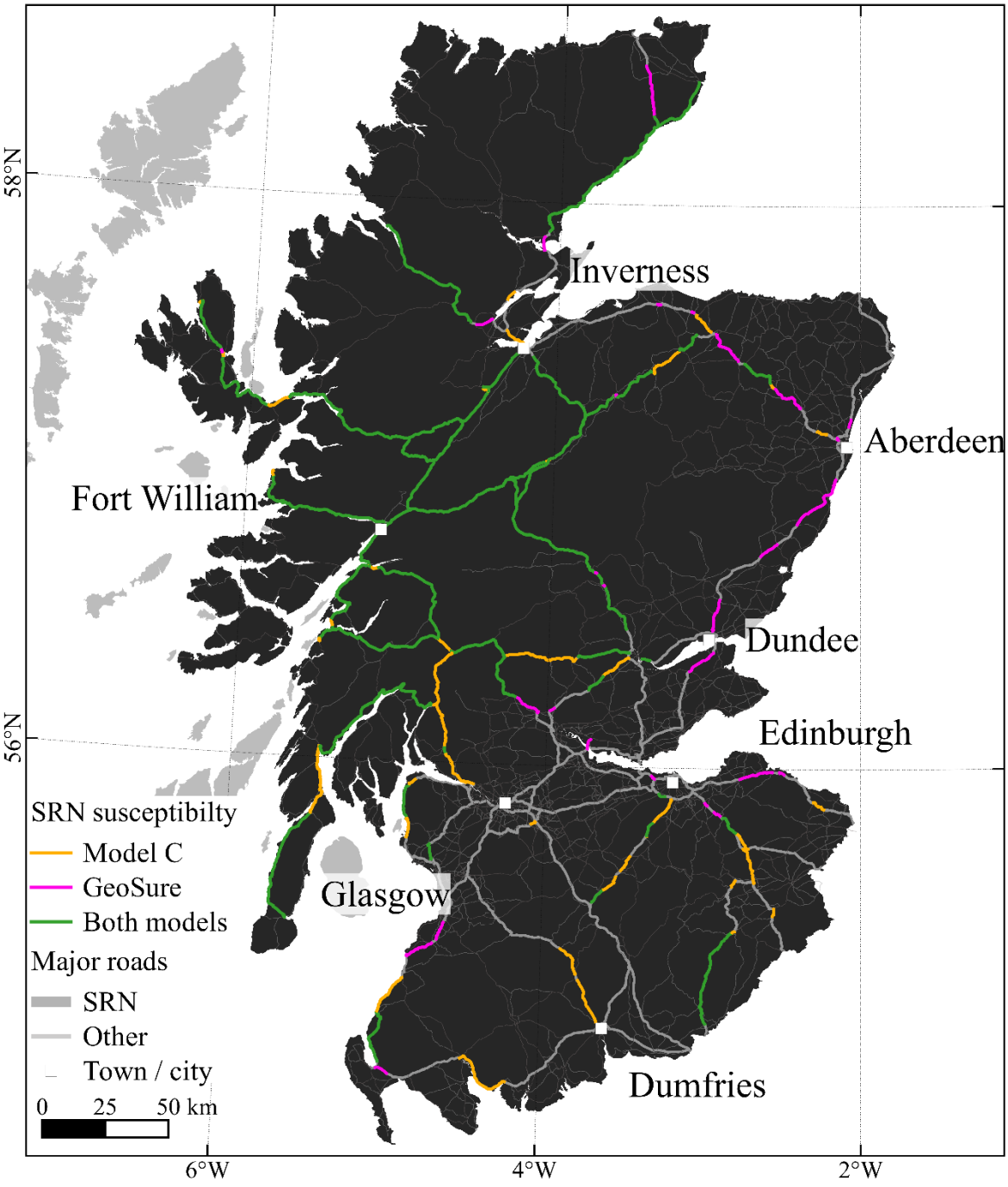

Figure 4.12. Map of Scotland showing susceptible SRN road segments identified by GeoSure and model C (green lines), just GeoSure (pink lines), and just model C (orange lines).

4.9 Discussion

Generating hillslopes:

River catchments are a fundamental geomorphic unit that outline the areas where precipitation collects and drains into a common outlet. Landslide susceptibility assessments are frequently conducted at the catchment scale (Catani *et al.* 2005; Guzzetti *et al.* 2006; Chevalier *et al.* 2013; Berenguer *et al.* 2015). Given that landslides (i.e. debris flows and shallow translational failures) predominantly occur in mountainous environments, the catchment units used in these assessments are typically headwater stream basins and upland valley's. The units are usually sourced from national hydrological authorities, for example, in the UK catchments are best captured by the integrated hydrological unit sections (IHUS) – the smallest official hydrometric area in the UK (Kral *et al.* 2015). As outlined in the literature review, a potential limitation of this approach is the fact that the individual hillslopes that comprise each catchment (i.e. the left and right side of a catchment) are likely to have different geomorphological and geological characteristics to one another, such as slope angle, mean aspect and soil type, and that influence their relative susceptibility to landslides. In addition, researchers have no control over the parameters used to create catchments, including their size.

For this study, six different sized sets of catchments and their component hillslopes were created. A minimum drainage area threshold was used to control the size of the catchments, ranging from 100-cells (> 0.0625 km^2) to 1600-cells (> 1.0 km^2) in 300 cell increments. As far as this author is aware, this is one of the first applications using hillslopes as a terrain unit in landslide susceptibility assessment. Consequently, there is limited opportunity for direct comparison to other investigations. In the central Pyrenees, a landslide susceptibility assessment was conducted using catchments created using a > 1 km^2 minimum drainage area threshold by Chevalier *et al* (2013): these units were also used by Berenguer *et al* (2015). Compared to the hillslopes created by this study (Table 4.1), the catchments have a larger mean area of 2.29 km^2. Similarly, in Scotland, the IHUS catchments also have a larger mean area 1.67 km^2 (min = 0.002, max 647.09 km^2). Therefore, the created hillslopes provide a new and relatively high-resolution modelling unit to examine landslide susceptibility.

Input variables:

Each hillslope was sampled for 14 geomorphological and geotechnical explanatory variables including: the mean, median and maximum slope angle; the mean, median and range of elevation; profile, plan and general curvature; soil texture, depth and grain size; Melton ratio and mean aspect.

Among the 14 variables, the median slope angle, maximum elevation, mean aspect and general curvature were the most skilful at distinguishing between landslide and non-landslide hillslopes (i.e. featured the smallest overlapping area between pdf, $A < 0.65$). These variables were used in more than 60 % of 145 landslide susceptibility studies (Süzen & Kaya 2011; Budimir *et al.* 2015). The Melton ratio exhibits relatively less skill ($A = 0.82$) yet this variable has been shown to be significant at distinguishing between flood, debris flood and debris flow producing slopes in other studies (Jackson *et al.* 1987; Bovis & Jakob 1999; Wilford *et al.* 2004; Welsh & Davies 2011; Berenguer *et al.* 2015), and is significant in this study area as well. A similar set of variables and results were found for an assessment of susceptible catchments in the central Pyrenees by Chevalier *et al* (2013) and Berenguer *et al* (2015). In contrast to this study, these authors used mean slope angle and this may be due to the fact that visually their data appears

to be more normally distributed (see figure 4 in Berenguer *et al* (2015)), whereas here the data is positively skewed (Figure 4.1D, E and F). This is likely because of the national scope of this study and increased number of hillslopes with low slope angles.

The variable for the mean aspect of hillslopes is of interest from the hydro-meteorological point of view as it reveals the influence that dominant weather patterns and differential weathering have on the spatial distribution of landslides (Dai & Lee 2001; Ayalew & Yamagishi 2005; Jaiswal *et al.* 2010). In the study area, and wider UK, west facing hillslopes are likely to be subject to increased rates of wind and precipitation due to low pressure and cyclonic weather systems driven north westerly by the North Atlantic Oscillation and polar front and amplified in high elevations (Wilby *et al.* 1997). In addition, southerly facing hillslopes experience more solar irradiance. In dry conditions, these factors can act to exacerbate soil desiccation and cracking, increasing the permeability of soils. In wet conditions, higher rates of water infiltration, and to greater depths, may lead to a critical increase of porewater pressure and reduction of effective stress, so that shear strength is reduced and a landslide occurs (Crozier 1997; Iverson *et al.* 1997; Iverson 2000; Stoffel *et al.* 2014). This observation is supported by the computed class frequencies and the hillslopes that are orientated to the SE-SW and SW-NW have the most landslides (Figure 4.1N and Figure 4.1O). In contrast, the Northerly aspect classes have lower frequencies.

The input variables obtained from the UK soil parent material model 'PMM' (Lawley & Smith 2008) provide near surface geotechnical information on soils, including soil depth, texture and grain size. A large proportion of landslides were confined to a single class for the soil depth (70 % of landslide are at 2 - 5 m bgl) and soil grain (85 % Argillaceous < 0.06 mm diameter) variables (Figure 4.1J, K and L). Tentatively, this may suggest that these classes are some of the best data to identify landslide susceptible hillslopes in Scotland. In support, most field observations note that landslide shearing planes and failed soil horizons are typically 1 – 4 m in depth (Ballantyne 1986; Milne *et al.* 2009). In addition, these observations and other photographic evidence (e.g. Figures 3.2 and 3.3) indicate that a large proportion of the landslide deposits in Scotland are comprised of fine clay to silt materials that are the result of weathering and accumulation within failure conduits (i.e. gulley's and hillslopes). These materials produce the liquified flows of material that are typical for landslides in Scotland, but these also contain larger size rocks and boulders (0.2 to 5 m in diameter) that are not reflected in the PMM data.

It is also reasonable to assume that there is a degree of bias in the PMM variables given the limited availability and limited spatial distribution of bore hole and detailed geotechnical investigation data used to construct the PMM. In the PMM, these data are generalised across the study area using heuristic, statistical and spatial analysis (Lawley & Smith 2008). For instance, there are very few hillslopes, landslide or non-landslide, in the larger soil grain size classes (e.g. < 10 % of hillslopes are in the medium, coarse and Rudaceous classes). Additionally, field observations note that most landslides and their deposits are comprised of fines mixed with medium to coarse grained materials (Ballantyne 1986; Milne *et al.* 2009; Dijkstra *et al.* 2016a). For these reasons, the soil depth and grain size variables were not used in the logistic regression models. It is however stressed that the parent material model represents the state-of-the-art in the UK and is perhaps the global standard for evaluating the near surface geotechnical properties of soils at national scale. The classes in the PMM soil texture variable were used the models as they exhibit a more even frequency distribution (Figure 4.1J). This is attributed to the wider range of high resolution input data sources,

primarily the interpretation of surface and vegetation cover via remotely sensed satellite and aerial imagery (Lawley & Smith 2008).

Logistic regression models:

The Pearson correlation coefficient and chi-square statistic were applied to select sets of independent explanatory variables and these were used to produce two different logistic regression models', model A and model B. Based on the AIC, AUC, pseudo R^2 and p-value measures for model goodness of fit and accuracy, model B was found to have higher performance than model A and included the variables, Melton ratio, median slope angle, intercardinal aspect, general curvature and soil texture. Following a leave-one-out strategy, a new model, model C, was formed by dropping the general curvature variable. This led to further improvements in the goodness of fit and accuracy measures and model C was selected as the final model. The variable coefficients and odds-ratios from each model indicate their contribution to increased or decreased hillslope susceptibility, highlighting several interesting trends:

- In model A, the poorest performing model, a per unit increase in the mean elevation of a hillslope contributes 3 % increase to its modelled susceptibility. The elevation variables are highly correlated ($r \geq 0.5$) to all the other variables except profile curvature, a limitation on their wider use in the models.
- The coefficient for maximum slope angle (1.042, model A) suggests that it has a smaller influence on susceptibility than the median slope angle (1.329 – 1.428, in model B and C). Though the comparison of model coefficients does not offer a conclusive assessment, the variables for median and mean slope are by far the most prevalent variables in landslide susceptibility literature (Dai *et al.* 2001; Catani *et al.* 2005; Glade *et al.* 2005; Guzzetti *et al.* 2005; Shahabi & Hashim 2015).
- Hillslope aspect is a significant variable in each of the models, with the SE-SW and SW-NW classes having the largest influence on increased hillslope susceptibility, relative to the NE-SE reference class. Hillslopes orientated to the South and West receive increased solar irradiation, wind and precipitation which may act to increase their relative susceptibility.
- The general curvature variable included three classes for, concave (< -0.001), flat (-0.001 to 0.001) and convex (> 0.001) hillslopes. Relative to flat (i.e. the reference class), convex and concave hillslopes were 130 % and 200 % more likely to be susceptible (model A and B).
- The soil texture classes clay (0.002 – 0.06 mm) and sand (0.06 – 2.0 mm) increase hillslope susceptibility by 165 % and 220 % relative to the reference class of peat, silt and loam soils (model C). The coarsest, sandy soils class consistently has the greatest influence on susceptibility across the three models (170 – 220 %) and this fits with the physical descriptions of Scottish landslides (Ballantyne 2002; Milne *et al.* 2009).
- The Melton ratio was a strong indicator of increasing hillslope susceptibility (model B and C). In British Columbia, the hillslopes that produce shallow landslides and debris flow were associated to Melton ratio values > 0.65 (Jackson *et al.* 1987; Wilford *et al.* 2004). Similarly, in New Zealand, a slightly lower Melton ratio criteria > 0.5 was found (Welsh & Davies 2011). Using the Melton ratio coefficient from model C, these values increase hillslope susceptibility by 164 % (0.65) and 111 % (0.50), respectively.

Optimal hillslope size:

Hillslopes, and other hydrological units such as catchments, differentiate areas of terrain characterised by distinct suites of hydrogeomorphic process (Bovis & Jakob 1999; Montgomery 1999; Wilford *et al.* 2004). As such, it is reasonable to assume that, for different landscapes, there exists an optimal hillslope size that best characterises the slopes capable of generating landslides. The logistic regression models were developed and evaluated using 6 different sized sets of hillslopes with the aim of selecting the most optimal hillslope size to assess landslide susceptibility. Pragmatically, the hillslopes created using a 1000-cell catchment threshold (> 0.625 km^2) were selected as the optimal based on an evaluation of the model performance measures obtained across the different hillslope sizes and for each model. Only the AIC measure was shown to improve with increasing hillslope size whilst model accuracy and statistical significance showed little change, but with marginally better values for the 1000-cell hillslopes.

The lack of a clear 'optimal' hillslope size may be due to limitations in the adopted method. First, the low 25 m^2 resolution of the digital terrain model and the software used to create the hillslopes. Whilst the 5 m^2 NEXTmap digital terrain model is available for the whole study area, there is limited application of < 10 m^2 resolution terrain data in current state-of-the-art hydrological software (Metz *et al.* 2011). Once these issues are resolved, higher resolution data and smaller hillslopes may provide improved modelling scores. The second limitation concerns the spatial scale of the study. In attempting to evaluate the susceptibility of a strategically important national road network, this study examines all hillslopes across this network in Scotland (i.e. national scale). The network traverses landscapes with varied geography, from heavily faulted and uplifted mountainous terrain in the north-west highlands and central north Grampians; more gentle, undulating mountains in the southern uplands; to lowland areas in the central south and east. Subsequently, the optimal hillslope size may differ between areas. In Italy, Segoni et al (2014) demonstrated an improved landslide warning system using a regionalised mosaic of landslide assessments – albeit for precipitation initiation thresholds. Such a strategy may also improve terrain susceptibility assessments. In this case, this was not possible given the relative paucity of landslide data in Scotland. Nonetheless, this study was the first to use hillslopes as a modelling unit and the first to compare and evaluate different hillslope sizes in landslide susceptibility assessment.

Predicted probabilities and warning levels:

The logistic regression model calculates a value of susceptibility for each hillslope between 0 and 1. To produce a susceptibility map, these values are divided into ranges for increasing susceptibility. In traditional applications of logistic regression modelling it is common to split the predicted values at 0.5, any values below 0.5 are assigned to the negative class (e.g. not susceptible) and values above 0.5 are assigned the positive class (e.g. susceptible). Many different methods have been adopted in the landslide susceptibility literature including using, the 0.5 threshold, equal intervals (e.g. 0.0 – 0.1, 0.1 – 0.2), natural breaks and standard deviations (Dai *et al.* 2001; Ayalew & Yamagishi 2005; Van Westen *et al.* 2008; Martinovic *et al.* 2016).

In this study, a new approach is demonstrated that was inspired from the parallel investigation examining different threshold selection techniques for landslide rainfall initiation thresholds (Chapter 4.3). As illustrated in the ROC plots (Figure 4.4, 4.5 and 4.6), three different

thresholds were used to give four susceptibility warning levels: marginal (grey), low (yellow), moderate (amber) and high (red). First, the low (yellow) warning level is selected by the optimal point threshold on the ROC curve: values below this level are assigned to the marginal susceptibility warning level. The high (red) warning level is given by the threat score threshold on the ROC curve. Respectively, these thresholds optimise landslide detection (i.e. optimal point) and accuracy (i.e. threat score). The moderate threshold is selected halfway between the low and high threshold values. The moderate threshold does not have a formal mathematical formula but is chosen as most other susceptibility maps contain three or more warning levels. A primary advantage to this system of thresholds is that each warning level is selected according to a measure of threshold detection or accuracy and their accuracy increases along the higher susceptibility levels. For instance, for model C and the 1000-cell hillslopes, the accuracy of the low-yellow susceptibility level is 80 % (threshold value = 0.57), consequently one fifth of hillslopes within this level are incorrectly labelled as susceptible or not-susceptible. In contrast, the moderate and high-red warning levels have accuracy of 91 % (0.77) and 99 % (0.98). Therefore, this system of thresholds serves to reduce false alarms for the higher susceptibility warning levels.

Susceptible hillslopes and road segments:

The final results are spatially attributed datasets that display the susceptibility warning level for each hillslope and road segment in Scotland. The new model and analysis using hillslopes is a first attempt to classify road network landslide susceptibility at the national scale. The majority of the hillslopes (75 %) were classified as having a very low, marginal susceptibility to landslides which is expected given that most hillslopes and road segments have been serviceable throughout the past century. When attributing the susceptibility of hillslopes to the individual segments in the major road network, the analysis indicates that 37 % of road segments are situated next to hillslopes that feature a low to high degree of landslide susceptibility. As a proportion of length, the strategic road network (SRN) is most susceptible (40 %). The selection of highly susceptible SRN includes road segments with no known history of failure in addition to previously identified landslide prone corridors, such as the A82, A83, A85 and A9 (Figure 4.10). The good agreement between the new model results and these previous assessments is a useful comparison as these were based on desktop geographical information system analysis in addition to detailed on-site surveying and geotechnical investigations (Winter *et al.* 2005). Similar results (e.g. susceptible road segments) were also obtained in a comparison to the BGS GeoSure susceptibility model. GeoSure was developed independent of this study and using a different methodology: however, the landslide database used by this study is a subset of the database used to develop GeoSure.

The model results highlight the hillslopes that feature combinations of slope angle, Melton ratio, aspect and soil texture associated with historic landslide activity: changing the number and value of these factors leads to an increase or decrease in the modelled susceptibility. For hillslopes, the values of these variables are unlikely to vary significantly on time scales of several years to decades making them suitable indicators of the present day and near future landslide potential (Guzzetti *et al.* 2005). This does not however mean that a landslide is certain to occur on a susceptible hillslope and the model does not provide any information to the size, pathway or likelihood of a landslide hazard. Landslides are usually initiated by medium to short term changes in the slope system such as, the weakening of slope soil materials by weathering or periods of intense rainfall, seasonal vegetation change, or due to the undercutting of a slope

by lateral fluvial erosion or by human activity. These factors are not accounted for in the new model. This is primarily due to the transient nature of these variables and the heterogeneity of conditions that lead to landslide occurrence. In the longer term, it is also unknown how several factors, including vegetation cover and superficial material strength, will respond to repeat seasonal cycles as climate changes (Dijkstra & Dixon 2010; Gibson *et al.* 2013). Thus by limiting the input variables to those that are relatively fixed, the developed model is applicable to a wide range of potential landslide locations and at a broad spatial scale (Meyer *et al.* 2014).

The practical applications and socio-economic value of the new model are in its potential to improve and increase the efficiency of highway hazard management. Hillslopes that are found to have heightened susceptibility may be prioritised for more costly and detailed desktop and on-site geotechnical investigations, aiding highway authorities in targeting limited management resources. The model may also feed into land planning and management strategy, highlighting the areas where future development and alterations to land use require a consideration of their effects to the landslide hazard. The method is applicable to other linear infrastructures such as, rail or power networks, and may also be adapted to consider other slope failure mechanisms including shrink swell or compressible ground by adjusting the input variables and training data sets.

A high susceptibility value indicates that any future changes in the hillslope condition, such as by intense rainfall or vegetation change, is likely to increase the possibility of landslide occurrence. Recently, several studies couple terrain susceptibility assessments with higher temporal and spatial resolution analysis of for example, vegetation change using NDVI (Shahabi & Hashim 2015; Chen *et al.* 2017) and rainfall initiation thresholds (Meyer *et al.* 2015; Segoni *et al.* 2015a). These represent the current state-of-the-art in regional to national scale landslide hazard assessment and warning systems. They are made possible by the increasing availability and now multi-decadal historic record of high resolution remotely sensed data. In sections 4.3 and 4.4, a set of new rainfall thresholds are developed for landslides in Scotland and a prototype hazard assessment system is demonstrated.

Chapter 5 Indirect Impact of Landslides on a Road Network

5.1 Introduction

In Chapter 4, a susceptibility model was developed and used to identify the strategic road network segments that are most susceptible to landslides in Scotland. In chapter 5, the susceptible road segments are used to form an event set of potential landslide disruptions and the impact of each event is calculated using a dynamic user equilibrium traffic simulation model. The traffic simulation is developed using comprehensive UK census data of for the annual average number of weekday commuter trips, an open source suite of micro-simulation software and the simulation is validated using a 12-year record of traffic flows at 36 different network locations. For each event in the event set, the simulation calculates the additional travel time. The economic losses of each event are derived by multiplying the additional travel time with a national value of user generalised-cost. The losses due to each event are examined at the national scale and in footprints of impact that reveal how populations are affected according to the zones where people live. The model is used to analyse several historic events and the results are compared to those reported in previous investigations. The rationale, method, results and conclusions of this study are also published in the journal *Environmental Research Letters* (Postance *et al.* 2017b).

5.2 A traffic simulation of Scotland's major road network

A user equilibrium simulation of traffic on Scotland's major road network is created. The model captures a single period of undisrupted peak traffic flow, representative of the weekday morning rush hour 03:00 to 10:00 am. The simulation calculates the routes taken by 1.37M commuter vehicles (1.50M people including passengers), or 81 % of the total weekday commuter traffic made on roads in Scotland (Chapter 3.4.4). The simulation is the result of combining the 2011 census commuter origin-destination trip matrix (OD, i.e. traffic demand), empirical traffic count data, and a model of route choice behaviours in an iterative procedure to determine the least cost route (i.e. shortest travel time) of each trip. A user equilibrium state is achieved when the routes can no longer be adjusted to reduce their travel cost. Practically, user equilibrium is quantified by the standard deviation of the trip travel times across each of the previous simulation iterations and the procedure is terminated when this value reaches < 0. 1 minutes (i.e. user equilibrium). All the simulations conducted for this study reached a user equilibrium condition and were terminated after 12 or less iterations.

The results of the traffic simulations are aggregated and presented according to 1,212 origin-destination zones: these are intermediate zones used in the 2011 UK census. For the undisrupted network (i.e. when no landslides have occurred), Figure 5.1A shows the average travel time of trips according to their origin zone. Travel times are short in urban areas (< 20 minutes) whereas the darker shading in the north and northwest regions indicates that average travel times are in the order of 40 to 80 minutes. Figure 5.1B displays the demand ratio of each zone. The demand ratio is given by the number of trips originating in a zone divided by the number of trips that end (destination) in a zone. The white shaded zones indicate demand sinks where there is a higher proportion of inwardly moving traffic (e.g. places of work), the darker shaded zones are sources of traffic (e.g. residential areas).

The undisrupted simulation is calibrated using traffic count data obtained at 35 different automatic traffic counting (ATC) locations on the strategic road network at 15-minute intervals for the period January 2004 to December 2015. The calibration computes the normalised Root Mean Square Error ($nRMSE$) between the ATC observations and the modelled traffic counts on road segments: the routine is described in section 3.4.6. Figure 5.1C and Figure 5.1D show the location of the ATC sites and a bar plot of the calibration results. For all road segments and ATC sites, the undisrupted simulation $nRMSE$ is 0.12, within the recommended 0.02 – 0.25 range (Smilowitz *et al.* 1999; Brockfeld *et al.* 2003; Ortuzar & Willumsen 2011). For each individual road segment and ATC site, the mean $nRMSE$ = 0.09 and only one road segment exceeds the recommended range (ATC03118 $nRMSE$ = 0.30). As most of the model $nRMSE$ are within the range of acceptable values, the calibration procedure was not applied to re-assign routes.

To evaluate the sensitivity of the undisrupted simulation, a sensitivity test was conducted by sequentially closing 30 roads with zero levels of traffic flow and re-running the simulation. The test calculates the error (i.e. standard deviation) of the trip travel times for each zone. The zones have an average error of $\pm$ 0.5 minutes with a maximum value of $\pm$ 5 minutes. Across the entire study area, the sum zone error is $\pm$ 1,802 minutes, or $\pm$ 8 seconds per trip. The minimum impact values are reported.

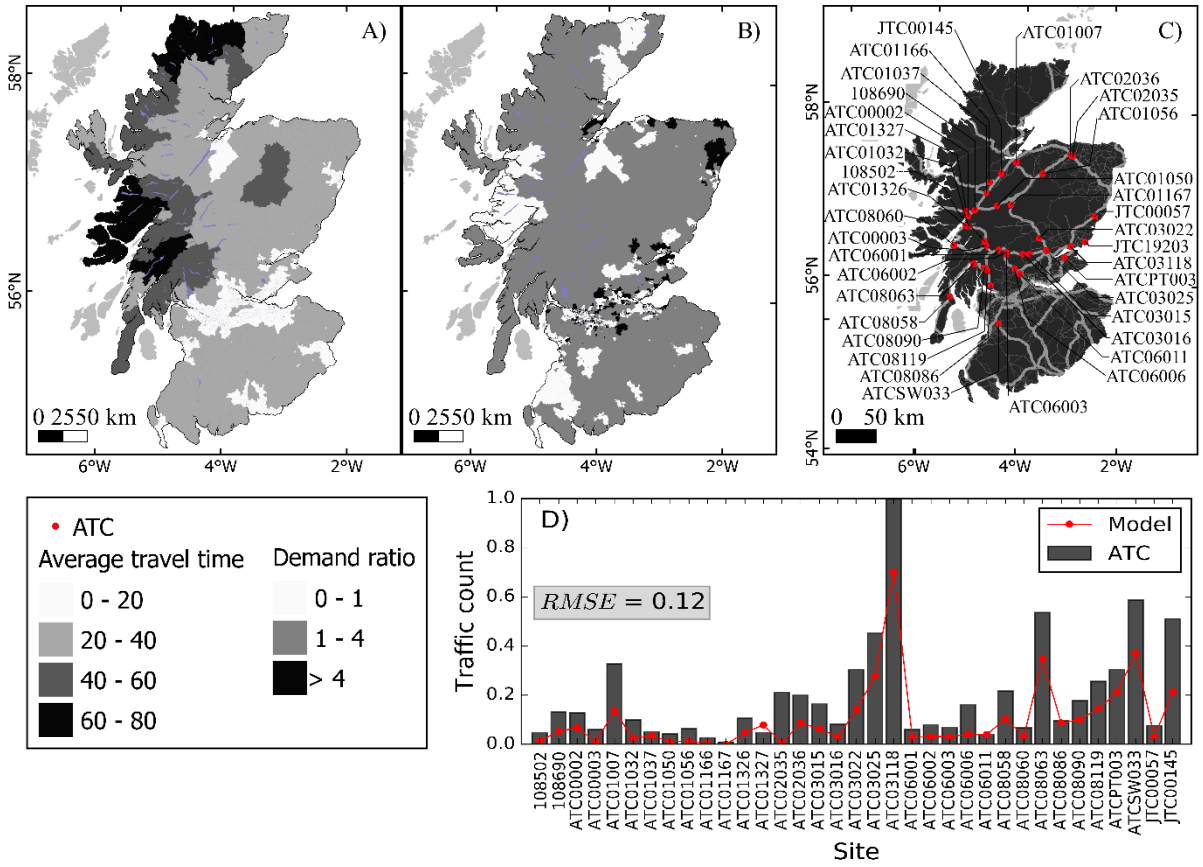

Figure 5.1. A) The average travel time of trips per origin zone for the undisrupted simulation. B) A map showing the demand ratio of each zone. C) a map showing the locations of 35 automatic traffic counting sites on the strategic road network. D) a bar plot showing the normalised root mean squared error between the observed, empirical traffic counts and those generated by the undisrupted simulation.

5.3 Event sets

A network disruption event is a hypothetical or historical event representing a conceivable manifestation of a landslide hazard disrupting the road network. An event set is comprised of multiple individual events. For this study, each event represents the closure of an individual road segment (i.e. between junction nodes) and assumes complete closure of the segment in all directions and for the duration of the simulation. Each simulation represents the annual average weekday morning commute 03:00 to 10:00 am. Events are only created on Scotland's 4,300 km strategic road network. Events are not created on junctions (i.e. intersection or slip roads) or on primary and secondary roads to constrain the scope and complexity of the study (Jenelius 2009; Nyberg & Johansson 2013; Demirel *et al.* 2015; Meyer *et al.* 2015) and to align with national government management of the strategic road network.

Two landslide event sets have been created. The first event set is comprised of the road segments identified as susceptible to landslides using the new hillslope logistic regression model developed by this study in section 4.17. The second uses the susceptible roads selected using the British Geological Survey GeoSure model described in section 4.18. The event sets are referred to as the 'Hillslope' and the 'GeoSure' event sets, respectively.

5.4 Nationwide indirect impact of landslide events

A traffic simulation is run to calculate the nationwide impact (NI) of each landslide event in the Hillslope and GeoSure event sets. For each event, the NI is the product of the total additional travel time in minutes, the monetary value of user generalised cost (£ per minute per person) and the vehicle occupancy rate (average number of persons per vehicle). The event NI values indicate the criticality (e.g. importance) of each road segment to the overall performance of the road transportation system. Higher NI values signify increasing travel costs and reduced network efficiency. Thus, NI is used to rank the relative impact of each event and importance of each road segment: rank 1 is the event with the greatest nationwide impact.

The NI values for all the Hillslope (n = 161) and GeoSure (n = 152) events are summarised in the maps and histograms displayed in Figure 5.2A and Figure 5.2B: the road segments are colour shaded according to their impact severity and these correspond to the histogram colours. The Hillslope and GeoSure event impacts follow an asymmetrical distribution with an average impact ($NI\mu$) of £64 k and £62 k per day of disruption (or $84 k USD and €72 k as of June 2017). The NI distributions are positively skewed by several events that incur relatively extreme impacts (NI > NIμ + 2σ). Eight extreme events were found in the Hillslope event set and six extreme events were found in the GeoSure event set (annotated in Figure 5.2A1 and Figure 5.2B1). These road segments have the highest criticality. Most of the extreme events in each event set are the same road segments except for Hillslope events 5, 6 and 7 and GeoSure event 3.

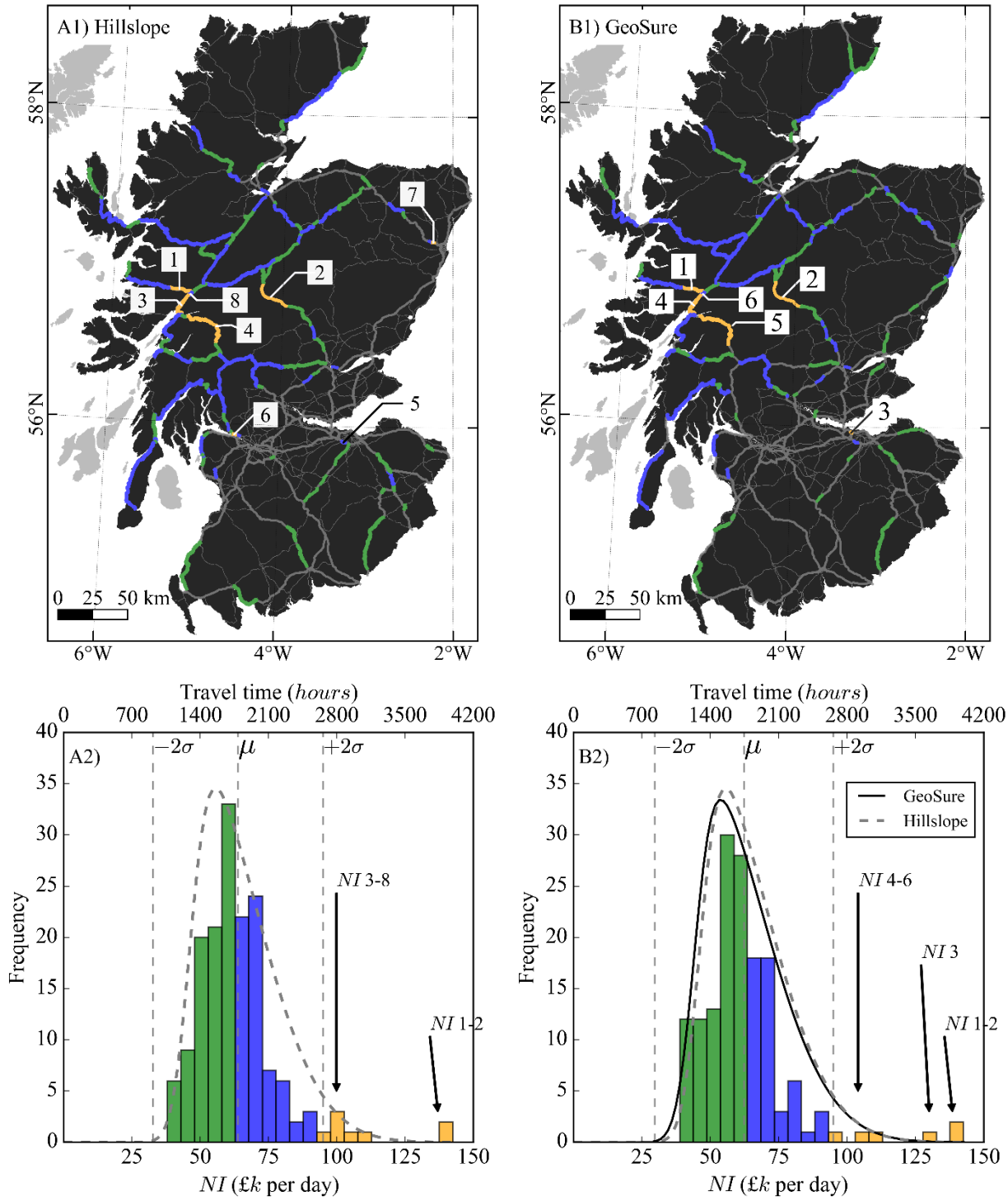

Figure 5.2. A map showing the location and net economic impact of susceptible road segments 'events' for the Hillslope (A1) and GeoSure (B1) event sets. The road segments are shaded according to their nationwide impact and the colours correspond to those in the histograms of nationwide impact in plots A2 and B2, respectively for the Hillslope and GeoSure event sets. Annotations highlight the location of extreme events. The non-susceptible strategic road network is the thick grey line, the thin grey lines are primary roads, and the other roads are not shown due to the scale and size of the map.

5.5 Extended hazard impact footprints

The spatial distribution of event impacts is examined through extended hazard impact footprints (Figure 5.3). These footprints illustrate how road users are effected according to where they live (i.e. origin zones), with darker shading indicating increased travel delay and cost.

Figure 5.3 displays the extended hazard impact footprints for the eight most extreme events (i.e. $NI1$ to $NI8$) within the Hillslope event set: several of these events are the same extreme events in the GeoSure (NI's 1, 2, 4, 5 and 6) event set. The footprints show that the impacts are generally distributed within the zone(s) that contain or are in proximity to the disrupted road segment. For several events, the footprints also highlight impacted zones and communities that are positioned far from the landslide location.

A notable, albeit qualitative, inference is that these impact footprints may be either spatially dispersed or spatially acute. For events $NI2$, $NI4$, $NI5$ and $NI6$, the maximum impact to any origin zone is < £5 k and the footprint of impacts is relatively dispersed across many zones covering a large area and proportion of the population (Figure 5.3). The zones where the impacts are concentrated (grey shading) have an average increase in travel time of 1 to 4 minutes per trip depending on the zones population: smaller zones have higher population densities and so the average increase is lower. In contrast, the other extreme events feature a more focussed, acute impact footprint where the increase in travel time and cost is distributed to within just a few zones. The events $NI1$, $NI3$, $NI7$ and $NI8$ have zones with impacts of £5 k – £50 k, equivalent to an average increase in travel time of between 35 and 65 minutes per trip in the darkest shaded zones (Figure 5.3).

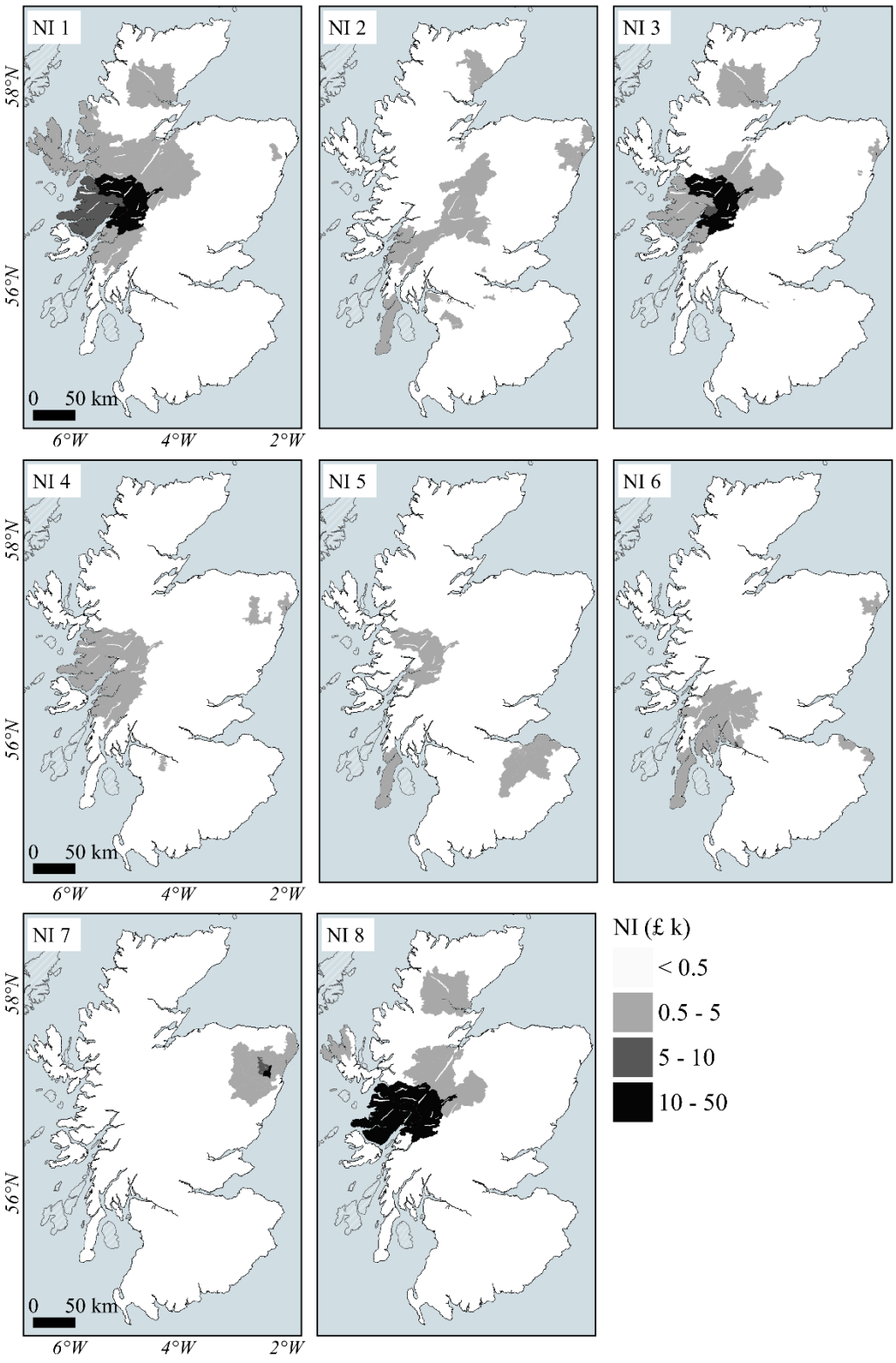

Figure 5.3. Extended hazard impact footprints for events *NI* 1 – *NI* 8 in the Hillslope event set.

Figure 5.4A displays a severity footprint, this is constructed by taking the sum of the impact footprints for each of the 161 events in the Hillslope event set. The severity footprint is not probabilistic, rather it shows the origin zones where impacts are aggregated for all the roads that were identified as being susceptible to landslides. The severity footprint indicates that the impact due to landslides is disproportionality focused to the central and north-west regions of Scotland, particularly around Fort William, and away from most major urban centres, including Glasgow and Edinburgh.

Figure 5.4B shows the distribution of landslides per zone that are recorded in the landslide database used to construct the susceptibility models (Chapter 4.1). Visually, there is a general association between the zones that feature high impact to traffic and high numbers of landslides. For example, in each figure there is a similar proportion of the population that resides within the shaded areas of 3.5 % (high impact NI > £20 k Figure 5.4A) and 2.5 % (Landslides > 1 Figure 5.4B). The contrast between these figures, such as shaded and non-shaded or lighter and darker zones, exposes some of the complex interactions that take place between landslide occurrence, the modelled susceptibility (i.e. location of events) and the impact to traffic in the road transportation system. For instance, in some areas there are high numbers of landslides and low impacts to traffic and in other areas this pattern is reversed. The association between zones with landslide occurrence, susceptibility and impact is non-linear as the spatial extent and severity of impact is dependent on a several dynamic traffic factors, such as the density and availability of alternative routes in the network and the level of user demand. These factors act to concentrate or disperse the event impacts beyond the landslides physical location.

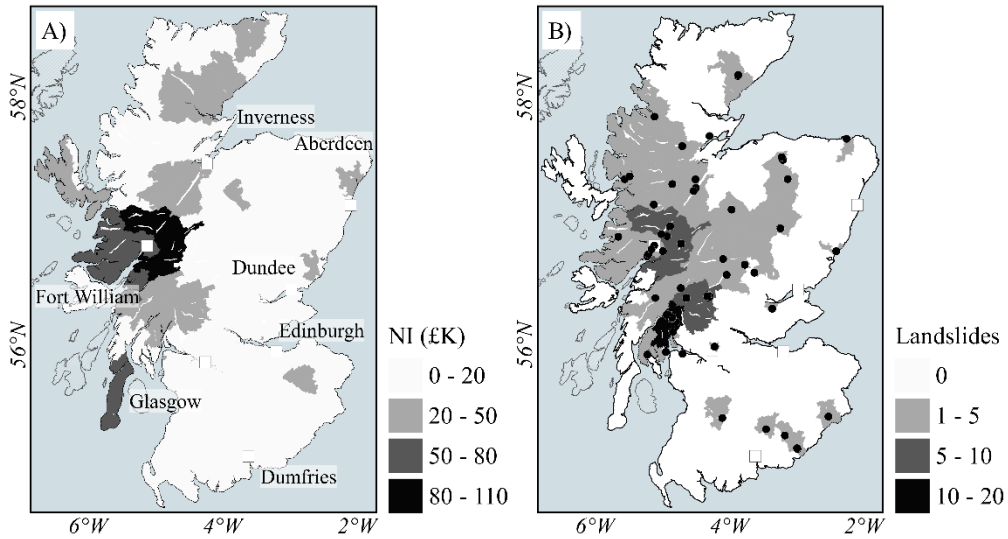

Figure 5.4. A) Severity footprint showing the combined impact of 161 landslide events in the Hillslope event set. B) Map showing the number of landslides in each zone recorded in the UK national landslide database: the black dots show the landslide locations.

5.6 Analysis of historic landslide events and comparing different traffic models

The traffic simulation model is applied to examine the indirect impacts of four historic landslide events in Scotland (Table 5.1). Three of the landslides occurred in quick succession over a period of 9 days in August 2004 following a series of North Atlantic cyclonic weather systems (Winter *et al.* 2005): many parts of Scotland received 150 to 250 % of the 1971 – 2000 30-year average August rainfall (Met Office 2017). The fourth landslide occurred on the 28th October 2007 following similarly wet conditions. In the context of UK landslide hazards and management, these four events are particularly significant as they were both high in magnitude, removing and depositing several 100's of tonnes of material, and high severity, posing a serious threat of injury or death and causing major disruption to the strategic road network.

Details of these four events are summarised in Table 5.1, including the duration of disruption to the strategic road network in days. Following the landslides, a detailed assessment of the costs of the emergency response (ER £k) and engineered remediation's (Eng £k) were made (Winter *et al.* 2005). Winter *et al* (2014) also investigated the indirect impact of these four events (i.e. the travel time delay and cost) using the 'Queues and Delays at Roadworks Model' QUADRO (DFT 2006). Similar to the SUMO model developed in this study, QUADRO calculates additional travel time according to the user equilibrium principle and this is converted to economic impact using the same user generalised cost values provided by the UK department for transport (DFT 2014a). Additionally, QUADRO uses the same automatic traffic counting data used in this study to approximate the traffic flow on each link. Crucially, however, the QUADRO model differs from the SUMO model in that in QUADRO traffic flow is constrained to a limited number prescribed diversionary routes. The diversionary routes are typically the new shortest path linking two end nodes of the disrupted road segment (i.e. a local scale assessment around the disrupted road segment). In contrast, in SUMO vehicles can utilise the entire road network selecting the diversionary route according to the shortest path between their origin and destination, and that may now be far from the disrupted segment.

	A83 RABT east (B828 to A815)		**A9 Dunkeld (B898 to A827)**		**A85 Glen Ogle (Lochearnhead to A827)**		**A83 RABT west (Arrochar to B828)**	
Date	09/08/2004		11/08/2004		18/08/2004		28/10/2007	
Duration	2		2		4		15	
ER (£k)	£300		£700		£500		£270	
Eng. (£k)	-		-		-		£1,156	
	£k /day	**£k total**	**£k /day**	**£k total**	**£k /day**	**£k total**	**£k /day**	**£k total**
QUADRO	47	94	150	300	40	160	49	735
SUMO	61	122	72	144	73	292	89	1,335
NI Rank	87		30		26		11	

Table 5.1. A comparison of the indirect economic impacts of four historic landslide events calculated using QUADRO and SUMO traffic models. The impacts are reported per day of disruption (£ / day) and for the duration of the road closure (£k total). The date of failure, duration in days, cost of emergency response (ER £k) and cost of engineered remediation (Eng. £k) are reported from (Winter *et al.* 2005). '*NI* Rank' is the rank impact of the event in relation to the 161 other events examined in the Hillslope event set compiled in this study.

In comparison to the QUADRO model, the SUMO model calculates that three of the landslide events have greater indirect economic impacts: A83 RABT west by + 29 %, A85 Glen Ogle + 83 % and A83 RABT east + 63 %. The A9 Dunkeld event saw a decrease (- 52 %) and this is believed to be the result of the prescribed diversionary routes. Although the diversions are not provided in Winter *et al* (2014), external reports note that the A9 diversions were established along a 132 km route via Aberdeen (BBC 2004). In contrast, the SUMO model would enable trips to take shorter routes via the local primary and secondary roads of 25 – 80 km.

5.7 Discussion

In this this study, a national scale simulation of commuter traffic was developed and used to assess the indirect impact of potential landslide hazards in Scotland: here, indirect impacts are defined as the economic losses accrued by road user's due to increasing travel distance and time. An event set of plausible landslide occurrences was created using the hillslope susceptibility and GeoSure models described in section 4.1. The work therefore demonstrates a novel coupled network-hazard model framework that can be used to assess the indirect impact of landslides to road transport. As far as this author is aware, this is the first application of traffic simulation, developed using national origin-destination matrix and traffic count data, to calculate landslide hazard impacts on a national-scale road transport network. The main advantages of this approach are that the data used to drive the open-source traffic model are readily available in most developed and developing nations worldwide (e.g. Eurostat, US census bureau, the department of statistics Malaysia, and the Australian bureau of transport statistics) and that the basic framework is applicable to the study of other hazards. It is however highlighted that in recent years similar frameworks have been demonstrated, but these use different network models, are at smaller regional to urban scales and are for different hazards, such as flooding, wind storms and earthworks (Jenelius *et al.* 2006b; Nyberg & Johansson 2013; Khademi *et al.* 2015; Meyer *et al.* 2015; Pregnolato *et al.* 2016). The study therefore provides a landslides specific contribution to the rapidly growing body of network-hazard literature.

The event sets are comprised of the road segments on the strategic road network (i.e. the trunk road network of motorways and arterial roads) that were found to have a heightened level of susceptibility to landslides. Although the method used to create the event sets is universally applicable to other road networks and other linear infrastructure (e.g. rail or pipelines), in this first application to Scotland the event sets omitted slip roads, junctions and lower priority primary and secondary roads to constrain the scope and complexity of the analysis. However, these roads are still present in the traffic simulation and their susceptibility was evaluated (Figure 4.9). Future studies may therefore use these data to evaluate the potential for indirect impacts and the relative criticality of these road segments.

A vital consideration for this study, and any other network-hazard study, is producing event sets that accurately reflect all the likely manifestations of a hazard (Murray *et al.* 2008). Due to the computational requirements of the traffic simulation, here the events were limited to individual landslide occurrences that caused the complete closure of the road segment for the duration of the modelled peak traffic flow period. This makes number of events computationally tractable in a national scale study. For landslide hazards, these criteria are a reasonable set of assumptions given that the occurrence of a landslide often leads to the

complete closure of a road segment lasting several days as the landslide debris is cleared and the stability of the failed slope is re-evaluated. In reality, and for the study of other hazards such as flooding, different criteria may be more suitable as the condition of the network during an event may be more varied, including, partial road closures and traffic control systems, area covering disruptions (e.g. snow), and wider speed restrictions caused by other factors, including heavy rain and strong winds.

Another source of event set limitations is the data and methods used in the hazard models (Chapter 4.1). Murray *et al* (2008) suggested using a variety of models to improve the quality of event sets in a multi-methodological approach (Mingers & Brocklesby 1997). In Scotland, detailed records of landslide activity are limited to within the most recent decades and to the slopes adjacent to the road network (Foster *et al.* 2008). To minimise this bias, the hillslope susceptibility model and event set were developed using only the slopes and landslides recorded on the road network. In addition, the susceptibility of the road network and another event set was created using the GeoSure susceptibility model: GeoSure was developed independent of this study using all landslide records in the UK (Walsby 2008). The two event sets were found to contain of a similar selection of road segments (Chapter 4.1.8) and each contains the same events with the most extreme indirect impacts (Figure 5.2).

In the traffic simulations, the commuter trips are calculated to user equilibrium condition where routes are chosen to minimise travel time and cost. Consequently, user equilibrium is analogous of a best-case user response whereas in reality there is often a degree of uncertainty for the best routes during a sudden network disruption event (Taylor & D'Este 2007; Knoop *et al.* 2008; Peeta *et al.* 2015): user equilibrium is often cited as being analogous to using modern navigation systems with live traffic updates. The results of the validation procedure indicate that the undisrupted simulation provides an accurate representation of the long-term traffic flows recorded by automatic traffic counters at 35 locations across the road network (Chapter 4.2.2). Attempts to validate the disruption event simulations using this data were unsuccessful due to: i) scarcity and missing traffic count data, ii) the short duration of captured disruption events, and iii) as many unknown additional factors are likely to have affected the traffic flows, such as roadworks, severe rainfall and flooding, that are not accounted for in the model. This may be feasible for other networks (e.g. urban networks with dense monitoring sensors) and as rich data sources such as telematics and intelligent infrastructure systems become more prevalent.

Comparing the results of different models offers a means of qualitative model validation (Mingers & Brocklesby 1997; Murray *et al.* 2008; Lucia *et al.* 2014). To validate the disruption simulations, a comparison was made to previous assessments made using a different traffic simulation (Winter *et al.* 2014). Where comparisons are available, the impacts are found to be 29 – 83 % greater than previous estimates (Table 5.1). For future assessments, these comparisons demonstrate the importance of methodological considerations for the choice of the network model used in relation to expected spatial distribution of the hazards impact.

The origin-destination matrix contains the trips made by 81 % of the daily commuter trips made by cars and their passengers in Scotland. Other trips made by other modes and vehicles, including public transport and cycles, were not included due to limitations in the SUMO software. In addition, there are no comparable scale origin-destination datasets available to include other road users, such as trips made for industry and for seasonal tourism. Given the

concentration of impacts to within Scotland's Highlands, the inclusion of seasonal tourism represents a significant improvement to the model. Analysis of the ATC data showed a marked increase the volume of traffic on weekdays in the peak tourism-season summer months (May to August) than in winter (November to February). Due to computational limitations the current model represents the annual average weekday traffic distribution obtained from ATC data. A suggested improvement to the model is therefore to derive and use separate seasonal weekday traffic distributions to better account for the seasonal variation in traffic flow. Though most landslides occur in winter, the increased volume of traffic during summer is likely to generate higher severity impact events that are not currently captured.

The economic impact of events is derived by multiplying the additional travel time and a national average value of road user generalised cost. The user generalised cost value accounts for the costs attributed to operating and maintaining a vehicle and values of work and none-work time set out by the UK department for transport's transport appraisal guidance (DFT 2014a). The landslide event indirect impacts should therefore be interpreted as minimum estimates and the full extent of indirect impacts is likely to be considerably higher. Nonetheless, the landslide events are shown to cause significant indirect impacts (Figure 5.2) and for several historic events these far exceed the cost of the emergency response and engineered solutions (Table 5.1). Consequently, the losses accrued by traffic disruption represent a significant proportion of the total impact of landslide hazards, contributing to increased landslide risk, yet these are not routinely considered in state of the art hazard risk assessment. This is in part due to the difficulty in approximating indirect impacts governed by non-linear processes, including, location of disruption, network topology, temporally and spatially varying levels of user demand. The method and results of this study may therefore be applied to conduct more complete landslide risk assessments and it is expected that these will be of interest to infrastructure operators who must evaluate and justify hazard mitigation expenditure on a cost benefit basis (Galbraith *et al.* 2005).

The results show the indirect impact of each landslide event expressed in terms of nationwide economic impact (Figure 5.2). Using this information, it is possible to identify those events that have the potential to cause high levels of disruption and may be considered critical road segments for sustaining network serviceability (Murray *et al.* 2008; Mattsson & Jenelius 2015). In the UK climate change risk assessment report (Krebs 2017), such assessments were identified as an urgent strategic requirement following the occurrence of several high impact events, including the closure of the M1 motorway at the Ulley reservoir following heavy rainfall in June 2007 and the storm surge that closed the South West rail main line in February 2014. In the case of the hillslope model landslide event set created for Scotland, eight events were found to have a relatively extreme level of national impact (i.e. NI 1 – 8 in Figure 5.2A and Figure 5.2A1) and this includes road segments that have been disrupted by landslides in the last decade (Winter *et al.* 2005) in addition to road segments with no prior history of failure.

The new dataset of event impacts may be used by the national highway authority in Scotland to target more detailed landslide hazard assessments (e.g. site surveys), and if required, to prioritise resources for hazard mitigation on these critical road segments. To illustrate its potential usage, in preparing this thesis a small landslide closed the A9 road south from Helmsdale, the first known recorded incident on this section of road. The road segment was identified as susceptible in both event sets and was found to have a high indirect impact (£90 k per day, NI rank 9). Fortunately no widespread traffic disruption was reported as the landslide

was relatively small, occurred in the evening and was cleared overnight (Transport Scotland 2016a). This example highlights the complexities of pre-determining the impact of landslide hazards (i.e. due to varying hazard magnitude and timing) and demonstrates the value of considering the indirect impact and road segment criticality in managing transport networks.

To be of most value to highway owners and operators the new dataset of event impacts can be combined with assessments for the potential likelihood of a landslide hazard on each road segment, or indeed any other potential hazard phenomena capable of closing the roads. Pragmatically, this is may be done by combining the three levels of road segment susceptibility outlined in Figure 4.10 and the three levels of nationwide impact displayed in Figure 5.2. The result is a 3×3 risk matrix and mapping of the roads according to their susceptibility to landslides and level of indirect impact to traffic flows (shown in Figure 5.5). The matrix and accompanying map enable the rapid identification of the road segments with low susceptibility low impact and those with high susceptibility high impact. For simplicity, the risk matrix is constructed using the three susceptibility and impact levels already provided in this study. To produce a more effective risk assessment, and for operational systems, these levels would be chosen to reflect the interests and concerns of a wider variety stakeholders (Wachinger *et al.* 2013; UNISDR 2015), including the different road user groups, the local communities, the network operators and other stakeholders.

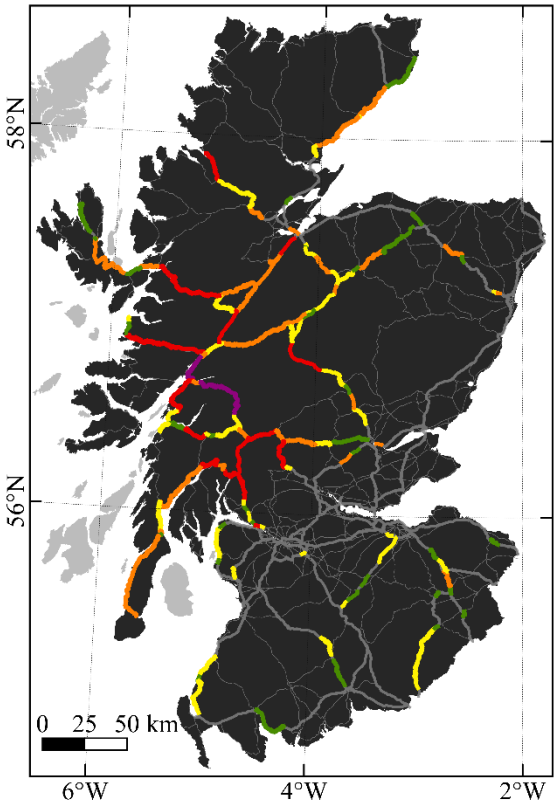

Road Susceptibility

Nationwide Impact (£k per day)	Low	Moderate	High
Low 30 – 60	1	2	3
Moderate 60 – 90	2	4	6
High > 90	3	6	9

Figure 5.5. A map and 3×3 risk matrix combining three levels of road segment landslide susceptibility and three levels of nationwide impact. The road segment colours correspond to the colours of the cells in the matrix.

The extended hazard impact footprints show how road users may be affected by landslides based on where they live. The combined severity footprint indicates that the Central and North-West regions of Scotland are the most exposed to traffic disruption by landslides on the strategic road network Figure 5.4. For a selection of the most extreme events, Figure 5.3 illustrates that the spatial distribution of impacts may be acute and focussed to a small number of zones, or dispersed and the zones are unexpectedly situated at great distances to the disrupted road segment. The acute impacts are explained by network topological characteristics, primarily the lack of equivalent length alternative routes so that the local population is the one most severely impacted (Jenelius 2010). The dispersed impact footprints reveal previously unidentified impacted communities and that comprise a significant part of the national impact. The dispersal of impacts is attributed to long distance trips adopting new circuitous routes to avoid the road segments. This can lead to a cascading and widespread effect of re-routing traffic onto alternative routes, increasing the travel time on other roads and further displacing traffic.

The impact footprints highlight several interesting issues that may be of great interest to hazard managers, politicians and the general public, particularly if the frequency of landslide occurrence were to increase given the projected scenarios of future climatic change (Dijkstra *et al.* 2016a). First, the impact footprints indicate the zones where the potential for traffic disruption is greatest. In the long term, this may lead to secondary landslide impacts such as decreasing levels of business investment, tourism and a gradual reduction in property prices in the most heavily disrupted zones (Winter *et al.* 2014). Second, there is the potential for political ramifications. Whereas the dispersed impact footprints indicate a landslide that affects a large number of people by a relatively small amount, an acute impact footprint represents a landslide event that disproportionately affects a certain community: typically, in rural communities. Such events are likely to gather a high level of public attention and with the potential for knock-on implications to the highway management authority, in this instance the Scottish parliament. This might include growing negative sentiment and reduction in community or business support to regional representatives and governing parties.

Chapter 6 Landslide Rain Initiation Thresholds

6.1 Introduction

Chapter 4 examined the spatial probability and attempts to answer 'where' landslides are most likely to occur in Scotland by analysing landslide records and information on the geomorphological and geotechnical characteristics of hillslopes on a road network. In Chapter 6, landslide rain initiation thresholds are developed to examine the temporal probability and 'when' landslides are most likely to occur. The results of this chapter are published in the journal *Earth Surface Processes and Landforms* (Postance *et al.* 2017a).

The study uses the same database of 75 shallow translational and debris flow landslides as used in the susceptibility analysis (Chapter 4). The timing of these landslides is analysed in relation to a site-specific-rain record (SSR) at each landslide location. The SSR are time series of rainfall variables derived from a high resolution (5 km^2 at 15 minutes) weather radar system for the period March 2004 to August 2016. The rain variables are calculated over ten antecedent periods of 1, 2, 3, 6, 12, 18, 24, 30, 50 and 60 days (n, e.g. 12-day normalised accumulation = NV_{12}). The variables include:

- Rain accumulation in mm (V_n).
- Normalised rain accumulation (NV_n) as multiples of the monthly rainy-day-normal accumulation (RDN). RDN is the monthly mean rain accumulation for days with rain. The RDN is calculated for each radar cell in Scotland to account for spatial rainfall variations, such as by elevation and orographic influence.
- Maximum rainfall intensity in mm h^{-1} ($Imax_n$).
- Rain duration in h^{-1} (RD_n). Rain duration is measured as the period of rainfall that exceeds the monthly rainy-day-normal-intensity ($RDNI$). $RDNI$ is analogous to RDN but measures the monthly mean rainfall intensity, it is used to indicate periods of above average intensity rainfall. The $RDNI$ is also calculated for each radar cell in Scotland.

For each variable, 250 candidate thresholds are created between their minimum and maximum observed values. For each of the 250 candidate threshold values, a binary classification procedure is applied to calculate contingency tables (i.e. counting the true positives, true negatives, false positives and false negatives of each threshold). Then, a receiver operating characteristic (ROC) analysis is used to measure the predictive performance of each rain variable using the area under the ROC curve (AUC). ROC analysis is also used to select two thresholds: the 'threat score' (TS) threshold offers the greatest level of predictive accuracy and minimizes false results (Staley *et al.* 2013), the 'optimal point' (OP) threshold provides the highest rate of landslide detection (true positives) for the lowest number of false results and is yet to be applied to landslides. The results include: the threshold values, and Bayesian probabilities that indicate the likelihood of threshold exceedance and the conditional probability of landslide occurrence given threshold exceedance (Chleborad *et al.* 2008; Berti *et al.* 2012). For each threshold, the effect of varying the SSR record length is systematically evaluated using 10 different record lengths representative of those implemented in past studies: these are daily SSR time series of 10, 20, 30, 45, 90, 180, 365, and 730 days before each landslide event, all days before ('Prior') and all ('All') that includes all data either side of landslide occurrence. The entire process is applied to determine thresholds for each rain variable and for pairs of variables found to be statistically independent by correlation analysis.

6.2 Normalised rain variables

Figure 6.1A and Figure 6.1B illustrate the RDN values for June and December, the driest and wettest months. Figure 6.1C shows a box whisker plot of the RDN and RDNI values for each month. One of the novel elements of this study is that thresholds are sought using spatially coherent radar rainfall data and monthly RDN and RDNI normalised variables. The variables and their landslide initiation thresholds are therefore normalised both spatially (i.e. to account for orographic influences in the West Highlands) and temporally (i.e. to account for seasonal variation) as illustrated in the Figure 6.1. Previous studies have used annual RDN normalisation (Wilson & Jayko 1997; Guzzetti *et al.* 2007) and these are shown for comparison in Figure 6.1C by the horizontal line connecting the black (annual RDN) and blue dots (annual RDNI). The plot illustrates how the annual values may overestimate the typical rainfall conditions in summer and underestimate conditions in winter, thus producing poorer quality thresholds.

Please turn over.

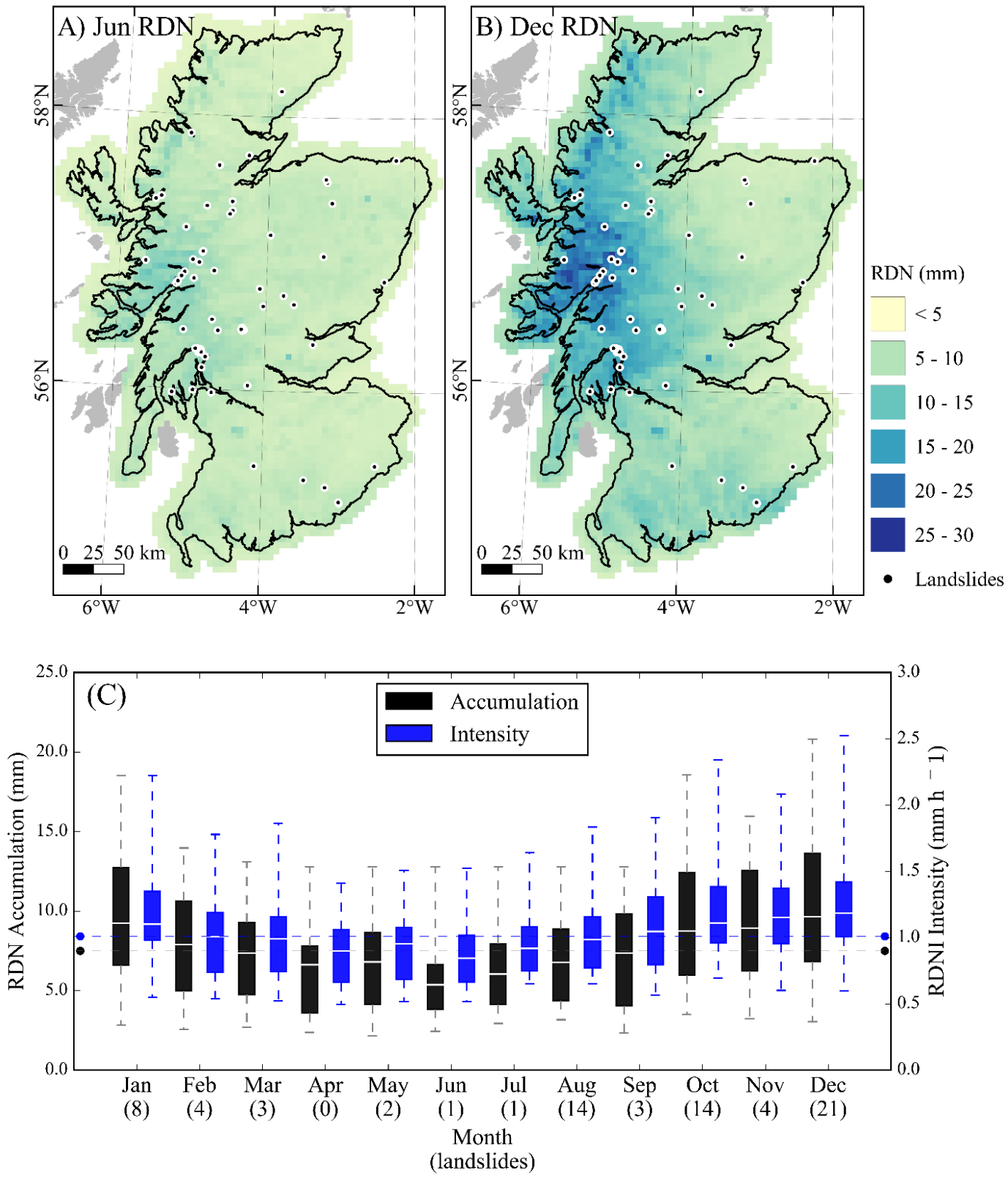

Figure 6.1. A and B show the spatial distribution of the rainy day normal (RDN) accumulation for June and December, respectively. C) A box whisker plot of the monthly RDN (black boxes) and rainy day normal intensity values (RDNI blue boxes). The boxplots are median centred and range from first to third quartiles with whiskers to minimum and maximum values. The x-axis labels indicate the number of landslides recorded in each month. The points and horizontal lines show the average annual RDN (black) and RDNI (blue).

6.3 Landslide thresholds for individual variables

Table 6.1 displays the threshold results for a selection of the highest performing rain variables: $Imax_1$ and $Imax_2$ are the thresholds for the maximum intensity of rainfall (mm h^{-1}) observed in the days preceding landslide occurrence; RD_1 and RD_2 are the thresholds for the duration (hours) of above average intensity rainfall; and NV_1, NV_2 and NV_{12} show the RDN normalised accumulation thresholds. The NV thresholds are multiples of a locations RDN. For instance, by adjusting the NV_1 thresholds to the pixel RDN values the thresholds translate to critical accumulations of approximately 11.0 to 36.5 mm in June, the driest month, and 19.6 to 65.0 mm in the wettest month December depending on location (Figure 6.1).

In Table 6.1, the average AUC value across the ten rain records indicates the overall predictive performance of each rain variable, with higher AUC for variables better able to distinguish landslide and non-landslide rain conditions. The optimal point (OP) and threat score (TS) thresholds are averaged over each of the different rain record lengths and the values in brackets show the range of threshold values between the shortest and longest rain records ('10-day' - 'All'). In comparison to the TS thresholds, the OP thresholds have lower values and lower probabilities but capture a greater number of the landslides (TP). The coefficient of variance (CV %) measures the change in the threshold value across the ten different rain record lengths, a higher CV % indicates greater threshold variance. The TS thresholds have higher variance of 14 – 44 % whereas the OP thresholds are relatively stable 7 – 20 %. The $p(TH)$ is the probability of the threshold and $p(LS|TH)$ is the Bayesian conditional probability of landslide occurrence given threshold exceedance, again the values in brackets show the range of probability values between the shortest and longest rain records ('10-day' - 'All'). The OP thresholds have higher probability of occurrence and lower conditional probability of initiating a landslide. Conversely, TS thresholds have lower probability of occurrence and higher conditional probability of initiating a landslide. The statistical significance of the thresholds, their probabilities and the observed number of landslides (TP) is evaluated using the binomial distribution. All the reported thresholds are significant to the 95 % confidence interval and thresholds with p-values above the critical value are discarded ($\alpha > 0.05$). For example, Figure 6.2 shows the result of the Bernoulli trial for $Imax_1$ TS threshold: the observed number of landslides (TP – black arrow) exceeds the number of landslides expected to co-occur with threshold exceedance by random chance at the common critical values (vertical grey lines).

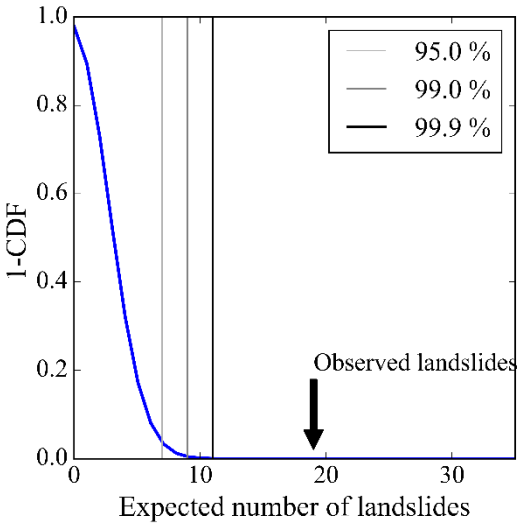

Figure 6.2. A plot showing the results of the Bernoulli trial test of statistical significance for the $Imax_1$ TS threshold. The x-axis is the number of landslides expected to co-occur with threshold exceedance by random chance, the y-axis is one minus the binomial cumulative density function (1–CDF). The black arrow indicates the actual number of landslides observed given $Imax_1$, and the grey lines indicate the critical number of landslides observed for different confidence intervals.

Individual variables		**Optimal Point**					**Threat Score**				
Variable	AUC	Threshold	CV %	$p(TH)$	$p(LS\|TH)$	TP	Threshold	CV %	$p(TH)$	$p(LS\|TH)$	TP
$Imax_1$	0.83	4.7 (5.6 - 4.4)	10	0.25 (0.36 - 0.18)	0.05 (0.18 - 9.6× 10^{-4})	59 (53 - 60)	12.4 (5.6 - 14.1)	23	0.05 (0.35 - 0.07)	0.11 (0.18 - 5.2× 10^{-3})	19 (53 - 12)
$Imax_2$	0.80	5.5 (6.6 - 4.8)	15	0.29 (0.36 - 0.25)	0.04 (0.16 - 7.3× 10^{-4})	59 (50 - 63)	13 (8.7 - 14.2)	14	0.05 (0.22 - 0.01)	0.09 (0.19 - 3.0× 10^{-3})	18 (35 - 13)
RD_1	0.86	4.0 (5.5 - 3.5)	20	0.22 (0.29 - 0.19)	0.06 (0.22 - 1.0× 10^{-3})	63 (55 - 65)	14.4 (8.3 - 20.3)	37	0.04 (0.14 - 0.1× 10^{-2})	0.21 (0.33 - 3.3× 10^{-2})	20 (39 - 6)
RD_2	0.85	7.9 (9.4 - 6.4)	11	0.22 (0.33 - 0.21	0.06 (0.20 - 9.1× 10^{-4})	60 (55 - 64)	22.6 (16.2 - 30.7)	31	0.03 (0.11 - 0.1× 10^{-2})	0.18 (0.35 - 2.1× 10^{-2})	19 (31 -7)
NV_1	0.88	1.9 (2.6 - 1.9)	13	0.18 (0.25 - 0.13)	0.07 (0.26 - 1.3× 10^{-3})	59 (54 - 59)	6.3 (3.6 - 9.1)	27	0.03 (0.14 - 0.1× 10^{-2})	0.22 (0.37 - 1.7× 10^{-2})	21 (41 - 7)
NV_2	0.87	3.7 (4.4 - 3.5)	07	0.18 (0.25 - 0.14)	0.07 (0.26 - 1.3× 10^{-3})	60 (55 - 61)	9.6 (7.0 - 20.7)	44	0.03 (0.10 - 0.1× 10^{-3})	0.22 (0.43 - 3.2× 10^{-2})	25 (37 - 11)
NV_{12}	0.81	15.0 (19.7 - 13.7)	12	0.26 (0.26 - 0.21)	0.05 (0.20 - 8.7× 10^{-4})	59 (44 - 62)	28.4 (22.8 - 46.8)	34	0.06 (0.12 - 0.2× 10^{-3})	0.105 (0.34 - 1.8× 10^{-2})	24 (34 - 11)

Table 6.1. Rain initiation thresholds for landslides in Scotland. Variable: rain variable used and antecedence period. Threshold: the mean threshold value across ten different rain records, brackets show the threshold values for (10-day - 'All') rain records. $CV\%$: the threshold coefficient of variance across ten different rain records. $p(TH)$ and $p(LS|TH)$: the threshold probability and the Bayes conditional probability of landslide occurrence for threshold exceedance, brackets show the range of probabilities for the '10-day' to 'All' rain records. TP: true positives are the number of landslides that co-occurred on days with threshold exceedance, the brackets show the range of values for the '10-day' to 'All' rain records.

6.4 Landslide thresholds for pairs of variables

Thresholds that are based on pairs of rain variables may produce more robust indicators of landslide occurrence as they are able to consider both the short-term rainfall conditions at the onset of landslide initiation in addition to longer term antecedent rainfall. The most suitable pairs of variables will be those that combine the high performing rain variables (i.e. high individual AUC) and that are statistically independent of one another. Spearman's rank order correlation coefficient (R) is used to test for independence and out of the 595 possible pairs, the mean $R = 0.52$ with range $R = 0.17$ - 0.99.

The criterion, mean AUC > 0.85 and $R < 0.50$ is applied to select suitable pairs of variables: previous studies used higher values $R < 0.8$ (Søren *et al.* 2014). Listed in Table 6.2, nineteen pairs of variables were identified using these criteria for different combinations of rain duration (RD_1, RD_2 and RD_{12}), normalized rain accumulation (NV_1, NV_2, $NV_{12}$and NV_{18}) and maximum rain intensity ($Imax_1$ and $Imax_2$). Most pairs are for combinations of different variables, although several suitable pairs were found for combinations of normalised rain accumulation at short (i.e. 1 – 2 days) and long (i.e. 12 – 18) antecedence periods.

					Rain record AUC		
Pair	Variable 1	Variable 2	R	p-value	10	All	Average AUC
1	RD_1	RD_{12}	0.39	< 0.001	0.83	0.93	0.90
2	RD_1	NV_{12}	0.37	< 0.001	0.85	0.93	0.91
3	RD_1	NV_{18}	0.31	< 0.001	0.85	0.95	0.92
4	RD_2	NV_{12}	0.48	< 0.001	0.83	0.92	0.89
5	RD_2	NV_{18}	0.39	< 0.001	0.83	0.94	0.91
6	RD_2	NV_{18}	0.45	< 0.001	0.81	0.93	0.90
7	NV_1	RD_{12}	0.37	< 0.001	0.85	0.93	0.91
8	NV_2	RD_{12}	0.46	< 0.001	0.84	0.92	0.90
9	$Imax_1$	RD_{12}	0.39	< 0.001	0.80	0.92	0.89
10	$Imax_2$	RD_{12}	0.46	< 0.001	0.79	0.91	0.87
11	NV_1	NV_{12}	0.37	< 0.001	0.85	0.93	0.91
12	NV_1	NV_{18}	0.31	< 0.001	0.86	0.95	0.92
13	NV_2	NV_{12}	0.48	< 0.001	0.84	0.91	0.89
14	NV_2	NV_{18}	0.39	< 0.001	0.85	0.94	0.92
15	NV_3	NV_{18}	0.46	< 0.001	0.83	0.93	0.90
16	$Imax_1$	NV_{12}	0.36	< 0.001	0.82	0.92	0.89
17	$Imax_2$	NV_{12}	0.43	< 0.001	0.80	0.91	0.88
18	$Imax_1$	NV_{18}	0.30	< 0.001	0.81	0.94	0.90
19	$Imax_2$	NV_{18}	0.36	< 0.001	0.80	0.93	0.89

Table 6.2. Nineteen pairs of rain variables. R: the Spearman rank correlation coefficient. p-value: statistical significance of the correlation. Rain record AUC: the AUC the scores for the 10-day and 'All' rain record. Average AUC; the average AUC score of the ten rain records.

Pairs of variables			Optimal Point					Threat Score				
Variables	AUC	R	Threshold	CV %	$p(TH)$	$p(LS\|TH)$	TP	Threshold	CV %	$p(TH)$	$p(LS\|TH)$	TP
$^{*}Imax_1$ $^{+}RD_{12}$	0.89	0.39	4.7_32.1 *(5.0 - 6.0) $^{+}$(39.0 - 21.6)	*28 $^{+}$28	0.16 (0.27 - 0.10)	0.08 (0.26 - 1.7× 10^{-3})	42 (38 - 40)	12.0_49.2 (13.0 - 13.0) (28.6 - 96.4)	29 62	0.01 (0.05 – 6.8× 10^{-4})	0.32 (0.6 - 8.6× 10^{-2})	9 (12 - 2)
$Imax_1$ NV_{12}	0.89	0.36	2.4_19.0 (4.0 - 2.0) (22.6 - 13.0)	35 17	0.12 (0.23 - 0.09)	0.11 (0.38 - 2.1× 10^{-3})	40 (34 - 48)	11.9_19.5 (2.0 - 13.0) (25.0 - 25.0)	29 25	0.02 (0.13 - 0.7× 10^{-2})	0.30 (0.45 - 3.2× 10^{-2})	12 (21 - 8)
RD_1 NV_{12}	0.91	0.37	3.5_17.4 (3.5 - 3.5) (22.0 - 15.0)	0 15	0.11 (0.17 - 0.08)	0.11 (0.38 - 2.3× 10^{-3})	45 (33 - 52)	12.1_18.6 (3.5 - 20.3) (24.0 - 18.0)	28 43	0.01 (0.10 - 0.3× 10^{-2})	0.41 (0.75 - 5.5× 10^{-2})	8 (23 - 6)

Table 6.3. Paired variable rain initiation thresholds for landslides in Scotland. Variables: rain variables used and antecedence period, the * and + are used to indicate the values of each variable. Threshold: the mean threshold value across ten different rain records, pairs are separated using "_" and brackets show the threshold values for (10-day - 'All') rain records. $CV\%$: the threshold coefficient of variance across ten different rain records. $p(TH)$ and $p(LS|TH)$: the threshold probability and the Bayes conditional probability of landslide occurrence for threshold exceedance, brackets show the range of probabilities for the '10-day' to 'All' rain records. TP: true positives are the number of landslides that co-occurred on days with threshold exceedance, the brackets show the range of values for the '10-day' to 'All' rain records.

Table 6.3 shows the threshold values, their probabilities and other scores for a selection of pairs with the best performance. As for the individual variables, the OP thresholds have lower values, variances and conditional probabilities and are more likely to occur than the TS thresholds. This is also illustrated in Figure 6.3A that shows a panel plot of the OP and TS thresholds for each of the different rain record lengths: the plots show the number of days with landslides (black dots) and the number days without landslides (grey dots) captured by each threshold (i.e. above and to the right of the threshold lines). The OP thresholds (dashed lines) are relatively stable with low CV, and these capture most landslide occurrences. In contrast, the TS thresholds adjust with respect to increasing rain record length to minimise the number of days where landslides did not occur. Figure 6.3B shows the reduction in the threshold conditional probability of landslide occurrence for increasing rain record length.

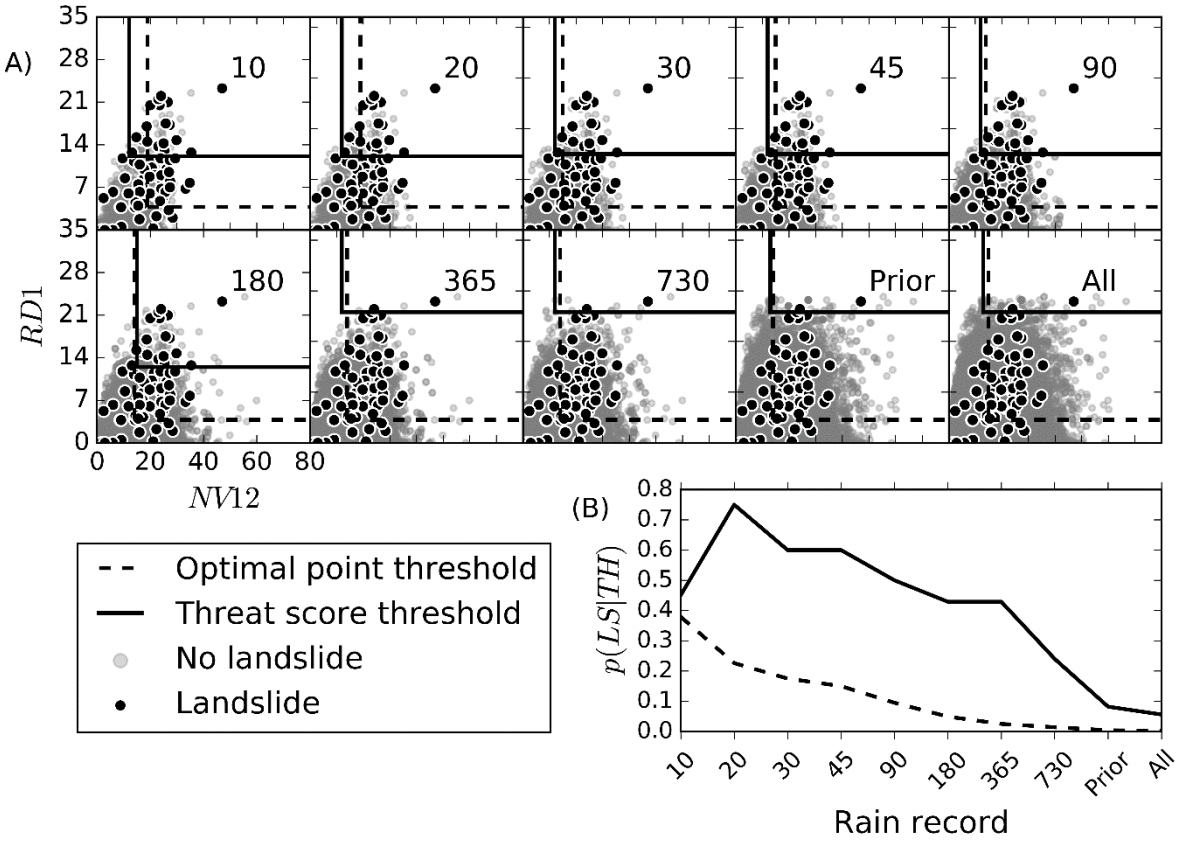

Figure 6.3. (A) Panel plot showing the OP (dashed line) and TS (solid line) thresholds for the combination of RD_1 and NV_{12} and for 10 different rain records. Black dots are the days with landslide occurrence whilst grey dots are the days with no landslides. (B) A plot of the conditional probability of landslide occurrence given OP or TS threshold exceedance for each rain record.

6.5 Comparing thresholds from other studies

Most landslide initiation thresholds are for critical rain accumulations and durations at certain intensities. Figure 6.4 compares the new RDN normalised rain accumulation and maximum intensity landslide thresholds to those published for other temperate regions and thresholds developed using: different threshold selection techniques; analyses using rainfall events; analyses using gauge rain data; absolute and normalized rain variables; and outputs for lower, middle and upper limit thresholds. Several of the intensity thresholds may be inaccurate (± 1 - 2 mm h^{-1}) due to the nature in which the thresholds are reported, for instance using mean or maximum values and results given in graphics.

In Figure 6.4, some of the most relevant thresholds to this study are those for the analysis of 16 landslide rain-events in Scotland (Winter *et al.* 2010) and 502 events in Norway (Meyer *et al.* 2012). For Scotland, the previous rain accumulation thresholds for 1 and 2 days antecedence (blue dots) correspond well with the OP thresholds of this study (red dots). Winter *et al* (2010) also noted the importance of 12-day antecedent accumulation as a contributory factor in landslide initiation, however, the new thresholds suggest that these may be lower 12-day accumulations. A similar pattern is observed for the 1-day Scottish rain intensity thresholds in Figure 6.4B. These differences are likely attributed to the fact that a greater number of landslides were analysed in this most recent study, thus greater variety of initiation conditions. In addition, the new rain accumulation values are normalised using RDN and so the thresholds will be higher or lower depending the on their location: the accumulation values in Figure 6.4 represent the mean RDN value across Scotland. For the Norwegian thresholds, rain intensities are within the range of the OP and TS thresholds found for Scotland. The Norwegian rain accumulation thresholds are higher but these also the include contributions of water supplied by melting ice and snow.

Thresholds from other regions and countries world-wide have different, higher values, but this is likely attributed to different physical constraints and methodology of analysis (Figure 6.4). For instance, the $Imax_1$ OP thresholds are lower than much of the rest, but when looking at the range of intensities (OP - TS) these seem to correspond well with those reported for similar landslide mechanisms and climates (Figure 6.4C). This review indicates that it is important to regionally constrain comparisons.

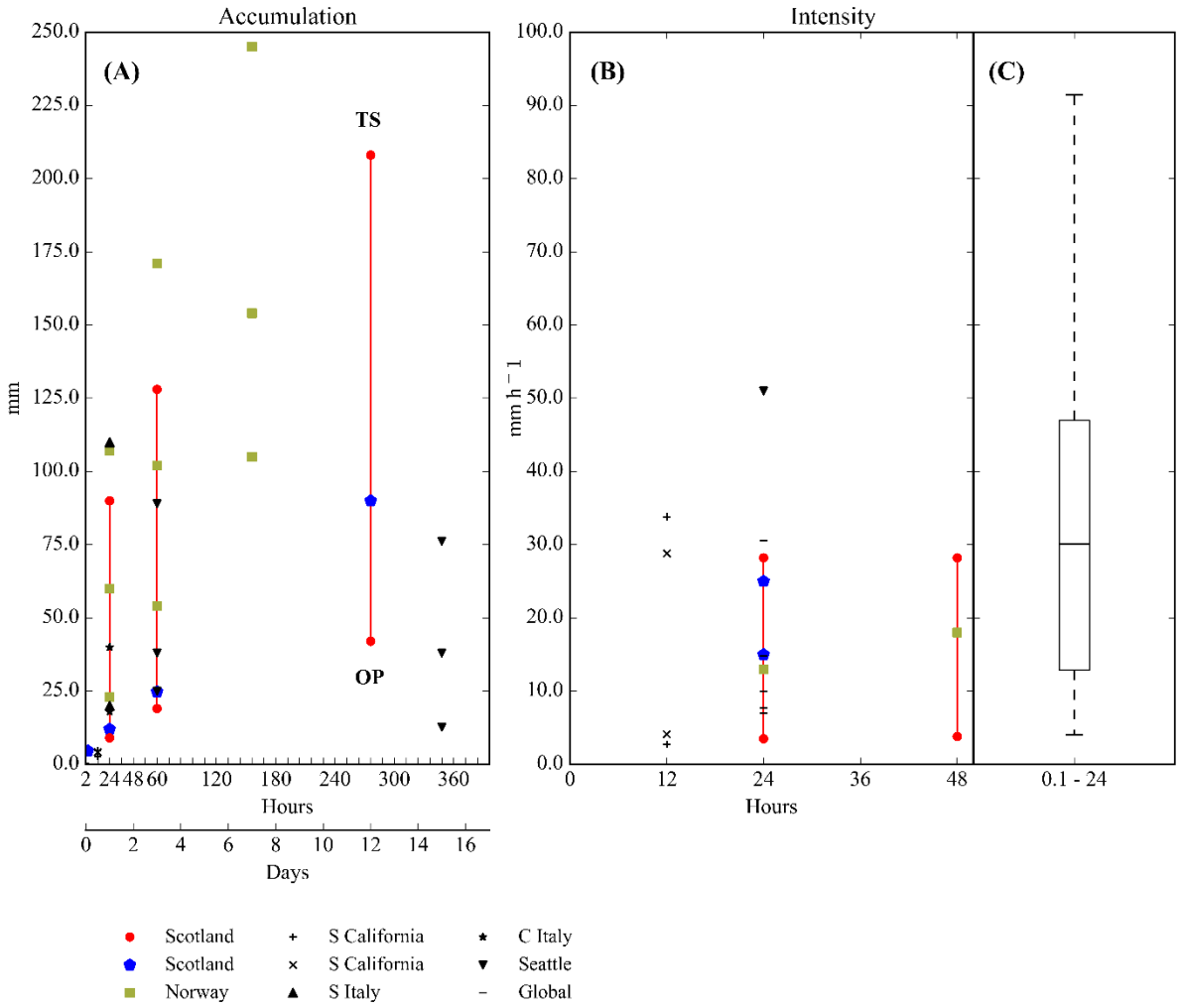

Figure 6.4. A comparison of new thresholds for Scotland (red dots and lines) and thresholds published in other temperate climates. (A) Shows rain accumulation thresholds from 0 - 17 days, and (B) rain intensity thresholds 0 - 48 h. Stacked symbols indicate studies reporting lower, middle and upper thresholds. Blue pentagons: Scotland (Winter *et al.* 2010). Green squares: Norway (Meyer *et al.* 2012). Cross: Southern California (Cannon *et al.* 2008). X: Southern California (Staley *et al.* 2013). Triangle: Southern Italy (Gariano *et al.* 2015). Star: Central Italy (Peruccacci *et al.* 2012). Inverted triangle: Seattle (Chleborad *et al.* 2008). Dash: Global (Guzzetti *et al.* 2007). (C) is a box whisker plot to show the range of 0.1 - 24 h maximum intensity thresholds for 25 different territories, including, Italy, Switzerland, Austria, Spain, North and South America, Indonesia, South East Asia and Japan (Guzzetti *et al.* 2007). The box is median centered and extends 1st to 3rd quartiles and whiskers 10 to 90%. Three thresholds are not shown at ~120 (2) and 180 (1) mm h^{-1}.

6.6 Discussion

The study evaluates the effect of varying the rainfall record length, the primary data input, on two different receiver operating characteristic (ROC) techniques used to define landslide rain initiation thresholds: these are the optimal point (OP) and threat score (TS) thresholds. One of the main inferences to be gained from this investigation is that the TS thresholds are more sensitive to changes in the rain record length and these have mean coefficient of variance 28 % across all the rain variables and pairs examined. Conversely, the OP thresholds proved relatively consistent and have lower variances (mean 11 %) with respect to changes in the rain record length. The length of the rain record is ultimately limited by data availability. For this study in Scotland a relatively unique 13 year radar precipitation record was used but most other investigations use rain gauge data and these are usually for longer periods of several decades. The method implemented here shows that changes to rain record length are shown to influence the OP and TS thresholds differently. This therefore constitutes a simple yet important consideration for past and future investigations and as the literature review identified a diversity of different strategies, including, using a number of days of the rain record prior to each landslide occurrence ranging 10 to 180 days, or using rain events defined between minimum dry periods of 2 – 120 hours.

The OP thresholds maximise landslide detection by selecting relatively low threshold values and this reduces the number of missed landslide alarms. In contrast, the TS thresholds have higher values and these are selected to maximise threshold accuracy by limiting the number false alarms. The two thresholds can be interpreted as a potential lower (OP) and upper (TS) limit range of thresholds that envelope the rain conditions most frequently associated to landslide occurrence in Scotland. Establishing such limits is a common objective in landslide hazard research as they clearly communicate the rain conditions below and above which landslides are least and most likely to occur (Guzzetti *et al.* 2008). In a first application to landslides, the OP thresholds are therefore suggested as suitable method to determine lower limit initiation thresholds and these may be beneficial for use in landslide early warning (Reid 2006; Wachinger *et al.* 2013; UNISDR 2015). Whilst TS thresholds have been used before by Staley *et al* (2013), these and other previously defined thresholds and limits were established irrespective of the rain record length and without consideration for the periods and rain events where no landslides are known to have occurred (Caine 1980; Guzzetti *et al.* 2007; Brunetti *et al.* 2010). The new thresholds for Scotland have been developed using all the available rain time series data at each landslide site.

To assess the value of the new thresholds, and prior to any operational use, the thresholds need to be rigorously tested and evaluated using a set of independent landslide records and rainfall radar of at least 2 – 4 years. In addition, there are several known limitations and possible improvements that may be made to further enhance their performance. First, the thresholds only consider water supplied to the slope materials by rainfall but other studies demonstrate improved thresholds by including additional sources, such as melting snow and ice pack or surface water flow (Meyer *et al.* 2012; Martelloni *et al.* 2013; Søren *et al.* 2014). This might also involve using more sophisticated rain variables for effective precipitation by taking account of evaporation and evapotranspiration (Dixon & Brook 2007; Dijkstra & Dixon 2010). These were not considered here given the time constraints of this study and the limited availability of input data of an equivalent period and scale as the radar data. Second, further improvements may be achieved by developing a set of independent thresholds for smaller

regions and sub-domains in the study area based on the spatial distribution of different slope lithologies and landslide characteristics (Segoni *et al*. 2014). A set of national thresholds were developed due to: i) the relatively limited number of landslide records within the study area, but also as these are comprised of similar landslide mechanisms and failures materials; and ii) as the thresholds are normalised spatially.

The best performing individual rain variables (Table 6.1) are the variables for the one and two day antecedence periods. The optimal point (OP) and threat score (TS) thresholds for normalized rain accumulation on the day of landslide occurrence (NV_1) range from 1.9 to 6.3 times the rainy-day-normal (RDN), respectively. For NV_2, the thresholds are greater at 3.7 to 9.6 times RDN. These thresholds indicate that in Scotland the flux in water supply to slopes prior to landslide occurrence is in the order of two to ten days' worth of the monthly daily average rain. For example, the NV_1 thresholds translate to critical rain accumulations of 11.0 to 36.5 mm in June, the driest month, to 19.6 to 65.0 mm in the wettest month December. This demonstrates how the monthly RDN is used to account for seasonal fluctuations of rainfall in Scotland. The NV thresholds are also normalised for spatial rainfall variation, such as by orographic affects, as the RDN is calculated for each pixel in the weather radar data (Figure 6.1A). The 1 and 2-day antecedence rain duration thresholds indicate that landslides are initiated following critical periods of 3.5 to 30 h above average intensity rainfall. As for the normalised rain accumulation thresholds, the rain duration thresholds are normalised for the seasonal and spatial variability of rain. The new thresholds are consistent with physical descriptions of landslides in Scotland namely: that most landslides occur on slopes with an impermeable substrata that features a shallow (< 3 m), overlain cover of relatively coarse granular matrix material that is highly susceptible to mobilization by both rapid water infiltration and saturation (Ballantyne 1986; 2002; Milne *et al*. 2009).

Similar threshold values of 4.7 to 5.5 mm h^{-1} (OP) and 12.4 to 13.0 mm h^{-1} (TS) are found for the 1 and 2-day antecedence period maximum rain intensity thresholds ($Imax$). These thresholds have lower performance measures relative to equivalent antecedence NV and RD ones. Assuming that landslides are initiated at or near the period of maximum intensity rainfall the results may indicate that there are lags in water supply to reach critical parts of the slope, for instance, due to groundwater flow (Iverson 1997, 2000), vegetation cover, or increased rates surface runoff during high intensity rain (Lu & Godt 2013). Alternatively, other studies report rainfall intensity thresholds that are far below the peak intensity, however, these are for landslides initiated in a different, post-fire environment (Staley *et al.* 2013). The relatively poor performance of $Imax$ is more likely attributed to: i) spatio-temporal rainfall variations as the $Imax$ is a non-normalized rain variable, and ii) data artefacts, as 22 % of the landslide records have > 48 h temporal resolution.

Thresholds that are formed of pairs of variables were selected using a criterion for high AUC and low Spearman's rank order correlation (Table 6.2). Several of the pairs included combinations with the 12 and 18-day rain duration variables. On reflection, these long antecedence period rain duration variables are ambiguous and are of limited value as they might capture durations of a single prolonged rain event or the cumulative duration of multiple short events. Consequently, the pairs with these variables were discarded. For future studies, it is recommended that the new RD variable is used only to measure rain durations at 1 and 2-day antecedence periods. For longer periods, a more appropriate strategy is to calculate the rain

duration by counting the number and duration of rain events between the dry periods, as in Melillo *et al* (2015).

A similar range of 1 and 2-day antecedence NV, RD and $Imax$ thresholds were obtained in the pairs combining the 12-day antecedent normalised rain accumulation (NV_{12}). The pairs with NV_{12} also featured the highest performance measures found in this study (Table 6.3). More robust thresholds are likely obtained as the 12-day antecedent rain accumulation contributes to an increase of the slope material pore water pressure and a reduction of effective stress, so that shear strength is reduced and a landslide occurs (Iverson *et al.* 1997; Wieczorek & Glade 2005; Napolitano *et al.* 2016). Other empirical thresholds developed in Scotland also highlight the role of the 12-day antecedent hydrological condition of soils as a precursory factor in controlling the rain thresholds that trigger landslides (Winter *et al.* 2010). The new results also support the observation that landslides occur more frequently in the UK during the early autumn and winter seasons when sequences or 'clustering' of multiple cyclonic-storm systems is common in periods lasting 5 to 15 days (Mailier *et al.* 2006; Kendon & McCarthy 2015; McCarthy *et al.* 2016). Lower performance measures were obtained for the pairs combining longer antecedent periods ($\geq NV_{18}$). This weakening of the threshold signal suggests that rainfall of more than 12 days prior to landslide occurrence is a less significant indicator of landslide initiation in Scotland. The longer antecedent periods may have a more limited influence as the geomorphological and geotechnical characteristics of the slope materials support effective drainage and resistance to protracted and evenly distributed rainfall, such as their steep slope angles, high permeability and granularity (Ballantyne 1986; Wieczorek 1996; Nettleton *et al.* 2005). Subsequently, it is believed that the 12-day antecedent rainfall is an important precursor to landslide occurrence in Scotland whereas the shorter, 1 to 2-day rain conditions are a likely indicator of their triggering.

Figure 6.5 illustrates a three tier, low (yellow), moderate (amber), high (red), landside warning system based on the RD_1 and NV_{12} pair thresholds obtained in the study area. Rain conditions that exceed the OP threshold and are below the TS threshold ('> OP & < TS' in Figure 6.5) are used to indicate a moderate 'amber' warning of landslide potential as these capture the rain conditions in which most past landslides have occurred (74 %). The TS thresholds and red portion of the plot only capture a small proportion of the landslides (6 %). As shown in Figure 6.3, the TS thresholds only capture a larger number of landslides for the ≤ 180 rain records and the TS thresholds are more sensitive to rainfall record length. Tentatively, to complete the warning system, a yellow 'low' warning may be given below the OP threshold (<OP) and a high 'red' warning of landslide potential is given for the rain conditions that exceed the TS threshold (>TS).

The yellow shaded area represents rain conditions with a high level of uncertainty for the landslide potential. This is because the yellow portion of the plot contains several landslide occurrences (20 %) and many days where no landslides were recorded. In addition, several of the landslides may have been initiated by other factors not captured in the rainfall variables and thresholds used, such as water supplied by snow melt or overland flow, and this may explain why several landslides occur in relatively low rainfall conditions. For instance, in the bottom left portion of the plot five landslides are shown to have been initiated in conditions of little to no 1-day rain duration and only 2 to 10 days' worth of the monthly rainy day normal rainfall in the preceding 12-days. Alternatively, and a more likely scenario, is that these represent several records within the landslides database that have poor spatial and temporal resolution or

that have been wrongly classified as planar and debris flow type failures – despite the data verification and cleaning processes applied for this study described section 3.1.2 Landslide database. One possible solution to improve the data verification process involves using plots such as Figure 6.5 to identify and eliminate landslide records with low rainfall profiles (e.g. those in the bottom left of Figure 6.5 that are unlikely to be triggered by rainfall). However, the author issues caution in adopting this approach as it represents a subjective selection and removal of data points to fit a pre-determined opinion on the rainfall conditions that cause landslides. More appropriate solutions include: i) to use threshold selection methods that provide tolerance to erroneous and outlier data points, such as those adopted here for OP thresholds; ii) make further improvements to the processes and accuracy of data collection, data cleansing and landslide classification; and iii) introduce additional variables and account for other physical processes that are known to initiate landslides, such as snow melt and rock fall.

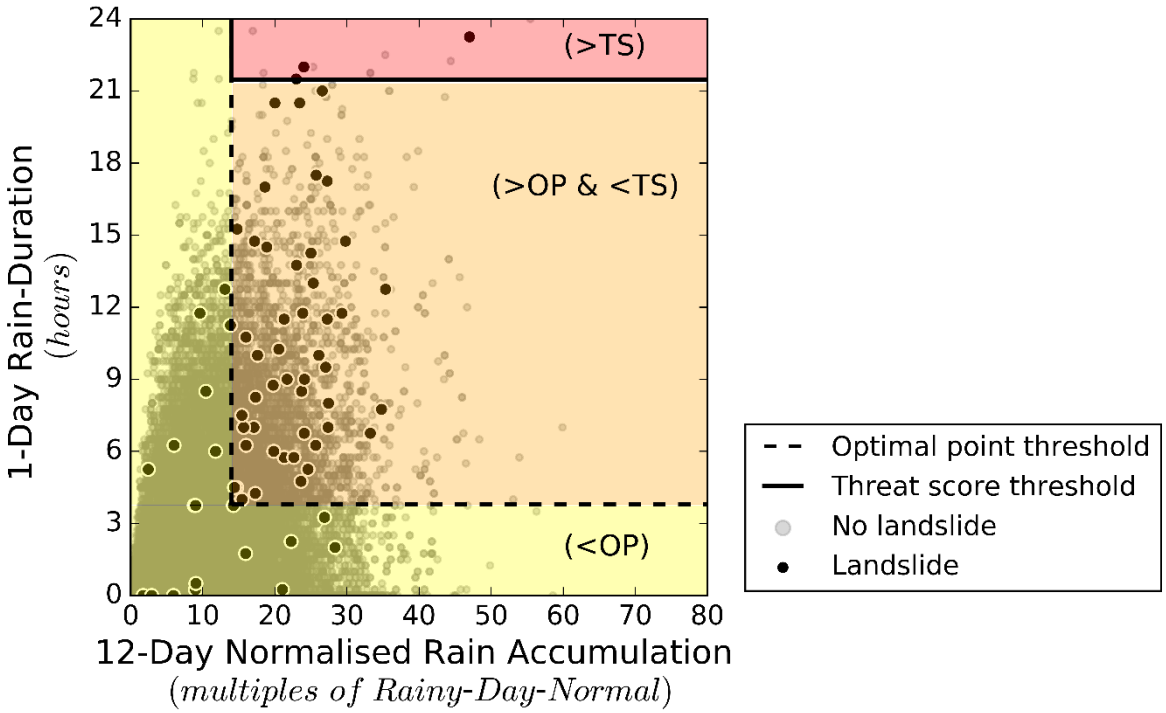

Figure 6.5. The OP (dashed line) and TS (solid line) thresholds for the combination of: hours of above average intensity Rain-Duration (RD_1) on the day of occurrence, and monthly rainy-day-normal normalised rain accumulation (NV_{12}) in the preceding 12 days. The thresholds are used to form a hypothetical traffic light warning system of landslide potential: uncertain / low = yellow, moderate = amber, and high = red.

Chapter 7 A Prototype Hazard-Network Catastrophe Model

7.1 Introduction

In this chapter, a catastrophe (CAT) model is demonstrated that combines the three key elements of this thesis: the model of hillslope susceptibility, the landslide initiation thresholds, and the traffic simulation of indirect impacts. The CAT model is used to estimate the potential losses due to landslide disruptions on the road network in Scotland, a landslide-network CAT model. It is stressed that the model developed and its outputs are intended for illustrative purposes only. Although the spatial-temporal probabilities (i.e. landslide susceptibility and triggering thresholds) and the landslide impacts (i.e. the network model) used in the model have been rigorously tested and evaluated in this thesis, several simplifying assumptions were made in order to produce a working model. These assumptions show how the CAT model framework may be used to evaluate factors that determine the overall level of landslide risk, such as the disruption duration. For operational applications this, and other factors (e.g. partial closure) require thorough evaluation and thus render the development of an operational standard model beyond the scope of this thesis. Nonetheless, as far as the author is aware this is the first application of CAT modelling to evaluate hazards in terms of their impact to the operation of infrastructure. Therefore, the modelling framework and its components are portable to investigations of other hazards in Scotland, such as flooding and severe wind, and to the study of other hazards and infrastructures in different regions.

7.2 Input data to the catastrophe model event set

The event set is a stochastically generated list of possible landslide events on the strategic road network in Scotland. Conceptually, the event set can be construed as 10,000 years' (number of model iterations; n = 10,000) worth of random re-realisations of the observed landslide data obtained in Scotland for the period 2004 to 2016. The event set is produced by Monte Carlo sampling of discrete probability mass functions (PMF) and continuous probability distribution functions (PDF) of observed empirical data and the modelled landslide hazard on road segments. Figure 7.1 shows the probability functions used in the CAT model:

- Figure 7.1A shows the PMF of the number of storms per year for the period 2004 to 2016 (red bars, mean = 11.4, standard deviation = 4.2) and the skewed normal PDF for period 1871 to 2016 (black line, mean = 9.1, standard deviation = 3.9). The CAT model samples the 2004 to 2016 period PMF to provide consistency with the period of landslide and rainfall observations.
- Figure 7.1B displays the PMF of the calibrated landslide hazard on each road segment (red bars). The landslide hazard PDF follows a lognormal distribution (black line) and the inset in Figure 7.1B shows a long right tail representing road segments with a relatively high hazard concentration. The landslide hazard PMF is sampled without replacement to select the road or roads that are disrupted by a landslide in each storm event (e.g. each event represents a storm with 0, 1 or more landslides on a road).
- Once the event set is formed, the number of landslide occurrences per storm is counted to produce a PMF of landslides per storm in Figure 7.1C. Thus, this PMF is an output

of the CAT model. It illustrates the underlying distribution formed by combining the storm and hazard occurrence probabilities (Figure 7.1A and Figure 7.1B).

- Figure 7.1D shows the distribution of losses for events with one landslide (solid line, 600 sampled events), two landslides (dashed line, 300 events) and three landslides (dotted line, 100 events).
- Figure 7.1E shows the PMF for the duration of road segment disruptions caused by landslides in Scotland for the period 2004 to 2016. Most of the landslides are reported to have caused between 0 (< 12 hours) and 4 days of road disruption, and up to 15 days duration in extreme cases. Acts as a multiplier to the event losses.

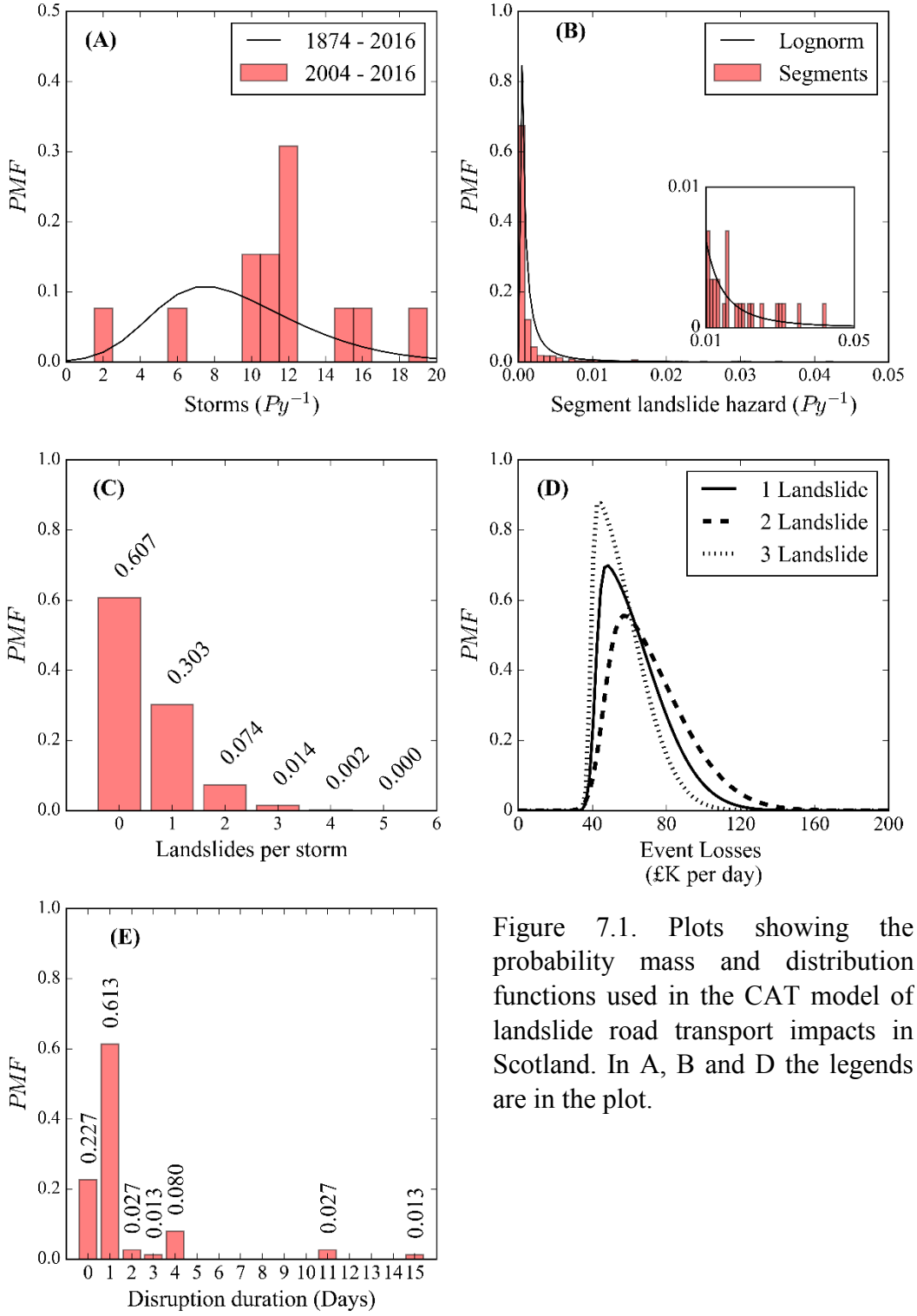

Figure 7.1. Plots showing the probability mass and distribution functions used in the CAT model of landslide road transport impacts in Scotland. In A, B and D the legends are in the plot.

7.3 Expected losses due to landslides

Figure 7.2 shows the expected losses due to landslide occurrences and disruptions to the road transport network. The AEP (Figure 7.2 A) is the probability that the sum of losses in any given year will exceed a certain level. The plot also shows the losses in terms of days of travel delay, or the total time lost across all users of the road network. Figure 7.2B shows the same AEP information but in the format of the expected losses at different return periods. For example, the aggregate expected losses due to landslides for the 1-in-10-year return period are approximately £1 M and this corresponds to an AEP of 0.1 (i.e. a 10 % chance each year). Figure 7.2 B also more clearly shows the expected losses at the rare and extreme end of the AEP distribution such as the 1-in-100-year (AEP = 0.01) and 1-in-250-year (AEP = 0.004) return period losses between £5 and £7 M.

In Figure 7.2 the grey shaded curve and boxes are the CAT model results using the observed disruption durations (Figure 7.1E), the dashed line curve and white boxes are the model results assuming each event has a disruption duration of 1 day. For the latter, the annual average loss (AAL) is approximately £ 0.35M and losses are very unlikely to exceed £ 1M at even the 1-in-1000-year return period (Figure 7.2 B). When the model is run using the events with different disruption durations the AAL = £ 0.50 M and the losses follow an exponential distribution over the higher return periods.

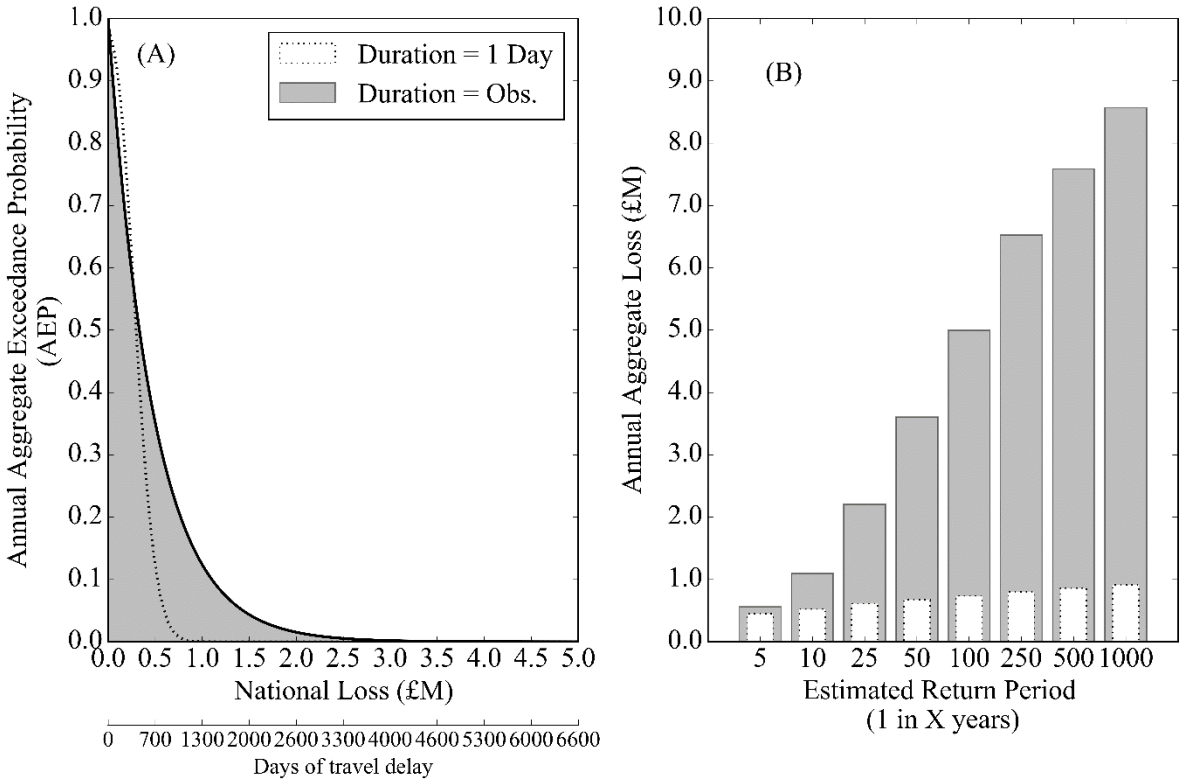

Figure 7.2. The modelled losses due to commuter travel disruption by landslides in Scotland. Plots A and B show the Aggregate Exceedance Probability (AEP) and return periods of losses for events with fixed1-day durations (dashed line and white boxes) and variable durations (solid line and grey boxes).

7.4 Discussion

The results presented above show the loss estimates produced by a catastrophe model of landslide disruptions of traffic on Scotland's strategic road network. The model has produced two AEP curves: one for the events with fixed 1-day disruption durations, and one for the events with varying disruption durations. The modelled AEP curves quantify and illustrate the influence of disruption duration to the expected level of loss. The losses for the model with varying event durations, and that were sampled from actual observations in Scotland, are found to be significantly higher. For instance, the 1-in-100-year losses were increased from £0.6 M to £5 M per year. Therefore, there is approximately a 10 % chance of a £5 M or more loss occurring in any ten-year period. To put these loss figures into context, for the decade 2015/16 to 2025/26 the road maintenance budget is £55 M per year (Transport Scotland 2016b). This is a meaningful insight for the hazard managers and network operators that are responsible for maintaining the road network. The model results may be used to supplement cost-benefit-analysis and to evaluate how policies and initiatives aimed at reducing remediation time can limit and reduce loss. For example, the AEP results may be considered in the design of road maintenance contracts with clauses that specify targets and incentives for limiting disruption duration. Such contracts and practices are already industry standard and routinely used for responsive maintenance and other scheduled works on the UK's road and rail infrastructure (NAO 2008; Cook 2011; DFT 2014b). These may therefore present a relatively quick to deploy mechanism to alleviate the level of landslide hazard risk in Scotland.

The model results also highlight the difficulty in producing robust AEP curves as the uncertainty associated with the disruption duration is quite large. For instance, the modelled distribution of event durations is based on a relatively limited sample of landslides (Figure 7.1E). In reality the duration of a disruption is determined by a number of interacting factors that are not presently accounted for in the model, including the availability of local resources, ease of access to the hazard location, the hazard magnitude and complexity (Glade *et al.* 2005; Winter *et al.* 2014). Furthermore, in this illustrative model, not all sources of uncertainty have been considered. For example, the model hazard and vulnerability modules may be extended to enable the simulation of events that cause partial road closures, and evaluating how this interacts with disruption duration, or by introducing information of the landslide defences and their failure rates.

Despite its shortcomings, these does not mean that the model has little or no value. The landslide hazard on each road segment has been evaluated by combining robust empirical assessments and modelling of the terrain susceptibility and the landslide triggering frequency. The landslide hazard was determined by combining the sum susceptibility and the maximum triggering frequency on each segment (Guzzetti *et al.* 2005; Meyer *et al.* 2015). However, the hazard module is intended to be extendable so that one could use and combine other definitions of the landslide hazard (e.g. using the mean recurrence interval). In addition, the model exposure module may be extended to beyond using the impacts to traffic calculated using the calibrated and national scale traffic simulation developed in this thesis. Therefore, although it is a challenge to deploy the catastrophe model to accurately predict the occurrence of specific threats and hazard scenarios, the model can still be used to assess the relative risk of each road segment within the network and to indicate the expected losses in any given year.

Chapter 8 Conclusions and Further Work

8.1 Introduction

The previous chapters of this thesis have provided the rationale, methodology, analysis results and discussion of the research. Here the conclusions are presented in relation to the research aim and objectives established in section 1.2.

8.2 Completion of the aim and objectives

The aim of the thesis was "*to develop a method to systematically quantify and evaluate the indirect impact of landslide hazards on transportation infrastructure networks*". Achievement of the thesis's aim was directed by several objectives:

To "*understand the present state of knowledge and its limitations with respect to quantifying the susceptibility of slopes adjacent to transportation infrastructure networks*" a literature review was conducted and it was found that the strategically important infrastructure networks in the UK are exposed to a variety of different landslide mechanisms and that vary depending upon their geographical setting. For the networks in upland and mountainous regions, such as in Scotland, most landslides and infrastructure disruption occurs in locations that feature terrain characteristics associated with increased landslide susceptibility. In the literature review it was found that areas that are of increased (or decreased) landslide susceptibility may be modelled using broad coverage spatial data sets, including digital elevation and soil material models, and empirical multi-variate techniques.

To "*develop a landslide susceptibility assessment for transportation infrastructure networks*" a case study was used. The strategic road network in Scotland was chosen as a suitable study area given the availability sufficient data of past landslide occurrences and as many of the reported landslide incidents are known to have caused substantial damage and disruption to national transportation. Guided by the findings of the literature review (Chapter 2.2), a method was devised that leverages the available data sets in Scotland and logistic regression to model landslide susceptibility (Chapter 3.2). The results (Chapter 4) indicate the terrain characteristics that are associated with increased landslide susceptibility and this is used to inform of the landslide processes. A primary output of the thesis, several new map products are produced that evaluate and portray the relative landslide susceptibility of each segment in the road transport network.

To "*understand the present state of knowledge and its limitations with respect to quantifying the indirect impact of landslide disruptions on transportation infrastructure networks*" a literature review was conducted. The literature review found that substantial economic losses arise due to the delays and congestion (indirect impacts) caused by landslide disruptions of rail and road networks, and that therefore these impacts represent a significant proportion of the total hazard risk that is largely unaccounted for in state-of-the-art hazard and risk assessment. In the literature, the methods used to quantify these impacts combine techniques from multiple disciplines including, traffic simulation and transport economics, complex network analysis, and risk assessment. For highway networks, it was established that user equilibrium traffic models may be used to calculate the routes and travel time-cost for undisrupted and disrupted network conditions.

I order to "*establish an appropriate traffic simulation model to quantify the indirect impact of landslide disruptions on a highway network*" the case study of Scotland was again used. Based on the knowledge gained from the review of literature in Chapter 2.3, a method was devised that combines automatic traffic counting data and UK census commuter origin-destination tables in a user equilibrium traffic simulation model described in Chapter 3.4. The model is calibrated and used to approximate the undisrupted travel patterns, routes, time and cost of commuter trips in Scotland. The traffic model is then applied to calculate the additional travel time and costs (indirect impacts) due to a series of hypothetical landslide events. These hypothetical landslide events are the selection of strategic road network segments that were identified as susceptible to landslides using the landslide susceptibility model developed in Chapter 3.2 and results shown in Chapter 4. A primary output of the thesis, in Chapter 5 the event impacts are aggregated to inform of the likely distribution of indirect impacts due to landslides in Scotland, and this information is used to rank and identify the critical (or most important) segments for maintaining road network serviceability.

To *"understand the present state of knowledge and its limitations with respect to the definition of landslide initiation thresholds"* a literature review was conducted and it was found that due to the landslide mechanisms, rainfall thresholds are most suited and far more developed for shallow translational landslides and debris flow than for deep seated, rotational and complex landslides. To develop thresholds several empirical analysis techniques have been demonstrated and each of these adheres to a similar method of analysis: to evaluate the timing of landslide occurrences in relation to time series of precipitation variables, such as intensity or accumulation and at different antecedence periods. The thresholds are used to inform of the landslide processes and to make probabilistic assessments of the threshold landslide recurrence intervals. An unresolved issue, and one that generates much threshold uncertainty, is in the lack of a coherent approach to evaluate the variance of threshold values and their probabilities to changes in the rainfall records used, including investigations that use gauge or remotely sensed rain data and the length of these observations.

To "*develop a set of landslide initiation thresholds utilising weather radar data"* a database of landslide occurrences was obtained for the period 2004 to 2016, and these were analysed in relation to rainfall time series from high-resolution radar using the methodology described in Chapter 3.3; again, using Scotland as a case study. The thresholds were developed using a range of different time series periods and this is used to inform of the threshold variance. A primary output of the thesis, In Chapter 6 the new landslide initiation thresholds for are presented and used to inform of the landslide processes.

To "*demonstrate a coupled hazard-network catastrophe model to quantify the annual average loss caused by travel disruption to commuters due to landslides in Scotland*" a brief literature review was conducted in Chapter 2.2 to summarise the present state of knowledge for landslide hazard and risk assessment, and catastrophe models. In Chapter 3.5 the method to produce a prototype catastrophe model is described. The model illustrates several of the key stages of catastrophe model development, made possible using the primary outputs of this thesis: a landslide susceptibility mode, a network impact model, and landslide initiation thresholds. The results of the catastrophe model are presented in Chapter 7 and these indicate the annual average loss due to landslides and the losses expected at different return periods.

8.3 Synthesis of key discussions

8.3.1 Landslide susceptibility

The thesis has developed a landslide susceptibility model of the hillslopes adjacent to the strategic road network in Scotland. Based on the findings of the literature review in Chapter 2, the susceptibility was model was developed using the well-established logistic regression technique that has been shown to outperform other multi-variate approaches in other landslide susceptibility investigations (Brenning 2005; Yilmaz 2010). Several high resolution data products were used as input to the model including: 5 m^2 NEXTmap digital elevation model, providing information for the slope elevation, angle, aspect, roughness and curvature; and the soil parent material model (Lawley & Smith 2008) for the superficial material soil depth, texture and classification. Three models (i.e. models A, B and C) were produced for different combinations of these input variables. A novel element of the method developed for this thesis was the use of hillslopes as a modelling unit; in contrast to previous studies that model susceptibility at the per pixel or per catchment scale. The decision to use hillslope units was informed by the results of other investigations that differentiate the hillslopes capable of producing translational landslides and debris flow using measures of hillslopes roughness (Wilford *et al.* 2004; Welsh & Davies 2011; Chevalier *et al.* 2013; Berenguer *et al.* 2015).

To determine a suitable hillslope unit scale, the logistic regression models were fitted and evaluated using six different hillslope sizes (Chapter 4.2). Pragmatically, the hillslopes created using a 1000-cell threshold (minimum area ≥ 0.625 km^2, mean area = 0.790 km^2) were selected based on the model performance measures, but these showed that the model goodness of fit and accuracy were only marginally improved for the 1000-cell hillslopes. The lack of a notable change in the performance measures of the models using the different sized hillslopes was attributed to the national scale of the study and as the optimal hillslope size may differ region to region. Nonetheless, the performance and accuracy of each model was found to be in a similar or higher range to those obtained in previous studies (Chapter 4.4).

The results indicated that the most suitable explanatory variables for landslides in Scotland are the hillslope median slope angle, the Melton ratio, slope aspect, and soil texture. Increased landslide susceptibility was identified for the hillslopes facing the South and West, and theoretically this is linked to: increased rates of solar irradiance exacerbating desiccation of the slope surface material leading to higher permeability; and increased precipitation and water infiltration due to the prevalence of westerly moving frontal systems and rain in the study area. In wet conditions, increased rates of water infiltration, and to greater depths, can lead to a critical increase of porewater pressure and a reduction of effective stress, so that shear strength is reduced and a landslide occurs (Crozier 1997; Iverson *et al.* 1997; Iverson 2000; Stoffel *et al.* 2014). Increased landslide susceptibility was also found for variables soil depth of 2 to 5 m bgl and for Argillaceous soils (< 0.06 mm diameter). These results are in line with process understanding and field observation of landslides in Scotland (Ballantyne 1986, 2002; Winter *et al.* 2005; Milne *et al.* 2009).

To account for known reporting bias in the landslide database used, the data use to train and test the models is limited to the landslides that occurred on the hillslopes that are adjacent to the road network. The hillslope susceptibilities were aggregated according to the road segments that they intersect, and this allows the relative susceptibility of each road segment to be evaluated. The susceptible road segments were compared to those identified as susceptible

using a different GeoSure susceptibility model, a national model developed by the British Geological Survey, and those identified using other techniques, such as detailed site and geotechnical investigations in Winter *et al* (2005). There was good agreement between the different models (Figure 4.12 in Chapter 4.8). The approach may therefore be used to identify the most susceptible road segments to improve the effectiveness of and efficiency of landslide hazard management in Scotland, for instance, conducting more on-site investigations on the high susceptibility segments. The method is applicable to other the evaluation of landslide susceptibility for other linear infrastructures, such as rail or pipelines, and in other landslide prone regions globally.

8.3.2 Landslide impacts

The study demonstrates an assessment of the indirect impacts of landslide hazards on a national road network. A national scale model of traffic in Scotland is developed using a combination of automatic traffic counting data, origin-destination data of commuter trips and a dynamic user equilibrium simulation model outline in Chapter 3.4. The model was calibrated for undisrupted network conditions and then it was used to calculate the additional travel time and cost due to different network disruption events. Previously, such assessments were limited to the study of travel disruptions in conceptual and in urban road networks, and there was a clearly identified need to develop and demonstrate these models at broader to national scales in order to address the threats posed by hazards distributed over a large spatial area, such as landslides, flooding or wind storms (Murray *et al.* 2008; Koetse & Rietveld 2009; Dijkstra & Dixon 2010; Mattsson & Jenelius 2015; Krebs 2017).

A series of potential landslide events were selected using the road segments identified as susceptible to landslides using a new model developed in Chapter 4. The average nationwide economic impact of each of the events was £64 k per day of disruption, and these impacts follow a positive skewed distribution representing the road segments where landslide-disruptions can generate relatively severe losses of up to £130 k per day. This information was used to identify the most critical road segments in Scotland (Figure 5.2). In addition, a risk matrix and map was produced that clearly identifies the road segments where there is a high potential for landslide hazards and that cause high economic impacts (Figure 5.5).

The hazard impact footprints show how the travel disruption and impacts caused by landslides are spatially distributed according to the zones and regions where people live. The analysis of the event footprints indicates that residents in the central and west of Scotland are most likely to be effected by landslides, and if the occurrence of landslides in the future continues in a similar pattern to that of the past, this may lead to further indirect and secondary socio-economic impacts in these areas, such as longer-term reductions in business investment and tourism.

8.3.3 Landslide thresholds

This study examined two methods to determine objective landslide thresholds in an assessment of shallow translational slides and debris flows in Scotland. Thresholds were produced using information for 75 recorded landslide events and radar precipitation data for the period 2004 to 2016. The results show that thresholds selected using threat score are more sensitive to rainfall record length, whereas the optimal point thresholds provide rational lower limit thresholds and these are least affected by the length of the rain record used. Changes to the rainfall record length is a factor not considered in past studies. The thresholds are developed

using several new rain variables that are normalised by the monthly rainy-day-normal. This normalisation produces thresholds that are both temporally (i.e. seasonally) and spatially (i.e. terrain) adjusted for rainfall variations.

The normalised variables provide the most robust landslide thresholds and the best performing threshold was observed for the threshold combining the duration of high intensity rain on the day of failure ($RD_1 \geq 3.5$ h) and the 12-day normalised rain accumulation ($NV_{12} \geq 17.4$). Other investigations in conducted in Scotland have also highlighted the role of the 12-day antecedence hydrological condition of soils as a precursory factor in controlling landslides triggering (Winter *et al.* 2010), and tentatively this supports the observation that the landslides most frequently occur during the seasons when sequences or 'clustering' of cyclonic-storm systems and fronts is typical and persists for periods of 2 to 15 days (Mailier *et al.* 2006; Kendon & McCarthy 2015; McCarthy *et al.* 2016). Threshold performance is shown to be weakened by the use of longer antecedent period rain variables (≥ 18 days) and this is believed to be attributed the geomorphological and geotechnical characteristics of the slope materials, namely steep slope angles, high permeability and granularity, that provisions effective drainage and resistance to protracted and more evenly distributed periods of rainfall (Ballantyne 1986; Wieczorek 1996; Nettleton *et al.* 2005). Subsequently, it is believed that the 12-day antecedent rainfall is an important precursor to landslide occurrence in Scotland whereas the shorter, 1 to 2-day rain conditions are a likely indicator of their triggering.

8.3.4 A catastrophe model of landslide losses

A catastrophe model was developed that is comprised of hazard, exposure, vulnerability and loss modules. The modelling framework is based on the logic and is comparable to that used by insurers to evaluate catastrophe risk (Foote *et al.* 2017). The components and results of each module were calibrated according to the historical records and hazard modelling results obtained in Scotland. The hazard module simulates a hazard event set. The event set is generated to represent 10,000 years' worth of simulated storms during which landslides may or may not have occurred. The event set is an list of potential landslides and their likelihood created using independent Monte Carlo sampling of: the observed frequency of storms per year; and the landslide hazard probability distribution of the road segments. The landslide hazard is obtained from the susceptibility and threshold models developed in this thesis. The exposure and vulnerability modules assess the level of road network disruption and the loss caused by each event, forming an inventory of event losses and their occurrence intervals. Lastly, the loss module is used to resample the events and their losses, producing metrics of the annual average loss and the aggregate exceedance probability of losses at different return periods. The study is the first known application of a catastrophe model to evaluate the risk posed by national travel disruption due to landslides. Each of the model components is portable to investigations of other hazards and other infrastructures in Scotland, and it is applicable to other regions.

The catastrophe model calculates the annual risk of indirect economic impacts due to travel disruption by landslides in Scotland. The model was run twice: once for run for events with fixed disruption durations of 1 day; and then for events with varying durations based on the historical record. For the latter, the annual average loss was increased £0.3 M to £ 0.5 M and the losses were increased significantly at return periods relevant to operational hazard management planning. For instance, the 1-in-100-year event losses were increased £0.6 M to £5 M per year. The results of this study emphasise the dramatic effect of disruption duration

on the loss estimates, and this information may be used to inform network management policies.

The results also highlight the significant effect that data and process uncertainties can have on loss estimates, and it is important that the developers and users of such models are aware of the data, limitations and assumptions on which they are based. The catastrophe model was developed in order to illustrate a framework for evaluating the impact and risk of landslide disruptions on transport infrastructure. At present, the hazard events are simulated using a calibrated, but simplified, storm driven process combining the annual frequency rainfall initiation threshold exceedance and the conditional probability of landslide occurrence. To improve the models simulation of hazard events, it is suggested that future investigations are concentrated on the application of these thresholds with more sophisticated and higher resolution re-analysis and stochastic precipitation series to quantify and reduce the uncertainties associated with landslide triggering (e.g. Jones *et al* (2009)). Another pertinent extension of the model is the evaluation of partial road closure events to examine the losses caused by lower magnitude hazards and to evaluate how partial restoration of the road segment influences the expected level of loss.

8.4 Uncertainties and implications for users

This section highlights the issues of uncertainty in the data, techniques and results of this thesis and considers its implications for potential users.

8.4.1 Landslide susceptibility

A series of data quality checks and processes were applied to cleanse the British Geological Survey national landslide database (NLD) as described in section 3.1.2 Landslide database. Despite these steps several uncertainties persist because of the condition of the NLD and the analytical techniques used. First, despite cleansing, the landslide data has a known spatial bias towards the built environment. The susceptibility analyses are therefore constrained to the areas adjacent to infrastructure networks and may not be directly applicable in other areas, such as on hillslopes in remote areas.

Second, the NLD is also known to be biased toward higher magnitude events as these are more likely to be reported. The extent that the data captures low magnitude landslides is unknown. The inclusion of data for low magnitude landslides might influence the terrain characteristics identified as being associated with higher or lower susceptibility in the logistic regression models as these smaller landslides may be initiated under different hydro-geological conditions. However, as most of the landslides are reported when they have some effect on the human or built environment, it might be assumed that the absence of records for lower magnitude landslides reflects the fact that these events are too small to incur any significant damage and thus irrelevant for evaluating susceptibility on transport networks.

Third, the landslide data are supplied as point coordinate-pairs at the landslide failure source and scarp location. These points are spatially joined to the hillslope units that are used to analyse and model the factors associated with increased or decreased landslide susceptibility. Landslides may inadvertently be spatially joined to the wrong hillslope given the spatial accuracy of the landslide point data and as landslide scarps may be situated on or near to the hillslope boundaries. Consequently, these errors may also occur due to the resolution of the digital terrain model and the technique used to create the hillslope units. For the latter scenario,

this is somewhat accounted for as various hillslope sizes were created and evaluated – selecting an appropriate hillslope unit size by maximising classification accuracy across several measures.

Lastly there are uncertainties due to the absence of several factors in the model that are known to influence the occurrence of landslides in the study area. This includes model inputs for seasonal vegetation and land cover change, due to the lack of equivalent resolution and geographic coverage data. Indeed, one potential area of future investigation involves evaluating how certain types of vegetation cover and sequences of vegetation change coincide with varying rates of landslide occurrence. Current techniques involve the use of remotely sensed data and vegetation indices such as NDVI and the Leaf Area Index (e.g. Shahabi & Hashim 2015; Chen *et al.* 2017). However, several challenges remain for these approaches due to the relatively shorting operating periods of state of the art remotely sensed data products. For those products with several years and decades of data there remains the trade-off between using data with high spatial resolution at long and irregular intervals, versus lower resolutions with higher revisit times. In a similar vein, there is a lack of suitable resolution data and methods to account for anthropogenic alterations in land cover, land use and slope morphology. For instance, due to engineered slope stabilisation work and vegetation restoration schemes. In Scotland, and the wider UK, soft and hard engineering remediation and mitigation works are typically conducted by private contracting agencies and as such it is generally only the most high-profile sites that are widely known and publicised (e.g. the A83 Rest and Be Thankful). An important consideration in future models exists in determining where such initiatives are in place. In addition to clearly distinguishing the type of work as these can act to either: reduce the landslide risk, such as introducing landslide fencing and other hard barriers that act to block or divert debris from disrupting the network; and those that reduce the landslide hazard on a slope, such as by restoring vegetation and improving hillslope drainage to reduce the overall susceptibility of the slope to landslides.

8.4.2 Landslide impacts

In addition to ongoing research use, it is envisaged that the model may applied to wider, practical challenges in highway management. For this thesis, the road network disruption events were chosen using landslide susceptibility model's and by their combination with landslide thresholds to evaluate the landslide hazard on each road segment. Nonetheless, the results and the traffic model are applicable to any event (e.g. a flood, fallen tree or road traffic incident etc.) that causes a complete closure of a road. The model may therefore be used to evaluate the impact of a wide variety of road closure events, combinations of hazards and to evaluate specific scenarios. For instance, the modelling results may be used in workshops involving key stakeholders and where specific hazards and worst-case scenarios are played out. In a similar vein the model may be used to aid cost benefit analysis, for instance, by evaluating the impacts to traffic under different remediation time scenarios, analogous to disruption duration. Anecdotal evidence and communications with stakeholders in the Scottish Highland Council suggests that a prominent issue is the fact that most highway incident resources (e.g. traffic incident teams, emergency responders, and heavy lifting equipment etc.) are situated near to the urban centres Glasgow and Edinburgh, a minimum 6 hours' drive away from the West Highland roads. In this case the traffic model may be used to evaluate and compare impacts under < 6 hr and > 6 hr response time scenarios and to evaluate the benefits of more evenly distributed resources.

Effective application of the traffic model requires understanding of the model's design limitations and constraints. First, it is important to highlight that the model was designed to provide a representation of the annual average weekday morning commute traffic flow only. The rationale for this is that the commute period represents the densest regularly-repeating period of traffic on Scotland's roads – and so can be used to capture a large proportion of a disruptions impact. In addition, the model is constructed and calibrated with a view to evaluate disruptions on the strategic road network (Motorway, A and B roads) and therefore the traffic dynamics are simplified in dense urban areas away from most landslide prone regions. The absence of other road user groups is a limitation of the model and one that is highly influenced by regional traffic characteristics. For instance, in urban areas the traffic dynamics are likely to be heavily influenced by public transport (e.g. bus and metro systems). More notable is the absence of traffic in the model due to seasonal tourism and industry (Winter *et al.* 2014). In the West Highlands for example, there are several key industries that rely heavily on road haulage, such as agriculture and distilling, in addition to an increase in traffic during the spring-summer "auto-touring" tourism season. Whilst these trips are evident in the ATC data (i.e. vehicle class counts) and from other sources (e.g. depot locations, registered businesses, employment figures etc), converting these sparse data to usable origin-destination tables represents a significant extension to the current approach (see e.g. Ortuzar & Willumsen 2011). Second, it is important to understand the behaviour of the user-equilibrium route assignment procedure. User equilibrium can be interpreted as a best-case user response and is analogous to users having perfect knowledge of network conditions, therefore minimising impacts. Whilst this is increasingly the case due to modern in-car navigation systems there may be scenarios when the best alternative route is not known. Strategies to account for these effects include stochastic user-equilibrium (see 2.3 Quantifying Impact on Transport Infrastructure Networks).

8.4.3 Landslide thresholds

The thresholds are developed using two primary data sources: the NLD, and UK Met Office radar rainfall data. The same set of data quality checks and processes were applied to cleanse the NLD used for threshold classification. The landslide data is again subject to the same location bias with a large proportion of records situated near to the built environment. Use of the landslide thresholds developed in this study should therefore be constrained to slopes adjacent infrastructure networks only. Again, the NLD contains relatively few records for low magnitude landslides. These landslides may be initiated under a different set of conditions and at lower rainfall accumulations than is captured in the current thresholds. Therefore, and in a similar fashion to the hillslope susceptibility model, the thresholds likely underrepresent the potential for low magnitude landslides.

The thresholds are constructed using combinations of absolute and normalised variables for rainfall accumulation, intensity and duration calculated at varying antecedence periods. As described in section 3.3.1 Input data, the C-band radar sensor array used to capture these data are calibrated for intensities greater than 0.1 mm/hr^{-1}. Therefore, the water supplied by low intensity rainfall is likely to be undervalued in the rain variable time series generated at each landslide site and used in the threshold classification. Similarly, the radar may underestimate the rate of high intensity rainfall, particularly high intensity rainfall caused by localised orographic effects such as in mountainous areas. Therefore, the thresholds may also understate the water supplied to slopes during periods of high intensity rainfall. This is because the radar data value is the spatially averaged rainfall intensity within each radar cell. In addition, there

are uncertainties due to the 5.0 km^2 spatial resolution of the radar data. Investigations comparing UK Met Office radar data and that of similar systems in Italy note that higher intensities are observed using higher resolution 0.5 to 2.0 km^2 radar data (Cole & Moore 2008; Villarini & Krajewski 2008; Marra *et al.* 2017). However, in Scotland the geographic coverage of the higher resolution radar data extends only a short distance beyond the radars location and thus fails to capture most landslide observations in the NLD. It is envisaged that future investigation may alleviate these issues by using combinations of the different resolution radar data, improving radar coverage and in-situ observations from gauge networks.

8.4.4 A catastrophe model of landslide losses

A catastrophe model was developed that is based on the structure and logic of models used by insurers to evaluate catastrophe risk (Foote *et al.* 2017). It is stressed that this is purely exploratory work, demonstrating fundamental modelling principles and establishing a framework for further study only. The results are not recommended for practical application. First, the modelled rate of landslide occurrence adheres to the historic experience and observations in Scotland whereas future rates of occurrence may change. Estimating the short to long term rate of landslide occurrence is subject much uncertainty given the interactions and varying rates of weather, climate, land use and vegetation change (Dijkstra *et al.* 2016a). Second, the model does not account for factors that are known to influence the rate of landslide occurrence at certain locations. This includes consideration for engineered interventions at landslide prone sites, such as the A83 Rest and Be Thankful, and accounting for the conduit recharge rate or interval between successive failures on single hillslope.

8.5 Further work

The identified areas of further research fall into two categories: there are tasks related to applying the method, results and lessons learned in this research to operational situations, for example through collaborative partnerships and engaging stakeholders in hazard and infrastructure management; and there are tasks related to improving the techniques and the method developed and used in this thesis that could further improve the understanding of landslides and their interaction with infrastructure networks.

A future research and engagement partnership with Transport Scotland, and its road management partners including Bear Ltd and the Transport Research Laboratory, could lead to translation of the findings of this thesis to provide operational value. For instance, the strategies used to improve hazard mitigation, such as soft engineering schemes and responsive site investigations, may benefit from the models and maps produced that show the road segments with high landslide susceptibility (Figure 4.10) and where the cost and impact of disruption to these segments is severe (Figure 5.5). The landslide thresholds may also be applied to establish a hazard warning system (Figure 6.5), for example combining the thresholds with forecast meteorological data, and to trigger the dispatch of responsive landslide patrols or site investigations. The estimates for the annual average loss and aggregated exceedance probability of losses (Figure 7.2) may also support Transport Scotland where it is involved in budget planning and the assignment of financial resources for hazard and high management.

The study could also be extended to the evaluate the landslide hazard and risk of other infrastructures in Scotland, such as the rail and power distribution networks, and this could be achieved relatively rapidly. The methodological framework may also be applied to other regions or the whole UK, conducting independent hazard and impact modelling according to areas with similar landslide processes, slope materials and hydro-meteorological conditions. For instance, Cumbria provides a similar set conditions to those found in Scotland and could be used as a comparative case study. Whereas regions in South Wales and Gloucestershire feature a different suite hazards and physical processes, including road disruptions due to rotational landslides and subsidence by the shrink-swelling of soils, necessitating different hazard modelling methods such as physical-process based models. These case studies, and investigations of the other hazard phenomena capable of causing disruption to transportation such as flooding, would extended the existing methodological framework to one capable of examine multi-hazard impact and risk. This could be applied to explore how the severity and distribution of impacts varies when considering other hazard phenomena (e.g. flooding and severe wind storms), simultaneous network disruptions, and the inclusion of other network users and modes of transport.

Several improvements to the analysis techniques have been identified. Perhaps most importantly, the landslide susceptibility model and initiation thresholds could be further developed and refined by drawing on a larger body of landslide data, including more detailed and more abundant records past and future failures. Detailed site surveys can be used to obtain more information on historic failures (e.g. see Ballantyne *et al.* 2014), though these are costly and obtaining accurate timing information remains a challenge. The methods used to obtain and record landslide data are continually improving and continued cooperation between researchers, land owners, infrastructure operators and government bodies should maintain this trend (Pennington *et al.* 2015). In the landslide database obtained, landslides are represented by point data and these do not capture the conditions across the entire landslide footprint. This

is clearly a very simplistic representation and likely leads to over-generalisation of geological, geomorphological and meteorological characteristics that differ across the landslide source or initiation, flow, and deposition zones. To resolve this issue, future investigations may conduct detailed digitalisation of the landslide zones using aerial imagery and site survey information where this information is available (Pareschi *et al.* 2000; Guzzetti *et al.* 2012). This information was found to be of limited availability for the landslide records obtained in Scotland, and this therefore represents a potential improvement for the UK National Landslide Database.

For the landslide susceptibility model, the DEMs available were at 5 to 25 m^2 resolutions so terrain features may be smoothed out. Higher resolution terrain data such as LIDAR exists, but this was not made available for this research and there is a lack of geospatial software able process these data and at large scales. The geotechnical properties of the landslide slope materials were derived from a 1 km^2 soil parent material model (Lawley & Smith 2008). More detailed geotechnical data at each landslide site would be of benefit to better evaluate the parent material data limitations and uncertainties particularly for soil depth and grain size. Looking forward, a particular interest to investigate how the spatial distribution of the variables identified with increased landslide susceptibility may develop in response to medium and long term climatic change.

For the traffic impact model, the available traffic count and UK census origin-destination data enabled the development and calibration of a simulation for road commuters at peak flow conditions. To improve the impact assessments the model may therefore be extended to include: the other road user groups for which the same origin-destination data are available, such as public transport; private and commercial road users and their costs of travel, including travel made freight and that has higher cost of delay due to greater business interruption; other modes of transportation using the multi-modal simulation procedures in SUMO, such as rail; and extending the model period to 24 hours. These developments are largely dependent on the availability of suitable data and computational resources to develop and run the models. In the coming years, it is envisaged that such data sources will be increasingly available due to the rapid development of intelligent transport systems, vehicle telematics and autonomous transportation. Lastly, these assessments can be combined with those made using different approaches and for other aspects of the hazard impact to provide a more holistic approach, such as including the remediation costs due to the landslides direct physical damage. Other novel additions might include, assessments of the socio-economic impact of landslides, or the costs attributed to the loss of tourism, business investment and depreciating property prices and derived macro-economic models (Winter *et al.* 2014).

For the landslide initiation thresholds, the results of this study should be compared and evaluated to other techniques including, thresholds developed using physical-process based models or semi-empirical water balance models (Brooks *et al.* 2004; Clarke & Smethurst 2010). In addition, comparing the new thresholds derived using the radar precipitation data to those obtained using rain gauge networks, would limit the uncertainties related to the different data sampling techniques and provide a clearer picture of the rainfall conditions associated with landslide occurrence.

References

Abancó, C., Hürlimann, M., Moya, J. and Berenguer, M. (2016) Critical rainfall conditions for the initiation of torrential flows. Results from the Rebaixader catchment (Central Pyrenees). *Journal of Hydrology*. [Online] 541218–229. Available at: doi:10.1016/j.jhydrol.2016.01.019 (Accessed: 23 October 2016).

Addison, K. (1987) Debris flow during intense rainfall in Snowdonia, North Wales: A preliminary survey. *Earth Surface Processes and Landforms*. [Online] 12 (5), 561–566. Available at: doi:10.1002/esp.3290120513 (Accessed: 23 February 2017).

Agresti, A. (2002) *Categorical Data Analysis*. [Online]. Available at: doi:10.1198/tech.2003.s28 (Accessed: 3 July 2017).

Albert, R. and Barabási, A.-L. (2002) Statistical mechanics of complex networks. *Reviews of Modern Physics*. [Online] 74 (1), 47–97. Available at: doi:10.1103/RevModPhys.74.47 (Accessed: 27 June 2016).

Aleotti, P. (2004) A warning system for rainfall-induced shallow failures. *Engineering Geology*. [Online] 73 (3–4), 247–265. Available at: doi:10.1016/j.enggeo.2004.01.007 (Accessed: 7 March 2017).

Aleotti, P. and Chowdhury, R. (1999) Landslide hazard assessment: summary review and new perspectives. *Bulletin of Engineering Geology and the Environment*. [Online] 58 (1), 21–44. Available at: doi:10.1007/s100640050066 (Accessed: 6 January 2017).

Anderson, M.G. and Howes, S. (1988) Development and application of a combined soil water-slope stability model. *Quarterly Journal of Engineering Geology and Hydrogeology*. [Online] 18 (3), 225. Available at: doi:10.1144/GSL.QJEG.1985.018.03.04 (Accessed: 6 March 2017).

Van Asch, T.W.J., Buma, J. and Van Beek, L.P.H. (1999) A view on some hydrological triggering systems in landslides. *Geomorphology*. [Online] 30 (1–2), 25–32. Available at: doi:10.1016/S0169-555X(99)00042-2.

Austin, P.M. (1987) Relation between Measured Radar Reflectivity and Surface Rainfall *Monthly Weather Review*. [Online]. 115 (5) pp.1053–1070. Available at: doi:10.1175/1520-0493(1987)115<1053:RBMRRA>2.0.CO;2 (Accessed: 13 October 2016).

Ayalew, L. and Yamagishi, H. (2005) The application of GIS-based logistic regression for landslide susceptibility mapping in the Kakuda-Yahiko Mountains, Central Japan. *Geomorphology*. [Online] 65 (1–2), 15–31. Available at: doi:10.1016/j.geomorph.2004.06.010.

Ballantyne, C.K. (2002) Debris flow activity in the Scottish Highlands: temporal trends and wider implications for dating. *Studia Geomorphologica Carpatho-Balcanica*. 367–27.

Ballantyne, C.K. (1986) Landslides and slope failures in Scotland: A review. *Scottish Geographical Magazine*. [Online] 102 (3), 134–150. Available at: doi:10.1080/00369228618736667 (Accessed: 22 February 2017).

Ballantyne, C.K., Sandeman, G.F., Stone, J.O. and Wilson, P. (2014) Rock-slope failure following Late Pleistocene deglaciation on tectonically stable mountainous terrain. *Quaternary Science Reviews*. [Online] 86144–157. Available at: doi:10.1016/j.quascirev.2013.12.021.

Banks, N., Bayliss, D. and Glaister, S. (2007) *Motoring towards 2050: roads and reality: technical report*.

Bathurst, J.C., Burton, A. and Ward, T.J. (1997) Debris Flow Run-Out and Landslide Sediment Delivery Model Tests. *Journal of Hydraulic Engineering*. [Online] 123 (5), 410–419. Available at: doi:10.1061/(ASCE)0733-9429(1997)123:5(410) (Accessed: 9 March 2017).

BBC (2004) A9 route reopens after landslide [12/09/04]. *BBC news channel*. [Online] 12 August. Available at: http://news.bbc.co.uk/1/hi/scotland/3557190.stm.

Bell, M.G.. (2000) A game theory approach to measuring the performance reliability of transport networks. *Transportation Research Part B: Methodological*. [Online] 34 (6), 533–545. Available at: doi:10.1016/S0191-2615(99)00042-9 (Accessed: 28 March 2017).

Bell, M.G.. G.H., Kanturska, U., Schmocker, J.-D., Fonzone, A., Schmöcker, J.-D. and Fonzone, A. (2008) Attacker-defender models and road network vulnerability. *Philosophical Transactions of the Royal Society A: Mathematical, Physical and Engineering Sciences*. [Online] 366 (1872), 1893–1906. Available at: doi:10.1098/rsta.2008.0019 (Accessed: 28 March 2017).

Bell, M.G.H. and Iida, Y. (2003) *The Network Reliability of Transport: Proceedings of the 1st International Symposium on Transportation Network Reliability (INSTR)*. [Online]. Pergamon. Available at: http://books.google.co.jp/books?id=9MwT9S-0Q3gC (Accessed: 27 June 2016).

Berdica, K. (2002) An introduction to road vulnerability: What has been done, is done and should be done. *Transport Policy*. [Online] 9 (2), 117–127. Available at: doi:10.1016/S0967-070X(02)00011-2.

Berdica, K., Andjic, Z. and Nicholson, A.J. (2003) Simulating road traffic interruptions -- Does it matter what model we use? In: *The Network Reliability of Transport*. [Online]. 8 May 2003 Emerald Group Publishing Limited. pp. 353–368. Available at: doi:10.1108/9781786359544-021 (Accessed: 31 March 2017).

Berdica, K. and Mattsson, L.. (2007) Vulnerability: A Mode-Based Case Study of the Road Network in Stockholm. In: *Critical Infrastructure: Reliability and Vulnerability*. [Online]. Berlin, Heidelberg, Springer Berlin Heidelberg. pp. 81–106. Available at: doi:10.1007/978-3-540-68056-7_5 (Accessed: 2 April 2017).

Berenguer, M., Sempere-Torres, D. and Hürlimann, M. (2015) Debris-flow forecasting at regional scale by combining susceptibility mapping and radar rainfall. *Natural Hazards and Earth System Sciences*. [Online] 15 (3), 587–602. Available at: doi:10.5194/nhess-15-587-2015 (Accessed: 15 November 2016).

Berti, M., Martina, M.L. V., Franceschini, S., Pignone, S., Simoni, A. and Pizziolo, M. (2012) Probabilistic rainfall thresholds for landslide occurrence using a Bayesian approach. *Journal of Geophysical Research: Earth Surface*. [Online] 117 (4). Available at: doi:10.1029/2012JF002367 (Accessed: 3 November 2016).

Beser, M. and Algers, S. (2002) SAMPERS—The new Swedish national travel demand forecasting tool. *National Transport Models*. [Online] 101–118. Available at: doi:10.1007/978-3-662-04853-5_9 (Accessed: 31 March 2017).

Beven, K. (2002) Towards a coherent philosophy for modelling the environment. *Proceedings of the Royal Society A: Mathematical, Physical and Engineering Sciences*. [Online] 458 (2026), 2465–2484. Available at: doi:10.1098/rspa.2002.0986 (Accessed: 6 March 2017).

BGS (2017) *How does BGS classify landslides? [Webpage]*. [Online]. 2017. British Geological Survey. Available at: http://www.bgs.ac.uk/landslides/how_does_BGS_classify_landslides.html (Accessed: 13 February 2017).

Blahut, J., van Westen, C.J. and Sterlacchini, S. (2010) Analysis of landslide inventories for accurate prediction of debris-flow source areas. *Geomorphology*. [Online] 119 (1–2), 36–51. Available at: doi:10.1016/j.geomorph.2010.02.017 (Accessed: 14 March 2017).

Boarnet, M.G. (1996) Business Losses, Transportation Damage and the Northridge Earthquake. *University o*. [Online] (341), 29. Available at: https://escholarship.org/uc/item/80w9g0rd.pdf (Accessed: 25 March 2017).

Bonham-Carter, G.E. and Cox, S.J.D. (1995) Geographic information systems for geoscientists: Modelling with GIS. *Economic Geology and the Bulletin of the Society of Economic Geologists*. 90 (5), 1352–1353.

Booth, K., Diaz Doce, D., Harrison, M. and Wildman, G. (2010) *User Guide for the British Geological Survey GeoSure dataset* [Online]. Available at: http://nora.nerc.ac.uk/511063/1/OR14012.pdf (Accessed: 29 June 2016).

Borga, M., Stoffel, M., Marchi, L., Marra, F. and Jakob, M. (2014) Hydrogeomorphic response to extreme rainfall in headwater systems: Flash floods and debris flows. *Journal of Hydrology*. [Online] 518 (PB), 194–205. Available at: doi:10.1016/j.jhydrol.2014.05.022.

Bourne, N., Gillan, W., Notley, S.O., Taylor, N. and Webster, D. (2008) *A review of literature on the nature of the impact of roadworks on traffic movement and delay. [Public report PPR348]* [Online]. Available at: https://trl.co.uk/reports/PPR348.

Bovis, M.J. and Dagg, B.R. (1992) Debris flow triggering by impulsive loading: mechanical modelling and case studies. *Canadian Geotechnical Journal*. [Online] 29345–352. Available at: doi:10.1139/t92-040 (Accessed: 24 February 2017).

Bovis, M.J. and Jakob, M. (1999) The role of debris supply conditions in predicting debris flow activity. *Earth Surface Processes and Landforms*. [Online] 24 (11), 1039–1054. Available at: doi:10.1002/(SICI)1096-9837(199910)24:11<1039::AID-ESP29>3.0.CO;2-U (Accessed: 15 November 2016).

Brabb, E.E. (1984) Innovative approaches to landslide hazard and risk mapping. In: *Proceedings of the 4th International Symposium of Landslides*. 1984 Toronto, Canada. pp. 307–324.

Bradley, A.P. (1997) The use of the area under the ROC curve in the evaluation of machine learning algorithms. *Pattern Recognition*. [Online] 30 (7), 1145–1159. Available at: doi:10.1016/S0031-3203(96)00142-2.

Brenning, A. (2005) Spatial prediction models for landslide hazards: review, comparison and evaluation. *Natural Hazards and Earth System Sciences*. [Online] 5 (6), 853–862. Available at: doi:10.5194/nhess-5-853-2005 (Accessed: 15 March 2017).

Brockfeld, E., Kühne, R., Skabardonis, A. and Wagner, P. (2003) Toward Benchmarking of Microscopic Traffic Flow Models. *Transportation Research Record*. [Online] 1852 (250), 124–129. Available at: doi:10.3141/1852-16 (Accessed: 2 December 2016).

Brooks, S.M., Crozier, M.J., Glade, T. and Anderson, M.G. (2004) Towards establishing climatic thresholds for slope instability: Use of a physically-based combined soil hydrology-

slope stability model. *Pure and Applied Geophysics*. [Online] 161 (4), 881–905. Available at: doi:10.1007/s00024-003-2477-y (Accessed: 20 February 2017).

Brunetti, M.T., Peruccacci, S., Rossi, M., Luciani, S., Valigi, D. and Guzzetti, F. (2010) Rainfall thresholds for the possible occurrence of landslides in Italy. *Natural Hazards and Earth System Science*. [Online] 10 (3), 447–458. Available at: doi:10.5194/nhess-10-447-2010 (Accessed: 19 September 2016).

Budimir, M.E.A., Atkinson, P.M. and Lewis, H.G. (2015) A systematic review of landslide probability mapping using logistic regression *Landslides*. [Online]. 12 (3) pp.419–436. Available at: doi:10.1007/s10346-014-0550-5 (Accessed: 16 November 2016).

Burgholzer, W., Bauer, G., Posset, M. and Jammernegg, W. (2013) Analysing the impact of disruptions in intermodal transport networks: A micro simulation-based model. In: *Decision Support Systems*. [Online]. March 2013 pp. 1580–1586. Available at: doi:10.1016/j.dss.2012.05.060 (Accessed: 1 April 2017).

Burghout, W., Koutsopoulos, H.N. and Andreasson, I. (2006) A Discrete-Event Mesoscopic Traffic Simulation Model for Hybrid Traffic simulation. *Proceedings of the IEEE Intelligent Transportation Systems Conference (ITSC)*. [Online] 1102–1107. Available at: doi:10.1109/ITSC.2006.1707369 (Accessed: 5 July 2016).

Burns, L.D. (2013) A vision of our transport future. *Nature*. [Online] 497 (7448), 181–182. Available at: doi:10.1038/497181a (Accessed: 1 March 2017).

Burton, K.J. (2010) *Transport economics*. 3rd edition. Elgar.

Butcher, L. (2016) *Local road maintenance, repairs and street works in England* [Online]. Available at: http://researchbriefings.parliament.uk/ResearchBriefing/Summary/SN00739 (Accessed: 27 February 2017).

Caine, N. (1980) The Rainfall Intensity: Duration Control of Shallow Landslides and Debris Flows. *Geografiska Annaler. Series A, Physical Geography*. [Online] 62 (1/2), 23–27. Available at: doi:10.2307/520449 (Accessed: 17 August 2016).

Can, T., Nefeslioglu, H.A., Gokceoglu, C., Sonmez, H. and Duman, T.Y. (2005) Susceptibility assessments of shallow earthflows triggered by heavy rainfall at three catchments by logistic regression analyses. *Geomorphology*. [Online] 72 (1–4), 250–271. Available at: doi:10.1016/j.geomorph.2005.05.011 (Accessed: 23 May 2017).

Cannon, S.H. and Ellen, S.D. (1985) Rainfall conditions for abundant debris avalanches, San Francisco Bay region, California. *California Geology*. [Online] 38 (12), 267–272. Available at: papers2://publication/uuid/232AA03A-A6E3-4D27-A66C-0DA0A8D7A407 (Accessed: 3 October 2016).

Cannon, S.H., Gartner, J.E., Wilson, R.C., Bowers, J.C. and Laber, J.L. (2008) Storm rainfall conditions for floods and debris flows from recently burned areas in southwestern Colorado and southern California. *Geomorphology*. [Online] 96 (3–4), 250–269. Available at: doi:10.1016/j.geomorph.2007.03.019.

Cardinali, M., Reichenbach, P., Guzzetti, F., Ardizzone, F., Antonini, G., Galli, M., Cacciano, M., Castellani, M. and Salvati, P. (2002) A geomorphological approach to the estimation of landslide hazards and risks in Umbria, Central Italy. *Natural Hazards and Earth System Sciences*. [Online] 2 (1–2), 57–72. Available at: doi:10.5194/nhess-2-57-2002 (Accessed: 14 March 2017).

Carrara, A., Cardinali, M., Guzzetti, F. and Reichenbach, P. (1995) Gis Technology in Mapping Landslide Hazard. In: Alberto Carrara and Fausto Guzzetti (eds.). *Geographical Information Systems in Assessing Natural Hazards*. [Online]. Dordrecht, Springer Netherlands. pp. 135–175. Available at: doi:10.1007/978-94-015-8404-3_8 (Accessed: 9 March 2017).

Carrara, A., Guzzetti, F., Cardinali, M. and Reichenbach, P. (2000) Use of GIS Technology in the Prediction and Monitoring of Landslide Hazard. *Natural Hazards*. [Online] 20 (2/3), 117–135. Available at: doi:10.1023/A:1008097111310 (Accessed: 6 March 2017).

Carrara, A. and Pike, R.J. (2008) GIS technology and models for assessing landslide hazard and risk *Geomorphology*. [Online]. 94 (3–4) pp.257–260. Available at: doi:10.1016/j.geomorph.2006.07.042 (Accessed: 19 August 2016).

Carvalho, L.F., Fernandes, G., De Assis, M.V.O., Rodrigues, J.J.P.C. and Lemes Proença, M. (2014) Digital signature of network segment for healthcare environments support *Irbm*. [Online]. 35 (6). Available at: doi:10.1016/j.patrec.2005.10.010.

Cascetta, E. (2001) *Transportation Systems Engineering: Theory and Methods*. Applied Optimization. [Online]. Boston, MA, Springer US. Available at: doi:10.1007/978-1-4757-6873-2 (Accessed: 27 June 2016).

Catani, F., Casagli, N., Ermini, L., Righini, G. and Menduni, G. (2005) Landslide hazard and risk mapping at catchment scale in the Arno River basin. *Landslides*. [Online] 2 (4), 329–342. Available at: doi:10.1007/s10346-005-0021-0 (Accessed: 13 March 2017).

Catani, F., Lagomarsino, D., Segoni, S. and Tofani, V. (2013) Landslide susceptibility estimation by random forests technique: Sensitivity and scaling issues. *Natural Hazards and Earth System Sciences*. [Online] 13 (11), 2815–2831. Available at: doi:10.5194/nhess-13-2815-2013 (Accessed: 13 March 2017).

Chang, K.T., Chiang, S.H. and Lei, F. (2008) Analysing the relationship between typhoon-triggered landslides and critical rainfall conditions. *Earth Surface Processes and Landforms*. [Online] 33 (8), 1261–1271. Available at: doi:10.1002/esp.1611 (Accessed: 18 March 2017).

Chang, S.E. and Nojima, N. (2001) Measuring post-disaster transportation system performance: The 1995 Kobe earthquake in comparative perspective. *Transportation Research Part A: Policy and Practice*. [Online] 35 (6), 475–494. Available at: doi:10.1016/S0965-8564(00)00003-3.

Chatterton, J., Viavattene, C., Morris, J., Penning-Rowsell, E. and Tapsell, S. (2011) *The costs of the summer 2007 floods in England [Public report SC070039/R1]* [Online]. Available at: doi:978-1-84911-146-1.

Chau, K.T. and Chan, J.E. (2005) Regional bias of landslide data in generating susceptibility maps using logistic regression: Case of Hong Kong Island. *Landslides*. [Online] 2 (4), 280–290. Available at: doi:10.1007/s10346-005-0024-x (Accessed: 8 June 2017).

Chen, A., Yang, C., Kongsomsaksakul, S. and Lee, M. (2007) Network-based acessibility measures for vulnerability analysis of degradable transportation networks. *Networks and Spatial Economics*. [Online] 7 (3), 241–256. Available at: doi:10.1007/s11067-006-9012-5 (Accessed: 27 June 2016).

Chen, H. and Lee, C.F. (2003) A dynamic model for rainfall-induced landslides on natural slopes. *Geomorphology*. [Online] 51 (4), 269–288. Available at: doi:10.1016/S0169-555X(02)00224-6 (Accessed: 9 March 2017).

Chen, L. and Miller-Hooks, E. (2012) Resilience: An Indicator of Recovery Capability in Intermodal Freight Transport. *Transportation Science*. [Online] 46 (1), 109–123. Available at: doi:10.1287/trsc.1110.0376 (Accessed: 27 March 2017).

Chen, W., Xie, X., Wang, J., Pradhan, B., Hong, H., Bui, D.T., Duan, Z. and Ma, J. (2017) A comparative study of logistic model tree, random forest, and classification and regression tree models for spatial prediction of landslide susceptibility. *CATENA*. [Online] 151147–160. Available at: doi:10.1016/j.catena.2016.11.032 (Accessed: 6 January 2017).

Chevalier, G.G., Medina, V., Hürlimann, M. and Bateman, A. (2013) Debris-flow susceptibility analysis using fluvio-morphological parameters and data mining: Application to the Central-Eastern Pyrenees. *Natural Hazards*. [Online] 67 (2), 213–238. Available at: doi:10.1007/s11069-013-0568-3 (Accessed: 15 November 2016).

Chiaro, G., Kiyota, T., Pokhrel, R.M., Goda, K., Katagiri, T. and Sharma, K. (2015) Reconnaissance report on geotechnical and structural damage caused by the 2015 Gorkha Earthquake, Nepal. *Soils and Foundations*. [Online] 55 (5), 1030–1043. Available at: doi:10.1016/j.sandf.2015.09.006.

Chleborad, A.F. (2000) Preliminary Method for Anticipating the Occurrence of Precipitation-Induced Landslides in Seattle, Washington. *U.S. Geological Survey Open file report 2000-469*. [Online] Open file29. Available at: doi:Open-File Report, vol. 00-469 (Accessed: 18 March 2017).

Chleborad, A.F., Baum, R.L., Godt, J.W. and Powers, P.S. (2008) A prototype system for forecasting landslides in the Seattle, Washington, area. *Reviews in Engineering Geology*. [Online] 20 (0), 103–120. Available at: doi:10.1130/2008.4020(06) (Accessed: 26 September 2016).

Chleborad, A.F., Baum, R.L., Godt, J.W. and Report, U.S.G.S.O. (2006) Rainfall Thresholds for Forecasting Landslides in the Seattle , Washington , Area — Exceedance and Probability. *U.S. Geological Survey Open file report 2006-1064*. [Online] 35 pages. Available at: doi:Open-File Report 2006–1064.

Cho, Y.H., Lee, G.W., Kim, K.E. and Zawadzki, I. (2006) Identification and removal of ground echoes and anomalous propagation using the characteristics of radar echoes. *Journal of Atmospheric and Oceanic Technology*. [Online] 23 (9), 1206–1222. Available at: doi:10.1175/JTECH1913.1 (Accessed: 18 May 2017).

Chung, C.-J.F., Fabbri, A.G. and others (1999) Probabilistic prediction models for landslide hazard mapping. *Photogrammetric engineering and remote sensing*. 65 (12), 1389–1399.

Clark, S. and Watling, D. (2005) Modelling network travel time reliability under stochastic demand *Transportation Research Part B: Methodological*. [Online]. 39 (2) pp.119–140. Available at: doi:10.1016/j.trb.2003.10.006 (Accessed: 27 March 2017).

Clark, W.A. V. and Hosking, P.L. (1986) *Statistical Methods for Geographers*. [Online]. Wiley. Available at: http://www.amazon.com/Statistical-Methods-Geographers-W-Clark/dp/0471818070 (Accessed: 25 May 2017).

Clarke, D. and Smethurst, J.A. (2010) Effects of climate change on cycles of wetting and drying in engineered clay slopes in England. *Quarterly Journal of Engineering Geology and Hydrogeology*. [Online] 43 (4), 473–486. Available at: doi:10.1144/1470-9236/08-106 (Accessed: 17 February 2017).

Cole, S.J. and Moore, R.J. (2008) Hydrological modelling using raingauge- and radar-based estimators of areal rainfall. *Journal of Hydrology*. [Online] 358 (3–4), 159–181. Available at: doi:10.1016/j.jhydrol.2008.05.025.

Cook, A. (2011) *A fresh start for the Strategic Road Network: Managing our roads better to drive economic growth, boost innovation and give road users more for their money*. [Online] (November), 91. Available at: https://www.gov.uk/government/uploads/system/uploads/attachment_data/file/4378/strategic-road-network.pdf (Accessed: 27 June 2016).

Crovelli, R.A. (2000) *Probability Models for Estimation of Number and Costs of Landslides* [Online]. Available at: http://citeseerx.ist.psu.edu/viewdoc/download?doi=10.1.1.593.5564&rep=rep1&type=pdf (Accessed: 21 March 2017).

Crozier, M.J. (1997) The climate-landslide couple: a Southern Hemisphere perspective. *Rapid mass movement as a source of climatic evidence for the Holocene. Stuttgart: Fischer*. 333–354.

Cruden, D.M. (1991) A simple definition of a landslide. *Bulletin of the International Association of Engineering Geology - Bulletin de l'Association Internationale de G??ologie de l'Ing??nieur*. [Online] 43 (1), 27–29. Available at: doi:10.1007/BF02590167 (Accessed: 13 February 2017).

Cruden, D.M. and Varnes, D.J. (1996) Landslide types and processes. In Special Report 247: Landslides: Investigation and Mitigation. *Transportation Research Board, Washington D.C*. (247).

Culshaw, M.G. and Harrison, M. (2010) Geo-information systems for use by the UK insurance industry for 'subsidence'risk. In: *Geologically active.'Proceedings of the 11th Congress of the International Association for Engineering Geology and the Environment, Auckland, New Zealand*. 2010 pp. 1043–1051.

D'Este, G.M. and Taylor, M.A.P. (2001) Modelling network vulnerability at the level of the national strategic transport network. *ournal of the Eastern Asia Society for Transportation Studies*. 4 (2), 1–14.

Dadson, S.J., Hovius, N., Chen, H., Dade, W.B., Lin, J.C., Hsu, M.L., Lin, C.W., Horng, M.J., Chen, T.C., Milliman, J. and Stark, C.P. (2004) Earthquake-triggered increase in sediment delivery from an active mountain belt. *Geology*. [Online] 32 (8), 733–736. Available at: doi:10.1130/G20639.1.

Dai, F.C. and Lee, C.F. (2001) Terrain-based mapping of landslide susceptibility using a geographical information system: a case study. *Canadian Geotechnical Journal*. [Online] 38 (5), 911–923. Available at: doi:10.1139/cgj-38-5-911 (Accessed: 9 February 2017).

Dai, F.C., Lee, C.F., Li, J. and Xu, Z.W. (2001) Assessment of landslide susceptibility on the natural terrain of Lantau Island, Hong Kong. *Environmental Geology*. [Online] 40 (3), 381–391. Available at: doi:10.1007/s002540000163 (Accessed: 3 July 2017).

Dai, F.C., Lee, C.F. and Ngai, Y.Y. (2002) Landslide risk assessment and management: An overview. *Engineering Geology*. [Online] 64 (1), 65–87. Available at: doi:10.1016/S0013-7952(01)00093-X (Accessed: 21 March 2017).

Dalziell, E. and Nicholson, A. (2001) Risk and impact of natural hazards on a road network.

Journal of transportation engineering. [Online] 127 (April), 159–166. Available at: doi:10.1061/(ASCE)0733-947X(2001)127:2(159) (Accessed: 27 June 2016).

Davies, O., Rouainia, M., Glendinning, S. and Birkinshaw, S.J. (2008) Assessing the Influence of Climate Change on t he Progressive Failure of a Railway Embankment. *Young*. [Online] (JANUARY), 1–6. Available at: https://www.researchgate.net/profile/M_Rouainia/publication/238100169_Assessing_The_Influence_Of_Climate_Change_On_The_Progressive_Failure_Of_A_Railway_Embankment/links/00b7d52bb1e927b4d0000000.pdf (Accessed: 7 March 2017).

Davies, O., Rouainia, M., Glendinning, S., Cash, M. and Trento, V. (2014) Investigation of a pore pressure driven slope failure using a coupled hydro-mechanical model. *Engineering Geology*. [Online] 17870–81. Available at: doi:10.1016/j.enggeo.2014.05.012.

Dawson, D., Shaw, J. and Gehrels, R. (2016a) Sea-level rise impacts on transport infrastructure: The notorious case of the coastal railway line at Dawlish, England. *Journal of Transport Geography*. [Online] 5197–109. Available at: doi:10.1016/j.jtrangeo.2015.11.009.

Dawson, R., Thompson, D., Johns, D., Gosling, S., Chapman, L., Darch, G., Watson, G., Powrie, W., Bell, S., Paulson, K., Hughes, P. and Wood, R. (2016b) *UK Climate Change Risk Assessment Evidence Report: Chapter 4, Infrastructure.* [Online]. Available at: https://www.theccc.org.uk/uk-climate-change-risk-assessment-2017/.

Dawson, R.J., Peppe, R. and Wang, M. (2011) An agent-based model for risk-based flood incident management. *Natural Hazards*. [Online] 59 (1), 167–189. Available at: doi:10.1007/s11069-011-9745-4 (Accessed: 29 June 2016).

Demirel, H., Kompil, M. and Nemry, F. (2015) A framework to analyze the vulnerability of European road networks due to Sea-Level Rise (SLR) and sea storm surges. *Transportation Research Part A: Policy and Practice*. [Online] 8162–76. Available at: doi:10.1016/j.tra.2015.05.002 (Accessed: 27 June 2016).

Demšar, U., Špatenková, O. and Virrantaus, K. (2008) Identifying critical locations in a spatial network with graph theory. *Transactions in GIS*. [Online] 12 (1), 61–82. Available at: doi:10.1111/j.1467-9671.2008.01086.x (Accessed: 30 March 2017).

DFT (2013a) *Action for roads: a network for the 21st century* [Online]. Available at: https://www.gov.uk/government/publications/action-for-roads-a-network-for-the-21st-century.

DFT (2012) *Department for transport business plan 2012 - 2015*. [Online]. 2012. Available at: https://www.gov.uk/government/uploads/system/uploads/attachment_data/file/3367/dft-2012-business-plan.pdf.

DFT (2006) *Design manual for roads and bridges (DMRB): volume 14: economic assessment of road maintenance—QUADRO4 user manual* [Online]. Available at: http://webarchive.nationalarchives.gov.uk/20120925153031/http:/www.dft.gov.uk/publications/quadro-4-manual/.

DFT (1999) *Design Manual for Roads and Bridges Part 3, TA 79/99 Traffic Capacity of Urban Roads*. [Online]. 1999. Available at: http://www.standardsforhighways.co.uk/ha/standards/dmrb/ (Accessed: 1 April 2017).

DFT (2015a) *Reliability of journeys on Highways Agency roads: England: January to March 2015*. [Online]. 2015. Road congestion and travel times. Available at:

https://www.gov.uk/government/statistics/reliability-of-journeys-on-highways-agency-roads-england-january-to-march-2015 (Accessed: 23 March 2017).

DFT (2013b) *Road network size and condition*. [Online]. 2013. Available at: https://www.gov.uk/government/statistical-data-sets/rdl02-road-lengths-kms (Accessed: 23 March 2016).

DFT (2015b) *Road Traffic Forecasts 2015*. [Online] 73. Available at: https://www.gov.uk/government/publications/road-traffic-forecasts-2015 (Accessed: 23 March 2017).

DFT (2014a) *Transport analysis guidance: WebTAG*. [Online]. 2014. Available at: https://www.gov.uk/guidance/transport-analysis-guidance-webtag.

DFT (2014b) *Transport Resilience Review: A review of the resilience of the transport network to extreme weather events* [Online]. Available at: https://www.gov.uk/government/uploads/system/uploads/attachment_data/file/335115/transport-resilience-review-web.pdf.

Dijkstra, E.W. (1959) A note on two problems in connexion with graphs. *Numerische Mathematik*. [Online] 1 (1), 269–271. Available at: doi:10.1007/BF01386390 (Accessed: 30 March 2017).

Dijkstra, T.A. and Dixon, N. (2010) Climate change and slope stability in the UK: challenges and approaches. *Quarterly Journal of Engineering Geology and Hydrogeology*. [Online] 43 (4), 371–385. Available at: doi:10.1144/1470-9236/09-036 (Accessed: 27 June 2016).

Dijkstra, T.A., Dixon, N., Crosby, C., Frost, M., Gunn, D., Fleming, P. and Wilks, J. (2014a) Forecasting infrastructure resilience to climate change. *Proceedings of the Institution of Civil Engineers: Transport*. [Online] 167 (5), 269–280. Available at: doi:10.1680/tran.13.00089 (Accessed: 27 June 2016).

Dijkstra, T.A., Jenkins, G.O., Freeborough, K., Parry, S., Wathall, S. and Ward, E. (2014b) *Landslide domain statistics and impact libraries; a report on GO-Science funded activity 2014-2015 [Open Report OR/15/049]*

Dijkstra, T.A., Jenkins, G.O., Gunn, D., Dashwood, C., Dankers, R., Dixon, N., Petley, D.N., Gibson, A. and Winter, M. (2016a) Landslides and climate change in the United Kingdom. In: Ken Ho, Suzanne Lacasse, and Luciano Picarelli (eds.). *Slope Safety Preparedness for Impact of Climate Change*. [Online]. Taylor & Francis Group, 6000 Broken Sound Parkway NW, Suite 300, Boca Raton, FL 33487-2742, CRC Press. pp. 437–478. Available at: doi:10.1201/9781315387789-15.

Dijkstra, T.A., Reeves, H., Freeborough, K., Dashwood, C., Pennington, C., Jordan, H., Hobbs, P., Richardson, J., Banks, V., Cole, S., Wells, S. and Moore, R. (2016b) *Landslides in Scotland - case studies, threshold models and early warning. British Geological Survey Commercial Report, CR/16/206*

Dixon, N. and Brook, E. (2007) Impact of predicted climate change on landslide reactivation: Case study of Mam Tor, UK. *Landslides*. [Online] 4 (2), 137–147. Available at: doi:10.1007/s10346-006-0071-y (Accessed: 10 January 2017).

Dixon, N., Dijkstra, T.A., Forster, A. and Connell, R. (2006) Climate change impact forecasting for slopes (CLIFFS) in the built environment. In: *Engineering Geology for Tomorrow's Cities: Proceedings, 10th International Association of Engineering Geology*

Congress. Geological Society, London. [Online]. 2006 pp. 1–8. Available at: http://iaeg2006.geolsoc.org.uk/cd/PAPERS/IAEG_528.PDF (Accessed: 14 February 2017).

Dixon, N., Dijkstra, T.A., Glendinning, S., Hughes, P.N., Hughes, D.A.B., Clarke, D., Smethurst, J., Powrie, W., Toll, D.G. and Mendes, A.C. (2008) *Climate change and slope stability - improving our forecasting capabilities*.

Domencich, T. and McFadden, D. (1975) *Urban Travel Demand: A Behavioral Analysis*. [Online]. Available at: https://trid.trb.org/view.aspx?id=48594 (Accessed: 25 May 2017).

Donat, M.G., Leckebusch, G.C., Wild, S. and Ulbrich, U. (2011) Future changes in European winter storm losses and extreme wind speeds inferred from GCM and RCM multi-model simulations. *Natural Hazards and Earth System Science*. [Online] 11 (5), 1351–1370. Available at: doi:10.5194/nhess-11-1351-2011 (Accessed: 27 June 2016).

Duan, Y. and Lu, F. (2014) Robustness of city road networks at different granularities. *Physica A: Statistical Mechanics and its Applications*. [Online] 41121–34. Available at: doi:10.1016/j.physa.2014.05.073 (Accessed: 29 March 2017).

Dueñas-Osorio, L. and Vemuru, S.M. (2009) Cascading failures in complex infrastructure systems. *Structural Safety*. [Online] 31 (2), 157–167. Available at: doi:10.1016/j.strusafe.2008.06.007.

Duncan, J.M. (1996) Soil slope stability analysis *Landslides, investigation and mitigation. US National Research Council. Transportation Research Board Special Report*. 247.

Early, K.R. and Jordant, P.G. (1985) Some landslipping encountered during construction of the A40 near Monmouth. *Quarterly Journal of Engineering Geology and Hydrogeology*. [Online] 18 (3), 207–224. Available at: doi:10.1144/GSL.QJEG.1985.018.03.03 (Accessed: 14 February 2017).

Eddington, R. (2006) *The Eddington Transport Study* [Online]. Available at: https://web.archive.org/web/20080324002356/http://www.dft.gov.uk/about/strategy/transportstrategy/eddingtonstudy/.

Ehlschlaeger, C. (1989) Using the AT Search Algorithm to Develop Hydrologic Models from Digital Elevation Data[r.watershed grass gis]. In: *Proceedings of International Geographic Information Systems (IGIS) Symposium*. [Online]. 1989 Baltimore. pp. 275–281. Available at: https://grass.osgeo.org/grass73/manuals/r.watershed.html#references.

El-Rashidy, R.A. and Grant-Muller, S.M. (2014) An assessment method for highway network vulnerability. *Journal of Transport Geography*. [Online] 3434–43. Available at: doi:10.1016/j.jtrangeo.2013.10.017.

Entwisle, D.C., Hobbs, P.R.N., Northmore, K.J., Skipper, J., Raines, M.R., Self, S.J., Ellison, R.A. and Jones, L.D. (2012) *Engineering Geology of British Rocks and Soils - Lambeth Group*. [Online] 323. Available at: http://nora.nerc.ac.uk/20421/ (Accessed: 17 February 2017).

Erath, A., Birdsall, J., Axhausen, K.W. and Hajdin, R. (2010) Vulnerability Assessment Methodology for Swiss Road Network. *Transportation Research Record: Journal of the Transportation Research Board*. [Online] 2137118–126. Available at: doi:10.3141/2137-13 (Accessed: 1 April 2017).

Ercanoglu, M., Gokceoglu, C. and Van Asch, T.W.J. (2004) Landslide susceptibility zoning north of Yenice (NW Turkey) by multivariate statistical techniques. *Natural Hazards*. [Online] 32 (1), 1–23. Available at: doi:10.1023/B:NHAZ.0000026786.85589.4a (Accessed: 10 March

2017).

Evans, A.W. (1994) Evaluating public transport and road safety measures. *Accident Analysis & Prevention*. [Online] 26 (4), 411–428. Available at: doi:10.1016/0001-4575(94)90033-7 (Accessed: 25 March 2017).

Fairman, J.G., Schultz, D.M., Kirshbaum, D.J., Gray, S.L. and Barrett, A.I. (2015) A radar-based rainfall climatology of Great Britain and Ireland. *Weather*. [Online] 70 (5), 153–158. Available at: doi:10.1002/wea.2486 (Accessed: 27 September 2016).

Fawcett, T. (2006) An introduction to ROC analysis. *Pattern Recognition Letters*. [Online] 27 (8), 861–874. Available at: doi:10.1016/j.patrec.2005.10.010.

Fell, R., Corominas, J., Bonnard, C., Cascini, L., Leroi, E. and Savage, W.Z. (2008) Guidelines for landslide susceptibility, hazard and risk zoning for land use planning. *Engineering Geology*. [Online] 102 (3–4), 85–98. Available at: doi:10.1016/j.enggeo.2008.03.022.

Flotterod, G., Chen, Y. and Nagel, K. (2012) Behavioral Calibration and Analysis of a Large-Scale Travel Microsimulation. *Networks and Spatial Economics*. [Online] 12 (4), 481–502. Available at: doi:10.1007/s11067-011-9164-9 (Accessed: 19 June 2017).

Flowerdew, R. and Feng, Z. (2005) *Scottish Neighbourhood Statistics: Intermediate Geography Background Information: Annex A: Methodology Report* [Online]. Available at: http://www.gov.scot/Publications/2005/02/20732/53084.

Foote, M., Hillier, J., Mitchell-Wallace, K. and Jones, M. (2017) *Natural catastrophe risk management and modelling*. [Online]. Oxford, UK, John Wiley & Sons, Ltd. Available at: doi:10.1002/9781118906057 (Accessed: 2 August 2017).

Forster, A. and Culshaw, M. (2004) Implications of climate change for hazardous ground conditions in the UK. *Geology Today*. [Online] 20 (2), 61–67. Available at: doi:10.1111/j.1365-2451.2004.00442.x (Accessed: 14 November 2016).

Forster, A., Culshaw, M., Wildman, G. and Harrison, M. (2006) Implications of climate change for urban areas in the UK from an engineering geological perspective. *IAEG2006 Paper Number 246, Geological Society of London*. [Online] (246), 1–6. Available at: http://www.academia.edu/download/44551016/Implications_of_climate_change_for_urban20160408-32600-1ma0xml.pdf (Accessed: 17 February 2017).

Foster, C., Gibson, A. and Wildman, G. (2008) The new National Landslide Database and Landslide Hazard Assessment of Great Britain. In: *First World Landslide Forum*. [Online]. 2008 Tokyo, Japan. pp. 203–206. Available at: http://nora.nerc.ac.uk/4694/1/CF_BGS_Tokyofinal.pdf (Accessed: 27 June 2016).

Francis, J.A. and Vavrus, S.J. (2012) Francis_2012_Evidence linking Arctic Amplification to Extreme Weather.pdf. *Geophysical Research Letters*. [Online] 39 (February), 1–6. Available at: doi:10.1029/2012GL051000 (Accessed: 2 March 2017).

Frattini, P., Crosta, G. and Carrara, A. (2010) Techniques for evaluating the performance of landslide susceptibility models. *Engineering Geology*. [Online] 111 (1–4), 62–72. Available at: doi:10.1016/j.enggeo.2009.12.004.

Frattini, P., Crosta, G. and Sosio, R. (2009) Approaches for defining thresholds and return periods for rainfall-triggered shallow landslides. *Hydrological Processes*. [Online] 23 (10), 1444–1460. Available at: doi:10.1002/hyp.7269 (Accessed: 23 September 2016).

Freeborough, K.A., Diaz Doce, D., Lethbridge, R., Jessamy, G., Dashwood, C., Pennington, C. and Reeves, H.J. (2016) Landslide Hazard Assessment for National Rail Network. *Procedia Engineering*. [Online] 143 (Ictg), 689–696. Available at: doi:10.1016/j.proeng.2016.06.104 (Accessed: 21 March 2017).

G.O. Jenkins, L.D.J. and A.D.G. (2006) Analysis of Hollin Hill landslide, Low Mouthorpe, New Yorkshire; Field Reconnaisance and proposed survey recommendations. *British Geological Survey Internal Report*. 12.

Galbraith, R.M., PRICE, D.J., Shackman, L. and others (2005) *Scottish road network climate change study*. Scottish Executive.

Gariano, S.L., Brunetti, M.T., Iovine, G., Melillo, M., Peruccacci, S., Terranova, O., Vennari, C. and Guzzetti, F. (2015) Calibration and validation of rainfall thresholds for shallow landslide forecasting in Sicily, southern Italy. *Geomorphology*. [Online] 228653–665. Available at: doi:10.1016/j.geomorph.2014.10.019.

Garrison, W. (1960) Connectivity of the Interstate Highway System. *Papers and Proceedings of the Regional Science Association*. [Online] 6 (1), 121–137. Available at: doi:10.1111/j.1435-5597.1960.tb01707.x (Accessed: 29 June 2016).

Gawron, C. (1998) An Iterative Algorithm to Determine the Dynamic User Equilibirium in A Traffic Simulation Model. *International Journal of Modern Physics C*. [Online] 9 (3), 393–407. Available at: doi:10.1142/S0129183198000303.

GCC and Amey Ltd (2014) *Gloucestershire County Council Highways Information Pack: West (Forest and Tewkesbury)* [Online]. Available at: http://www.gloucestershire.gov.uk/roads-parking-and-rights-of-way/major-schemes/highways-information-packs-hips/.

Giannecchini, R., Galanti, Y., D'Amato Avanzi, G. and Barsanti, M. (2016) Probabilistic rainfall thresholds for triggering debris flows in a human-modified landscape. *Geomorphology*. [Online] 25794–107. Available at: doi:10.1016/j.geomorph.2015.12.012.

Gibson, A.D., Culshaw, M.G., Dashwood, C. and Pennington, C.V.L. (2013) Landslide management in the UK-the problem of managing hazards in a 'low-risk' environment. *Landslides*. [Online] 10 (5), 599–610. Available at: doi:10.1007/s10346-012-0346-4 (Accessed: 27 June 2016).

Glade, T., Anderson, M. and Crozier, M.J. (2005) NULL. *Landslide Hazard and Risk*. [Online]. John Wiley & Sons. Available at: doi:10.2113/gseegeosci.13.1.80.

Glaister, S. and Graham, D. (2006) Proper pricing for transport infrastructure and the case of urban road congestion. *Urban Studies*. [Online] 43 (8), 1395–1418. Available at: doi:10.1080/00420980600776475 (Accessed: 23 March 2017).

Glendinning, S., Hughes, P.N., Hughes, D.A.B., Clarke, D., Smethurst, J., Powrie, W., Dixon, N., Dijkstra, T.A., Toll, D.G. and Mendes, J. (2008) *Biological and engineering impacts of climate on slopes – learning from full-scale*. 1553–1558.

Grandin, R., Vallée, M., Satriano, C., Lacassin, R., Klinger, Y., Simoes, M. and Bollinger, L. (2015) Rupture process of the Mw= 7.9 2015 Gorkha earthquake (Nepal): insights into Himalayan megathrust segmentation. *Geophysical Research Letters*. 42 (20), 8373–8382.

Green, D., Yu, D., Pattison, I., Wilby, R., Bosher, L., Patel, R., Thompson, P., Trowell, K., Draycon, J., Halse, M., Yang, L. and Ryley, T. (2017) City-scale accessibility of emergency responders operating during flood events. *Natural Hazards and Earth System Sciences*.

[Online] 17 (1), 1–16. Available at: doi:10.5194/nhess-17-1-2017 (Accessed: 7 February 2017).

Greenwood, J.R., Norris, J.E. and Wint, J. (2004) Assessing the contribution of vegetation to slope stability. In: *Proceedings of the ICE - Geotechnical Engineering*. [Online]. 2004 pp. 199–207. Available at: doi:10.1680/geng.2004.157.4.199 (Accessed: 13 February 2017).

Grossi, P. and Kunreuther, H. (2005) *Catastrophe Modeling: A New Approach to Managing Risk*. Catastrophe Modeling. Partricia Grossi and Howard Kunreuther (eds.). [Online]. Boston, Kluwer Academic Publishers. Available at: doi:10.1007/b100669 (Accessed: 22 November 2016).

Guidicini, G. and Iwasa, O.Y. (1977) Tentative correlation between rainfall and landslides in a humid tropical environment. *Bulletin of the International Association of Engineering Geology - Bulletin de l'Association Internationale de Géologie de l'Ingénieur*. [Online] 16 (1), 13–20. Available at: doi:10.1007/BF02591434 (Accessed: 16 March 2017).

Gunn, D.A., Chambers, J.E., Uhlemann, S., Wilkinson, P.B., Meldrum, P.I., Dijkstra, T.A., Haslam, E., Kirkham, M., Wragg, J., Holyoake, S., Hughes, P.N., Hen-Jones, R. and Glendinning, S. (2015) Moisture monitoring in clay embankments using electrical resistivity tomography. *Construction and Building Materials*. [Online] 9282–94. Available at: doi:10.1016/j.conbuildmat.2014.06.007.

Guzzetti, F. (1998) Hydrological triggers of diffused landsliding: Editorial *Environmental Geology*. [Online]. 35 (2–3) pp.79–80. Available at: doi:10.1007/s002540050294 (Accessed: 23 February 2017).

Guzzetti, F., Carrara, A., Cardinali, M. and Reichenbach, P. (1999) Landslide hazard evaluation: A review of current techniques and their application in a multi-scale study, Central Italy. In: *Geomorphology*. [Online]. December 1999 pp. 181–216. Available at: doi:10.1016/S0169-555X(99)00078-1 (Accessed: 6 March 2017).

Guzzetti, F., Mondini, A.C., Cardinali, M., Fiorucci, F., Santangelo, M. and Chang, K.T. (2012) Landslide inventory maps: New tools for an old problem *Earth-Science Reviews*. [Online]. 112 (1–2) pp.42–66. Available at: doi:10.1016/j.earscirev.2012.02.001 (Accessed: 8 June 2017).

Guzzetti, F., Peruccacci, S., Rossi, M. and Stark, C.P. (2007) Rainfall thresholds for the initiation of landslides in central and southern Europe. *Meteorology and Atmospheric Physics*. [Online] 98 (3–4), 239–267. Available at: doi:10.1007/s00703-007-0262-7 (Accessed: 21 September 2016).

Guzzetti, F., Peruccacci, S., Rossi, M. and Stark, C.P. (2008) The rainfall intensity-duration control of shallow landslides and debris flows: An update. *Landslides*. [Online] 5 (1), 3–17. Available at: doi:10.1007/s10346-007-0112-1 (Accessed: 19 August 2016).

Guzzetti, F., Reichenbach, P., Ardizzone, F., Cardinali, M. and Galli, M. (2006) Estimating the quality of landslide susceptibility models. *Geomorphology*. [Online] 81 (1–2), 166–184. Available at: doi:10.1016/j.geomorph.2006.04.007 (Accessed: 6 January 2017).

Guzzetti, F., Reichenbach, P., Cardinali, M., Galli, M. and Ardizzone, F. (2005) Probabilistic landslide hazard assessment at the basin scale. *Geomorphology*. [Online] 72 (1–4), 272–299. Available at: doi:10.1016/j.geomorph.2005.06.002 (Accessed: 9 March 2017).

Haimes, Y.Y. (2006) On the definition of vulnerabilities in measuring risks to infrastructures *Risk Analysis*. [Online]. 26 (2) pp.293–296. Available at: doi:10.1111/j.1539-

6924.2006.00755.x (Accessed: 25 March 2017).

Hand, D.J. (1997) NULL. *Construction and Sssessment of Classification Rules*. [Online]. Wiley. Available at: http://cds.cern.ch/record/324349 (Accessed: 15 March 2017).

Hansen, A. (1984) Landslide hazard analysis. In: D Brunsden and D.B Prior (eds.). *Slope Stability*. [Online]. New York, Wiley. pp. 532–602. Available at: https://trid.trb.org/view.aspx?id=267068 (Accessed: 10 March 2017).

Harrison, A.M., Plim, J.F.M., Harrison, M., Jones, L.D. and Culshaw, M.G. (2012) The relationship between shrink–swell occurrence and climate in south-east England. *Proceedings of the Geologists' Association*. [Online] 123 (4), 556–575. Available at: doi:10.1016/j.pgeola.2012.05.002 (Accessed: 13 July 2016).

Harrison, D., Driscoll, S.J. and Kitchen, M. (2000) Improving precipitation estimates from weather radar using quality control and correction techniques. *Meteorol. Appl.* [Online] 6 (2), 135–144. Available at: doi:10.1017/S1350482700001468 (Accessed: 30 September 2016).

Harrison, D.L., Kitchen, M. and Scovell, R.W. (2009) High-resolution precipitation estimates for hydrological uses. *Proceedings of the ICE - Water Management*. [Online] 162 (April 2009), 125–135. Available at: doi:10.1680/wama.2009.162.2.125 (Accessed: 27 September 2016).

HMEP (2012) *Guidance on the management of Highways Drainage Assets* [Online]. Available at: http://www.highwaysefficiency.org.uk/efficiency-resources/asset-management/guidance-on-the-management-of-highways.html.

Hodgson, J.M. (1997) *Soil Survey Field Handbook - Describing and Sampling Soil Profiles*. 3rd ed. [Online]. Silsoe Beds., Soil Survey of Great Britain (England and Wales). Available at: http://www.worldcat.org/title/soil-survey-field-handbook-describing-and-sampling-soil-profiles/oclc/123376160?referer=di&ht=edition (Accessed: 11 May 2017).

Hofierka, J., Mitásová, H. and Neteler, M. (2009) *Geomorphometry in GRASS GIS*. [Online]. Available at: doi:10.1016/S0166-2481(08)00017-2 (Accessed: 11 May 2017).

Holmgren, P. (1994) Multiple flow direction algorithms for runoff modelling in grid based elevation models: An empirical evaluation. *Hydrological Processes*. [Online] 8 (4), 327–334. Available at: doi:10.1002/hyp.3360080405 (Accessed: 13 May 2017).

Hong, Y., Alder, R. and Huffman, G. (2006) Evaluation of the potential of NASA multi-satellite precipitation analysis in global landslide hazard assessment. *Geophysical Research Letters*. [Online] 33 (22), L22402. Available at: doi:10.1029/2006GL028010 (Accessed: 31 October 2016).

Hooper, E., Chapman, L. and Quinn, A. (2014) The impact of precipitation on speed–flow relationships along a UK motorway corridor. *Theoretical and Applied Climatology*. [Online] 117 (1), 303–316. Available at: doi:10.1007/s00704-013-0999-5 (Accessed: 23 March 2017).

Horn, B.K.P. (1981) Hill Shading and the Reflectance Map. *Proceedings of the IEEE*. [Online] 69 (1), 14–47. Available at: doi:10.1109/PROC.1981.11918 (Accessed: 11 May 2017).

HSE (2014) *Avoiding danger from underground services: HSG47 (Third edition)*. [Online]. 2014. Available at: http://www.hse.gov.uk/pubns/books/hsg47.htm (Accessed: 27 February 2017).

Hughes, P.N., Glendinning, S., Mendes, J., Parkin, G., Toll, D.G., Gallipoli, D. and Miller, P.E. (2009) Full-scale testing to assess climate effects on embankments. *Proceedings of the*

Institution of Civil Engineers - Engineering Sustainability. [Online] 162 (2), 67–79. Available at: doi:10.1680/ensu.2009.162.2.67 (Accessed: 2 March 2017).

Hungr, O. (1987) An extension of Bishop's simplified method of slope stability analysis to three dimensions. *Géotechnique*. [Online] 37 (1), 113–117. Available at: doi:10.1680/geot.1987.37.1.113 (Accessed: 6 March 2017).

Hungr, O., Leroueil, S. and Picarelli, L. (2014) The Varnes classification of landslide types, an update. *Landslides*. [Online] 11 (2), 167–194. Available at: doi:10.1007/s10346-013-0436-y (Accessed: 13 February 2017).

Iida, Y. (1999) Basic concepts and future directions of road network reliability analysis. *Journal of Advanced Transportation*. [Online] 33 (2), 125–134. Available at: doi:10.1002/atr.5670330203 (Accessed: 27 March 2017).

Innes, J.L. (1983) Debris flows. *Progress in Physical Geography*. [Online] 7 (4), 469–501. Available at: doi:10.1177/030913338300700401 (Accessed: 3 October 2016).

IntermapTechnologies (2009) *NEXTMap British Digital Terrain (DTM) Model Data by Intermap* [Online]. Available at: http://catalogue.ceda.ac.uk/uuid/998a28d8a5ed4564863a0daa0f731e8d.

Issacharoff, L., Lämmer, S., Rosato, V. and Helbing, D. (2008) Critical infrastructures vulnerability: The highway networks. *Understanding Complex Systems*. [Online] 2008201–216. Available at: doi:10.1007/978-3-540-75261-5_9 (Accessed: 27 June 2016).

Iverson, R.M. (2000) Landslide triggering by rain infiltration. *Water Resources Research*. [Online] 36 (7), 1897. Available at: doi:10.1029/2000WR900090 (Accessed: 24 October 2016).

Iverson, R.M. (1997) The physics of debris flows. *Reviews of Geophysics*. [Online] 35 (3), 245. Available at: doi:10.1029/97RG00426 (Accessed: 17 August 2016).

Iverson, R.M., George, D.L., Allstadt, K., Reid, M.E., Collins, B.D., Vallance, J.W., Schilling, S.P., Godt, J.W., Cannon, C.M., Magirl, C.S., Baum, R.L., Coe, J.A., Schulz, W.H. and Bower, J.B. (2015) Landslide mobility and hazards: Implications of the 2014 Oso disaster. *Earth and Planetary Science Letters*. [Online] 412197–208. Available at: doi:10.1016/j.epsl.2014.12.020.

Iverson, R.M., Reid, M.E. and LaHusen, R.G. (1997) Debris-Flow Mobilization From Landslides 1. *Annual Review of Earth and Planetary Sciences*. [Online] 25 (1), 85–138. Available at: doi:10.1146/annurev.earth.25.1.85 (Accessed: 24 October 2016).

Jackson, I. (2004) Britain beneath our feet: an atlas of digital information on Britain's land quality, underground hazards, natural resources and geology. *BGS Occasional Publication*. 4.

Jackson, L.E., Kostaschuk, R.A. and MacDonald, G.M. (1987) Identification of debris flow hazard on alluvial fans in the Canadian Rocky Mountains. *Geol. Soc. Amer., Rev. eng. Geol.* [Online] 7 (NOVEMBER 1984), 115–124. Available at: doi:10.13140/2.1.2321.1206 (Accessed: 15 November 2016).

Jaedicke, C., Lied, K. and Kronholm, K. (2009) Integrated database for rapid mass movements in Norway. *Natural Hazards and Earth System Science*. [Online] 9 (2), 469–479. Available at: doi:10.5194/nhess-9-469-2009 (Accessed: 8 June 2017).

Jaiswal, P., van Westen, C.J. and Jetten, V. (2010) Quantitative landslide hazard assessment along a transportation corridor in southern India. *Engineering Geology*. [Online] 116 (3–4),

236–250. Available at: doi:10.1016/j.enggeo.2010.09.005 (Accessed: 23 May 2017).

Jakob, M. (2005) Debris-flow hazard analysis. *Debris-flow Hazards and Related Phenomena*. [Online] 411–443. Available at: doi:10.1007/3-540-27129-5_17 (Accessed: 23 February 2017).

Jakob, M., Bovis, M. and Oden, M. (2005) The significance of channel recharge rates for estimating debris-flow magnitude and frequency. *Earth Surface Processes and Landforms*. [Online] 30 (6), 755–766. Available at: doi:10.1002/esp.1188 (Accessed: 22 February 2017).

Jakob, M. and Weatherly, H. (2003) A hydroclimatic threshold for landslide initiation on the North Shore Mountains of Vancouver, British Columbia. *Geomorphology*. [Online] 54 (3–4), 137–156. Available at: doi:10.1016/S0169-555X(02)00339-2.

Jaroszweski, D., Chapman, L. and Petts, J. (2010) Assessing the potential impact of climate change on transportation: the need for an interdisciplinary approach. *Journal of Transport Geography*. [Online] 18 (2), 331–335. Available at: doi:10.1016/j.jtrangeo.2009.07.005 (Accessed: 27 June 2016).

Jaroszweski, D., Hooper, E., Baker, C., Chapman, L. and Quinn, A. (2015) The impacts of the 28 June 2012 storms on UK road and rail transport. *Meteorological Applications*. [Online] 22 (3), 470–476. Available at: doi:10.1002/met.1477 (Accessed: 27 February 2017).

Jenelius, E. (2009) Network structure and travel patterns: explaining the geographical disparities of road network vulnerability. *Journal of Transport Geography*. [Online] 17 (3), 234–244. Available at: doi:10.1016/j.jtrangeo.2008.06.002.

Jenelius, E. (2010) Redundancy importance: Links as rerouting alternatives during road network disruptions. In: *Procedia Engineering*. [Online]. 2010 Elsevier. pp. 129–137. Available at: doi:10.1016/j.proeng.2010.07.013 (Accessed: 27 June 2016).

Jenelius, E. and Mattsson, L.. (2012) Road network vulnerability analysis of area-covering disruptions: A grid-based approach with case study. *Transportation Research Part A: Policy and Practice*. [Online] 46 (5), 746–760. Available at: doi:10.1016/j.tra.2012.02.003.

Jenelius, E., Petersen, T. and Mattsson, L.. (2006a) Importance and exposure in road network vulnerability analysis. *Transportation Research Part A: Policy and Practice*. [Online] 40 (7), 537–560. Available at: doi:10.1016/j.tra.2005.11.003.

Jenelius, E., Petersen, T. and Mattsson, L.. (2006b) Road network vulnerability: Identifying important links and exposed regions. *Transportation Research A*. 40 (7), 537–560.

Jenkins, G.J., Murphy, J.M., Sexton, D.M.H., Lowe, J.A., Jones, P. and Kilsby, C.G. (2009) *UK Climate Projections: Briefing report*. [Online]. Met Office Hadley Centre. Available at: doi:ISBN 978-1-906360-04-7.

Jenkins, G.O., Foster, C. and Hopson, P.M. (2011) Geology as a control on landslides on the Isle of Wight: An overview. *Proceedings of the Geologists' Association*. [Online] 122 (5), 906–922. Available at: doi:10.1016/j.pgeola.2011.09.003 (Accessed: 20 February 2017).

Jenkinson, A.F. and Collison, F.P. (1977) An initial climatology of gales over the North Sea. *Synoptic Climatology Branch Memorandum*. 62Meteorological Office: Bracknell; 18 pp.

Jones, P., Jones, P., Harpham, C., Harpham, C., Kilsby, C., Kilsby, C., Glenis, V., Glenis, V., Burton, A. and Burton, A. (2009) *Projections of future daily climate for the UK from the Weather Generator*. [Online]. University of Newcastle. Available at:

http://ukclimateprojections.defra.gov.uk (Accessed: 1 March 2017).

Jones, P.D., Harpham, C. and Briffa, K.R. (2013) Lamb weather types derived from reanalysis products. *International Journal of Climatology*. [Online] 33 (5), 1129–1139. Available at: doi:10.1002/joc.3498 (Accessed: 16 September 2017).

Jordan, F. (2008) Predicting target selection by terrorists: A network analysis of the 2005 London underground attacks. *International journal of critical infrastructures*. 4 (1–2), 206–214.

Kaplan, S., Garrick, B.J., Kaplin, S. and Garrick, G.J. (1981) On the quantitative definition of risk. *Risk analysis*. [Online] 1 (1), 11–27. Available at: doi:10.1111/j.1539-6924.1981.tb01350.x (Accessed: 29 June 2016).

Kappes, M.S., Keiler, M., von Elverfeldt, K. and Glade, T. (2012) Challenges of analyzing multi-hazard risk: A review *Natural Hazards*. [Online]. 64 (2) pp.1925–1958. Available at: doi:10.1007/s11069-012-0294-2 (Accessed: 27 June 2016).

Keefer, D.K. (1984) Landslides caused by earthquakes. *Geological Society of America Bulletin*. [Online]. 95 (4) pp.406–421. Available at: doi:10.1130/0016-7606(1984)95<406:LCBE>2.0.CO.

Kendon, E., Roberts, N. and Fowler, H. (2014) Heavier summer downpours with climate change revealed by weather forecast resolution model. *Nature Climate Change*. [Online] 4 (June), 1–7. Available at: doi:10.1038/NCLIMATE2258 (Accessed: 3 March 2017).

Kendon, M. and McCarthy, M. (2015) The UK's wet and stormy winter of 2013/2014. *Weather*. [Online] 70 (2), 40–47. Available at: doi:10.1002/wea.2465 (Accessed: 27 June 2016).

Khademi, N., Balaei, B., Shahri, M., Mirzaei, M., Sarrafi, B., Zahabiun, M. and Mohaymany, A.S. (2015) Transportation network vulnerability analysis for the case of a catastrophic earthquake. *International Journal of Disaster Risk Reduction*. [Online] 12234–254. Available at: doi:10.1016/j.ijdrr.2015.01.009 (Accessed: 7 February 2017).

Kilsby, C., Glendinning, S., Hughes, P.N., Parkin, G. and Bransby, M.F. (2009) Climate-change impacts on long-term performance of slopes. *Proceedings of the Institution of Civil Engineers - Engineering Sustainability*. [Online] 162 (ES2), 59–66. Available at: doi:10.1680/ensu.2009.162.

Kim, S.K., Hong, W.P. and Kim, Y.M. (1991) Prediction of rainfall-triggered landslides in Korea. *Landslides*. 2989–994.

King, G. and Zeng, L. (2001) Logistic Regression in Rare Events Data. *Political analysis*. [Online] 9 (2), 137–163. Available at: doi:10.1162/00208180152507597 (Accessed: 23 May 2017).

Kinner, D., Mitasova, H., Harmon, R., Toma, L. and Stallard, R. (2005) GIS-based stream network analysis for the Chagres River Basin, Republic of Panama. *Chagres: A Multidisciplinary …*

Kirschbaum, D., Stanley, T. and Zhou, Y. (2015) Spatial and temporal analysis of a global landslide catalog. *Geomorphology*. [Online] 2494–15. Available at: doi:10.1016/j.geomorph.2015.03.016 (Accessed: 8 June 2017).

Kirschbaum, D.B., Adler, R., Hong, Y., Kumar, S., Peters-Lidard, C. and Lerner-Lam, A.

(2012) Advances in landslide nowcasting: Evaluation of a global and regional modeling approach. *Environmental Earth Sciences*. [Online] 66 (6), 1683–1696. Available at: doi:10.1007/s12665-011-0990-3 (Accessed: 31 May 2017).

Knoop, V., van Zuylen, H. and Hoogendoorn, S. (2008) The influence of spillback modelling when assessing consequences of blockings in a road network. *European Journal of Transport and Infrastructure Research*. [Online] 8 (4), 287–300. Available at: www.ejtir.tbm.tudelft.nl (Accessed: 27 June 2016).

Knoop, V.L., Hoogendoorn, S.P. and van Zuylen, H.J. (2007) Quantification of the Impact of Spillback Modeling in Assessing Network Reliability. In: *86th Annual Meeting of the Transportation Research Board*. 2007 p.

Knoop, V.L., Snelder, M., van Zuylen, H.J. and Hoogendoorn, S.P. (2012) Link-level vulnerability indicators for real-world networks. *Transportation Research Part A: Policy and Practice*. [Online] 46 (5), 843–854. Available at: doi:10.1016/j.tra.2012.02.004 (Accessed: 29 June 2016).

Koetse, M.J. and Rietveld, P. (2009) The impact of climate change and weather on transport: An overview of empirical findings. *Transportation Research Part D: Transport and Environment*. [Online] 14 (3), 205–221. Available at: doi:10.1016/j.trd.2008.12.004.

Konis, K.P. (2007) *Linear Programming Algorithms for Detecting Separated Data in Binary Logistic Regression Models*. [Online] Available at: https://ora.ox.ac.uk/objects/uuid:8f9ee0d0-d78e-4101-9ab4-f9cbceed2a2a (Accessed: 23 May 2017).

Korup, O. (2010) Earthquake-triggered landslides—spatial patterns and impacts. *COGEAR, Module 1a-Report*.

Korup, O. (2004) Landslide-induced river channel avulsions in mountain catchments of southwest New Zealand. *Geomorphology*. [Online] 63 (1–2), 57–80. Available at: doi:10.1016/j.geomorph.2004.03.005 (Accessed: 13 March 2017).

Kovacevic, N., Potts, D.M. and Vaughan, P.R. (2001) Progressive failure in clay embankments due to seasonal climate changes. In: *15th International conference on Soil Mechanics & Geotechnical Engineering*. 2001 pp. 2127–2130.

Kraan, M., Schereuder, M. and Tamminga, G. (2008) Vulnerability of a National Road Network. In: *Proceedings of the 87th Annual Meeting of the Transportation Research Board*. [Online]. 2008 p. Available at: https://trid.trb.org/view.aspx?id=848068 (Accessed: 1 April 2017).

Krajzewicz, D., Erdmann, J., Behrisch, M. and Bieker, L. (2012) Recent Development and Applications of {SUMO - Simulation of Urban MObility}. *International Journal On Advances in Systems and Measurements*. [Online] 5 (3), 128–138. Available at: http://citeseerx.ist.psu.edu/viewdoc/download?doi=10.1.1.303.4746&rep=rep1&type=pdf#page=48 (Accessed: 5 July 2016).

Kral, F., Fry, M. and Dixon, H. (2015) *Integrated Hydrological Units of the United Kingdom: Sections [dataset]* [Online]. Available at: doi:10.5285/a6e37e39-9e10-4647-a110-12d902403095.

Kraus, S., Wagner, P. and Gawron, C. (1997) Metastable States in a Microscopic Model of Traffic Flow. *Physical Review E*. [Online] 55 (304), 55–97. Available at: doi:10.1103/PhysRevE.55.5597 (Accessed: 16 June 2017).

Krebs (2017) *UK Climate Change Risk Assessment 2017 Synthesis report: priorities for the next five years* [Online]. Available at: https://www.theccc.org.uk/uk-climate-change-risk-assessment-2017/.

Kuhn, M. and Johnson, K. (2013a) Measuring Performance in Regression Models. In: *Applied Predictive Modeling*. [Online]. New York, NY, Springer New York. pp. 95–100. Available at: doi:10.1007/978-1-4614-6849-3_5 (Accessed: 24 May 2017).

Kuhn, M. and Johnson, K. (2013b) Remedies for Severe Class Imbalance. In: *Applied Predictive Modeling*. [Online]. New York, NY, Springer New York. pp. 419–443. Available at: doi:10.1007/978-1-4614-6849-3_16 (Accessed: 24 May 2017).

Lane, S.N., Tayefi, V., Reid, S.C., Yu, D. and Hardy, R.J. (2007) Interactions between sediment delivery, channel change, climate change and flood risk in a temperate upland environment. *Earth Surface Processes and Landforms*. [Online] 32 (3), 429–446. Available at: doi:10.1002/esp.1404 (Accessed: 2 March 2017).

Larsen, M.C. and Parks, J.E. (1997) How wide is a road? The association of roads and mass-wasting in a forested montane environment. *Earth Surface Processes and Landforms*. [Online] 22 (9), 835–848. Available at: doi:10.1002/(SICI)1096-9837(199709)22:9<835::AID-ESP782>3.0.CO;2-C (Accessed: 9 March 2017).

Lawley, R. and Smith, B. (2008) Digital soil mapping at a national scale: A knowledge and GIS based approach to improving parent material and property information. In: *Digital Soil Mapping with Limited Data*. [Online]. Dordrecht, Springer Netherlands. pp. 173–182. Available at: doi:10.1007/978-1-4020-8592-5_14 (Accessed: 11 April 2017).

Lee, E.M. and Jones, D.K.C. (2014) *Landslide Risk Assessment*. [Online] 454. Available at: doi:10.1680/lra.31715 (Accessed: 5 March 2017).

Lee, J.R., Booth, S.J., Hamblin, R.J.O., Jarrow, A.M., Kessler, H., Moorlock, B.S.P., Morigi, A.N., Palmer, A., Pawley, S.J., Riding, J.B. and Rose, J. (2004a) A new stratigraphy for the glacial deposits around Lowestoft, Great Yarmouth, North Walsham and Cromer, East Anglia, UK. *Bulletin of the geological Society of Norfolk*. 533–60.

Lee, S., Choi, J. and Woo, I. (2004b) The effect of spatial resolution on the accuracy of landslide susceptibility mapping: a case study in Boun, Korea. *Geosciences Journal*. [Online] 8 (1), 51–60. Available at: doi:10.1007/BF02910278 (Accessed: 13 March 2017).

Lees, B. (1996) Neural network applications in the geosciences: an introduction. *Computers & Geosciences*.

Leroueil, S. (2001) Natural slopes and cuts: movement and failure mechanisms. *Géotechnique*. [Online] 51 (3), 197–243. Available at: doi:10.1680/geot.2001.51.3.197 (Accessed: 13 February 2017).

Levinson, D. (2010) Equity Effects of Road Pricing: A Review. *Transport Reviews*. [Online] 30 (1), 33–57. Available at: doi:10.1080/01441640903189304 (Accessed: 23 March 2017).

Little, R.G. (2002) Controlling Cascading Failure: Understanding the Vulnerabilities of Interconnected Infrastructures. *Journal of Urban Technology*. [Online] 9 (1), 109–123. Available at: doi:10.1080/106307302317379855 (Accessed: 27 February 2017).

Lords Hansard (2013) *Ansford Railway Bridge*. [Online]. 2013. House of Commons Hansard . Available at: https://hansard.parliament.uk/Commons/2013-10-16/debates/13101682000002/AnsfordRailwayBridge (Accessed: 28 February 2017).

Lords Hansard (2007) *Roads: Motorway Lanes Closures. Lord Bassam of Brighton in answer to a question posed by Earl Attlee. 21 Nov 2007 : Column WA84*. [Online]. 2007. House of Commons Hansard. Available at: http://www.publications.parliament.uk/pa/ld200708/ldhansrd/text/71121w0004.htm.

Lorente, A., Beguería, S., Bathurst, J.C. and García-Ruiz, J.M. (2003) Debris flow characteristics and relationships in the Central Spanish Pyrenees. *Natural Hazards and Earth System Science*. [Online] 3683–691. Available at: doi:10.5194/nhess-3-683-2003.

Loveridge, F.A., Spink, T.W., O'Brien, A.S., Briggs, K.M. and Butcher, D. (2010) The impact of climate and climate change on infrastructure slopes, with particular reference to southern England. *Quarterly Journal of Engineering Geology and Hydrogeology*. [Online] 43 (4), 461–472. Available at: doi:10.1144/1470-9236/09-050 (Accessed: 27 February 2017).

Lu, N. and Godt, J.W. (2013) *Hillslope, Hydrology and Stability*. [Online] 435. Available at: doi:10.1017/CBO9781139108164.

Lu, Q.-C. and Peng, Z.-R. (2011) Vulnerability Analysis of Transportation Network Under Scenarios of Sea Level Rise. *Transportation Research Record: Journal of the Transportation Research Board*. [Online] 2263 (1), 174–181. Available at: doi:10.3141/2263-19 (Accessed: 2 April 2017).

Lucia, S., Andersson, J.A.E., Brandt, H., Diehl, M. and Engell, S. (2014) Handling uncertainty in economic nonlinear model predictive control: A comparative case study. *Journal of Process Control*. [Online] 24 (8), 1247–1259. Available at: doi:10.1016/j.jprocont.2014.05.008.

MacLeod, A., Hofmeister, R.J., Wang, Y. and Burns, S. (2005) Landslide indirect losses: methods and case studies from Oregon. *Open File Report O-05-X. Oregon Department of Geology and Mineral Industries*.

Mailier, P.J., Stephenson, D.B., Ferro, C.A.T. and Hodges, K.I. (2006) Serial Clustering of Extratropical Cyclones. *Monthly Weather Review*. [Online] 134 (8), 2224–2240. Available at: doi:10.1175/MWR3160.1 (Accessed: 30 May 2017).

Malamud, B.D., Turcotte, D.L., Guzzetti, F. and Reichenbach, P. (2004) Landslide inventories and their statistical properties. *Earth Surface Processes and Landforms*. [Online] 29 (6), 687–711. Available at: doi:10.1002/esp.1064 (Accessed: 5 January 2017).

Malet, J.-P., van Asch, T.W.J., van Beek, R. and Maquaire, O. (2005) Forecasting the behaviour of complex landslides with a spatially distributed hydrological model. *Natural Hazards and Earth System Science*. [Online] 5 (1), 71–85. Available at: doi:10.5194/nhess-5-71-2005 (Accessed: 6 March 2017).

Mansour, M.F., Morgenstern, N.R. and Martin, C.D. (2011) Expected damage from displacement of slow-moving slides. *Landslides*. [Online] 8 (1), 117–131. Available at: doi:10.1007/s10346-010-0227-7 (Accessed: 15 February 2017).

Marjanović, M., Kovačević, M., Bajat, B. and Voženílek, V. (2011) Landslide susceptibility assessment using SVM machine learning algorithm. *Engineering Geology*. [Online] 123 (3), 225–234. Available at: doi:10.1016/j.enggeo.2011.09.006 (Accessed: 9 March 2017).

Marra, F., Destro, E., Nikolopoulos, E.I., Zoccatelli, D., Dominique Creutin, J., Guzzetti, F. and Borga, M. (2017) Impact of rainfall spatial aggregation on the identification of debris flow occurrence thresholds. *Hydrology and Earth System Sciences*. [Online] 21 (9), 4525–4532. Available at: doi:10.5194/hess-21-4525-2017 (Accessed: 17 December 2017).

Marra, F., Nikolopoulos, E.I., Creutin, J.D. and Borga, M. (2014) Radar rainfall estimation for the identification of debris-flow occurrence thresholds. *Journal of Hydrology*. [Online] 519 (PB), 1607–1619. Available at: doi:10.1016/j.jhydrol.2014.09.039.

Martelloni, G., Segoni, S., Lagomarsino, D., Fanti, R. and Catani, F. (2013) Snow accumulation/melting model (SAMM) for integrated use in regional scale landslide early warning systems. *Hydrology and Earth System Sciences*. [Online] 17 (3), 1229–1240. Available at: doi:10.5194/hess-17-1229-2013 (Accessed: 5 April 2017).

Martha, T.R., van Westen, C.J., Kerle, N., Jetten, V. and Vinod Kumar, K. (2013) Landslide hazard and risk assessment using semi-automatically created landslide inventories. *Geomorphology*. [Online] 184139–150. Available at: doi:10.1016/j.geomorph.2012.12.001 (Accessed: 14 March 2017).

Martinovic, K., Gavin, K. and Reale, C. (2016) Development of a landslide susceptibility assessment for a rail network. *Engineering Geology*. [Online] 2151–9. Available at: doi:10.1016/j.enggeo.2016.10.011.

Matisziw, T.C. and Murray, A.T. (2009) Modeling s-t path availability to support disaster vulnerability assessment of network infrastructure. *Computers and Operations Research*. [Online] 36 (1), 16–26. Available at: doi:10.1016/j.cor.2007.09.004 (Accessed: 28 March 2017).

Matthews, T., Murphy, C., Wilby, R.L. and Harrigan, S. (2016) A cyclone climatology of the British-Irish Isles 1871-2012. *International Journal of Climatology*. [Online] 36 (3), 1299–1312. Available at: doi:10.1002/joc.4425 (Accessed: 16 December 2017).

Mattsson, L.. and Jenelius, E. (2015) Vulnerability and resilience of transport systems - A discussion of recent research. *Transportation Research Part A: Policy and Practice*. [Online] 8116–34. Available at: doi:10.1016/j.tra.2015.06.002.

McCarthy, M., Spillane, S., Walsh, S. and Kendon, M. (2016) The meteorology of the exceptional winter of 2015/2016 across the UK and Ireland. *Weather*. [Online] 71 (12), 305–313. Available at: doi:10.1002/wea.2823 (Accessed: 2 March 2017).

McFadden, D. (1974) Conditional Logit Analysis of Qualitative Choice Behavior. *Frontiers of Economics*. [Online] 105–142. Available at: https://elsa.berkeley.edu/reprints/mcfadden/zarembka.pdf (Accessed: 25 May 2017).

McMillan, A A and Powell, J. (1999) Classification of artificial (man-made) ground and natural superficial deposits applications to geological maps and datasets in the UK. *BGS Rock Classification Scheme*. 4.

Melillo, M., Brunetti, M.T., Peruccacci, S., Gariano, S.L. and Guzzetti, F. (2015) An algorithm for the objective reconstruction of rainfall events responsible for landslides. *Landslides*. [Online] 12 (2), 311–320. Available at: doi:10.1007/s10346-014-0471-3 (Accessed: 20 March 2017).

Melton, M.A. (1957) *An analysis of the relation among elements of climate, surface properties and geomorphology*. [Online]. Available at: http://oai.dtic.mil/oai/oai?verb=getRecord&metadataPrefix=html&identifier=AD0148373 (Accessed: 15 November 2016).

Menard, S. (1997) NULL. *Applied logistic regression analysis*. [Online]. Sage. Available at: https://books.google.co.uk/books?hl=en&lr=&id=EAI1QmUUsbUC&oi=fnd&pg=PR5&dq=

menard+Applied+logistic+regression+analysis.&ots=4TJSN1oQLW&sig=tfEJfABlEQ3yrst YHirU2f6wyzk (Accessed: 15 March 2017).

Merz, B., Kreibich, H., Thieken, A. and Schmidtke, R. (2004) Estimation uncertainty of direct monetary flood damage to buildings. *Natural Hazards and Earth System Science*. [Online] 4 (1), 153–163. Available at: doi:10.5194/nhess-4-153-2004 (Accessed: 19 September 2017).

Met Office (2003) *5 km Resolution UK Composite Rainfall Data from the Met Office Nimrod System. NCAS British Atmospheric Data Centre, Oxford. [ONLINE] http://catalogue.ceda.ac.uk/uuid/82adec1f896af6169112d09cc1174499* [Online]. Available at: http://catalogue.ceda.ac.uk/uuid/f91b2c5399c5bf689e29bb15ab45da8a.

Met Office (2017) *UK climate: summaries and averages*. [Online]. 2017. Available at: http://www.Met Office.gov.uk/climate (Accessed: 2 March 2017).

Metz, M., Mitasova, H. and Harmon, R.S.R. (2011) Efficient extraction of drainage networks from massive, radar-based elevation models with least cost path search. *Hydrology and Earth System Sciences*. [Online] 15 (2), 667–678. Available at: doi:10.5194/hess-15-667-2011 (Accessed: 6 January 2017).

Meunier, P., Hovius, N. and Haines, J.A. (2008) Topographic site effects and the location of earthquake induced landslides. *Earth and Planetary Science Letters*. [Online] 275 (3–4), 221–232. Available at: doi:10.1016/j.epsl.2008.07.020.

Meyer, N.K., Dyrrdal, A. V., Frauenfelder, R., EtzelmÃller, B. and Nadim, F. (2012) Hydrometeorological threshold conditions for debris flow initiation in Norway. *Natural Hazards and Earth System Science*. [Online] 12 (10), 3059–3073. Available at: doi:10.5194/nhess-12-3059-2012 (Accessed: 21 September 2016).

Meyer, N.K., Schwanghart, W., Korup, O. and Nadim, F. (2015) Roads at risk: traffic detours from debris flows in southern Norway. *Natural Hazards and Earth System Science*. [Online] 15 (5), 985–995. Available at: doi:10.5194/nhess-15-985-2015 (Accessed: 29 June 2016).

Meyer, N.K., Schwanghart, W., Korup, O., Romstad, B. and Etzelmüller, B. (2014) Estimating the topographic predictability of debris flows. *Geomorphology*. [Online] 207114–125. Available at: doi:10.1016/j.geomorph.2013.10.030.

Milne, F.D., Werritty, A., Davies, M.C.R. and Brown, M.J. (2009) A recent debris flow event and implications for hazard management. *Quarterly Journal of Engineering Geology and Hydrogeology*. [Online] 42 (1), 51–60. Available at: doi:10.1144/1470-9236/07-073 (Accessed: 27 September 2016).

Minderhoud, M., Botma, H. and Bovy, P. (1997) Assessment of Roadway Capacity Estimation Methods *Transportation Research Record*. [Online]. 1572 (1) pp.59–67. Available at: doi:10.3141/1572-08 (Accessed: 1 April 2017).

Mingers, J. and Brocklesby, J. (1997) Multimethodology: Towards a framework for mixing methodologies. *Omega*. [Online] 25 (5), 489–509. Available at: doi:10.1016/S0305-0483(97)00018-2 (Accessed: 27 June 2016).

Montgomery, D.R. (1999) Process domains and the river continuum. *Journal of the American Water Resources Association*. [Online] 35 (2), 397–410. Available at: doi:10.1111/j.1752-1688.1999.tb03598.x (Accessed: 9 March 2017).

Mott MacDonald and Patterson, D. (2014) *HA Slope Geotechnical Hazard Rating: Highways Agency Task 197*

Muchan, K., Lewis, M., Hannaford, J. and Parry, S. (2015) The winter storms of 2013/2014 in the UK: hydrological responses and impacts. *Weather*. [Online] 70 (2), 55–61. Available at: doi:10.1002/wea.2469 (Accessed: 21 February 2017).

Murphy, J., Sexton, D.M.H., Jenkins, G., Boorman, P.M., Booth, B.B.B., Brown, C.C., Clark, R., Collins, M., Harris, G., Kendon, E., Betts, R., Brown, S., Howard, T.P., Humphrey, K.A., McCarthy, M.P., McDonald, R.E., Stephens, A., Wallace, C., Warren, R., et al. (2010) *UK Climate Projections Science Report: Climate change projections*. [Online]. Met Office Hadley Centre. Available at: doi:10.1787/9789264086876-5-en.

Murray-Tuite, P. and Mahmassani, H. (2004) Methodology for Determining Vulnerable Links in a Transportation Network. *Transportation Research Record*. [Online] 1882 (JANUARY), 88–96. Available at: doi:10.3141/1882-11 (Accessed: 25 March 2017).

Murray-Tuite, P.M. and Fei, X. (2010) A Methodology for assessing transportation network terrorism risk with attacker and defender interactions. *Computer-Aided Civil and Infrastructure Engineering*. [Online] 25 (6), 396–410. Available at: doi:10.1111/j.1467-8667.2010.00655.x (Accessed: 2 April 2017).

Murray, A.T., Matisziw, T.C. and Grubesic, T.H. (2008) A Methodological Overview of Network Vulnerability Analysis. *Growth and Change*. [Online] 39 (4), 573–592. Available at: doi:10.1111/j.1468-2257.2008.00447.x (Accessed: 27 June 2016).

Nagurney, A., Qiang, Q. and Nagurney, L.S. (2010) Environmental impact assessment of transportation networks with degradable links in an era of climate change. *International Journal of Sustainable Transportation*. [Online] 4 (3), 154–171. Available at: doi:10.1080/15568310802627328 (Accessed: 2 April 2017).

Nakicenovic, N. and Swart, R. (2000) *Special Report on Emissions Scenarios*.

NAO (2008) *Reducing passenger rail delays by better management of incidents*. 2008.

Napolitano, E., Fusco, F., Baum, R.L., Godt, J.W. and De Vita, P. (2016) Effect of antecedent-hydrological conditions on rainfall triggering of debris flows in ash-fall pyroclastic mantled slopes of Campania (southern Italy). *Landslides*. [Online] 13 (5), 967–983. Available at: doi:10.1007/s10346-015-0647-5 (Accessed: 30 May 2017).

Nettleton, I., Martin, S., Hencher, S. and Moore, R. (2005) Debris flow types and mechanisms *In: 'Winter M.G., Macgregor, F. and Shackman, L. (eds) 'Scottish Road Network Landslides Study'*. [Online]. (August). Available at: http://www.scotland.gov.uk/Publications/2005/07/08131738/17395.

Newman, M.E.J. (2003) The structure and function of complex networks. *e-print cond-mat/0303516*. [Online] Available at: http://epubs.siam.org/doi/abs/10.1137/s003614450342480 (Accessed: 28 March 2017).

Nicholson, A.J. and Dalziell, E. (2003) Risk evaluation and management: A road network reliability study. *The Network Reliability of Transport*. [Online] 45–59. Available at: doi:10.1108/9781786359544-003 (Accessed: 27 February 2017).

Notley, S., Bourne, N. and Taylor, N. (2008) Speed, flow and density of motorway traffic. *(Insight Report INS003).*

Nyambayo, V.P., Potts, D.M. and Addenbrooke, T.I. (2004) The Influence Of Permeability On The Stability Of Embankments Experiencing Seasonal Cyclic Pore Water Pressure Changes. In: *Advances in geotechnical engineering: The Skempton conference*. [Online]. pp. 898–910.

Available at: doi:10.1680/aigev2.32644.0019.

Nyberg, R. and Johansson, M. (2013) Indicators of road network vulnerability to storm-felled trees. *Natural Hazards*. [Online] 69 (1), 185–199. Available at: doi:10.1007/s11069-013-0693-z (Accessed: 29 June 2016).

O'Brien, A.S. (2007) Rehabilitation of urban railway embankments - Investigation, analysis and stabilisation. In: *14th International Conference on SMGE*. 2007 p.

Ohlmacher, G.C. and Davis, J.C. (2003) Using multiple logistic regression and GIS technology to predict landslide hazard in northeast Kansas, USA. *Engineering Geology*. [Online] 69 (3–4), 331–343. Available at: doi:10.1016/S0013-7952(03)00069-3 (Accessed: 5 March 2017).

Oliphant, T.E. (2007) Python for scientific computing. *Computing in Science and Engineering*. [Online] 9 (3), 10–20. Available at: doi:10.1109/MCSE.2007.58 (Accessed: 22 May 2017).

Onodera, T., Yoshinaka, R. and Kazama, H. (1974) Slope failures caused by heavy rainfall in Japan. In: *Proceedings of the 2nd International Congress of the International Association of Engineering Geology*. 1974 Sao Paulo. p. 11:1-10.

ONS (2011a) *2011 Census: Special Workplace Statistics (United Kingdom) [WU03UK_msoa]. UK Data Service Census Support. Downloaded from: https://wicid.ukdataservice.ac.uk* [Online]. Available at: https://wicid.ukdataservice.ac.uk.

ONS (2011b) *2011 Census aggregate data. UK Data Service (Edition: June 2016).* [Online]. Available at: doi:http://dx.doi.org/10.5257/census/aggregate-2011-1.

Ordnance Survey (2016) *OS MasterMap Integrated Transport Network Layer (ITN)[shapefile]*

ORR (2015) *Economic enforcement policy and penalties statement for railway licence holders*. [Online]. 2015. Office of Rail and Road. Available at: http://orr.gov.uk/publications/policies-and-statements (Accessed: 28 February 2017).

Ortuzar, J. de D. and Willumsen, L. (2011) *Modelling Transport*. [Online]. Wiley-Blackwell. Available at: doi:10.1002/9781119993308.

PAC (2014) *Maintaining strategic infrastructure: roads* [Online]. Available at: http://www.publications.parliament.uk/pa/cm201415/cmselect/cmpubacc/105/10502.htm (Accessed: 27 February 2017).

Pachauri, R.K., Allen, M.R., Barros, V.R., Broome, J., Cramer, W., Christ, R., Church, J.A., Clarke, L., Dahe, Q.D., Dasqupta, P., Dubash, N.K., Edenhofer, O., Elgizouli, I., Field, C.B., Forster, P., Friedlingstein, P., Fuglestvedt, J., Gomez-Echeverri, L., Hallegatte, S., et al. (2014) *Climate change 2014 synthesis report. contribution of working groups I, II, and III to the fifth assessment report of the Intergovernmental Panel on Climate Change*. IPCC.

Pallottino, S. and Scutell, M.G. (1998) *Shorest path algorithms in transportation models:classical and innovative aspects. In Equilibrium and Advanced Transportation Modelling*. [Online]. Boston, MA, Springer US. Available at: doi:10.1007/978-1-4615-5757-9_11 (Accessed: 30 March 2017).

Pardeshi, S.D., Autade, S.E. and Pardeshi, S.S. (2013) Landslide hazard assessment: recent trends and techniques. *SpringerPlus*. [Online] 2 (1), 1–11. Available at: doi:10.1186/2193-1801-2-523 (Accessed: 13 March 2017).

Pareschi, M.T., Favalli, M., Giannini, F., Sulpizio, R., Zanchetta, G. and Santacroce, R. (2000)

May 5, 1998, debris flows in circum-Vesuvian areas (Southern Italy): Insights for hazard assessment. *Geology*. [Online] 28 (7), 639–642. Available at: doi:10.1130/0091-7613(2000)28<639:MDFICA>2.0.CO;2 (Accessed: 9 March 2017).

Parkes, B.L., Wetterhall, F., Pappenberger, F., He, Y., Malamud, B.D. and Cloke, H.L. (2013) Assessment of a 1-hour gridded precipitation dataset to drive a hydrological model: a case study of the summer 2007 floods in the Upper Severn, UK. *Hydrology Research*. 44 (1).

Parry, S., Barker, L., Prosdocimi, I., Lewis, M., Hannaford, J. and Clemas, S. (2015) *Hydrological Summary for the United Kingdom: December 2015*

Peeta, S., Liu, H. and He, X. (2015) *Traffic network modeling*. [Online]. Routledge Handbooks Online. Available at: doi:10.4324/9781315756684.

Peeta, S., Sibel Salman, F., Gunnec, D. and Viswanath, K. (2010) Pre-disaster investment decisions for strengthening a highway network. *Computers and Operations Research*. [Online] 37 (10), 1708–1719. Available at: doi:10.1016/j.cor.2009.12.006 (Accessed: 30 March 2017).

Pennington, C., Dijkstra, T.A., Lark, M., Dashwood, C., Harrison, A. and Freeborough, K. (2014) Antecedent Precipitation as a Potential Proxy for Landslide Incidence in South West United Kingdom. In: Kyoji Sassa, Paolo Canuti, and Yueping Yin (eds.). *Landslide Science for a Safer Geoenvironment: Vol.1: The International Programme on Landslides (IPL)*. [Online]. Cham, Springer International Publishing. pp. 253–259. Available at: doi:10.1007/978-3-319-04999-1_34 (Accessed: 19 August 2016).

Pennington, C., Freeborough, K., Dashwood, C., Dijkstra, T.T.A. and Lawrie, K. (2015) The National Landslide Database of Great Britain: Acquisition, communication and the role of social media. *Geomorphology*. [Online] 24944–51. Available at: doi:10.1016/j.geomorph.2015.03.013 (Accessed: 13 July 2016).

Pennington, C. and Harrison, A. (2013) *2012: landslide year?* [Online]. 2013. Geoscientist Online [Available at http://www.geolsoc.org.uk/Geoscientist/Archive/June-2013/2012-Landslide-year]. Available at: http://nora.nerc.ac.uk/514719/ (Accessed: 22 February 2017).

Perkins, N.J. and Schisterman, E.F. (2006a) The Inconsistency of ‘ Optimal ’ Cut-points Using Two ROC Based Criteria. *Am J Epidemiol*. [Online] 163 (7), 670–675. Available at: doi:10.1093/aje/kwj063 (Accessed: 7 November 2016).

Perkins, N.J. and Schisterman, E.F. (2006b) The inconsistency of ‘optimal’ cutpoints obtained using two criteria based on the receiver operating characteristic curve. *American Journal of Epidemiology*. [Online] 163 (7), 670–675. Available at: doi:10.1093/aje/kwj063 (Accessed: 5 October 2016).

Perry, J. (1989) A survey of slope condition on motorway earthworks in England and Wales *Research report- Transport and Road Research Laboratory*. [Online]. (199). Available at: doi:10.1016/0148-9062(90)90380-K.

Peruccacci, S., Brunetti, M.T., Luciani, S., Vennari, C. and Guzzetti, F. (2012) Lithological and seasonal control on rainfall thresholds for the possible initiation of landslides in central Italy. *Geomorphology*. [Online] 139–14079–90. Available at: doi:10.1016/j.geomorph.2011.10.005.

Petley, D. (2012) Global patterns of loss of life from landslides. *Geology*. [Online] 40 (10), 927–930. Available at: doi:10.1130/G33217.1 (Accessed: 13 February 2017).

Petley, D. (2015) Landslides triggered by Storm Desmond in the UK last weekend *The*

Landslide Blog, AGU Blogosphere. [Online]. Available at: http://blogs.agu.org/landslideblog/2015/12/10/storm-desmond-1/ (Accessed: 23 February 2017).

Petley, D.N., Hearn, G.J., Hart, A., Rosser, N.J., Dunning, S.A., Oven, K. and Mitchell, W.A. (2007) Trends in landslide occurrence in Nepal. *Natural Hazards*. [Online] 43 (1), 23–44. Available at: doi:10.1007/s11069-006-9100-3 (Accessed: 25 February 2017).

Phipps, P.J. (2003) Geomorphological assessments for transport infrastructure projects. *Proceedings of the Institution of Civil Engineers - Transport*. [Online] 156 (3), 131–143. Available at: doi:10.1680/tran.156.3.131.37703 (Accessed: 20 February 2017).

Piacentini, D., Troiani, F., Soldati, M., Notarnicola, C., Savelli, D., Schneiderbauer, S. and Strada, C. (2012) Statistical analysis for assessing shallow-landslide susceptibility in South Tyrol (south-eastern Alps, Italy). *Geomorphology*. [Online] 151–152196–206. Available at: doi:10.1016/j.geomorph.2012.02.003 (Accessed: 14 March 2017).

Piciullo, L., Gariano, S.L., Melillo, M., Brunetti, M.T., Peruccacci, S., Guzzetti, F. and Calvello, M. (2016) Definition and performance of a threshold-based regional early warning model for rainfall-induced landslides. *Landslides*. [Online] 24 September, 1–14. Available at: doi:10.1007/s10346-016-0750-2 (Accessed: 20 November 2016).

Porta, S., Crucitti, P. and Latora, V. (2006) The network analysis of urban streets: A dual approach. *Physica A: Statistical Mechanics and its Applications*. [Online] 369 (2), 853–866. Available at: doi:10.1016/j.physa.2005.12.063 (Accessed: 30 March 2017).

Postance, B., Hillier, J., Dijkstra, T.A. and Dixon, N. (2017a) Comparing threshold definition techniques for rainfall induced landslides: a national assessment using radar rainfall. *Earth Surface Exchanges In 'Earth Surface Processes and Landforms'*. [Online] Available at: doi:10.1002/esp.4202 (Accessed: 31 July 2017).

Postance, B., Hillier, J., Dijkstra, T. and Dixon, N. (2017b) Extending natural hazard impacts: an assessment of landslide disruptions on a national road transportation network. *Environmental Research Letters*. [Online] 12 (1), 14010. Available at: doi:10.1088/1748-9326/aa5555 (Accessed: 11 January 2017).

Pradhan, B. and Lee, S. (2009) Landslide risk analysis using artificial neural network model focussing on different training sites. *International Journal*. [Online] 4 (1), 001–015. Available at: http://www.academicjournals.org/journal/IJPS/article-abstract/F7906B417691 (Accessed: 15 March 2017).

Pradhan, B., Oh, H.-J. and Buchroithner, M. (2010) Weights-of-evidence model applied to landslide susceptibility mapping in a tropical hilly area. *Geomatics, Natural Hazards and Risk*. [Online] 1 (3), 199–223. Available at: doi:10.1080/19475705.2010.498151 (Accessed: 14 March 2017).

Pregnolato, M., Ford, A., Robson, C., Glenis, V., Barr, S. and Dawson, R. (2016) Assessing urban strategies for reducing the impacts of extreme weather on infrastructure networks. *Royal Society Open Science*. 3 (5).

Pritchard, O.G., Hallett, S.H. and Farewell, T.S. (2014) Soil impacts on UK infrastructure: current and future climate. *Proceedings of the Institution of Civil Engineers - Engineering Sustainability*. [Online] 167 (4), 170–184. Available at: doi:10.1680/ensu.13.00035 (Accessed: 14 February 2017).

Qiang, Q. and Nagurney, A. (2008) A unified network performance measure with importance identification and the ranking of network components. *Optimization Letters*. [Online] 2 (1), 127–142. Available at: doi:10.1007/s11590-007-0049-2.

Quinn, P.E., Hutchinson, D.J., Diederichs, M.S. and Rowe, R.K. (2010) Regional-scale landslide susceptibility mapping using the weights of evidence method: an example applied to linear infrastructure. *Canadian Geotechnical Journal*. [Online] 47 (8), 905–927. Available at: doi:10.1139/T09-144 (Accessed: 14 March 2017).

RAIB (2008) *Network Rail's management of existing earthworks*. [Online]. Available at: https://www.gov.uk/raib-reports/network-rail-s-management-of-existing-earthworks.

Rail Engineer (2015) *The Harbury Slip*. [Online]. 2015. Rail Engineer. Available at: https://www.railengineer.uk/2015/05/06/the-harbury-slip/ (Accessed: 27 February 2017).

RailwaysAct (1993) *Railways Act 1993, 57B*. [Online]. Available at: http://www.legislation.gov.uk/ukpga/1993/43 (Accessed: 28 February 2017).

Reid, B. (2006) Global early warning systems for natural hazards: systematic and people-centred. *Phil. Trans. R. Soc. A*. [Online] 364 (1845), 2167–2182. Available at: doi:10.1098/rsta.2006.1819 (Accessed: 10 January 2017).

Reid, M.E. and Lahusen, R.G. (1998) Real-time monitoring of active landslides along highway 50, El Dorado County. *California Geology*. 51 (3), 17–20.

Ridley, A., McGinnity, B. and Vaughan, P. (2004) Role of pore water pressures in embankment stability. *Proceedings of the ICE - Geotechnical Engineering*. [Online] 157 (4), 193–198. Available at: doi:10.1680/geng.2004.157.4.193 (Accessed: 17 February 2017).

Rossi, M., Luciani, S., Valigi, D., Kirschbaum, D., Brunetti, M.T., Peruccacci, S. and Guzzetti, F. (2017) Statistical approaches for the definition of landslide rainfall thresholds and their uncertainty using rain gauge and satellite data. *Geomorphology*. [Online] Available at: doi:10.1016/j.geomorph.2017.02.001 (Accessed: 13 February 2017).

Rota, M. and Antolini, L. (2014) Finding the optimal cut-point for Gaussian and Gamma distributed biomarkers. *Computational Statistics and Data Analysis*. [Online] 691–14. Available at: doi:10.1016/j.csda.2013.07.015.

Rouainia, M., Davies, O., Brien, T.O., Glendinning, S., O'Brien, T. and Glendinning, S. (2009) Numerical modelling of climate effects on slope stability. *Engineering Sustainability*. [Online] 162 (ES2), 81–89. Available at: doi:10.1680/ensu.2009.162 (Accessed: 3 March 2017).

Rupi, F., Bernardi, S., Rossi, G. and Danesi, A. (2014) The Evaluation of Road Network Vulnerability in Mountainous Areas : A Case Study. *Networks and Spatial Economics*. [Online] 15 (2), 397–411. Available at: doi:10.1007/s11067-014-9260-8 (Accessed: 5 July 2016).

Saito, H., Nakayama, D. and Matsuyama, H. (2010) Relationship between the initiation of a shallow landslide and rainfall intensity-duration thresholds in Japan. *Geomorphology*. [Online] 118 (1–2), 167–175. Available at: doi:10.1016/j.geomorph.2009.12.016.

Sampson, C.C., Fewtrell, T.J., O'Loughlin, F., Pappenberger, F., Bates, P.B., Freer, J.E. and Cloke, H.L. (2014) The impact of uncertain precipitation data on insurance loss estimates using a flood catastrophe model. *Hydrology and Earth System Sciences*. [Online] 18 (6), 2305–2324. Available at: doi:10.5194/hess-18-2305-2014 (Accessed: 19 September 2017).

Schaefer, J.T. (1990) The Critical Success Index as an Indicator of Warning Skill *Weather and Forecasting*. [Online]. 5 (4) pp.570–575. Available at: doi:10.1175/1520-0434(1990)005<0570:TCSIAA>2.0.CO;2 (Accessed: 7 November 2016).

Schellart, A.N.A., Shepherd, W.J. and Saul, A.J. (2012) Influence of rainfall estimation error and spatial variability on sewer flow prediction at a small urban scale. *Advances in Water Resources*. [Online] 4565–75. Available at: doi:10.1016/j.advwatres.2011.10.012.

Schisterman, E.F., Perkins, N.J., Liu, A. and Bondell, H. (2005) Optimal cut-point and its corresponding Youden Index to discriminate individuals using pooled blood samples. *Epidemiology (Cambridge, Mass.)*. [Online] 16 (1), 73–81. Available at: doi:10.1097/01.ede.0000147512.81966.ba (Accessed: 7 November 2016).

Scott, D.M., Novak, D.C., Aultman-Hall, L. and Guo, F. (2006) Network Robustness Index: A new method for identifying critical links and evaluating the performance of transportation networks. *Journal of Transport Geography*. [Online] 14 (3), 215–227. Available at: doi:10.1016/j.jtrangeo.2005.10.003 (Accessed: 27 June 2016).

Seabold, S. and Perktold, J. (2010) Statsmodels: econometric and statistical modeling with Python. In: *Proceedings of the 9th Python in Science Conference*. [Online]. 2010 pp. 57–61. Available at: http://conference.scipy.org/proceedings/scipy2010/pdfs/seabold.pdf (Accessed: 22 May 2017).

Segoni, S., Battistini, A., Rossi, G., Rosi, A., Lagomarsino, D., Catani, F., Moretti, S. and Casagli, N. (2015a) Technical Note: An operational landslide early warning system at regional scale based on space-time-variable rainfall thresholds. *Natural Hazards and Earth System Sciences*. [Online] 15 (4), 853–861. Available at: doi:10.5194/nhess-15-853-2015 (Accessed: 24 March 2017).

Segoni, S., Lagomarsino, D., Fanti, R., Moretti, S. and Casagli, N. (2015b) Integration of rainfall thresholds and susceptibility maps in the Emilia Romagna (Italy) regional-scale landslide warning system. *Landslides*. [Online] 12 (4), 773–785. Available at: doi:10.1007/s10346-014-0502-0 (Accessed: 9 April 2017).

Segoni, S., Rosi, A., Rossi, G., Catani, F. and Casagli, N. (2014a) Analysing the relationship between rainfalls and landslides to define a mosaic of triggering thresholds for regional-scale warning systems. *Natural Hazards and Earth System Sciences*. [Online] 14 (9), 2637–2648. Available at: doi:10.5194/nhess-14-2637-2014 (Accessed: 6 April 2017).

Segoni, S., Rossi, G., Rosi, A. and Catani, F. (2014b) Landslides triggered by rainfall: A semi-automated procedure to define consistent intensity-duration thresholds. *Computers and Geosciences*. [Online] 63123–131. Available at: doi:10.1016/j.cageo.2013.10.009 (Accessed: 24 March 2017).

Shahabi, H. and Hashim, M. (2015) Landslide susceptibility mapping using GIS-based statistical models and Remote sensing data in tropical environment. *Scientific Reports*. [Online] 59899. Available at: doi:10.1038/srep09899 (Accessed: 1 December 2016).

Sidle, R.C. and Ochiai, H. (2013) *Landslides: Processes, Prediction, and Land Use*. Water Resources Monograph. [Online]. Washington, D. C., American Geophysical Union. Available at: doi:10.1029/WM018 (Accessed: 31 October 2016).

Skempton, A.W. (1996) Embankments and Cuttings on the early Railways. *Construction History*. [Online] Vol. 1133–49. Available at: http://www.jstor.org/stable/41615443?seq=1#page_scan_tab_contents (Accessed: 14

February 2017).

Smedley, M.I., Paulson, R. and Tucker, A. (2009) Remote sensing for highway management of landslides. *Proceedings of the Institution of Civil Engineers-Geotechnical Engineering*. [Online] 162 (3), 141–150. Available at: doi:DOI 10.1680/geng.2009.162.3.141.

Smilowitz, K., Daganzo, C., Cassidy, M. and Bertini, R. (1999) Some Observations of Highway Traffic in Long Queues. *Transportation Research Record*. [Online] 1678 (99), 225–233. Available at: doi:10.3141/1678-27 (Accessed: 2 December 2016).

Soeters, R. and van Westen, C.J. (1996) Slope instability recognition, analysis and zonation. In: *Special report 247 Transportation Research Board, National Research Council*. [Online]. Washington, D.C, National Academy Press. pp. 129–173. Available at: https://trid.trb.org/view.aspx?id=462506 (Accessed: 14 March 2017).

Sohn, J. (2006) Evaluating the significance of highway network links under the flood damage: An accessibility approach. *Transportation Research Part A: Policy and Practice*. [Online] 40 (6), 491–506. Available at: doi:10.1016/j.tra.2005.08.006 (Accessed: 30 March 2017).

Sohn, J., Kim, T.J., Hewings, G.J.D., Lee, J.S. and Jang, S.G. (2003) Retrofit priority of transport network links under an earthquake. *Journal of Urban Planning and Development*. [Online] 129 (4), 195–210. Available at: doi:10.1061/(asce)0733-9488(2003)129:4(195) (Accessed: 30 March 2017).

Søren, B., Graziella, D., José, C. and Hervé, C. (2014) Landslide thresholds at regional scale for an early warning system in Norway. In: *Proceedings of World Landslide Forum 3*. 2014 Beijing. pp. 2–6.

Srinivasan, K.K. (2002) TRANSPORTATION NETWORK VULNERABILITY ASSESSMENT: A QUANTITATIVE FRAMEWORK. *Transportation Security Papers 2002*. [Online] Available at: https://trid.trb.org/view.aspx?id=723261 (Accessed: 25 March 2017).

Staley, D.M., Kean, J.W., Cannon, S.H., Schmidt, K.M. and Laber, J.L. (2013) Objective definition of rainfall intensity-duration thresholds for the initiation of post-fire debris flows in southern California. *Landslides*. [Online] 10 (5), 547–562. Available at: doi:10.1007/s10346-012-0341-9 (Accessed: 23 September 2016).

Stanley, T. and Kirschbaum, D.B. (2017) A heuristic approach to global landslide susceptibility mapping. *Natural Hazards*. [Online] 87 (1), 145–164. Available at: doi:10.1007/s11069-017-2757-y (Accessed: 8 June 2017).

Steger, S., Brenning, A., Bell, R. and Glade, T. (2017) The influence of systematically incomplete shallow landslide inventories on statistical susceptibility models and suggestions for improvements. *Landslides*. [Online] 7 April, 1–15. Available at: doi:10.1007/s10346-017-0820-0 (Accessed: 22 May 2017).

Sterlacchini, S., Ballabio, C., Blahut, J., Masetti, M. and Sorichetta, A. (2011) Spatial agreement of predicted patterns in landslide susceptibility maps. *Geomorphology*. [Online] 125 (1), 51–61. Available at: doi:10.1016/j.geomorph.2010.09.004 (Accessed: 14 March 2017).

Stern (2006) The stern review on the economic effects of climate change *Population and Development Review*. [Online]. 32 (4) pp.793–798. Available at: doi:10.1111/j.1728-4457.2006.00153.x (Accessed: 27 June 2016).

Stoffel, M., Tiranti, D. and Huggel, C. (2014) Climate change impacts on mass movements - Case studies from the European Alps. *Science of the Total Environment*. [Online] 4931255–

1266. Available at: doi:10.1016/j.scitotenv.2014.02.102.

Suits, D.B. (1957) Use of Dummy Variables in Regression Equations. *Journal of the American Statistical Association*. [Online] 52 (280), 548–551. Available at: doi:10.2307/2281705 (Accessed: 9 December 2016).

Sullivan, J.L., Novak, D.C., Aultman-Hall, L. and Scott, D.M. (2010) Identifying critical road segments and measuring system-wide robustness in transportation networks with isolating links: A link-based capacity-reduction approach. *Transportation Research Part A: Policy and Practice*. [Online] 44 (5), 323–336. Available at: doi:10.1016/j.tra.2010.02.003.

Süzen, M.L. and Kaya, B.Ş. (2011) Evaluation of environmental parameters in logistic regression models for landslide susceptibility mapping. *International Journal of Digital Earth*. [Online] 5 (February 2015), 338–355. Available at: doi:10.1080/17538947.2011.586443 (Accessed: 9 March 2017).

Swiss Re (2016) *Natural catastrophes and man-made disasters in 2015 - ReliefWeb* [Online]. Available at: reliefweb.int/sites/reliefweb.int/files/resources/sigma1_2016_en.pdf.

Tampère, C.M.J., Stada, J., Immers, B., Peetermans, E. and Organe, K. (2008) Methodology for Identifying Vulnerable Sections in a National Road Network. *Transportation Research Record*. [Online] 2012 (1), 1–10. Available at: doi:10.3141/2012-01 (Accessed: 30 March 2017).

Taylor, M.A.P. and D'Este, G.M. (2007) Transport Network Vulnerability: a Method for Diagnosis of Critical Locations in Transport Infrastructure Systems. In: *Critical Infrastructure*. [Online]. Berlin, Heidelberg, Springer Berlin Heidelberg. pp. 9–30. Available at: doi:10.1007/978-3-540-68056-7_2 (Accessed: 29 June 2016).

Terlien, M.T.J. (1998) The determination of statistical and deterministic hydrological landslide-triggering thresholds. *Environmental Geology*. [Online] 35 (2–3), 124–130. Available at: doi:10.1007/s002540050299 (Accessed: 17 March 2017).

Terzaghi, K. (1950) Mechanism of Landslides: In Engineering Geology (Berkeley) Vol. *Geological Society of America, New York*.

Thiery, Y., Malet, J.P., Sterlacchini, S., Puissant, A. and Maquaire, O. (2007) Landslide susceptibility assessment by bivariate methods at large scales: Application to a complex mountainous environment. *Geomorphology*. [Online] 92 (1–2), 38–59. Available at: doi:10.1016/j.geomorph.2007.02.020 (Accessed: 14 March 2017).

Tian, Y., Xiao, C., Liu, Y. and Wu, L. (2008) Effects of raster resolution on landslide susceptibility mapping: A case study of Shenzhen. *Science in China, Series E: Technological Sciences*. [Online] 51 (SUPPL. 2), 188–198. Available at: doi:10.1007/s11431-008-6009-y (Accessed: 11 March 2017).

Transport Scotland (2016a) *A9 *CLOSED* at Helmsdale due to hill debris affecting the route.* [Online]. 2016. Available at: https://twitter.com/trafficscotland/status/694426190812155904?ref_src=twsrc%255Etfw.

Transport Scotland (2016b) *Road asset management plan for Scottish trunk roads, January 2016* [Online]. Available at: https://www.transport.gov.scot/publication/road-asset-management-plan-for-scottish-trunk-roads-january-2016/ (Accessed: 26 September 2017).

Treiber, M. and Kanagaraj, V. (2015) Comparing numerical integration schemes for time-continuous car-following models. *Physica A: Statistical Mechanics and its Applications*.

[Online] 419183–195. Available at: doi:10.1016/j.physa.2014.09.061 (Accessed: 16 June 2017).

Trewin, N.H. (2002) *The geology of Scotland.* 4th Revise. [Online]. London, United Kingdom, Geological Society of London. Available at: doi:10.1144/GOS4P.

Tsiampousi, A., Zdravkovic, L. and Potts, D.M. (2016) Numerical study of the effect of soil – atmosphere interaction on the stability and serviceability of cut slopes in London clay. *Canadian Geotechnical Journal*. [Online] 14 (October), 1–14. Available at: doi:10.1139/cgj-2016-0319 (Accessed: 7 March 2017).

Tsukamoto, Y., Ohta, T. and Noguchi, H. (1982) Hydrogeological and geomorphological studies of debris slides on forested hillslopes in Japan. In: *Recent Developments in the Explanation and Prediction of Erosion and Sediment Yield (Proceedings of the Exeter Symposium, July 1982). IAHS Publ. 137*. 1982 [Wallingford, England?] : International Association of Hydrological Sciences, 1982. pp. 89–98.

UNISDR (2015) *United Nations International Strategy for Disaster: Sendai framework for disaster risk reduction 2015–2030.* [Online]. (March). Available at: doi:A/CONF.224/CRP.1.

Vandre, B.C. (1985) Rudd Creek debris flow. *Delineation of landslide, flash flood and debris flow hazards in Utah, edited by Bowles, DS, Utah Water Res. Lab., Logan, Utah*.

Varnes, D.J. (1978) Slope Movement Types and Processes. *Transportation Research Board Special Report*. (176).

Varnes, D.J. and the I.C. on L. and other M.-M. (1984) Landslide hazard zonation: a review of principles and practice. *The UNESCO Press, Paris*. [Online] (3), 63. Available at: https://trid.trb.org/view.aspx?id=281932 (Accessed: 5 March 2017).

Villarini, G. and Krajewski, W.F. (2008) Empirically-based modeling of spatial sampling uncertainties associated with rainfall measurements by rain gauges. *Advances in Water Resources*. [Online] 31 (7), 1015–1023. Available at: doi:10.1016/j.advwatres.2008.04.007.

Villarini, G., Mandapaka, P. V., Krajewski, W.F. and Moore, R.J. (2008) Rainfall and sampling uncertainties: A rain gauge perspective. *Journal of Geophysical Research Atmospheres*. [Online] 113 (11), D11102. Available at: doi:10.1029/2007JD009214 (Accessed: 30 September 2016).

De Vita, P., Reichenbach, P., Bathurst, J.C., Borga, M., Crozier, G.M., Glade, T., Guzzetti, F., Hansen, A. and Wasowski, J. (1998) Rainfall-triggered landslides: A reference list. *Environmental Geology*. [Online] 35 (2–3), 219–233. Available at: doi:10.1007/s002540050308 (Accessed: 23 February 2017).

Voumard, J., Caspar, O., Derron, M.H. and Jaboyedoff, M. (2013) Dynamic risk simulation to assess natural hazards risk along roads. *Natural Hazards and Earth System Sciences*. [Online] 13 (11), 2763–2777. Available at: doi:10.5194/nhess-13-2763-2013 (Accessed: 10 February 2017).

Wachinger, G., Renn, O., Begg, C. and Kuhlicke, C. (2013) The risk perception paradox-implications for governance and communication of natural hazards. *Risk Analysis*. [Online] 33 (6), 1049–1065. Available at: doi:10.1111/j.1539-6924.2012.01942.x (Accessed: 10 January 2017).

Walsby, J. (2008) GeoSure : a bridge between geology and decision makers C Liverman, D. G. E Pereira and B Marker (eds.). *Communicating Environmental Geoscience*. [Online] 305

(c), 81–87. Available at: doi:10.1144/SP305.9 (Accessed: 27 June 2016).

Walsby, J.C. (2007) Geohazard information to meet the needs of the British public and government policy. *Quaternary International*. [Online] 171–172 (SPEC. ISS.), 179–185. Available at: doi:10.1016/j.quaint.2007.02.015.

Waltham, A.C. and Dixon, N. (2000) Movement of the Mam Tor landslide, Derbyshire, UK. *Quarterly Journal of Engineering Geology and Hydrogeology*. [Online] 33 (2), 105–123. Available at: doi:10.1144/qjegh.33.2.105 (Accessed: 26 September 2016).

Wang, S., Hong, L., Ouyang, M., Zhang, J. and Chen, X. (2013) Vulnerability analysis of interdependent infrastructure systems under edge attack strategies. *Safety Science*. [Online] 51 (1), 328–337. Available at: doi:10.1016/j.ssci.2012.07.003 (Accessed: 28 March 2017).

Wang, Z., Chan, A.P.C., Yuan, J., Xia, B., Skitmore, M. and Li, Q. (2014) Recent Advances in Modeling the Vulnerability of Transportation Networks. *Journal of Infrastructure Systems*. [Online] 21 (2), 1–9. Available at: doi:10.1061/(ASCE)IS.1943-555X.0000232.

Wardrop, J.G. and Whitehead, J.I. (1952) Correspondence. Some Theoretical Aspects of Road Traffic Research. *ICE Proceedings: Engineering Divisions*. [Online] 1 (5), 767–768. Available at: doi:10.1680/ipeds.1952.11362 (Accessed: 27 June 2016).

Watling, D. and Balijepalli, N.C. (2012) A method to assess demand growth vulnerability of travel times on road network links. *Transportation Research Part A: Policy and Practice*. [Online] 46 (5), 772–789. Available at: doi:10.1016/j.tra.2012.02.009 (Accessed: 1 April 2017).

Watts, D.J. and Strogatz, S.H.H. (1999) Collective dynamics of 'small-world' networks. *Nature*. [Online] 393 (6684), 440–442. Available at: doi:10.1038/30918 (Accessed: 27 March 2017).

Welsh, A. and Davies, T. (2011) Identification of alluvial fans susceptible to debris-flow hazards. *Landslides*. [Online] 8 (2), 183–194. Available at: doi:10.1007/s10346-010-0238-4 (Accessed: 9 March 2017).

van Westen, C.J., van Asch, T.W.J. and Soeters, R. (2006) Landslide hazard and risk zonation—why is it still so difficult? *Bulletin of Engineering Geology and the Environment*. [Online] 65 (2), 167–184. Available at: doi:10.1007/s10064-005-0023-0 (Accessed: 5 March 2017).

Van Westen, C.J., Van Asch, T.W.J. and Soeters, R. (2006) Landslide hazard and risk zonation - Why is it still so difficult? *Bulletin of Engineering Geology and the Environment*. [Online] 65 (2), 167–184. Available at: doi:10.1007/s10064-005-0023-0 (Accessed: 23 February 2017).

Van Westen, C.J., Castellanos, E. and Kuriakose, S.L. (2008) Spatial data for landslide susceptibility, hazard, and vulnerability assessment: An overview. *Engineering Geology*. [Online] 102 (3–4), 112–131. Available at: doi:10.1016/j.enggeo.2008.03.010.

Van Westen, C.J., Rengers, N. and Soeters, R. (2003) Use of geomorphological information in indirect landslide susceptibility assessment. *Natural Hazards*. [Online] 30 (3), 399–419. Available at: doi:10.1023/B:NHAZ.0000007097.42735.9e (Accessed: 13 February 2017).

Whitehead, P.G., Wilby, R.L., Battarbee, R.W., Kernan, M. and Wade, A.J. (2009) A review of the potential impacts of climate change on surface water quality. *Hydrological Sciences Journal*. [Online] 54 (1), 101–123. Available at: doi:10.1623/hysj.54.1.101 (Accessed: 2 March 2017).

Wieczorek, G.F. (1987) Effect of rainfall intensity and duration on debris flows in central Santa Cruz Mountains, California. In: *Reviews in Engineering Geology*. [Online]. Geological Society of America. pp. 93–104. Available at: doi:10.1130/REG7-p93 (Accessed: 17 March 2017).

Wieczorek, G.F. (1996) Landslide triggering mechanisms. In: A. Keith Turner and Robert L. Schuster (eds.). *Landslides : investigation and mitigation, Transportation Research Board, National Research Council, special report*. Washington, D.C, National Academy Press. p. 673.

Wieczorek, G.F. and Glade, T. (2005) Climatic factors influencing occurrence of debris flows. In: *Debris-flow Hazards and Related Phenomena*. [Online]. Berlin, Heidelberg, Springer Berlin Heidelberg. pp. 325–362. Available at: doi:10.1007/3-540-27129-5_14 (Accessed: 21 September 2016).

Wieczorek, G.F. and Sarmiento, J. (1982) Rainfall, piezometric levels, and debris flows near La Honda, California, in storms between 1975 and 1983. *Landslides, floods, and marine effects of the storm of January*. 3–5.

Wilby, R.L., O'Hare, G. and Barnsley, N. (1997) The North Atlantic Oscillation and British Isles climate variability, 1865-1996. *Weather*. [Online] 52 (9), 266–276. Available at: doi:10.1002/j.1477-8696.1997.tb06323.x (Accessed: 2 March 2017).

Wilford, D.J., Sakals, M.E., Innes, J.L., Sidle, R.C. and Bergerud, W.A. (2004) Recognition of debris flow, debris flood and flood hazard through watershed morphometrics. *Landslides*. [Online] 1 (1), 61–66. Available at: doi:10.1007/s10346-003-0002-0 (Accessed: 15 November 2016).

Wilks, D.S. (2006) *Statistical Methods in the Atmospheric Sciences*. 3rd edition. [Online]. Cambridge, MA, United States, Academic Press. Available at: doi:10.1198/jasa.2007.s163.

Wilson, R.C. and Jayko, A.S. (1997) Preliminary Maps Showing Rainfall Thresholds for Debris- Flow Activity, San Francisco Bay Region, California. *U.S. Geological Survey Open file report 97-745*. [Online] 1–20. Available at: http://pubs.er.usgs.gov/publication/ofr97745F (Accessed: 3 October 2016).

Winter, M., Macgregor, F. and Shackman, L. (2005) *Scottish Road Network Landslide Study* [Online]. Available at: http://www.gov.scot/Publications/2005/07/08131738/17395.

Winter, M.G. (2014) Debris Flow Hazard and Risk on the Scottish Road Network in a Changing Climate. In: *Recent Advances in Material, Analysis, Monitoring, and Evaluation in Foundation and Bridge Engineering*. [Online]. 23 June 2014 Reston, VA, American Society of Civil Engineers. pp. 150–158. Available at: doi:10.1061/9780784478530.019 (Accessed: 23 February 2017).

Winter, M.G., Dent, J., Macgregor, F., Dempsey, P., Motion, A. and Shackman, L. (2010) Debris flow, rainfall and climate change in Scotland. *Quarterly Journal of Engineering Geology and Hydrogeology*. [Online] 43 (4), 429–446. Available at: doi:10.1144/1470-9236/08-108 (Accessed: 27 September 2016).

Winter, M.G., Palmer, D., Sharpe, J., Shearer, B. and Harmer, C. (2014) Economic Impact Assessment of Landslide Events. In: *Proceedings of the World Landslide Forum*. [Online]. 2014 Cham, Springer International Publishing. pp. 2–6. Available at: doi:10.1007/978-3-319-04999-1 (Accessed: 27 June 2016).

Yang, H., Lo, K.K. and Tang, W.H. (2001) TRAVEL TIME VERSUS CAPACITY RELIABILITY OF A ROAD NETWORK. In: *RELIABILITY OF TRANSPORT NETWORKS*.

[Online]. Hertfordshire, United Kingdom, Research Studies Press. pp. 119–138. Available at: https://trid.trb.org/view.aspx?id=696249 (Accessed: 27 March 2017).

Yao, X., Tham, L.G. and Dai, F.C. (2008) Landslide susceptibility mapping based on Support Vector Machine: A case study on natural slopes of Hong Kong, China. *Geomorphology*. [Online] 101 (4), 572–582. Available at: doi:10.1016/j.geomorph.2008.02.011 (Accessed: 15 March 2017).

Yee, A., Leung, S.K. and Wesemann, L. (1996) The 1994 Northridge Earthquake--A Transportation Impact Overview. *Transportation Research Circular*. (462).

Yi-Ming, C., Dachrahn, W. and Cheng-Kuang, W. (2009) A Game Theory Approach for Evaluating Terrorist Threats and Deploying Response Agents in Urban Environments. *Journal of Homeland Security & Emergency Management*. [Online] 6 (1), 1–25. Available at: doi:10.2202/1547-7355.1488 (Accessed: 28 March 2017).

Yilmaz, I. (2010) Comparison of landslide susceptibility mapping methodologies for Koyulhisar, Turkey: conditional probability, logistic regression, artificial neural networks, and support vector machine. *Environmental Earth Sciences*. [Online] 61 (4), 821–836. Available at: doi:10.1007/s12665-009-0394-9 (Accessed: 9 March 2017).